

W. Cijssouw

# A continuous superstructure for the Sognefjord bridge





# A continuous superstructure for the Sognefjord bridge

by

W. (Willem) Cijssouw  
4451171

[w\\*\\*\\*\\*\\*@gmail.com](mailto:w*****@gmail.com)

in partial fulfilment of the requirements for obtaining the degree of

**Master of Science**  
in Structural Engineering

Thesis committee:

**Prof. M. Veljkovic** (chairman)

Chair of Steel and Composite Structures, Delft University of Technology, Faculty of Civil Engineering and Geosciences

**Ing. S. M. Molenaar** (supervisor)

Structural Engineer at Iv-Consult, Section of Steel Structures

**Dr. ir. R. Abspoel**

Researcher Steel Structures, Delft University of Technology, Faculty of Civil Engineering and Geosciences

**Ir. A.C.M. van der Stap**

Associate Professor Offshore Engineering, Delft University of Technology, Faculty of Civil Engineering and Geosciences

**Ir. W.M. Visser**

Manager Structural Design at Iv-Consult, Section of Steel Structures

An electronic version of this thesis is available at <http://repository.tudelft.nl/>.



---

*“If I have ever seen far, it was because I was standing on the shoulders of Giants”*

**- Isaac Newton**

In a letter to his rival Robert Hooke, 1676



## PREFACE

When I started my thesis project, I was prepared for a long and difficult journey. Fortunately however, the project never got to a point where I got completely stuck in my work. For that, I think, there are two reasons. First of all, I was very lucky in finding such a diverse topic as the Sognefjord bridge. At any point in time there were always multiple challenging aspects of research to work on, which kept the project interesting and the work diverse.

Secondly my thesis committee was always there to guide me, give a much needed critical look at my work and steer me back in the right direction whenever I lost track. André, Marius, Milan, Roland and Wouter never ceased to devote their time and energy whenever I needed it and with their different backgrounds they helped me look at things from different perspectives. Especially the help of Marius during my daily work was invaluable to me. His advice and engineering experience have spared me much time and have much improved the quality of my research. I am very grateful to my committee for all the time, energy and advice they have given me.

This report finishes my master in Structural Engineering and thereby finalises my time as a student. From the first moments on, being a student has been a great journey for me. Over the years I had the fortune to meet fantastic people, study great fields of knowledge and get experiences that I will remember for the rest of my life. It has enriched my life and for that I am very grateful.

Finally, most important for me is the knowledge that my friends and family were always there to support me. Next to good council, they provided a place to blow off steam whenever I needed that. They were an important part of what made life as a student so great for me. I feel proud to know I can call them friends and family and owe them the world.

Willem Cijssouw  
Delft, May 2018

## ABSTRACT

For the E39 highway in Norway a project is underway to replace the ferry crossing in the Sognefjord with a fixed crossing. Previous thesis projects have resulted in a design for a 4500 m long buoyancy bridge which consists of 22 concrete pontoons that carry a steel truss superstructure. To reduce lateral movements the pontoons are fixed to a submerged anchoring cable system. In the middle of the bridge a 400 m wide, 70 m high ship fairway is created. In previous bridge designs the superstructure consisted of separate girders for every span which were connected to the pontoons through hinges. The purpose of this research was to investigate the structural feasibility of creating a continuous superstructure without internal hinges for the Sognefjord bridge. After making a design for a continuous CHS steel truss superstructure, behaviour of the whole Sognefjord bridge with the new superstructure was researched for different load combinations. It was found that maximum lateral displacement of the bridge is 27 m, while maximum longitudinal displacement is 46 m. These were deemed acceptable values. A research was conducted into which parameters influence bridge behaviour the most. It was found that of the bridge structure, rotational stiffness of the pontoons influences bridge deformations the most. A two times higher rotational stiffness of the pontoons leads to a maximum reduction in lateral bridge displacements of 44%. The stiffness of the superstructure was found to have only minor effect on bridge behaviour. Internal loads in the superstructure were found to be mainly determined by displacements of the top of the pontoons, upon which the superstructure rests. Internal loads in individual truss members under a ULS storm situation were investigated. Member stress levels under a ULS storm are very diverse in value, with a maximum peak member stress of 590 N/mm<sup>2</sup>, resulting in a unity check for stability of 1.36. Under reduced bridge deformations from double rotational stiffness of the pontoons, member stress in the superstructure on average drops by half. Peak member stress in the superstructure under a ULS storm with double pontoon rotational stiffness is 293 N/mm<sup>2</sup>, resulting in a unity check for stability of 0.67. Preliminary investigations into bridge dynamics and ship collision were performed. Vortex-induced vibrations of structural elements, as well as pontoon displacements and shockwave effects under ship impact are challenges that require more investigation. The results of this research suggest that creating a continuous bridge girder without internal hinges for the Sognefjord buoyancy bridge is structurally feasible. This would require doubling the rotational stiffness of the pontoons, which is expected to come with large material costs. More in-depth research into other load situations is recommended.

## LIST OF CONTENTS

Preface.....	vi
Abstract.....	vii
<b>1. Introduction .....</b>	<b>1</b>
1.1 The E39 Coastal Highway Route.....	1
1.2 Introduction to the Sognefjord bridge.....	1
1.3 Previous research.....	2
1.4 Problem statement and research scope.....	3
1.5 Research workflow.....	4
1.6 Bridge terminology and global coordinate system.....	5
1.7 Main structural analysis models used.....	6
1.8 Report structure.....	7
<b>2. Design information and literature study.....</b>	<b>8</b>
2.1 Crossing properties.....	8
2.2 Crossing requirements.....	9
2.3 Environmental data.....	11
2.4 Other literature research.....	14
2.5 Conclusions from literature research.....	16
<b>3. Bridge modelling and bridge design evaluation.....</b>	<b>17</b>
3.1 Validating modelling cables in SCIA Engineer.....	17
3.2 Investigating alternative superstructure concepts.....	19
3.3 Re-building the model in SCIA Engineer.....	21
<b>4. Designing a new superstructure.....</b>	<b>25</b>
4.1 Superstructure concept.....	25
4.2 Truss girder modelling.....	25
4.3 Main span girder design.....	27
4.4 Sub span girder designs.....	27
4.5 Continuous girder boundary conditions.....	29
4.6 Results.....	29
<b>5. Bridge behaviour research.....</b>	<b>31</b>
5.1 Modelling.....	31
5.2 Parameter research.....	31
5.3 General deformation behaviour of Sognefjord bridge.....	31
5.4 Bridge sensitivity analysis.....	33
5.5 Parameter research results.....	34
5.6 Range of governing parameters.....	37
5.7 Discussion.....	37
5.8 Conclusions of parameter research.....	39



<b>6. Girder behaviour research .....</b>	<b>41</b>
6.1 Coordinate system forces .....	41
6.2 Modelling imposed deformations on the bridge girders .....	41
6.3 Boundary conditions and imposed deformations in Scia model #2 of the full truss girder .....	43
6.4 Global forces and bending moments in ULS storm situation in girders .....	43
6.5 Forces and bending moments in ULS storm situation in truss girder members .....	45
6.6 Stress levels.....	48
6.7 Effect of stiffer pontoons .....	48
6.8 Discussion.....	52
6.9 Conclusion .....	52
<b>7. Investigating ship collision .....</b>	<b>54</b>
7.1 Modelling ship impact .....	54
7.2 Ship collision analysis results .....	55
7.3 Bridge behaviour under impact .....	56
7.4 Dynamic response under impact .....	56
7.5 Pontoon buoyancy under impact .....	56
7.6 Conclusions .....	57
<b>8. Bridge dynamics .....</b>	<b>59</b>
8.1 Possible dynamic behaviour .....	59
8.2 Eigenfrequency analysis modelling.....	59
8.3 Eigenfrequency analysis results .....	60
8.4 Vortex-induced vibrations .....	60
8.5 Reducing dynamic effects.....	61
8.6 Conclusions .....	62
<b>9. Main conclusions from research .....</b>	<b>63</b>
9.1 Creating a continuous girder without internal hinges for the Sognefjord bridge .....	63
9.2 Behaviour of the Sognefjord bridge in conventional load situations .....	63
9.3 Behaviour of the superstructure in conventional load situations.....	65
9.4 Ship collision and bridge dynamics.....	66
9.5 Limitations in this research .....	66
9.6 Recommendations for further research .....	66
<b>10. References.....</b>	<b>68</b>
<b>ANNEX A: Bridge concept from previous research .....</b>	<b>A-1</b>
A.1 Bridge design from previous study.....	A-1
A.2 Bridge design by Yip (2015) characteristics.....	A-1
A.3 Modelling and calculations.....	A-4
<b>ANNEX B: Full conclusions on research by Yip (2015).....</b>	<b>B-1</b>
<b>ANNEX C: Model validation in ansys .....</b>	<b>C-1</b>
C.1 Difficulties in modelling .....	C-1

C.2	Stepwise elaboration in modelling .....	C-1
C.3	Results .....	C-5
<b>ANNEX D:</b>	<b>Researching different superstructure concepts .....</b>	<b>D-1</b>
D.1	Torsional check for preliminary investigation feasibility curved girder .....	D-1
D.2	Calculations to check simple preliminary bridge girder concepts .....	D-1
<b>ANNEX E:</b>	<b>Building SCIA analysis model #1 .....</b>	<b>E-1</b>
E.1	Geometry .....	E-1
E.2	Superstructure .....	E-1
E.3	Pontoon modelling .....	E-2
E.4	Loads .....	E-3
<b>ANNEX F:</b>	<b>External Loads calculation file output.....</b>	<b>F-1</b>
<b>ANNEX G:</b>	<b>New superstructure design .....</b>	<b>G-1</b>
G.1	Search for truss layout .....	G-1
G.2	Elaborating the Warren truss .....	G-1
G.3	Girder properties .....	G-2
G.4	Designing sub spans.....	G-2
G.5	Stability .....	G-3
<b>ANNEX H:</b>	<b>Bridge behaviour under different load situations .....</b>	<b>H-1</b>
H.1	Load combinations .....	H-1
H.2	Bridge behaviour .....	H-2
<b>ANNEX I:</b>	<b>Bridge parameter research results .....</b>	<b>I-1</b>
I.1	Pontoon rotational stiffness.....	I-1
I.2	Pontoon vertical stiffness .....	I-2
I.3	Bending stiffness bridge girder .....	I-3
I.4	Shear stiffness bridge girder .....	I-4
I.5	Anchoring system stiffness .....	I-5
I.6	Wind loads .....	I-6
I.7	Wind wave loads.....	I-7
I.8	Effect of anchoring system on pontoon rotations.....	I-8
<b>ANNEX J:</b>	<b>Tripod pontoon design investigation .....</b>	<b>J-1</b>
<b>ANNEX K:</b>	<b>Girder modelling validation .....</b>	<b>K-1</b>
K.1	Numerical cross-sections vs. geometric cross-sections .....	K-1
K.2	Modelling imposed deformations .....	K-2
K.3	Modelling deformations on the full truss girder .....	K-3
<b>ANNEX L:</b>	<b>Girder displacement analysis results.....</b>	<b>L-1</b>
L.1	Global forces and bending moments in bridge girder .....	L-1
L.2	Global forces and bending moments in girder for double pontoon rotational stiffness .....	L-3

---

L.3	Global forces and bending moments in girders without imposed deformations.....	L-6
<b>ANNEX M:</b>	<b>Ship impact analysis set-up and script.....</b>	<b>M-1</b>
M.1	Ship impact analysis model .....	M-1
M.2	Python script for ship impact analysis model .....	M-3
M.3	Buoyancy calculation of a pontoon with compartments after ship impact.....	M-5
<b>ANNEX N:</b>	<b>eigenperiods, dynamic behaviour and measures .....</b>	<b>N-1</b>
N.1	Eigenperiod analysis modelling .....	N-1
N.2	Eigenperiod analysis results .....	N-1
N.3	Measures to reduce behaviour .....	N-2
N.4	Qualitative analysis of dynamic behaviour measures .....	N-4





## 1. INTRODUCTION

### 1.1 The E39 Coastal Highway Route

The starting point of this study is the Project Coastal Highway E39 which has been planned by the Norwegian Ministry of Transport and Communications. See figure 1.1. The project concerns eliminating all the fjord ferries along the western corridor (E39) of almost 1100 km long. The E39 is part of the European trunk road system and it contains the highest number of ferries (8) for a single road in Europe. The fjords have different lengths, widths, soil characteristics, depths of water and climate conditions. This complex multidisciplinary technical challenge reaches its apex with the Sognefjord bridge. This is a bridge designed to cross the largest fjord of Norway, the Sognefjord (see figure 1.2).

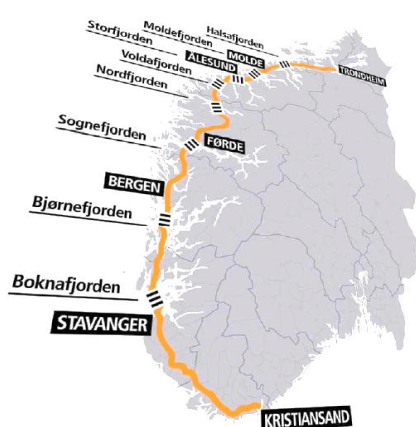


FIGURE 1.1: E39 HIGHWAY PROJECT

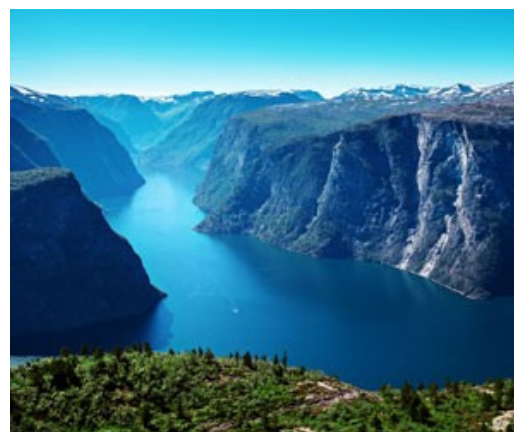


FIGURE 1.2: THE SOGNEFJORD

In 2014, engineering company Iv-Consult and architecture firm Zwart & Jansma Architecten teamed up with the TU Delft to investigate the feasibility of creating a floating crossing for Sognefjord. The Sognefjord is Norway's largest fjord, being 3700 m wide and 1250 m deep. The depth of the fjord, in combination with its large width and the architectural vision of creating panoramic views of the fjord, resulted in the choice for a floating bridge concept. This concept was first developed by Hermans (2014) in his graduation research. Work on the Sognefjord bridge was continued in the thesis by Yip (2015), in which the bridge design was adjusted. The result of the latter thesis has been used as the starting point for this research.

### 1.2 Introduction to the Sognefjord bridge

The design for the Sognefjord buoyancy bridge by Yip (2015) was taken as a starting point for this research. It consists of 22 large floating concrete pontoons, which support steel bridge girders that cross 21 spans over a total length of 4500 m. The pontoons are connected to a submerged cable anchoring system, which is designed to restrain lateral displacements of the pontoons. Each pontoon is connected to two lateral anchoring cables, which themselves are connected to two large main anchoring cables. The main anchoring cables are fixed to the shores. See figure 1.3.

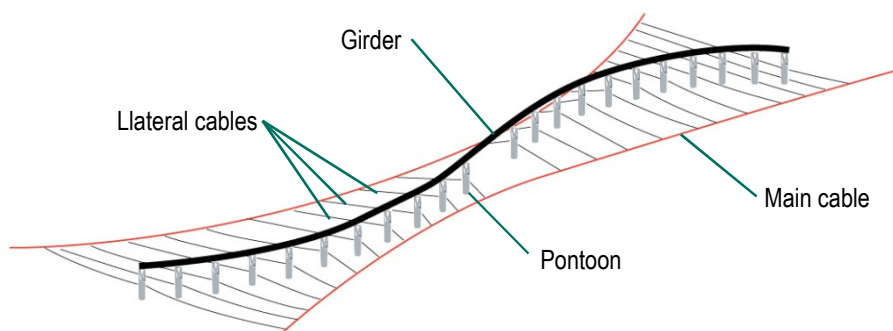


FIGURE 1.3: SCHEMATIC OVERVIEW OF THE SOGNEFJORD BUOYANCY BRIDGE

There are 20 side spans of 200 m each and a large central main span of 465 m. The bridge deck elevates up to 70 m above water level in the mid of the fjord to create a large fairway clearance under the bridge. The radii and lengths of the pontoons vary respectively from 15 to 26 m and from 100 to 220 m. The pontoons provide upward buoyancy forces and restoring moments to limit the rotations of the structure. See figures 1.4 and 1.5.

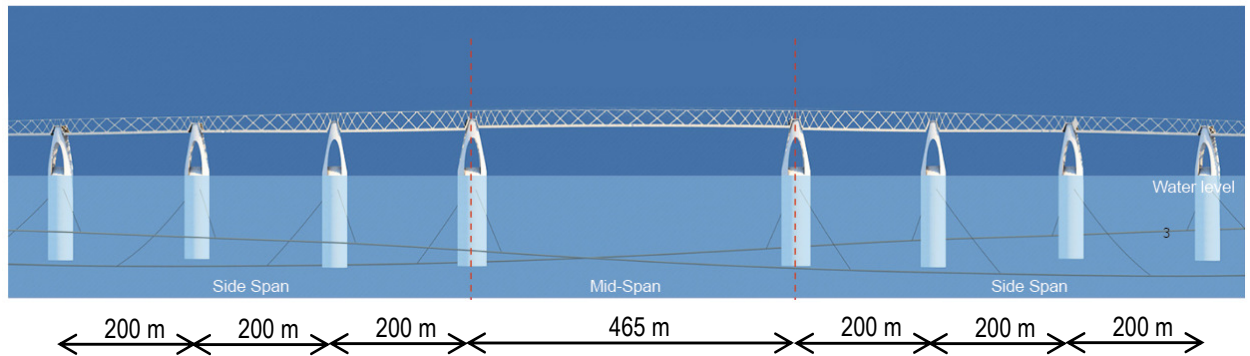


FIGURE 1.4: ELEVATION VIEW OF THE SOGNEFJORD BRIDGE, WITH THE LARGER MAIN SPAN IN THE MIDDLE. THE PONTOONS ARE FOR THE LARGEST PART SUBMERGED. THE ANCHORING CABLES DO NOT HANG EVENLY HIGH ON BOTH SIDES OF THE PONTOONS.



FIGURE 1.5: RENDER OF THE SOGNEFJORD BRIDGE. CRUISE SHIP FOR SIZE REFERENCE. RETRIEVED FROM ZWARTS & JANSMA ARCHITECTEN.

### 1.3 Previous research

Two theses have been submitted prior to this research. Hermans (2014) has conducted extensive studies into the Sognefjord environment and the requirements and environmental loads for the design. Yip (2015) built further on the initial design and investigated new options for the girders, pontoons and anchoring system, especially focusing on an alternative anchoring cable design. Their bridge concepts are displayed in figures 1.6 and 1.7. Both thesis reports have been used gratefully for this research.

#### 1.3.1 Feasibility study by Yip (2015)

Preceding design work was studied thoroughly for useful input. A full description of the design by Yip (2015) can be found in Annex A. Main conclusions on this design are made below.

- Yip (2015) started her research by changing the anchoring concept from anchoring just four pontoons, to applying a double horizontal suspension anchoring system. In this way, each pontoon is individually anchored. This concept has its benefits and drawbacks, but was upon evaluation still deemed the most feasible. Therefore this will be maintained as a starting point for this research.



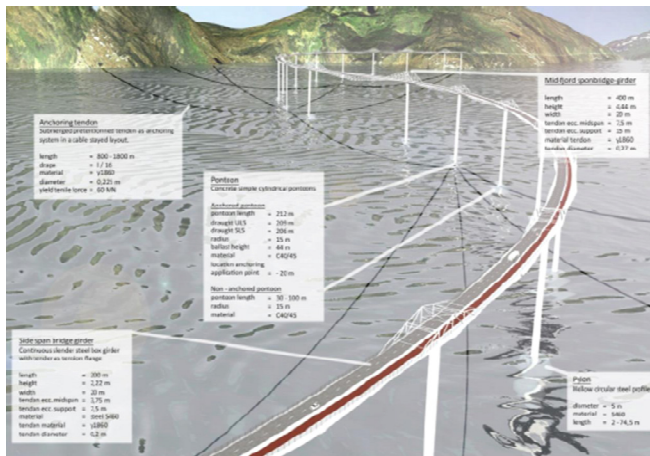


FIGURE 1.6: BRIDGE CONCEPT BY HERMANS (2014)



FIGURE 1.7: BRIDGE CONCEPT BY YIP (2015) (IMAGE BY ZWARTS & JANSMA ARCHITECTEN)

- The architects stated their desire for a single clear line for the superstructure. The choice was eventually made on designing for a steel lattice girder with circular hollow sections. However, design justification was partly missing and it was mentioned that the girder needed more optimisation. Therefore it was concluded that further design work on the bridge girder was needed.
- Bridge dynamics and ship impact for example have not been researched yet. These are both considered as risks for the overall bridge feasibility, and need to be addressed at least to the point where something can be said about their effect on bridge feasibility.

The conclusions made above are the three main remarks made on the research done so far. Extended versions of these conclusions are given in Annex B. In chapter 3, additional in-depth conclusions about design aspects by Yip (2015) are made as well.

### 1.3.2 Verification of previous design for maintenance intensity

Environmental properties have a large influence on the bridge design. Sognefjord is a very low-density area, where rather extreme weather conditions can occur and where for example equipment for bridge repair work is far away from the site. These conditions make performing maintenance activities very challenging and costly. Furthermore, the floating nature of the bridge further increases the cost of replacing bridge parts, since it would almost always be needed to temporarily fix other bridge parts in place during maintenance. Therefore it was concluded that designing a bridge that requires little maintenance during its lifespan should be a goal.

### 1.3.3 Verification of previous design for ship collision and bridge dynamics

In previous research by both Hermans (2014) and Yip (2015), it was decided not to consider ship collision or dynamic loading on the bridge. Both could however have disastrous consequences for a bridge that is not well designed. For this study it was therefore found appropriate to further investigate ship impact and bridge dynamics and use this research in refining the bridge design.

## 1.4 Problem statement and research scope

At the start of this thesis, the main challenges of the current bridge concept were defined. These are minimising bridge maintenance over its service life (at least 100 years), collision of a ship with the pontoons, coping with hazardous dynamic behaviour of the structure, erection of the bridge and resisting fatigue loading on the bridge.

In chapter 2 it was found that maintenance costs can be high, sometimes exceeding original construction costs. Since hinges for the superstructure have a service life that is lower than the design service life of the bridge, replacement cannot be evaded. The costs of replacing such joints will however be unacceptably high. This would not abide the goal of designing a low-maintenance structure. This means internal hinges in the bridge, which

require expensive maintenance, will have to be evaded. Therefore creating a continuous bridge girder without internal hinges for the Sognefjord will be the main research goal for this thesis.

A structure like the Sognefjord buoyancy bridge is currently unprecedented. In understanding the behaviour of a structure like this, so far, the effect of the girder on the overall bridge behaviour has not been investigated. Deformations of the bridge are expected to impose loads on the bridge girder. This thesis will investigate the range of these loads and whether the girder can withstand these loads. It can then be concluded whether it is possible to create a continuous girder without internal hinges in the current Sognefjord design concept.

Upon evaluation it was concluded that ship impact and bridge dynamics potentially pose serious threats to the feasibility of the Sognefjord bridge, and therefore need to be addressed. This will be done in this research. The Sognefjord bridge design is still in preliminary phase. Fatigue loads and erection of the bridge will not be taken into account in this research.

To conclude: this thesis investigates minimising maintenance by creating a continuous girder, the structural behaviour of the buoyancy bridge, bridge dynamics and ship collision. It was chosen to keep bridge erection and fatigue out of the scope of this research.

This led to the following research sub questions:

- **What behaviour (displacements and rotations) can be expected from a bridge structure like this in conventional load situations?**
- **What loads can be expected in the superstructure of the Sognefjord in conventional load situations?**
- **Is there a risk of structural collapse of the Sognefjord bridge in a ship collision event?**
- **Can hazardous dynamic behaviour of the Sognefjord bridge be expected?**

The overall research goal is to answer the main research question:

**Is creating a continuous girder without internal hinges for the Sognefjord buoyancy bridge feasible?**

## 1.5 Research workflow

To start, the design by Yip (2015) as starting point was evaluated, focusing especially on the bridge girder design. Together with this, the calculations and modelling done by Yip (2015) were evaluated as well. Where deemed needed, these were adjusted. When the modelling was set the bridge design was adjusted to fit the new requirements of the bridge. The bridge girder was completely redesigned.

Then, the new bridge design was tested to investigate its behaviour (its deformations under load situations). Structural properties of the bridge as well as the external loads on the bridge were tested for their influence on this bridge behaviour.

When the behaviour of the bridge was known the bridge girder itself was tested for its reaction under this behaviour. This was done to check if a continuous girder without internal hinges is able to absorb the deformations the deforming bridge imposes on it.

Preliminary studies into ship collision and the dynamic behaviour of the Sognefjord bridge were made. This thesis research ends with combining the results and conclusions of all parts of research into one concluding chapter. The research questions were discussed and recommendations for further research and design were given. Figure 1.8 summarises the workflow of this thesis research.

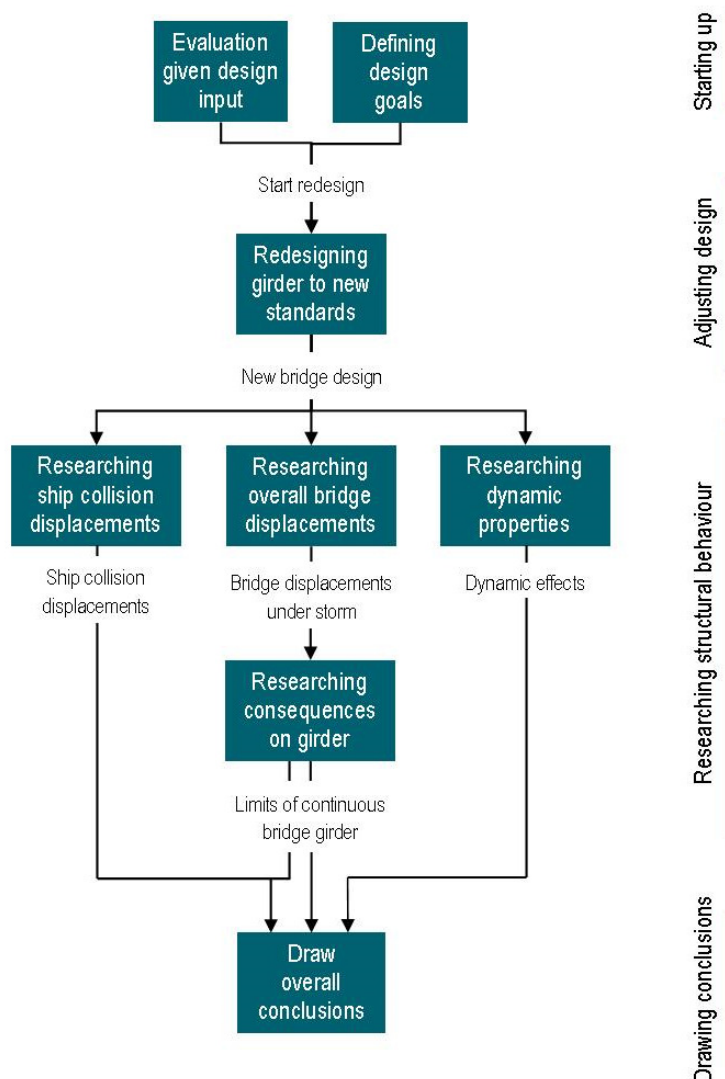


FIGURE 1.8: THESIS RESEARCH WORKFLOW

## 1.6 Bridge terminology and global coordinate system

In figure 1.9 a schematic cross-section of a pontoon with the girder and anchoring system is given for reference. The terminology described here will be used throughout the whole report. Although sizes differ per pontoon and per span, the structural layout indicated in this sketch holds for the whole bridge.

In describing displacements and rotations, the coordinate system displayed in figure 1.10 is used. This means for example lateral bridge displacements are denoted in the x-direction, while longitudinal bridge displacements are in the y-direction. This coordinate system is used throughout the whole report.

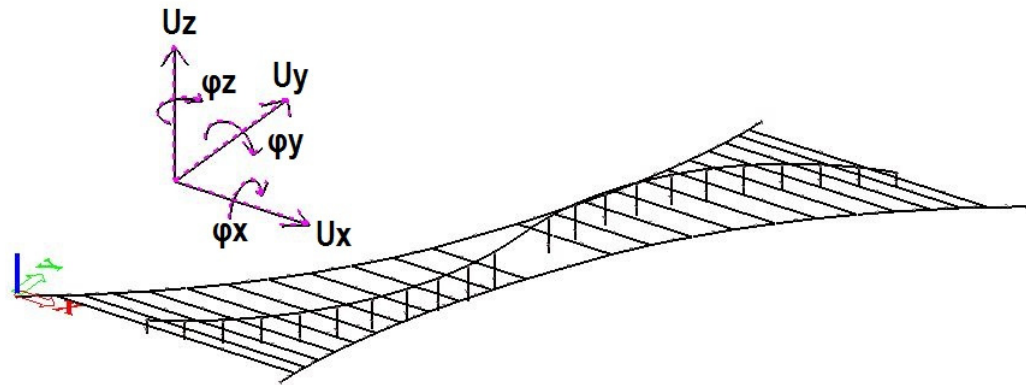


FIGURE 1.10: GLOBAL COORDINATE SYSTEM USED IN THIS RESEARCH

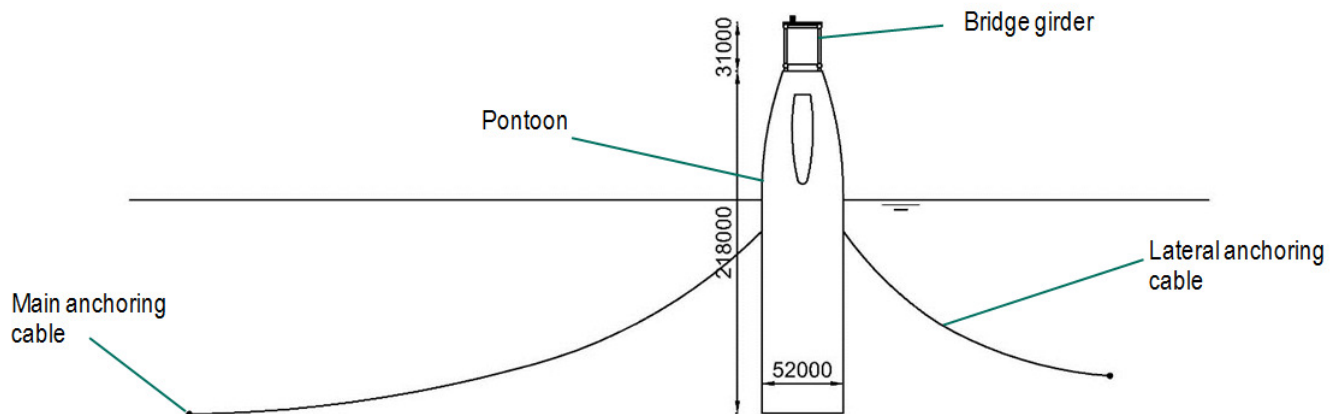
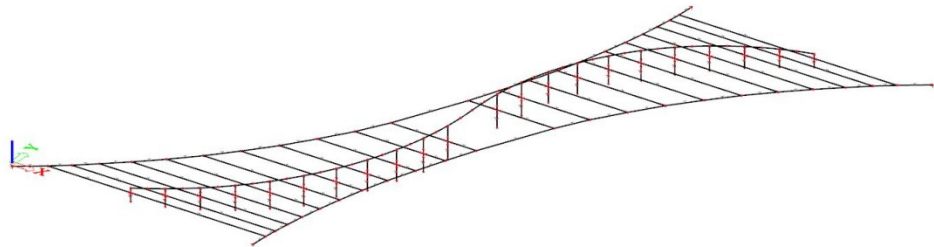
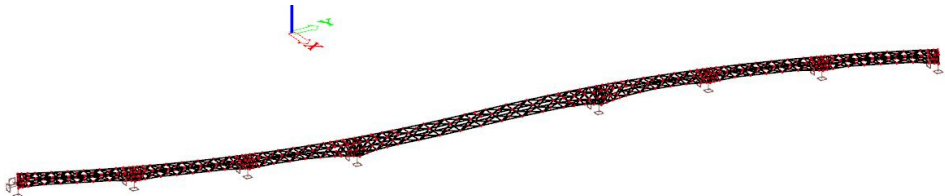
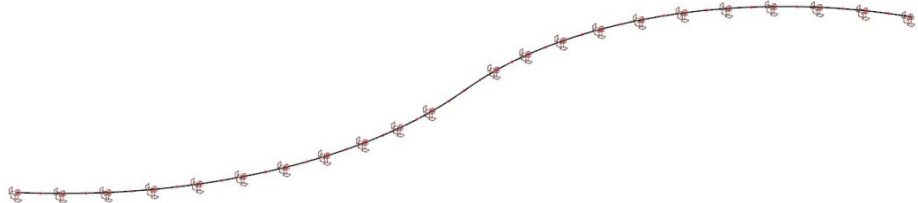


FIGURE 1.9: SCHEMATIC CROSS-SECTION OF THE SOGNEFJORD BRIDGE AT ONE PONTOON. TRUCK ON TOP OF THE GIRDER FOR SIZE REFERENCE.

## 1.7 Main structural analysis models used

In this thesis, three different models in Scia Engineer were used to analyse the Sognefjord bridge. In Scia model #1, the Sognefjord buoyancy bridge as a whole was modelled. In this model, the bridge girders were replaced by prismatic beams with the same stiffness properties, to increase calculation efficiency. This model was used to analyse global bridge behaviour. To analyse forces and stresses in the truss girders in more detail, a second Scia model #2 was made. In this model the 7 central spans of the bridge were modelled in full detail. Lastly, a third Scia model #3 was made. This model is an exact copy of the prismatic girders used in Scia model #1 of the whole bridge, but of these bridge girders only. The rest of the bridge was deleted and replaced by equivalent boundary conditions. This model was used mainly to investigate global forces. See table 1.1. The analysis models are further discussed in chapter 6.

TABLE 1.1: SCIA STRUCTURAL ANALYSIS MODELS USED IN THIS THESIS RESEARCH

Scia model	Description
#1	<p>Main model of whole Sognefjord bridge. Bridge girders simplified as prismatic beams with equivalent stiffness properties. Mainly used to analyse global bridge behaviour.</p> 
#2	<p>Model of only the girders at the central 7 spans of the bridge. Fully elaborated 3D truss girders. Mainly used to analyse structural behaviour of individual truss members.</p> 
#3	<p>Copy of only the bridge girders of Scia model #1. Mainly used to validate modelling imposed deformations on a structure, and to evaluate global forces on the bridge girders.</p> 

## 1.8 Report structure

This report starts with a literature study into the previous research and into related bridge research. It then continues by investigating and designing a new bridge girder design, after which the behaviour of the whole Sognefjord bridge and its consequences for the bridge girder are investigated. After this, collision of a ship with the bridge is preliminary researched as well, together with a preliminary study into the dynamics of the bridge. The conclusions are summarised in the last chapter. Here, general conclusions about the bridge, recommendations for its design and for further research are made.



## 2. DESIGN INFORMATION AND LITERATURE STUDY

Extensive research in investigating a floating bridge proposal has already been conducted by Hermans (2014) and Yip (2015). This research also included investigations in load conditions, by considering different codes and research reports. This provided a list of environmental and load properties which should be resisted by the bridge. These conditions, which are used for this thesis as well, are discussed in the following paragraph. This chapter then continues with other literature that has been studied for this research – topics that have not been looked upon yet in this design.

### 2.1 Crossing properties

The current crossing of the fjord by the E39 is between Lavik on the north bank and Oppedal on the south bank, and utilizes a ferry service. The location of the crossing is about 20-25 km inland. The buoyancy bridge will be located on this crossing as well. Because this is the location of the current ferry link, extension of the existing highway will be limited here. The location of the buoyancy bridge is indicated in purple in figure 2.1.

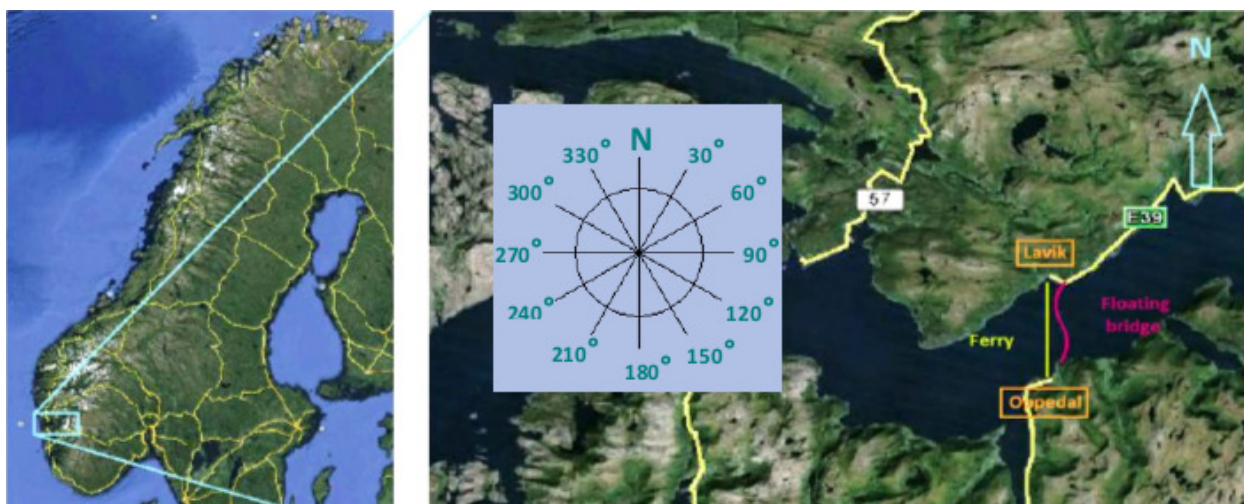


FIGURE 2.1: SOGNEFJORD BUOYANCY BRIDGE PLANNED LOCATION

The cross-section of the Sognefjord at the location around the crossing is shown in figure 2.2. The crossing is around 3700 meters wide and 1250 meters deep. The sides of the shores are relatively shallow, but going more mid-fjord they reach slopes of 30 to 50 degrees. At the bottom of the Sognefjord, the soil consists of 200-300 meters clay. The steep inclined parts at the sides consists of rock (Hermans, 2014).

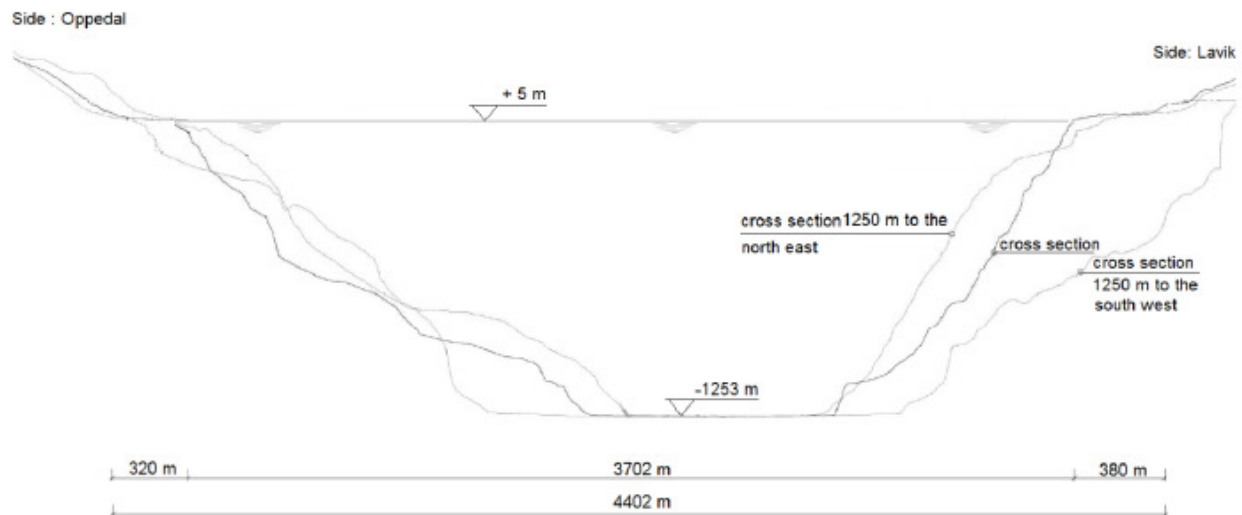


FIGURE 2.2: CROSS-SECTION OF THE SOGNEFJORD. RETRIEVED FROM YIP (2015).

## 2.2 Crossing requirements

The Eurocodes do not specifically give requirement for the movement of floating bridges. Movement here is defined as deflection, rotations and accelerations. Hermans (2014) has put a lot of research in requirements for structural and serviceability properties of a buoyancy bridge over Sognefjorden. The requirements set in this research will be gratefully used for this thesis as well, although found values were reviewed and adjusted when deemed necessary.

### 2.2.1 Functional requirements

The design life span of the crossing is 100 years. In terms of traffic, the aim of the NPRA is to provide enough capacity to meet the requirements for the traffic situation in 2040. Hermans (2014) proposed a road layout based on road class S4 set by the NRPA. This layout was also assumed by Yip (2015). After evaluation it was however concluded that road class H7 was better suited for this study, since this class has double traffic lanes in each direction. It is assumed that in the far future, when all crossings in the E39 highway are fixed, it will be desirable to have a two-lane road everywhere. This cross-section design is prepared for that. This gives the following requirements:

Average daily traffic:	12000 vehicles
Design speed:	80 km/h
Road class:	H7, double lane in each direction
Road width:	20 m (H7, excluding separate pedestrian/cycling plane)
Clearance height:	4.5 m

H7 is a road class specified by the NPRA in the N100 Road Design Handbook, in which however the pedestrian lane width is not specified. At evaluation, it was concluded that the slow traffic lane proposed by Hermans (2014) and Yip (2015) was too wide. Together with the different road class, this lead to a different proposed road section layout. See figure 2.3 for a drawing.

Furthermore the crossing should allow ship traffic to pass. The following requirements set for the fairway clearance by Hermans (2014) were maintained:

#### Ship clearance in fairway

Annual number large vessels:	3300
Width passage:	400m
Height passage:	70m
Draught:	20 m

#### Outside fairway

Height:	8m
Draught:	15 m

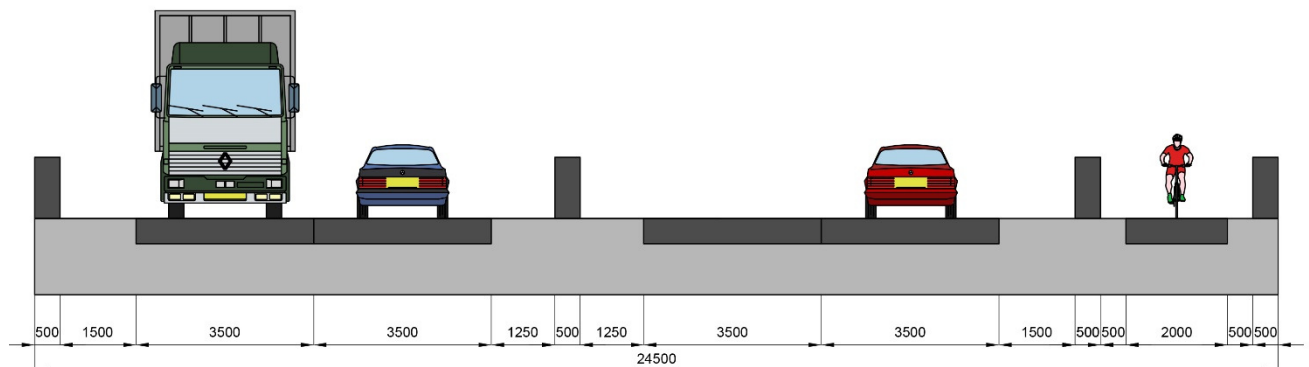


FIGURE 2.3: PROPOSED LAYOUT OF THE ROAD ON TOP OF THE SOGNEFJORD BRIDGE

### 2.2.2 Serviceability and user comfort

Eurocode 3-2 states that deflections in the bridge deck should be uniform without any abrupt changes. This means deflections are allowed to become large, as long as the bridge shape remains uniform and accelerations limited.

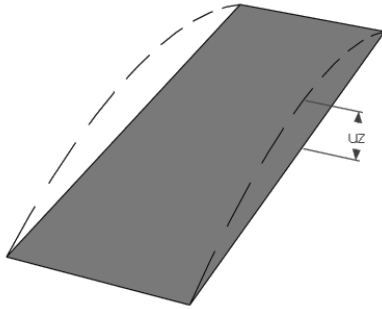
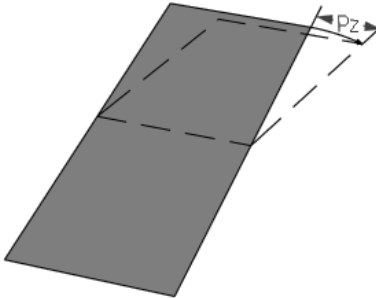
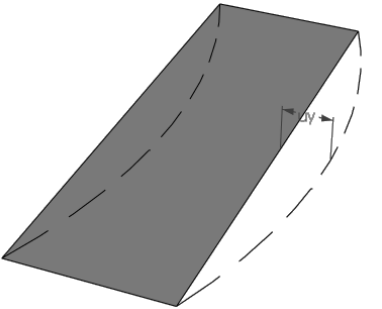
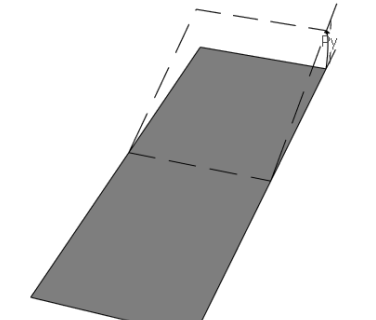
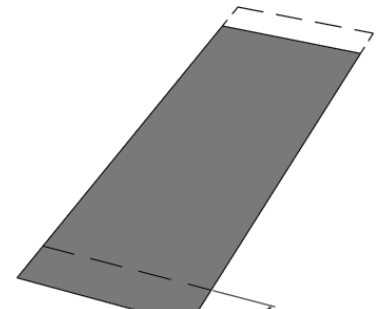
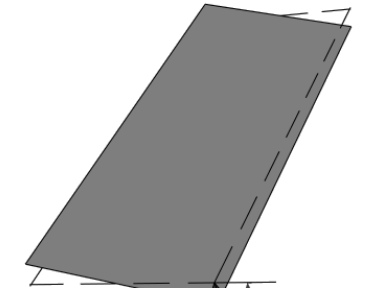
In their report, both Hermans (2014) and Yip (2015) set the maximum allowable deflection at the length of the span divided by 350. Upon evaluation in this research, this value was considered to be unnecessary strict and therefore set to the span length divided by 200 for this research. This is a value often used in engineering practice, and for example also used in other studies for a crossing over Sognefjord (Jakobsen et al., 2013). The same value was set for the maximum allowed translation in y-direction.

In their research, both Hermans (2014) and Yip (2015) set maximum vertical rotation at 0.030 rad. The NPRA has set the maximum road inclination at 6% for the H4 road class. This corresponds to a maximum rotation around the x-axis of 0.060 rad. Therefore it was decided to adjust the rotation requirement to this value. Since requirements for horizontal inclinations in the N100 Handbook are less strict than for vertical inclinations, it was decided to set the same value for the horizontal rotation requirement.

The torsional rotation values as set by Hermans (2014), who requested the Dutch ROA 2007, were deemed still suitable and were therefore also used in this thesis. The same holds for the maximum accelerations, for which Hermans (2014) requested Eurocode 1. For more information refer to Hermans (2014) Annex D. Eventually, this leads to the following (partly new) demands for deflections displayed in table 2.1.



TABLE 2.1: DISPLACEMENT AND ACCELERATION LIMITS

Vertical deflection $u_z$		Lateral plane rotation $\phi_z$	
	$u_z \leq L/200$ [m]		$\phi_z \leq 0.060$ [rad] or $3.43^\circ$
	$a_z \leq 0.7$ [m/s <sup>2</sup> ]		$\zeta_z \leq 0.050$ [rad/s <sup>2</sup> ]
Lateral deflection $u_y$		Vertical plane rotation $\phi_x$	
	$u_y \leq L/200$ [m]		$\phi_x \leq 0.060$ [rad] or $3.43^\circ$
	$a_y \leq 0.5$ [m/s <sup>2</sup> ]		$\zeta_x \leq 0.07$ [rad/s <sup>2</sup> ]
Longitudinal deflection $u_x$		Cross section plane rotation $\phi_y$	
	Not considered		$\phi_y \leq 0.044$ [rad] or $2.52^\circ$
	$a_x \leq 0.5$ [m/s <sup>2</sup> ]		$\zeta_y \leq 0.107$ [rad/s <sup>2</sup> ]

## 2.3 Environmental data

### 2.3.1 Wind loading

In previous research, the basis of design for wind loads was a once in a 100 year storm, as is often the basis in the offshore engineering sector. Environmental data such as wind and wave loads were extensively investigated by Lothe et al. (2011) for SINTEF, a Norwegian research institute. They found that the outline with the mountains nearby causes a reduced wind effect and the dominant wind flow is in fjord direction. For the extreme wind load case, a 10-minute wind speed of 35 m/s at a reference height of 10 meters was found to be used for design. The according hourly mean wind velocity is 32 m/s for a similar 100 year return period (Rp). The mean wind direction ranges from 180 – 240 degrees relative to the north. See figure 2.4 for an overview.

For higher elevations, different curves are available for determining the corresponding wind speed (DNV-C205) (EC1-1-4). See figure 2.5. Hermans (2014) decided on taking the logarithmic curve from the DNV code because this curve coincides with the curve given in the Eurocode. This recommendation is also used for this thesis.

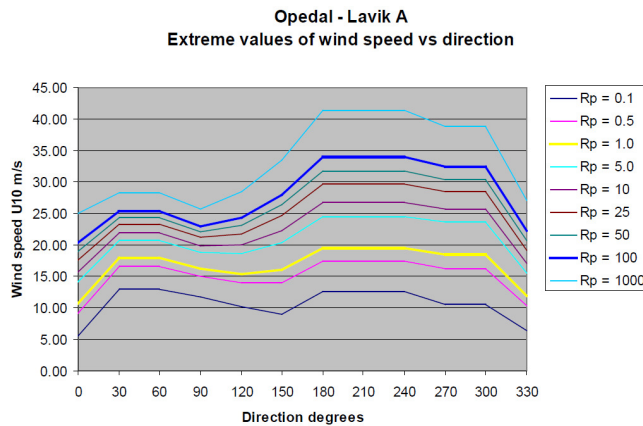


FIGURE 2.4: EXTREME VALUES FOR 10-MINUTE WIND SPEED

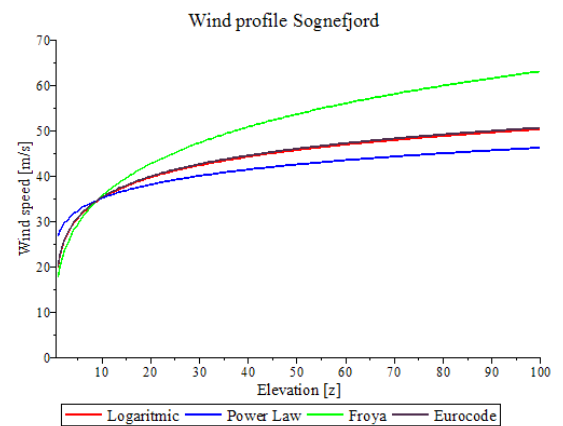


FIGURE 2.5: ELEVATION WIND CURVES

### 2.3.2 Wave loading

The waves in the Sognefjord were assumed to come in three categories: wind waves, swell waves and land slide induced waves. Lothe et al. (2011) investigated their magnitude for different directions and return periods. The topography of the fjord and the presence of riffs and islands resulted in a large reduction in swell wave energy and thus swell wave height. The SINTEF report uses a 0.01 coefficient for this reduction.

For wind induced waves, three locations in the fjord were considered: at the north shore, in the middle and at the south shore. These are named point A, B and C respectively. Wind wave height values are plotted against wind direction, the results of which are shown by figures 2.6. Characteristic wind loads and properties are taken for the 100-year return period and are given in table 2.2 (Lothe et al. 2011). It can be seen that wind characteristics differ significantly along the crossing.

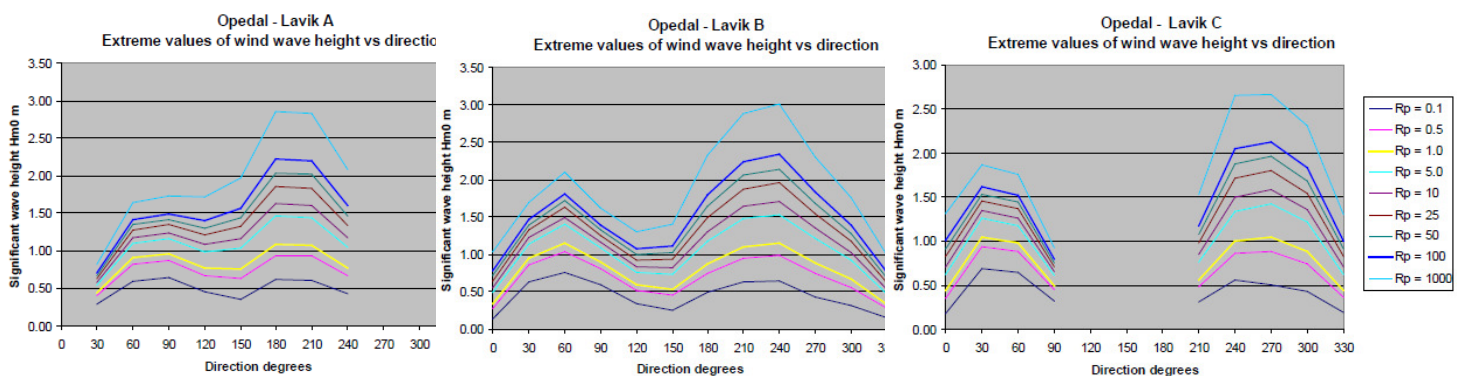


FIGURE 2.6: EXTREME VALUES OF WIND WAVE HEIGHTS FOR POINTS A, B AND C. RETRIEVED FROM LOTHE ET AL. (2011).

TABLE 2.2: WAVE CHARACTERISTICS

Parameter		Wind waves			Swell wave	Land slide
		North side	Mid-fjord	South side		
Sign. wave height	[m]	2.22	2.34	2.13	0.1	0.2
Spectral top period	[s]	4.6	4.8	4.8	13-14	85
Dominant direction	[°]	180	240	270		
Max. single wave height	[m]	4.55	4.79	4.36	0.2	0.2
Wave length	[m]	33	36	36	250	

### 2.3.3 Currents

Lothe et al. (2011) investigated currents and corrected the data with a safety margin, as uncertainty in measurements was quite high. The flow direction is assumed to be along the fjord longitudinal axis. An adapted overview from the SINTEF report is given in table 2.3.

TABLE 2.3: CURRENT VELOCITIES

Water depth [m]	Velocity outward [m/s]	Mean velocity [m/s]	Velocity inward [m/s]
<b>Mid-fjord</b>			
0-10	-1.06	-0.53	1.27
30	-0.55	0.26	0.48
75	-0.44	0.26	0.39
<b>Shore line</b>			
0-10	-0.86	-0.52	0.96
30	-0.49	0.25	0.43
75	-0.38	0.25	0.33

### 2.3.4 Seawater and tides

The mean density of seawater is 1015 kg/m<sup>3</sup>. In general a 1.0% variation can be taken into account due to variations in salinity. The corresponding specific weight is 9858 to 10055 kN/m<sup>3</sup>.

Tidal water levels in Norway could only be retrieved for recent years at major national points of interest. Therefore, in the absence of better data, values from a feasibility report on a submerged floating tunnel were used. These come from measurements at Ålesund and are taken as representative for Sognefjord as well. They are displayed in table 2.4 and show a design water level difference of 3.43 m (Fjeld et al., 2012).

TABLE 2.4 WATER LEVELS (MEASURED AT ÅLESUND AND TAKEN AS REPRESENTATIVE FOR SOGNEFJORD)

	Parameter	Highest sea level [m]	Lowest sea level [m]
Normal	Lowest astronomical tide (LAT)	0.00	0.00
	Mean Sea level (MSL)	+1.20	+1.20
	Highest astronomical tide (HAT)	+2.39	+2.39
Design	Return period of 1 year	+2.61	-0.10
	Return period of 10 years	+2.88	-0.27
	Return period of 20 years	+2.97	-0.32
	Return period of 100 years	+3.05	-0.38

### 2.3.5 Temperature, snow and ice

Eurocode 1-1-5 has set design values for the air temperature for a return period of 50 years (a return period of 100 years is not given). Sea water temperature values are based on measurements from a website on weather reports ([www.seatemperature.org](http://www.seatemperature.org)). No temperature history is given on this website. Values are displayed in table 2.5.

TABLE 2.5: AIR AND WATER TEMPERATURES

	$T_{\min}$ [°C]	$T_{\max}$ [°C]
Air temperature at water surface	-20	32
Water temperature at water surface	4	20

In Eurocode 1-1-5 snow loads are estimated at a value of 2.5 kN/m<sup>2</sup>. This is far lower than the expected traffic load and it is also assumed that these two loads won't occur at the same time. Therefore, the snow load is not taken into account for the superstructure. For the substructure, snow loads are expected to be negligible in comparison with the self-weight of the pontoons. At this stage of design, no ice conditions are considered either.

### 2.3.6 Marine growth

It is assumed that marine growth will develop on the submerged parts of the bridge (up to 0.5 m above the water line). DNV-C205 provides values for marine growth thickness and density, which are displayed in table 2.6. Note that marine growth will increase weight and thereby tensioning of the anchoring cables.

TABLE 2.6: MARINE GROWTH

Depth [m]	Thickness [mm]	Dry mass [kg/m <sup>2</sup> ]	Submerged weight [N/m <sup>2</sup> ]
+ 2 to -40	80	106	255
Below -40	40	53	128

## 2.4 Other literature research

### 2.4.1 Low-maintenance bridge design

Maintenance of a bridge can comprise a very high portion of the total costs, and over the life span, prove to be even higher than the original costs of construction (Estes et al., 2001). To keep maintenance costs at a minimum, it is key to integrate maintenance aspects into the design from an early point on. Examples of this are designing good accessibility to maintenance-intensive components or making sure water and dirt don't accumulate but run off smoothly.

Joints are large-scale bridge components which typically are determining factors in bridge maintenance. Especially for expansion joints, direct replacement costs are generally much higher than initial installation costs (Spuler et al., 2012). This stimulates avoiding the need for joint replacement, but since the maximum service life of expansion joints is currently 40 years (Spuler et al., 2012), replacement would be necessary over the service life of the bridge. Expansion joint service life can be significantly improved by proper maintenance, but this would run against the low-maintenance requirement for this study. This holds even more considering that costs of maintenance are hard to predict and can be significantly larger than initially assumed (Estes et al., 2001).

It is therefore considered best to set minimising the amount of joints in the bridge as a design goal. If using a joint at a certain point can't be avoided, this joint should be designed such that it will show minimum wear and tear over its service life.

### 2.4.2 Ship collision risk and magnitude

Studies on ship impact load, more specifically for Sognefjorden, already exist. Hermans (2014) did limited analysis, by only considering a collision as a short impulse load of 50 MN, which seems rather low.

In a study into ship collision in the Sognefjord area, specifically for a to-be built fixed crossing, Hansen et al. (2013) established a collision risk model based on current traffic intensity (3300 large vessels per year) and defined collision scenarios. This was used to calculate the probability of impact per ship class (size and speed), which can be used to define a design ship collision. For a floating bridge, the maximum impact energy was determined at 781

MNm. As an indication for comparison, Eurocode 1-7 defines a ‘large’ sea vessel as having a weight of 40.000 t and colliding with a speed of 5.0 m/s (which results in an impact energy of 500 MNm). Eurocode 1 defines the impact area as 20.8 m in width and 10.4 m in height, with the centre at sea level.

A second type of ship impact is sideways collision, where a ship has drifted off due to propulsion malfunction, thereby hitting a pontoon with its side. This will however result in a significantly lower impact energy (Hansen, 2013) and will therefore not be further considered in this research.

### 2.4.3 Designing for ship impact

Collision is considered as a design accidental load which a bridge has to sustain. Since Sognefjorden is sailed by a lot of ships daily, ship collision is a risk that has to be considered. Fixed bridge piers are almost always clad with protection devices, with dissipating impact energy through deformation of the device as design goal. In general, the collision component with the lowest stiffness will deform. Hence, the stiffer a protection device, the higher the damage to the ship.

Collision design for bridge piers differs from that for floating structures of course, since the latter can dissipate energy through displacement. When designing for collision with the pontoons in this study, different concepts can be considered. First fixing a conventional collision protection device on the pontoon. Multiple studies into designing such a device have been conducted, mostly focusing on developing some component with low stiffness that by deformation can take up impact energy. Note that in this design case such devices would have to be placed below water level, to fulfil aesthetical demands.

Wang et al. (2008) studied the dynamics of ship-bridge collision and used this to develop a ‘bumper’ for bridge piers. This device consists of steel-wire-rope coils (SWRC) that can deform significantly on impact, making it possible for the ship to adjust its direction. This in turn would carry off a large amount of kinetic energy, which makes for a large decrease in impact force on both the pier (up to 60%) and the vessel, thereby keeping them both intact. Such a bumper system would hang on the pontoon, which would have to be bigger to compensate for the negative forces.

Fang et al. (2016) developed a fender system made from polymers (FRP) to avoid conventional drawbacks such as low corrosion resistance. This system is made of FRP ring-shaped segments. FE modelling results show a reduction of impact force on the bridge of up to 34%. However, this system floats, which is a large aesthetic disadvantage.

Other studies consider more traditional steel fenders, which are attached to the bridge pier and generally consist of thin-walled membranes and bracing members. Wei et al. (2015) discuss a steel fender with a reinforced concrete panel, whereas Hua et al. (2016) propose a floating steel fender. These systems show a maximum reduction in collision force on the bridge of about 25% and 55%, respectively. Other currently wide-used concepts are installing pile structures, dolphin structures or artificial islands. Since these all need to be fixed at the sea bottom, they won't be discussed in this study. Figure 2.7 shows an overview of the previously discussed systems.

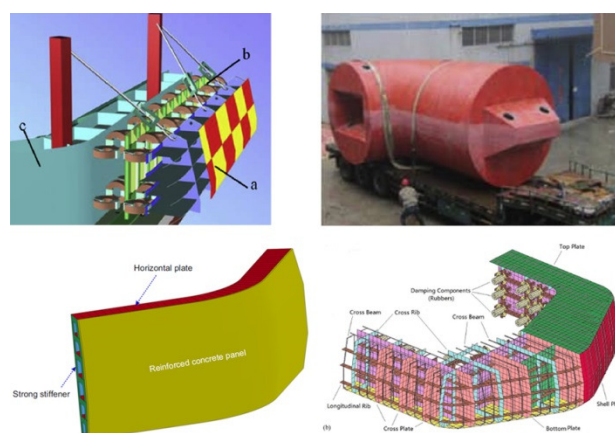


FIGURE 2.7: SWRC, FRP, FLOATING AND COMPOSITE FENDER SYSTEMS (CLOCKWISE FROM TOP LEFT)

A second design concept is designing inherently redundant pontoons, by splitting them up in compartments. In case of collision and fracture of the pontoon shell, only one or two of these compartments would fill with water, leaving the rest of the pontoon still floating. This brings inherent safety, but fixing a broken compartment could be costly. Normally offshore spar structures are designed in this way (De Jonge, 2013). Another way of dissipating energy is by adding dampers to the bridge structure. More on this topic is discussed in chapter 8.

## 2.5 Conclusions from literature research

The serviceability requirements for the Sognefjord bridge set by Hermans (2014) were compared with those of the NRPA. Upon evaluation it was concluded some requirements could be loosened a bit. Of the environmental properties of the Sognefjord, especially the wind is expected to have a big impact on bridge displacements.

It was found that maintenance on a bridge, especially on a floating bridge, can pose the largest part of its total service life costs. To minimise these costs it is key to incorporate maintenance in the bridge design as early as possible. It was further found that joints are generally maintenance-intensive components with a limited service life. With a service life at most half of the total required service life of the Sognefjord bridge, replacement during service life of any large bridge joints cannot be evaded.

Replacement work on such components in a floating bridge could bring costs running into substantial amounts of the original bridge costs. This has to be avoided. It is therefore concluded that the only way to reach a low-maintenance bridge design is by eliminating large internal hinges in the bridge. The design by Yip (2015) incorporated hinged connected bridge girders. This thesis will research the possibilities of creating a continuous bridge girder without internal hinges for the Sognefjord buoyancy bridge.

When considering ship collision events, the design ship impact has a big influence on the design. An impact energy of 781 MNm was chosen for this thesis. Many options for reducing structural damage from ship impact are external components that have to be attached to the bridge pontoons. This would however not comply with the aesthetic demands set for this bridge. It is therefore chosen to create different compartments in (part of) the pontoons. Next to complying aesthetical demands, this will make the pontoons inherently redundant against ship collision: upon collision, only a small part of the pontoon will flood with water.

### 3. BRIDGE MODELLING AND BRIDGE DESIGN EVALUATION

At the start of this thesis, the results of the research of Yip (2015) were presented for use as a starting point for this thesis. It was decided to first have a critical look at the prior design and its results, so that it could be affirmed that the current thesis would be conducted on a solid foundation. This evaluation is described in this chapter. It was done in three ways. First, the modelling software used to test the design was investigated and validated for its quality of results. Second, the superstructure concept was investigated and compared to other superstructure designs. Third, the analysis model was re-built, so that every model property could be evaluated again.

#### 3.1 Validating modelling cables in SCIA Engineer

In her thesis, Yip (2015) did research on the configuration of the anchoring net structure. However, doubts over the quality of the results of the cable system rose up. Therefore it was decided to validate the calculations in SCIA Engineer, by comparing its results with calculations made by Ansys. Both are FEA (Finite Element Analysis) suites, but Ansys has a wider range of properties and appliances. If both software suits would give the same displacement results under the same loads, it was assumed that for this phase of research, the cable system-model in SCIA would be sufficient to use for investigating the bridge design.

##### 3.1.1 Comparing model results between SCIA Engineer and Ansys

Generally, cable modelling in Ansys is sensitive to stability errors. Therefore, it was decided to build a cable system model that is similar to the anchoring system of the Sognefjord bridge, but simplified.

Modelling was done in several steps, increasing the model complexity at each iteration. Annex C reports on this. The final system composed of two 'horizontal suspension' main cables (as is the case in the Sognefjord anchoring system) connected by smaller sub cables. The model was however compared to the Sognefjord system reduced in size, to reduce analysis time. For more on the model properties and simplifications, refer to Annex C. For a top view of the structure geometry, see figure 3.1.

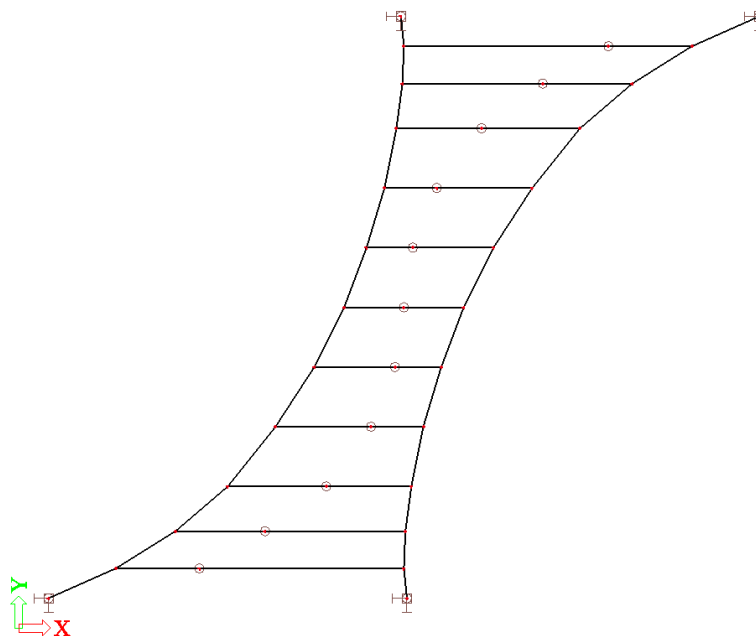


FIGURE 3.1: OVERVIEW OF FINAL MODEL GEOMETRY



This cable system was modelled both in SCIA Engineer as in Ansys with the exact same properties. Then both cable models were subjected to their self-weight. If the two models would give the same displacement results, it could be assumed that for now, using SCIA Engineer to model the anchoring system gives results that are of sufficient quality. The main properties of the models are given in table 3.1.

**TABLE 3.1: MODEL PROPERTIES AND BOUNDARY CONDITIONS**

Property	Value
Main cable diameter	70 mm
Side cable diameter	20 mm
Length main cable	110 m (model #1) – 243 m (models #4 and #5)
Length sub cable	50 m (model #1) – 40 m to 96.5 m (models #4 and #5)
Boundary conditions	Main cables fixed supported, pontoons free for x, y direction and fixed for z-direction (models #4 and #5)
Applied load	Self-weight only (models #1-4), self-weight + external load on pontoons (model #5)
Analysis type	Geometrical non-linear

Modelling was done in five steps. In every step the model was made more similar to the Sognefjord buoyancy bridge model. In the first three steps, the complexity of the cable geometry was increased. In the fourth step pontoons were added to the cable structure. Again, all these models were built in both SCIA Engineer as Ansys in exactly the same way. At calculation, all four models showed the same displacement and stress results, with differences deemed sufficiently small (maximum 1.8%). See table 3.2 for results in vertical displacements. Refer to Annex C for results of the pontoons in model #4.

### 3.1.2 Results and conclusions

**TABLE 3.2: COMPARISON OF VERTICAL DISPLACEMENTS IN DIFFERENT MODELLING SOFTWARE**

Model #	Description	Max. $u_z$ in Ansys [mm]	Max. $u_z$ in SCIA [mm]	Difference
1	Rectangle system with 4 sub cables	5129	5182	1.0%
2	Slightly curved system with 7 sub cables	5316	5344	0.5%
3	Proper curved system with 11 sub cables	11133	11329	1.8%
4	Proper curved system, 11 sub cables and pontoons	7230	7359	1.8%
5	Proper curved system, 11 sub cables, pontoons and external load	7619	9551	20.2%

Models #1 to #4 were loaded by self-weight only. In the last model #5, the geometry was kept the same, but next to self-weight, the system was now also subjected to a horizontal external load. However, this was when limitations of SCIA Engineer became clear. In SCIA, it is not possible to add loads in different time steps for non-linear FE-analysis (which is possible in Ansys). This means it is not possible to add different type of loads after each other at different points in time. However, in real-life, the cable system of the Sognefjord bridge will first be loaded by its self-weight during construction. Only after this, will the system be loaded by external loads, for example from the pontoons. Contrary to real-life, SCIA imposes all these loads simultaneously.

Cable systems that are loaded by their self-weight become stiffer, with the self-weight load acting as prestress, and will therefore deform less. This means that systems to which all loads are imposed simultaneously show larger displacements, and thus give too conservative results. This can be seen in the much larger vertical displacement of the SCIA model #5 in table 3.2.

Even though results from SCIA Engineer, with its limitations to model load steps, differ significantly from Ansys, they are on the conservative side. More elaborate modelling in the future will show more accurate cable system



results (lower displacements than now outputted by SCIA). SCIA does show the correct deformed shape, but with conservative values. It is therefore concluded that for this preliminary design phase, in modelling the anchoring system, SCIA Engineer gives results that are accurate enough. See figures 3.2 and 3.3 for the final deformed shapes of the models.

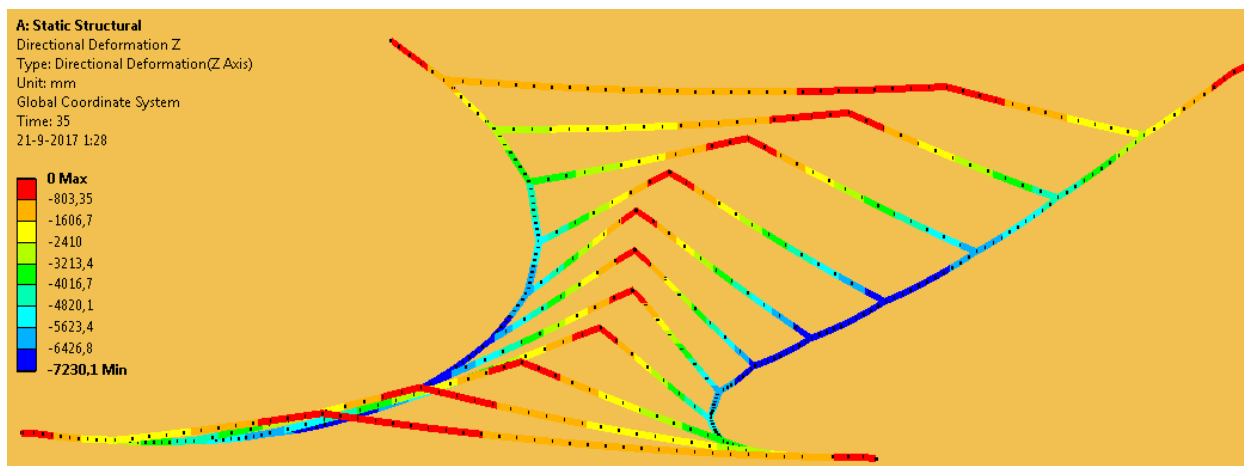


FIGURE 3.2: FINAL DEFORMED SHAPE OF MODEL #4 IN ANSYS

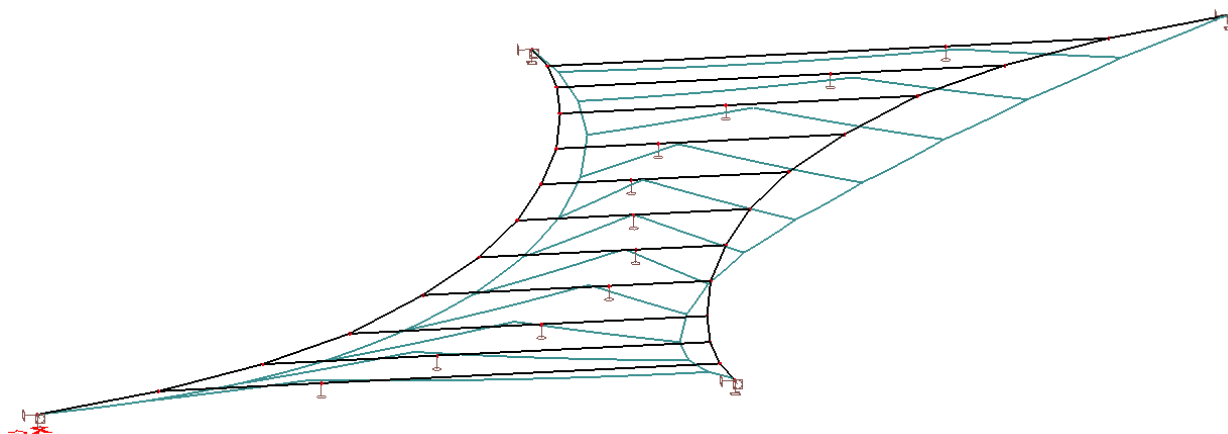


FIGURE 3.3: FINAL DEFORMED SHAPE OF MODEL #4 IN SCIA ENGINEER

For this design phase, SCIA Engineer will therefore remain to be used to model the bridge. Modelling a stable full anchoring system in Ansys, will probably be enough work for an additional full thesis. It is however recommended to use different modelling software when the full bridge design develops to the next step of detailed design.

### 3.2 Investigating alternative superstructure concepts

Since a justification on the choice for a lattice girder for the superstructure concept was absent in previous research, it was chosen to research the possibilities for alternative bridge girders and compare these to a lattice girder. The goal in mind was to prove which girder concept proved the most feasible (material efficiency, stresses and deflections and aesthetically). This could still be the lattice girder of course.

### 3.2.1 Assumptions in design and calculations

The truss girder as designed by Yip (2015) was wide enough to allow a straight girder with a curved road on top, in order to not introduce any additional torsional stresses coming from the curve in the girder. At evaluation, this was deemed too conservative and therefore it was decided to do a simple check on torsional stresses. Calculation gave a maximum additional member stress from torsional load of 79 N/mm<sup>2</sup> (see Annex D). It was concluded that creating a curved girder should not be ruled off immediately. Therefore designing a curved bridge girder will be investigated in this research. As an initial assumption, a width of 14 meters (allowing for two traffic lanes and one slow traffic lane) was taken. Note that deck structure weight was taken into account in the calculations, but not in the sketches in figures 3.4 and 3.5.

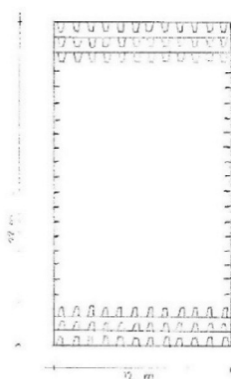


FIGURE 3.4: BOX GIRDER CROSS-SECTION

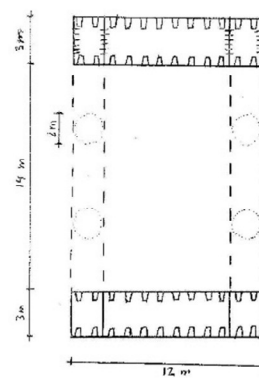


FIGURE 3.5: BOX GIRDER-TRUSS COMBINATION CROSS-SECTION

As a start, simple construction mechanics checks were made using Maple. In these checks, a few girder designs were calculated for their stiffness and self-weight, after which the deflection at mid-span for the main girder was determined. Some assumptions were made in these checks. First of all, the girders were assumed to be prismatic. Second, the cross-sections designs were slightly simplified, in order to allow quick calculations. Lastly, the shear lag effect, often present in steel bridge girders, was not taken into account. Annex D contains Maple calculation output together with sketches of the girder designs assumed and calculated.

### 3.2.2 Results

The first alternative that was investigated was a box girder with stiffeners. See figure 3.4 for an illustrative sketch. These girders however showed to give deflections that did not meet the requirement for maximum deflection at mid-span.

Furthermore, increasing geometric complexity in a box girder largely decreases the ease of fabrication. Extra steel would also make for a heavier and costlier girder. Therefore it was concluded that a box girder was not feasible, both structurally, fabrication-wise and in terms of costs.

A new box-truss combination girder was investigated. In this design, the flanges of the girder were small box girders, the webs were circular hollow truss members. See figure 3.5 for a sketch. A girder with a height of about 19 meters (a reduction in height of 33%) showed to give the same deflection as the truss girder designed by Yip (2015).

As mentioned these initial calculations did not incorporate the shear lag effect. However, with stresses introduced at the two outer edges of the boxes only, this effect is present in this design. This means the flanges would not be fully activated – stresses in the middle will be very low compared to the outer edge. Extra problems come from the fabrication complexity and high girder weight. Therefore it was concluded that a box-truss combination girder was not feasible.

### 3.2.3 Conclusions

A last alternative design was to reduce the amount of material in the middle and bring more material towards the outer corners of the girders. In this case it was directly clear that using all-circular sections would be more efficient. This is supported by literature (Romeijn, 2006). By this it was concluded that creating a truss girder was the structurally the most efficient solution and thus the truss girder concept as introduced by Yip (2015) was maintained. Figure 3.6 for a sketch that summarises the design process.

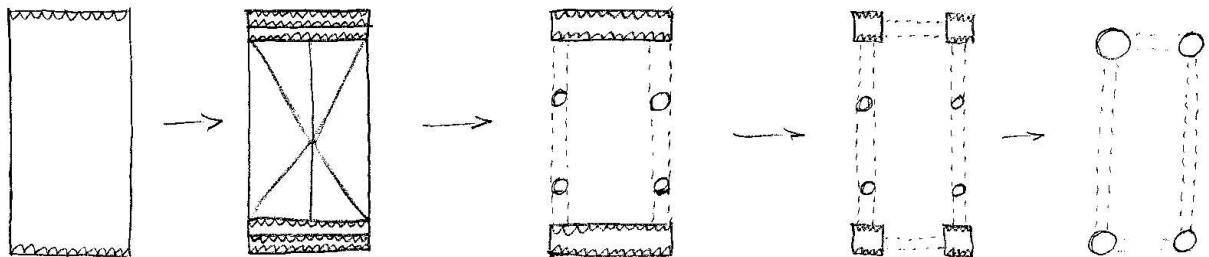


FIGURE 3.6: DEVELOPMENTS IN SUPERSTRUCTURE CROSS-SECTION INVESTIGATION

### 3.3 Re-building the model in SCIA Engineer

For this research, the whole Sognefjord bridge was again modelled from scratch in SCIA Engineer. This was done to make a fresh start in modelling the whole bridge, to have a critical look at the way modelling should be done and to experience the process of building an elaborate analysis model. During this, new findings on assumptions for loading and geometry were imposed. This resulted in the Scia model #1: the model of the whole Sognefjord bridge (see figure 3.7). This chapter describes the adjustments made in modelling the whole Sognefjord bridge, compared to the Scia model used by Yip (2015) in her research.

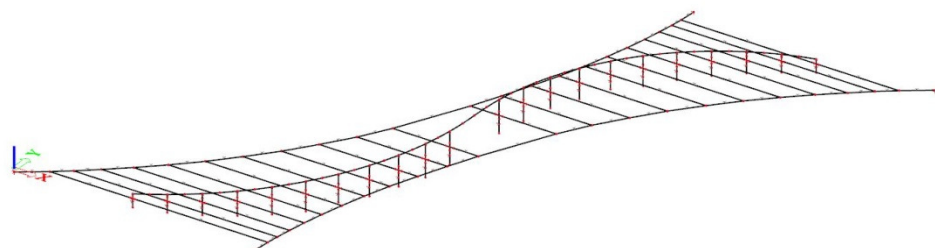


FIGURE 3.7: SCIA MODEL #1 OF THE WHOLE SOGNEFJORD BRIDGE

#### 3.3.1 Small adjustments in geometry

In the Sognefjord bridge, the shape of the main anchoring cables has a large influence on the loads from this cable on the pontoons. The smoother the curve of the cable, the more distributed these loads are. Therefore, some small adjustments in this main cable curve were made to smoothen it and improve the load distribution on the rest of the structure.

The bridge girder was modelled by Yip (2015) as a weightless arbitrary beam, which was deemed not realistic. Now, the girder was still modelled as an a prismatic beam to have efficient model calculations, but its weight and stiffness properties were according to the first superstructure design as discussed in chapter 4. For more on that, refer to Annex E. Furthermore, Yip (2015) designed each bridge girder as a straight beam. Now, the girders were given a curve, according to the architectural design. For a detailed overview of all the initial changes in the SCIA model, refer to Annex E.

### 3.3.2 Calculating structural properties for Scia model

In modelling the Sognefjord bridge in Scia Engineer, Yip (2015) made calculations for the properties of the pontoons. The pontoon buoyancy was determined by calculating the required volume to keep the pontoons floating. The rotational stiffness of the pontoons was determined by calculating the restoring moment of the pontoons under a rotation. This restoring moment is mainly created by the ballast of the pontoons. See figure 3.8 of a sketch of the way this calculation was done.

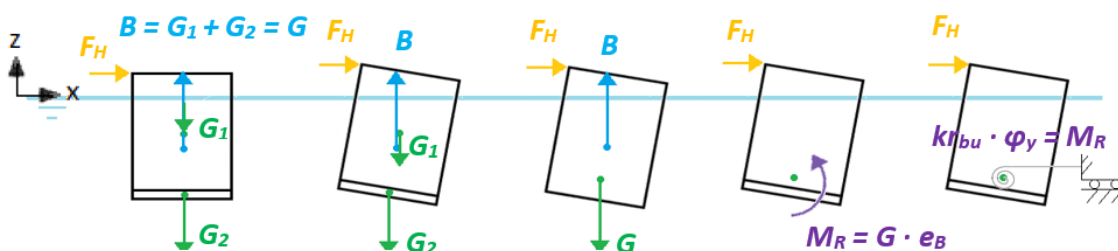


FIGURE 3.8: CALCULATING ROTATIONAL STIFFNESS OF THE PONTOONS. RETRIEVED FROM YIP (2015).

The calculations of the pontoon properties were evaluated and considered sufficient for this preliminary stage of design. All calculations can be found in the report by Yip (2015). The buoyancy and rotational stiffness of the pontoons can be modelled as springs in the Scia model. These springs were maintained for this research as well.

### 3.3.3 Scia model details

Figure 3.9 displays a schematic sketch of the way the pontoons were inputted in Scia model #1. The pontoons themselves were modelled as prismatic concrete cylinders, as they were designed by Yip (2015). Their density properties were adjusted for the real-life weight. More info on this modelling can be found in Annex E. The lateral anchoring cables are connected to the sides of the pontoon, 20 m below the water level. The pontoon side width was modelled by adding two weightless infinitely stiff dummy beams on each side of the central pontoon beam. The lateral anchoring cables the were hinged connected to these dummy beams.

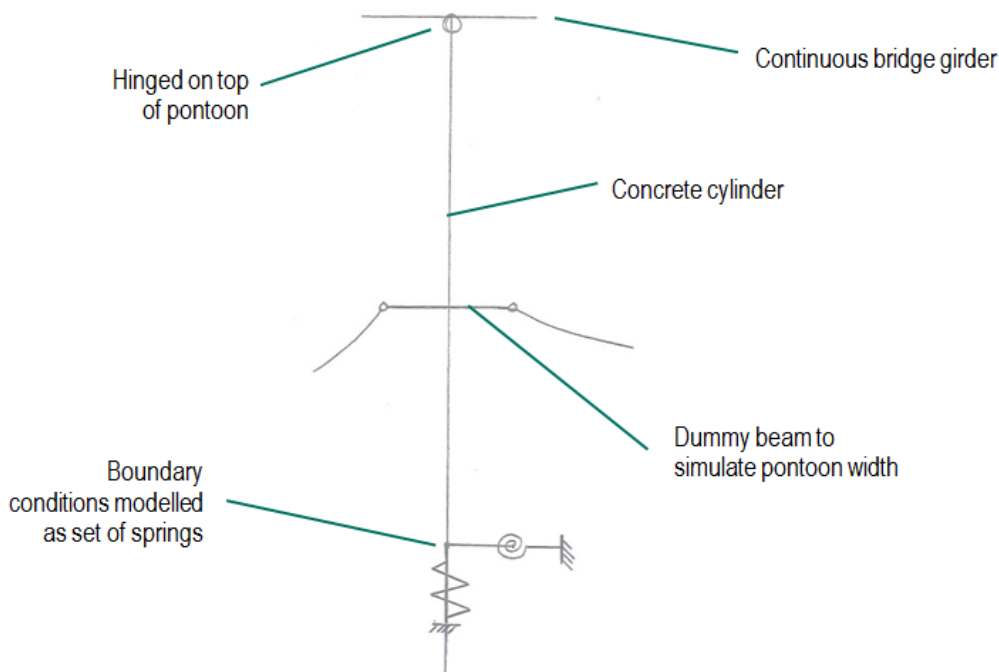


FIGURE 3.9: SCHEMATIC REPRESENTATION OF HOW THE PONTOONS WERE MODELLED IN SCIA MODEL #1

The top of the pontoon was hinged connected to the bridge girder, to maintain the boundary conditions of the girder (continuous, laying on two rubber blocks that allow small  $\phi$ y-rotations, see also chapter 4). At the centre of buoyancy of each pontoon, the pontoon properties were modelled by a set of springs. The buoyancy was modelled as a vertical translational spring and the pontoon rotational stiffness by two rotational springs (to include rotations in all directions).

### 3.3.4 Adjustments in loading

In the Scia bridge model used by Yip (2015) all the loads from the superstructure (including self-weight and traffic loads) were modelled as concentrated loads on the pontoons. This omits the external moments resulting from these loads, which was deemed not realistic. The load modelling was therefore adjusted in Scia model #1 for this research. By modelling self-weight, the loads will become distributed (as is the case in real life) which also introduces resulting external moments.

In the Scia model by Yip (2015), the water current and wind loads were modelled as concentrated loads on specific points of the bridge. In this research these loads were as distributed loads, as is the case in real-life. In modelling, loads were adjusted according to their location (e.g. large wind load at higher elevation, or lower current load at larger depth) and were given the right angle (instead of only modelling these orthogonally). Figure 3.10 summarises the new way of modelling loads. Figure 3.11 shows how the wind loads are modelled in SCIA.

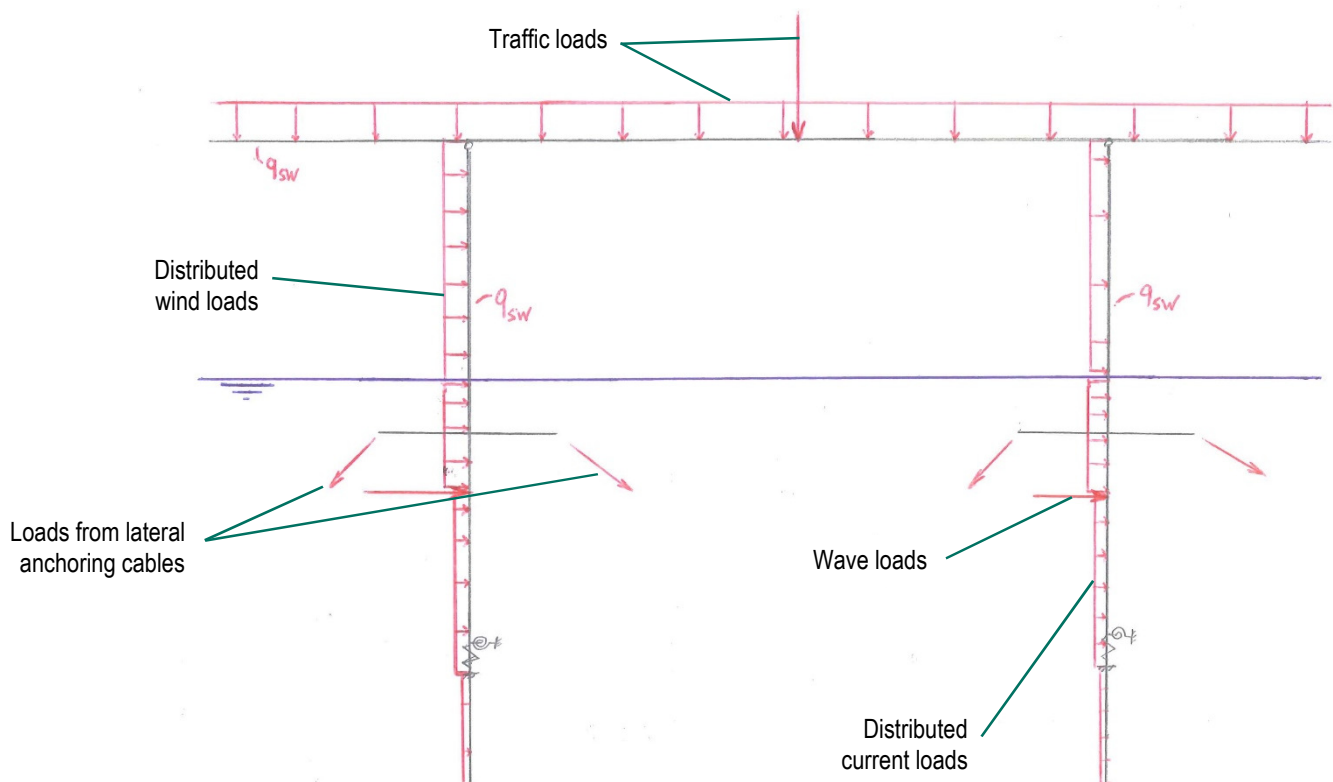
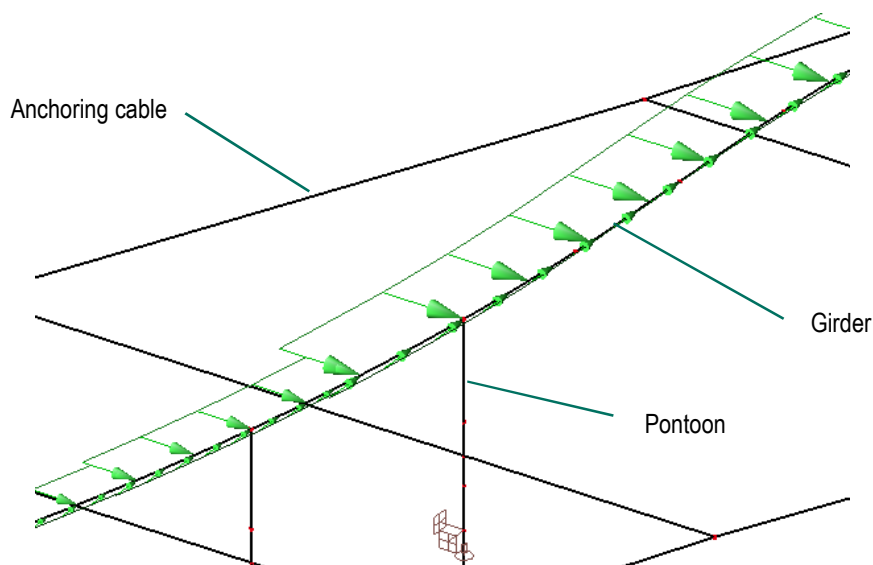


FIGURE 3.10: MODELLING OF LOADS IN SCIA MODEL #1 OF THE WHOLE SOGNEFJORD BRIDGE



**FIGURE 3.11: DISTRIBUTED WIND LOAD MODELLING ON BRIDGE GIRDER, ADJUSTED FOR GIRDER HEIGHT AND WIND DIRECTION**

The values of the external loads used in the research by Yip (2015) were evaluated. Assumptions used in design codes, such as environmental factors, were deemed too optimistic. Therefore all the external loads (wind, current and waves) were re-calculated. Annex F reports the calculation file and elaborations. In modelling wave loads, both Hermans (2014) and Yip (2015) assumed fully reflected waves on a straight wall as an initial conservative approach. It was decided that this was not realistic and therefore the Morison Equation was used for modelling loads. See table 3.3 for an overview of the most important adjustments in load calculations of Scia model #1 used in this research, as opposed to the loads used in the previous research by Yip (2015). Annex E reports further on how Scia model #1 of the whole Sognefjord bridge was modelled.

In the environmental loads, a division between ULS and SLS was now made. The ULS demand was that the bridge has to be able to withstand a 100-year return period storm. For SLS, the criterion was that the bridge may on average be closed for traffic only once every 10 years. Thus, deformations of a 5-year storm had to be withstood.

**TABLE 3.3: OVERVIEW OF BIGGEST CHANGES IN EXTERNAL LOADS IN CALCULATION MODEL**

Aspect	Old assumption	New assumption
Bridge deck	20 kN/m self-weight	75 kN/m self-weight
Traffic load	35 kN/m (one lane)	70 kN/m + 2400 kN concentrated load on each span (two lanes)
Wind load	Environmental category 0, maximum height 70 m, no $\gamma_{0.07}$ -factor in terrain factor. Wind modelled as concentrated loads.	Environmental category 1, maximum height 82 m. Results in almost twice higher loads. Load now modelled in real-life wind direction. Modelled as distributed loads.
Wave load	Fully reflected load on straight wall	Inertia and drag force assumed, using Morison Equation. Leads to about four times higher loads.
Current load	Modelled as point load in orthogonal direction	Modelled as distributed load, in real-life direction, decreasing in magnitude with larger depth. Leads to about twice as high loads.

As can be seen in table 3.3, the new calculation of external loads results in significantly higher loads compared to the calculated loads in previous research. All the exact values of loads, the formulas used for their calculations and the codes used to obtain these formulas are displayed in Annex F.

## 4. DESIGNING A NEW SUPERSTRUCTURE

Yip (2015) mentioned that the bridge girder needed more investigation. Furthermore the superstructure design needed to be optimised for low maintenance. In this chapter a new bridge girder design was investigated. This was a continuous girder without internal hinges, keeping in mind the goal of creating a flexible and light-weight structure.

### 4.1 Superstructure concept

In chapter 3.2 course alternative girder concepts were considered, after which it was chosen to design a lattice truss girder with circular hollow sections (CHS). In literature research it was concluded that internal hinges in the superstructure pose serious maintenance issues. It was therefore decided to minimise the amount of hinges in the superstructure. Instead of being simply supported, the bridge girder would become a continuous girder without internal hinges.

This decision comes with great consequences. The superstructure becomes statically indeterminate. Compared to simply supported girders in the Sognefjord bridge, a continuous structure might bring bigger challenges in construction. However, a continuous girder without internal hinges also gives possibilities to create a more light-weight structure due to lower global bending moments (see figure 4.1). As boundary conditions, in this research the bridge girder was assumed to lay on two large rubber blocks. That would still allow for small  $\varphi_y$ -rotations, while blocking all displacements and  $\varphi_x$  and  $\varphi_z$ -rotations.

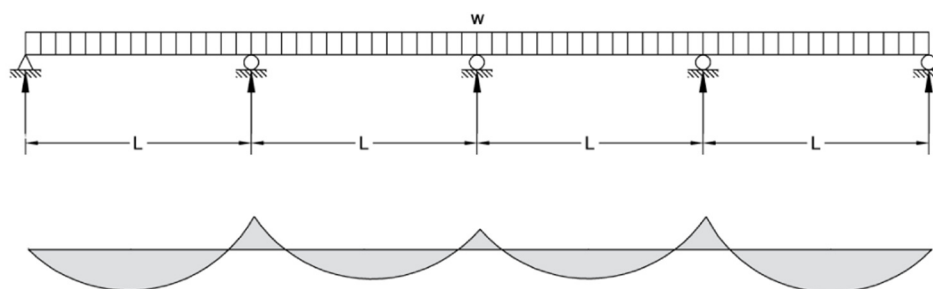


FIGURE 4.1: BENDING MOMENT DIAGRAM FOR A CONTINUOUS BEAM

In a structurally indeterminate structure stiffer parts draw more forces towards themselves. The bridge girders were therefore designed as light-weight and flexible as possible. Because of the expected loads through imposed deformations, a margin in the stress levels of individual truss members was retained, to account for later additional stresses.

### 4.2 Truss girder modelling

Design started with a comparison of different truss types. See Annex G for an elaboration on the process and its results. It was decided to continue designing a Warren truss.

A Scia model of the 3D truss girder was made. This was Scia model #2 as described in chapter 1. To save modelling and calculation time, it was decided to model only the 7 middle spans of the Sognefjord bridge. See figure 4.2. Because the largest bridge deformations occur in the middle of the bridge, and because the mid-span girder (the largest girder covering the longest span of the bridge) is located here, this was deemed acceptable. It was assumed that if the truss girder design is sufficient for these middle 7 spans, it would be sufficient for the rest of the Sognefjord bridge as well.

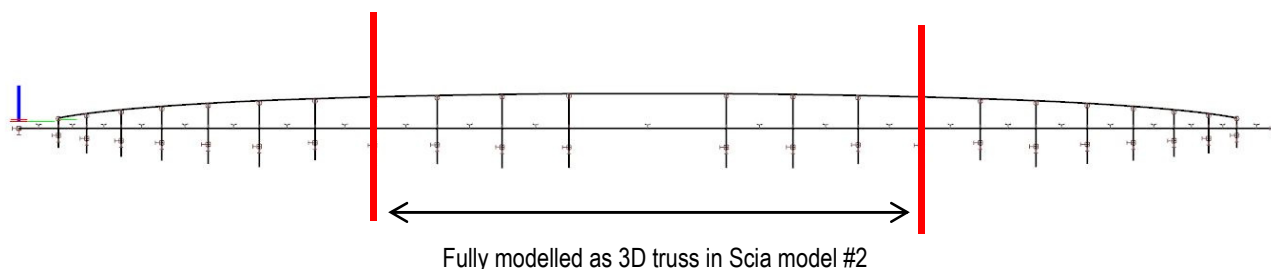


FIGURE 4.2: PART OF THE SOGNEFJORD BRIDGE SUPERSTRUCTURE THAT IS ELABORATELY MODELLED IN SCIA MODEL #2.

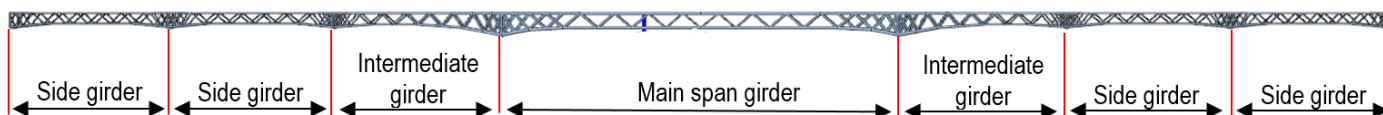


FIGURE 4.3: DISTRIBUTION OF MAIN GIRDER, INTERMEDIATE GIRDERS AND SIDE GIRDERS IN SCIA MODEL #2

In the middle of the bridge, a fairway for ship traffic had to be created. The span is here 465 meters. This is the main span. All the other spans have a length of 200 meters. These are the side spans. The two spans located directly adjacent to the main span were given a specialised truss design. This was to provide a smooth transfer of loads from the main span to the other spans. More on this is discussed in chapter 4.2.3. These two girders are the intermediate girders between the main span girder and the side span girders. See figure 4.3 for an overview.

#### 4.2.1 Loads

The truss girders were designed taking self-weight, wind and traffic loads into account (see table 4.1). These loads differ in value from the loads in the girder design research by Yip (2015). Chapter 3.3 elaborates on the reasons for these changes. Further in this research, the girder was subjected to imposed deformations as well.

TABLE 4.1: LOADS TAKEN INTO ACCOUNT IN FIRST SUPERSTRUCTURE DESIGN LOOP

Load	Value
Bridge deck	Self-weight of 75 kN/m
Traffic	70 kN/m
Wind load	As defined in Annex F, largest: 27.4 kN/m laterally

Load factors were used according to EC0: basis of structural design for traffic bridges. These were 1.25 for the permanent (self-weight) loads and 1.35 for the variable (external) loads.



### 4.3 Main span girder design

The Warren truss layout was optimised. To accommodate high forces at the supports, chords and braces near the supports were made bigger, and braces near the supports slightly denser. The girder was made tapering towards the middle to reduce weight and fulfil aesthetic demands for slenderness. This led to members with a maximum heart-to-heart distance of 25 m, resulting in a total girder height of 28 m. The layout for the main span is displayed in figure 4.4.

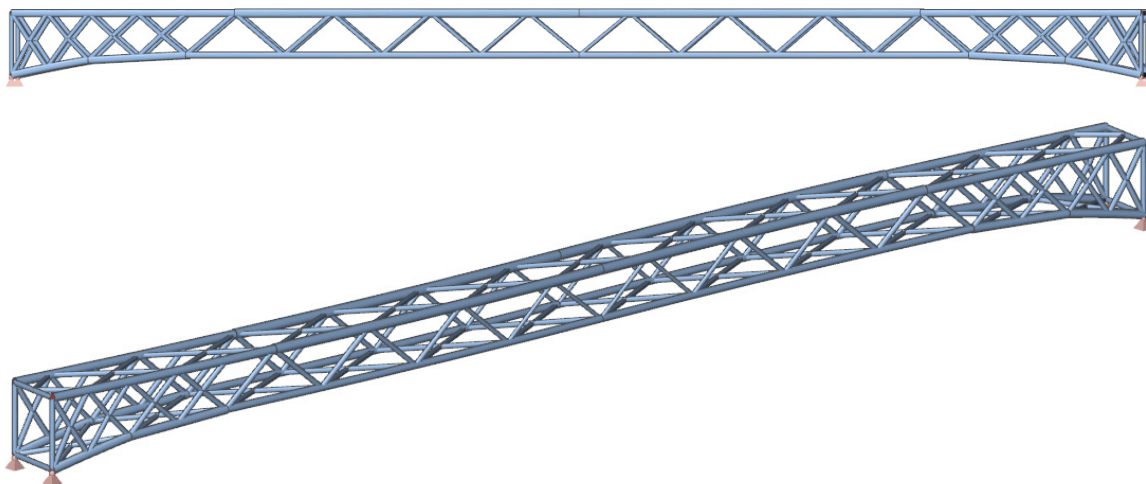


FIGURE 4.4: MAIN GIRDER LAYOUT (SIDE VIEW ON THE TOP, 3D VIEW ON THE BOTTOM)

The general properties of the main span truss girder and individual members are given in table 4.2. Annex G elaborates on the specifics of the main girder design.

TABLE 4.2: MAIN GIRDER PROPERTIES

Property	Value
Span	465 m
Girder self-weight	Average 333 kN/m
Width	Centre-to-centre distance 21.5 m, absolute distance 23 m
Height	Centre-to-centre distance 17 m (mid-span) to 25 m (supports), absolute distance 20 m (mid-span) to 28 m (supports)
Girder curvature	3.1 m lateral difference
Chord member sizes	From 2500x35 mm (smallest) to 3500x80 mm (largest)
Brace member sizes	From 1310x27 mm (smallest) to 1800x40 mm (largest)
Steel grade	S460

### 4.4 Sub span girder designs

The other spans were designed with the same layout concept. Because the main span girder is larger than the other girders, it was chosen to design an intermediate span girder between the main span and side span girders. This smooth transition reduces global force peaks from the main span on the side span girders. All side girders have the same girder design.

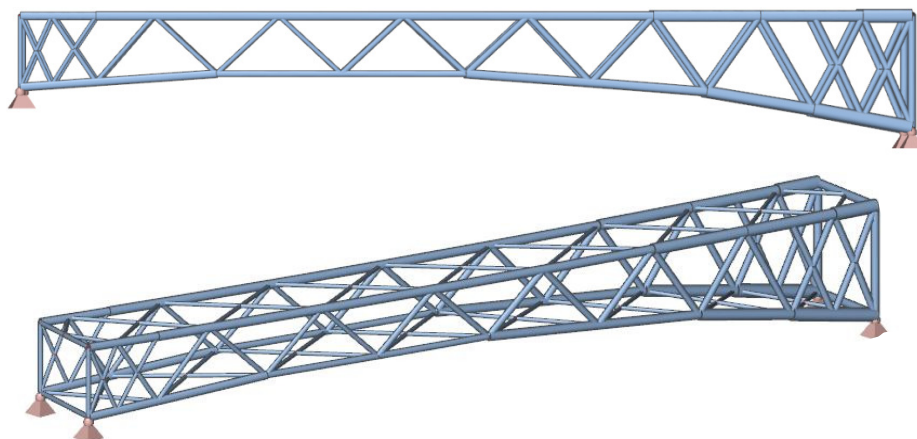


FIGURE 4.4: INTERMEDIATE GIRDER LAYOUT: SIDE VIEW ON THE TOP, 3D VIEW ON THE BOTTOM

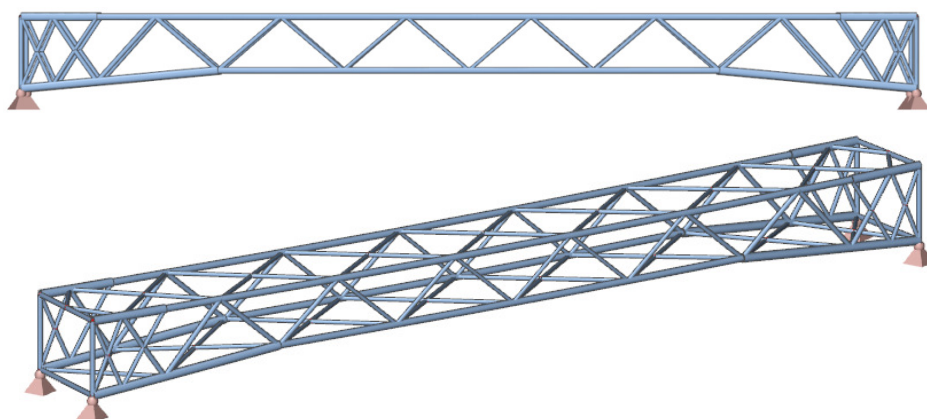


FIGURE 4.5: SIDE GIRDER LAYOUT: SIDE VIEW ON THE TOP, 3D VIEW ON THE BOTTOM

See figures 4.4 and 4.5 for the layout of the side girder and the intermediate girder. The general properties of both designs are given in table 4.3. Annex G elaborates on the specifics of the design.

TABLE 4.3: INTERMEDIATE AND SIDE GIRDER PROPERTIES

Property	Value
Span	200 m
Girder self-weight	Intermediate girder average 155 kN/m Side span girder average 87 kN/m
Width	Heart-to-heart distance 21.5 m, absolute distance 23 m
Height	Centre-to-centre distance 12 m (mid-span) to 16 m (supports), absolute distance 13.4 m (mid-span) to 17.8 m (supports)
Girder curvature	Side span: 2.6 m lateral difference
Chord member sizes	Side span: from 1400x32 mm (smallest) to 1800x40 mm (largest)
Brace member sizes	Side span: from 900x18 mm (smallest) to 900x20 mm (largest)
Steel grade	S460

## 4.5 Continuous girder boundary conditions

Eliminating internal hinges has large consequences for the boundary conditions of the superstructure. At this stage of design assumptions were therefore made. The superstructure was assumed to be supported at each pontoon by two large rubber blocks. More on this is discussed in chapter 6. See figure 4.6 for a view of the continuous girder as modelled in Scia model #2. See figure 4.7 for a sketch of the support assumption. The exact design of the supports of each span is to be made in further research. See figure 4.8 for an impression of the scale of the superstructure.

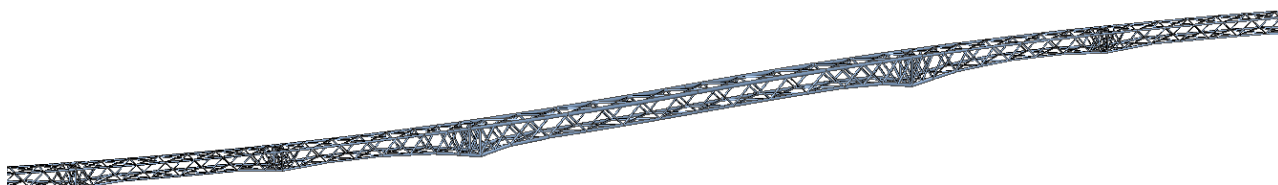


FIGURE 4.6: SCIA MODEL #2 OF THE CONTINUOUS CURVED GIRDER

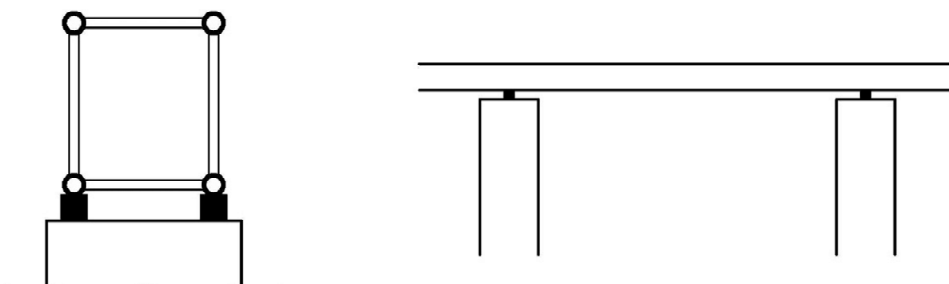


FIGURE 4.7: IT WAS ASSUMED THAT THE GIRDER LIES ON TWO LARGE RUBBER BLOCKS, ON TOP OF THE PONTOONS

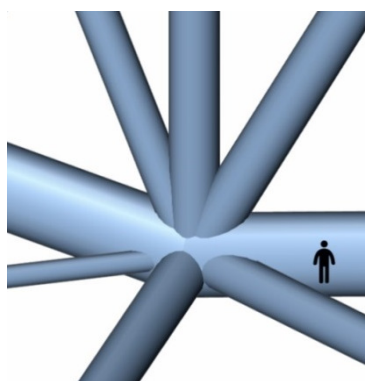


FIGURE 4.8: SUPPORT JOINT IN MAIN SPAN GIRDER. HUMAN FIGURE FOR SIZE REFERENCE.

## 4.6 Results

### 4.6.1 Displacements and rotations

The consequences of a continuous superstructure can be seen at the intermediate spans. Because of the large weight of the main span, the intermediate spans displace upwards under self-weight loading rather than downwards. See table 4.4.

**TABLE 4.4: DISPLACEMENT AND ROTATION RESULTS**

Result	Main span	Intermediate span	Side spans
Uz from self-weight only	1464 mm	-115 mm (upwards)	258 mm
Maximum Uz (SW, traffic and wind)	1763 mm	-37 mm (upwards)	391 mm
Maximum vertical rotation $\phi_x$ (SW, traffic and wind)	2.9 mrad	-3.8 mrad	4.8 mrad
Maximum horizontal rotation $\phi_z$ (SW, traffic and wind)	1.4 mrad	0.6 mrad	0.9 mrad

The displacements and rotations are below the requirements set in chapter 2. Furthermore, the girders will be precambered so that they will only deflect from external loading. This further decreases displacements and rotations.

#### 4.6.2 Stability

During design, checks were made for stability. First Scia was used to check whether buckling of a whole girder or buckling of members would be decisive. It was found that member buckling was governing the design.

Using Eurocode 3-1-1 maximum buckling stresses for each member were calculated. The lowest member buckling stress was 435 N/mm<sup>2</sup>. This value was set as upper limit for member stress at the preliminary design stage. Annex G elaborates on the stability calculations made.

#### 4.6.3 Stress unity checks

**TABLE 4.5: STRESS RESULTS**

Load case	Maximum stress	Unity check for stability
Self-weight (girder + bridge deck) only	262 N/mm <sup>2</sup>	0.60
Self-weight and traffic	313 N/mm <sup>2</sup>	0.72
Self-weight, traffic and wind load	319 N/mm <sup>2</sup>	0.73

In the design check with only self-weight, traffic and wind loads, the maximum member stress level in the superstructure was 319 N/mm<sup>2</sup>. This was deemed a sufficient margin to allow for additional stress under imposed deformations under storm in later research.

In chapter 3 it was concluded that investigating curved (instead of straight) girders was worthwhile. Yip (2015) designed straight girders to avoid additional torsional stresses. In this stage of design the exact same girder was designed both straight, as well as curved. The difference in member stresses was on average around 50 N/mm<sup>2</sup>. Moreover, connecting two girders at a pontoon would be easier with curved girders, as there is no need for an extra structure to accommodate the change in curve.

#### 4.6.4 Investigating higher steel grade

The research of Yip (2015) recommended the investigation of S690 grade steel for the superstructure. The superstructure was governed by buckling of individual members. The stress limits for this failure mode are below the yield stress of S460 steel. It was therefore concluded that investigating the use of a higher steel grade is not useful.

Fatigue loading will have to be investigated in later research. Nussbaumer et al. (2011) show that increasing the steel strength has little effect to the fatigue strength. It was therefore concluded that using a higher steel grade is not efficient.

## 5. BRIDGE BEHAVIOUR RESEARCH

Since the Sognefjord bridge is a structure currently unprecedented in the world, its behaviour when constructed was largely unknown. This chapter investigated behaviour (displacements under loads) of the Sognefjord bridge as a whole. First, the displacements and rotations of the bridge under all considered load situations were calculated. Then different bridge parameters were researched for their influence on displacements of the bridge.

### 5.1 Modelling

Investigating the bridge behaviour was done using Scia model #1, the model of the whole bridge. In this research, the interest lay in the deformations of the tops of the pontoons, since these support the superstructure. Any deformations of the pontoons would impose deformations on the bridge girders as well. It was expected this would result in large forces on the superstructure.

Furthermore, the bridge properties that determine these deformations had to be found. This was done by conducting a parameter research. All considered parameters were modelled in Scia model #1 as numerical input. Changing a parameter was done by changing the input value.

### 5.2 Parameter research

A parameter investigation was conducted to find the bridge parameters that determine displacements and rotations of the supports of the girders. The bridge parameters investigated were:

- Rotational stiffness of the pontoons
- Vertical (buoyancy) stiffness of the pontoons
- Bending stiffness of the bridge girders
- Shear stiffness of the bridge girders
- Cable stiffness of the anchoring system
- Wind loads on the bridge
- Wave loads on the bridge

The parameter research was done using Scia model #1 of the whole Sognefjord bridge. At every research step, one parameter was adjusted. Then, bridge deformations were re-calculated to check the effect of the change. If the effect would be large, then it could be concluded that the specific parameter investigated has a large influence on bridge displacements.

The interest lay in the influence of each parameter on displacements of the top of the pontoons, e.g. the supports of the superstructure. Deformations in all six degrees of freedom were considered. In the parameter research, every parameter was increased 1.5 and 2 times and decreased 1.5 and 2 times, compared to the original value.

### 5.3 General deformation behaviour of Sognefjord bridge

In this research, 6 different load situations were defined. Even though in real-life many more load situations might occur, these were deemed a sufficient first impression of the bridge behaviour.

The displacements and rotations of the Sognefjord bridge, with the new superstructure as designed in chapter 4, were calculated for these load situations first. Extreme values of deformations of the superstructure of the Sognefjord bridge are given in table 5.1. Under almost no loads, displacements are fairly small (<6 m), while in storm situations these can be more than 5 times as big. The maximum lateral and horizontal displacements were found to be 27 and 46 m, respectively. This was deemed acceptable compared to the scale of the Sognefjord bridge. See figure 5.1 for an impression of the way the bridge deforms under different load combinations. Refer to Annex H for the loads involved in each load combination.

TABLE 5.1: OVERVIEW OF ABSOLUTE VALUES OF DISPLACEMENTS AND ROTATIONS OF SOGNEFJORD BRIDGE

Load combination	Ux [m]		Uy [m]		Uz [m]		$\phi_x$ [mrad]		$\phi_y$ [mrad]		$\phi_z$ [mrad]	
	Max	Min	Max	Min	Max	Min	Max	Min	Max	Min	Max	Min
Quiet day, no wind	5.9	0.1	6.1	2.1	3.0	1.3	24.0	0.2	16.4	0.9	13.6	0.4
Max. SLS storm	20.4	3.3	33.8	21.3	7.8	0.6	38.6	1.9	29.4	1.3	18.4	0.4
Max. ULS storm	25.2	3.5	38.0	23.1	3.1	0.1	8.4	0.2	12.8	0.2	18.7	1.6
Contrary loads	27.2	3.4	45.8	28.8	3.1	0.0	9.2	0.8	13.5	0.0	22.5	2.4
Unsymmetrical loads	26.4	2.8	21.5	0.6	0.2	0.0	3.8	0.0	2.9	0.1	58.7	5.9
Max. lateral loads	26.1	2.0	9.5	0.3	2.7	0.1	8.7	0.1	24.3	0.4	23.1	7.1

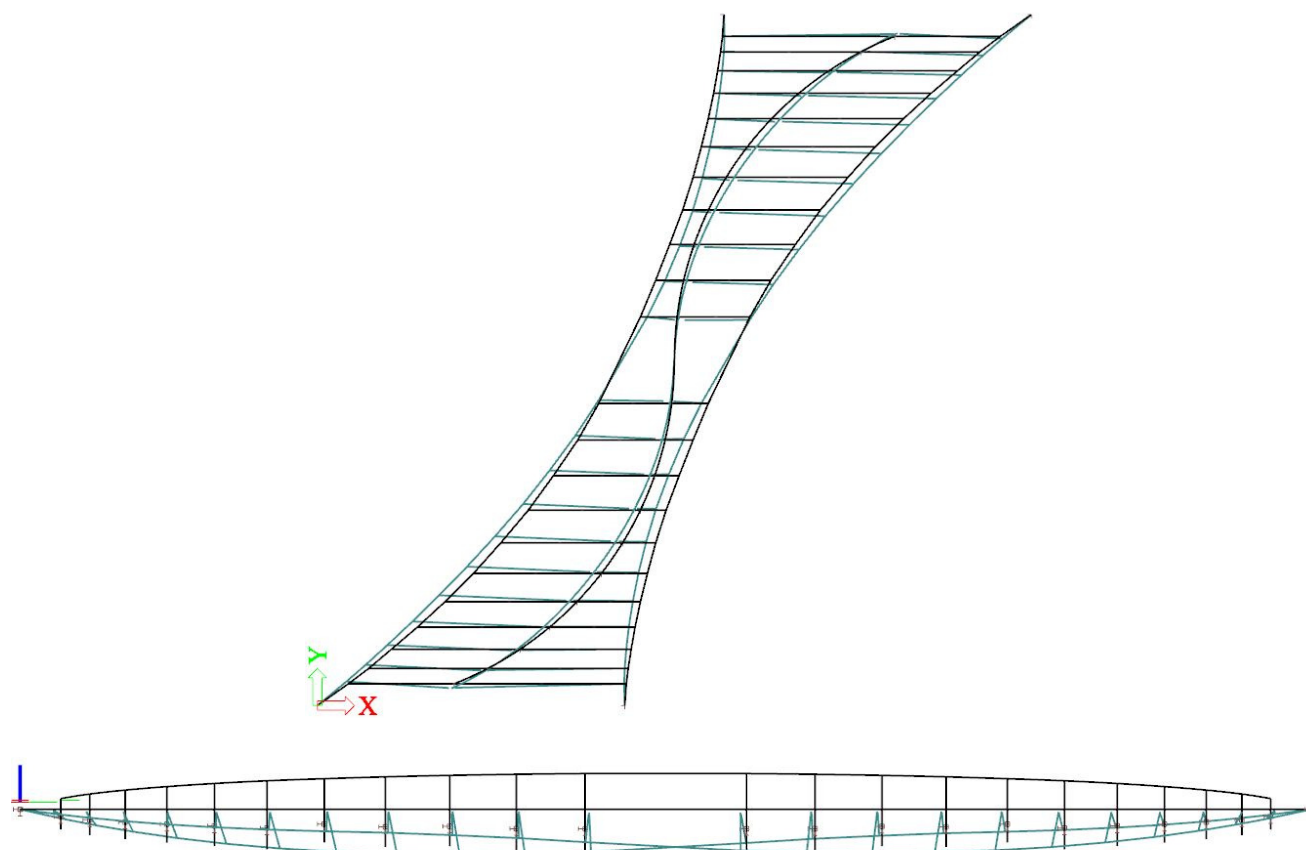


FIGURE 5.1: DEFORMED SHAPE OF THE BRIDGE GIRDERS AND ANCHORING SYSTEM IN LC2

Annex H gives all considered load cases and all bridge displacements and rotations results under different loads. Shapes of the deformed structure under different loads can also be found here. Bridge behaviour is very diverse, with large differences in deformations between different load situations. This is illustrated in figure 5.2. Wind loads cause the biggest deflections of the bridge. The direction of the wind therefore has significant effect on the direction of displacement of the bridge girder.

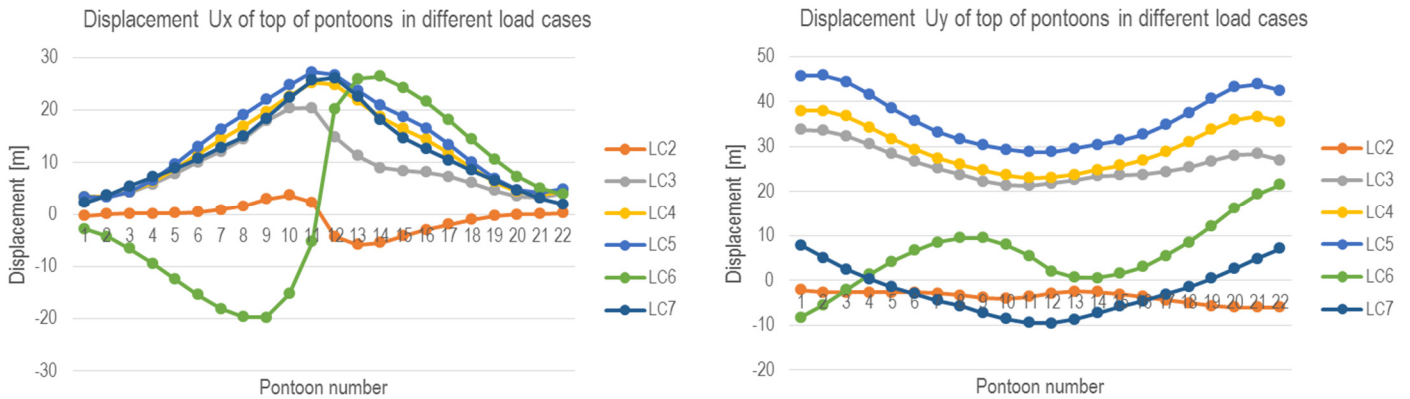


FIGURE 5.2: BRIDGE DEFORMATIONS (UX AND UY) UNDER THE DIFFERENT CONSIDERED LOAD COMBINATIONS

### 5.4 Bridge sensitivity analysis

The severest bridge deformations occur under a ULS storm. This situation was therefore used as the load situation for the parameter research. In every load combination the bridge deforms overall a little different. Considering only one load situation is therefore not representative for the full bridge behaviour. By taking the severest load situation it was however expected that sufficient knowledge for other load situations would be found. In the deformation results, the deformations in the self-weight only situation were subtracted from the deformations in the ULS storm, since the self-weight situation is the starting position of the bridge. The interest in this research lies in the deviations from the self-weight situation, since these impose loads on the superstructure.

Then the parameter research was conducted. Every parameter was increased and decreased both 1.5 times and 2 times, and with every parameter change the deformations of the Sognefjord bridge under a ULS storm were calculated. From these results the sensitivity of the Sognefjord bridge behaviour for each parameter was obtained.

Figure 5.3 shows the effect of each parameter on the lateral displacement (x-direction) of the top of the pontoons, at mid-span (the most deflecting part of the bridge). It can be seen that wind loads have the biggest influence on

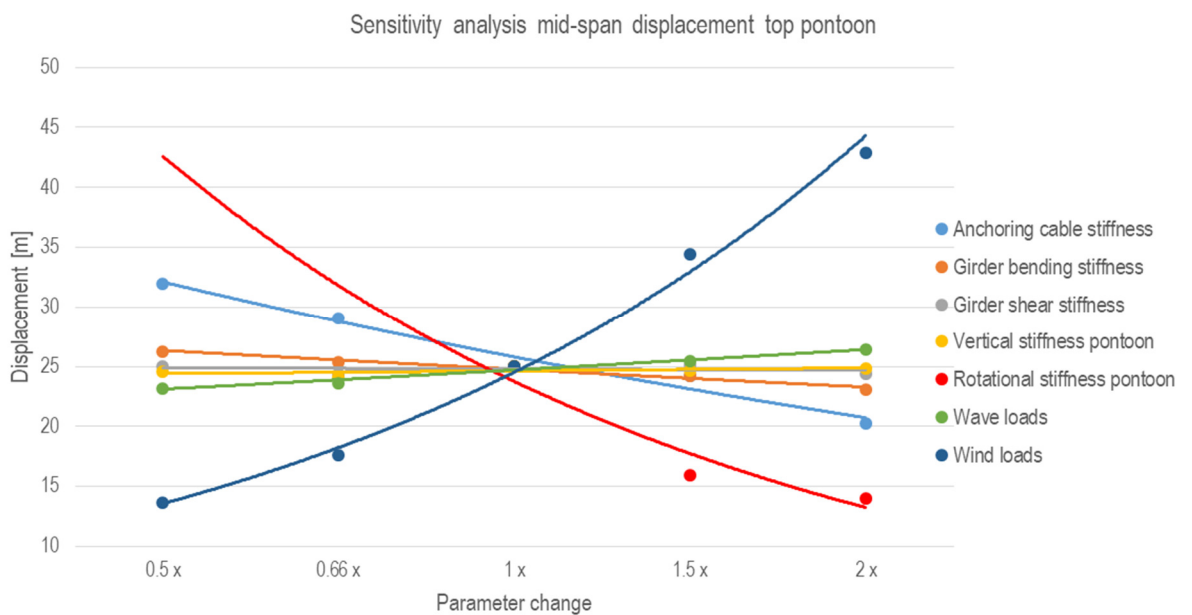


FIGURE 5.3: PARAMETER SENSITIVITY ON LATERAL DISPLACEMENTS OF THE BRIDGE AT MID-SPAN. THE STEEPER THE CURVE, THE BIGGER THE INFLUENCE OF THE PARAMETER ON DISPLACEMENTS.



lateral bridge displacements. A second parameter with large influence on lateral bridge displacements is the rotational stability of the pontoons, followed by the stiffness of the anchoring cables. Other bridge properties, such as the stiffness of the superstructure, have a less steep curve in the graph. Their effect on bridge behaviour is small.

## 5.5 Parameter research results

On the following pages the results from the parameter research are displayed. The full results from the parameter research can be found in Annex I.

Of the bridge properties rotational stability of the pontoons has the biggest influence on deformations of the supports of the girder. For double rotational stiffness, lateral displacement (x-direction) and longitudinal displacement (y-direction), two movements imposing large stresses on the bridge girder, reduce up to 44% and 26%, respectively. See figures 5.4 and 5.5. Note that for this parameter an extra alterations has been tested (1.25x higher as well). Due to modelling limitations, lower rotational stiffness could not be tested.

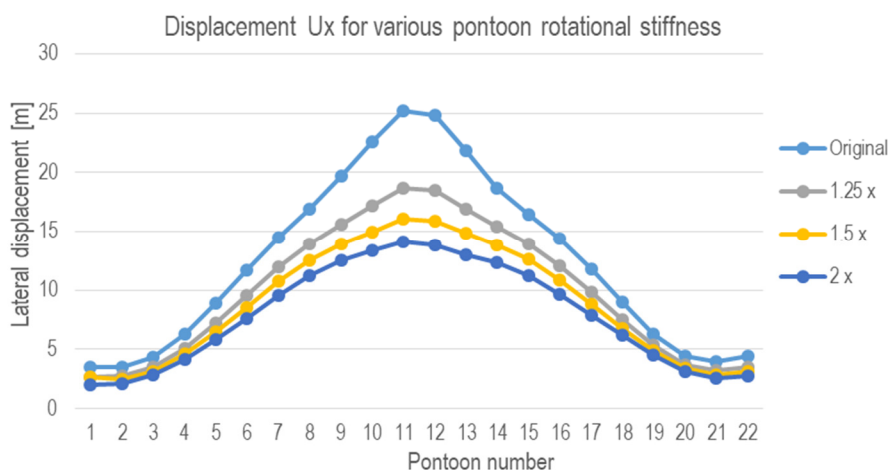


FIGURE 5.4: LATERAL DISPLACEMENT OF TOP OF PONTOONS FOR DIFFERENT ROTATIONAL STABILITY. MAXIMUM REDUCTION IN LATERAL DISPLACEMENT FOR A 2 TIMES STIFFER PONTOON IS 44%.

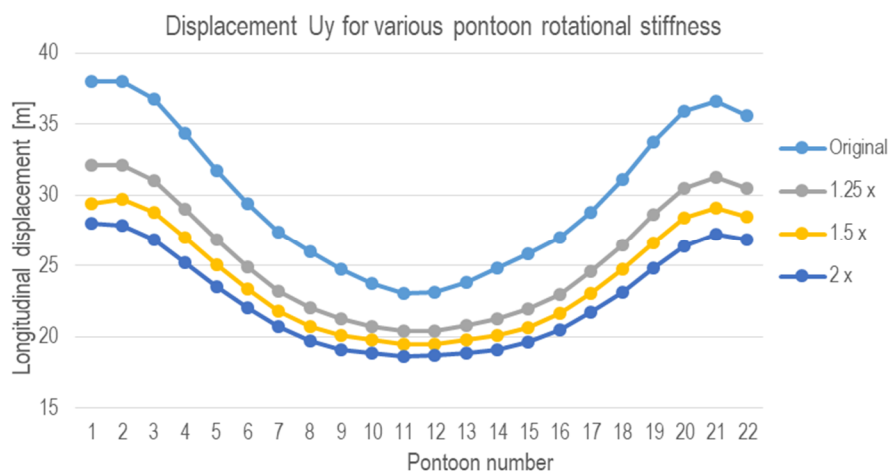


FIGURE 5.5: LONGITUDINAL DISPLACEMENT OF TOP OF PONTOONS FOR DIFFERENT ROTATIONAL STABILITY. MAXIMUM REDUCTION IN LONGITUDINAL DISPLACEMENT FOR A 2 TIMES STIFFER PONTOON IS 26%.



The stiffness of the anchoring cables has a much smaller, but still significant effect on bridge deformations. For a double stiffness, lateral and longitudinal displacements reduce up to 19% and 15%, respectively. See figures 5.6 and 5.7.

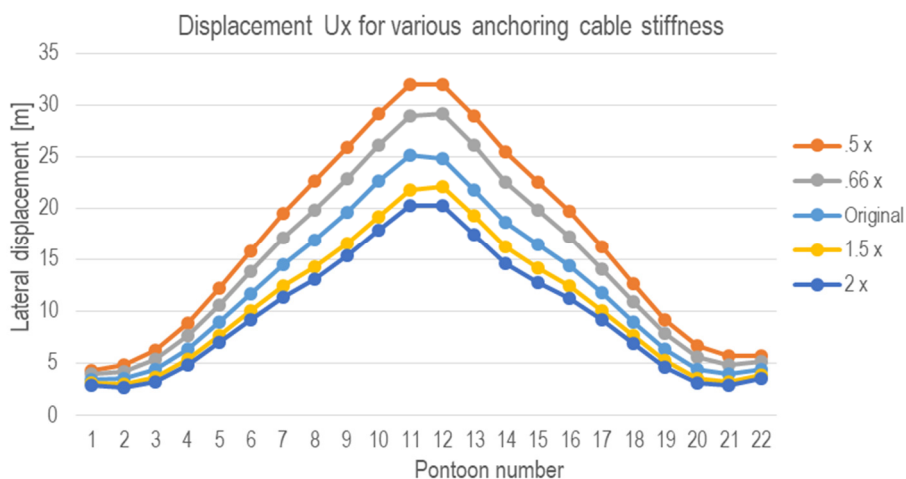


FIGURE 5.6: LATERAL DISPLACEMENT OF TOP OF PONTOONS FOR DIFFERENT ANCHORING CABLE STIFFNESSES. MAXIMUM REDUCTION IN DISPLACEMENT FOR A 2 TIMES STIFFER CABLE IS 19%.

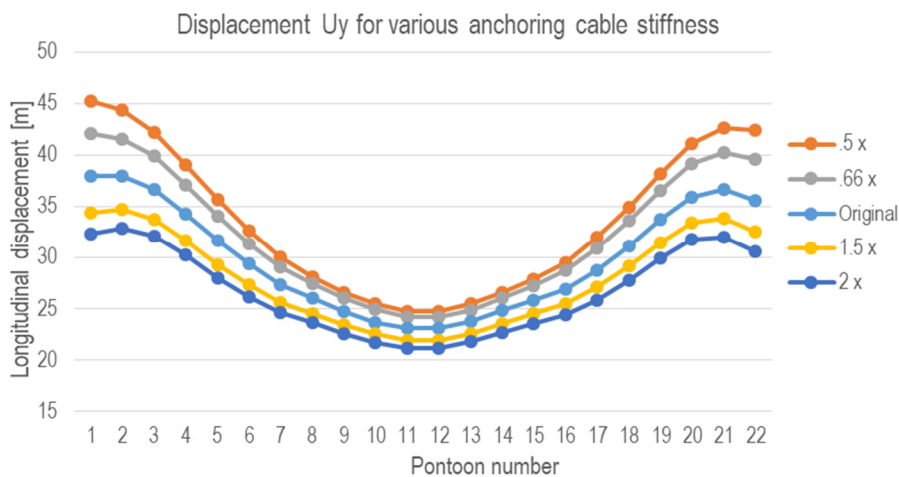
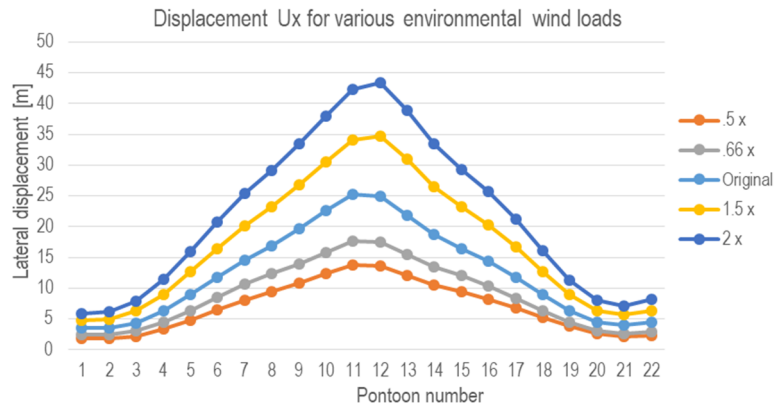
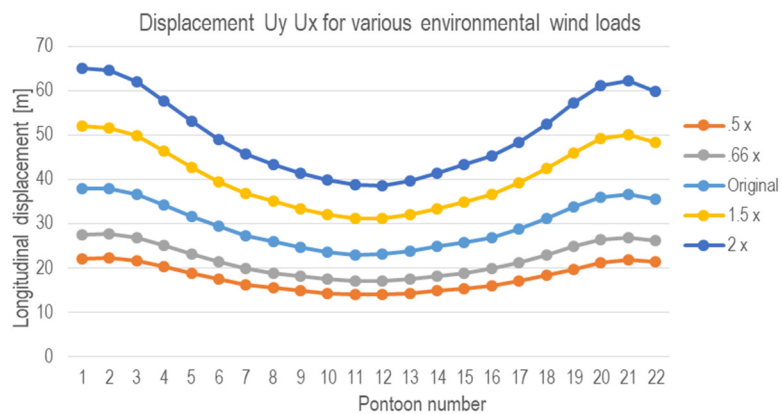


FIGURE 5.7: LONGITUDINAL DISPLACEMENT OF TOP OF PONTOONS FOR DIFFERENT ANCHORING CABLE STIFFNESSES. MAXIMUM REDUCTION IN DISPLACEMENT FOR A 2 TIMES STIFFER CABLE IS 15%.

It was found that wind loads have the biggest influence on bridge deformations. At main span, a twice as strong wind load gives lateral displacements (x-direction) that are 75% higher. At the end span, longitudinal displacements (y-direction) are 71% higher. See figures 5.8 and 5.9.



**FIGURE 5.8: LATERAL DISPLACEMENT OF TOP OF PONTOONS FOR DIFFERENT WIND LOADS. MAXIMUM INCREASE IN DISPLACEMENT FOR A 2 TIMES HIGHER LOAD IS 75%.**



**FIGURE 5.9: LONGITUDINAL DISPLACEMENT OF TOP OF PONTOONS FOR DIFFERENT WIND LOADS. MAXIMUM INCREASE IN DISPLACEMENT FOR A 2 TIMES HIGHER LOAD IS 81%.**

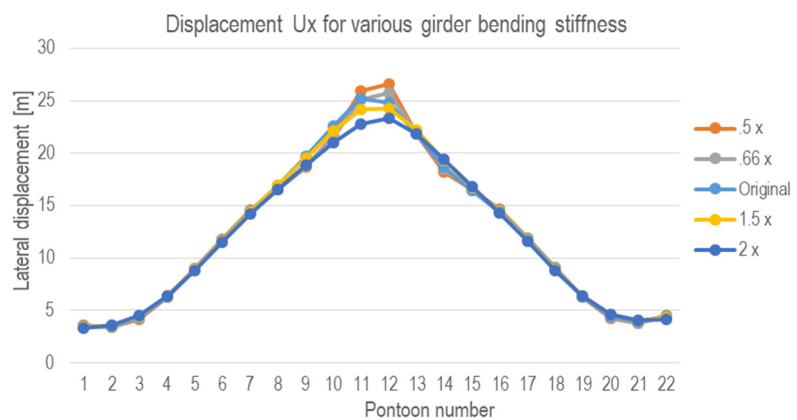


**FIGURE 5.10: LATERAL DISPLACEMENT OF TOP OF PONTOONS FOR DIFFERENT GIRDER BENDING STIFFNESSES. MAXIMUM REDUCTION IN DISPLACEMENT IS 9% FOR A 2 TIMES HIGHER STIFFNESS.**

Influence of the other bridge parameters, such as girder properties, on girder support deformations were much lower. As an indication  $U_x$ -results for girder bending stiffness are displayed in figure 5.10. The full research results for all displacements and rotations under all parameters can be found in Annex I.

## 5.6 Range of governing parameters

Three bridge parameters have significant effect on the bridge displacements: wind loads, pontoon rotational stiffness and anchoring cable stiffness. The range of effectiveness of pontoon rotational stiffness and cable stiffness on reducing overall bridge deformations was investigated.

The results are summarised in figure 5.11, in which the lateral displacement of Sognefjord bridge at mid-span for higher pontoon rotational stiffness and anchoring cable stiffness, is displayed. Increasing these parameters significantly initially reduces bridge deformations. The effectiveness of increasing the parameters diminishes when they become higher however. This is visualised by the flattening of the curves.

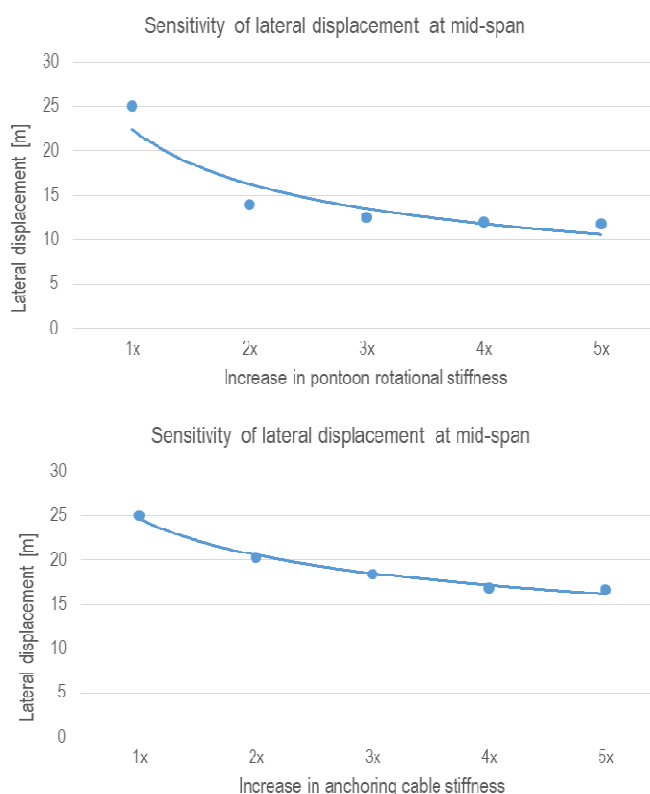


**FIGURE 5.11: LATERAL DISPLACEMENTS AT BRIDGE MID-SPAN UNDER INCREASING STIFFNESS OF THE PONTOONS (TOP) AND ANCHORING SYSTEM (BOTTOM).**

After a certain value of a parameter, other parameters become governing in bridge behaviour. It shows that a minimum amount of bridge displacements cannot be evaded.

## 5.7 Discussion

The largest influence on movements of the girder supports come from the rotational stability of the pontoons and the wind loads. Both these parameters' influence is strong because they activate the very large lever arm of the pontoons. For the mid-span pontoons for example this distance between the centre of buoyancy and the top of the pontoon is 157 m. This causes very large bending moments at small loads, and large displacements at small rotations. See figure 5.12.

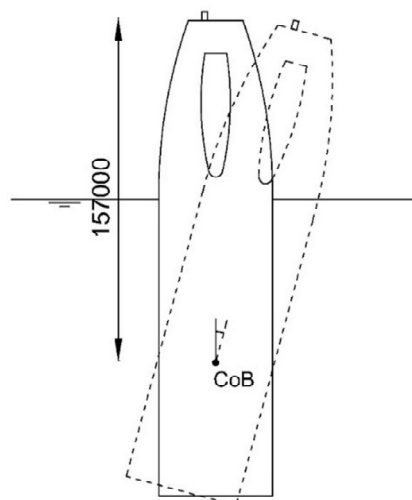


FIGURE 5.12: ROTATED PONTOON. THE LARGE LEVER ARM MAKES FOR LARGE DISPLACEMENTS AT THE TOP. TRUCK AT THE TOP FOR SIZE REFERENCE.

Of the other bridge parameters, only the anchoring cable stiffness was of significance, albeit less strong than the pontoon rotational stiffness and the environmental wind loads. This is because the effect of the anchoring system on pontoon rotations was found to be very low (see also Annex I.8). The anchoring system reduces lateral displacements of pontoon as a whole significantly, but pontoon rotation only little.

Other bridge parameters have little influence on bridge behaviour. Increasing the stiffness of the superstructure for example will have little effect in decreasing bridge displacements.

More important than general deformations are deformation differences between adjacent pontoons. To a certain degree the bridge as a whole is free to move. If two adjacent pontoons both displace the same, then no support displacements will be imposed upon the in-between girder. See figure 5.13.

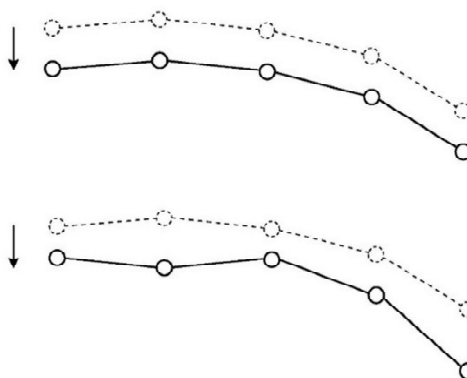
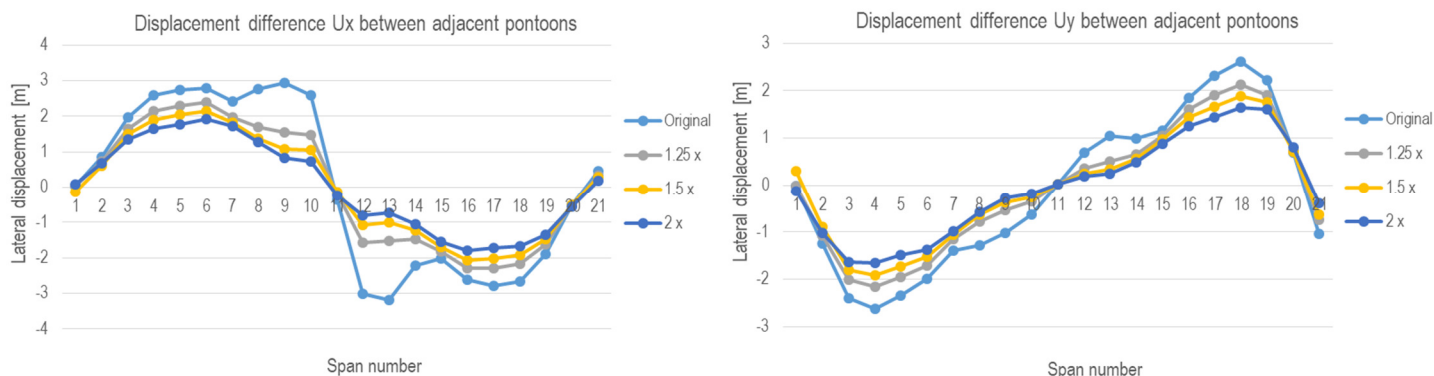


FIGURE 5.13: ALL PONTOONS DISPLACING THE SAME (TOP) OR ADJACENT PONTOONS DISPLACING DIFFERENTLY (BOTTOM). THE LATTER GIVES STRESS IN THE GIRDERS.

Differences between deformations of adjacent pontoons impose loads on the bridge girders. These deformations are therefore determining stresses in the superstructure. Graphs of the deformation differences between adjacent pontoons are given in figure 5.14.



**FIGURE 5.14: DEFORMATION DIFFERENCES BETWEEN ADJACENT PONTOONS UNDER DIFFERENT PONTOON ROTATIONAL STABILITY. LATERAL DISPLACEMENT (LEFT) DECREASES UP TO 81%, LONGITUDINAL DISPLACEMENT (RIGHT) DECREASES UP TO 37%.**

Compared to the absolute bridge deformations, these have a much smaller scale (about 3 meters max.). The effect of a double pontoon rotational stiffness is here higher compared to general deformations. When the pontoon rotational stiffness is doubled, lateral and longitudinal displacements decrease up to 81% and 37%, respectively.

Increasing pontoon rotational stability has a significant effect on decreasing girder support displacements. This offers possibilities for increasing the structural feasibility of a continuous bridge girder. In Annex J the feasibility of improving pontoon rotational stiffness was therefore investigated. For this, a preliminary tripod spar pontoon design was checked. This pontoon design had a 2.2 times higher rotational stiffness. It was thereby concluded that using increased pontoon rotational stability to decrease deformations of the girder supports is structurally feasible. However, in this tripod concept it would require about twice the amount of concrete compared to the original spar pontoon concept. For further research it is strongly recommended to evaluate pontoon design and investigate other pontoon structure concepts.

Large displacements of the bridge as a whole impose challenges on the two outer shore spans, since the shores are fixed points. Designing the connections from the bridge to land is out of the scope of this research. They pose a big engineering challenge however and it is recommended to investigate shore span design in further research.

## 5.8 Conclusions of parameter research

Deformations imposed on a continuous girder can cause large loads on this girder. For Sognefjord bridge, the displacements and rotations of the top of the pontoons must therefore be limited. Maximum longitudinal and lateral displacements of the bridge are 46 and 27 m, respectively. These were deemed acceptable. Displacement differences between adjacent pontoons are around 3 m.

Wind loads and pontoon rotational stability have the largest influence in movements of the pontoons. Stiffness of the anchoring cables has a two times lower effect compared to the rotational stiffness of the pontoons. Other parameters such as girder stiffness were found to have insignificant effects on bridge deformations.

To limit forces in the girder, it is best to investigate reducing pontoon deformations. The most important in this is the difference in deformations between adjacent pontoons. These have to be limited to make a continuous bridge girder structurally feasible. However, the size difference between the scale deformations of the bridge as a whole and the scale of deformation differences between individual pontoons is very large. This decreases feasibility of limiting the deformations imposed on the bridge girder. More on this is discussed in chapter 6.

To achieve lower deformations between adjacent pontoons, pontoon rotational stability could be increased, anchoring cable stiffness could be increased or wind loads could be decreased. Since the lattice girder is already an aerodynamically very efficient girder concept, and the same holds for the round pontoons, it is not expected that significant improvement in reducing wind loads can be made.

Increasing cable stiffness is only possible by prestressing, increasing cable cross-sections or choosing a new anchoring system layout. The first two are not considered feasible for construction and structural reasons.

Researching other anchoring system layouts is out of the scope of this research. In future research, this could be investigated for beneficial effects.

In the design by Yip (2015), pontoon design was limited to simple spar hulls only. In Annex J it was found that the current design offers good possibilities for optimisation. It is concluded that increasing pontoon rotational stability has the highest potential for decreasing imposed forces on the bridge girder.

This research only defined six load situations, of which only one was researched in-depth. Sognefjord bridge behaviour differs significantly between different load situations. It is therefore recommended that more load situations are investigated in further research. For this design stage however, the considered load situations were deemed representative.

## 6. GIRDER BEHAVIOUR RESEARCH

The Sognefjord bridge will displace under storm loads, imposing large deformations on the girder. This chapter investigates the forces in the truss girder that result from these storm deformations, and thereby if the concept of a continuous girder without internal hinges for the Sognefjord bridge is structurally feasible.

This was done by taking the bridge deformations resulting from a ULS storm situation, as calculated in Scia model #1, and imposing these on the truss girder of Scia model #2. Modelling imposed deformations on the bridge girders was first validated for its quality of results.

The member forces and bending moments in the truss girder of Scia model #2 were evaluated. From the results of these tests, conclusions were drawn on making a continuous bridge girder in the Sognefjord buoyancy bridge.

### 6.1 Coordinate system forces

Forces in this chapter are denoted in the local coordinate system of members or girders. See figure 6.1. For example,  $M_x$  means a torsional moment about the longitudinal axis of a member or girder. Likewise,  $V_z$  is a shear force in vertical direction.

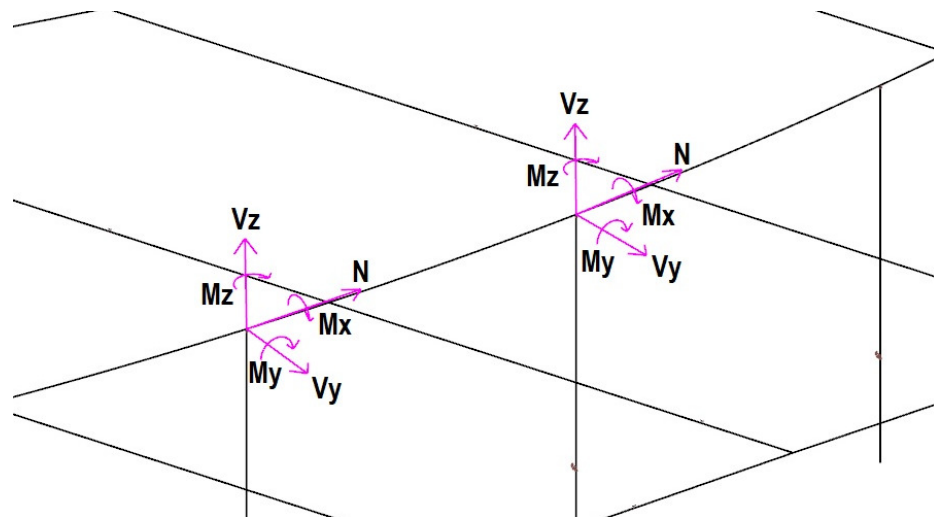


FIGURE 6.1: COORDINATE SYSTEM OF FORCES

### 6.2 Modelling imposed deformations on the bridge girders

In this thesis research three different calculation models were built using Scia Engineer. The first model was of the Sognefjord bridge as a whole, including the pontoons and anchoring system. This was Scia model #1. In a second model, only a part of the 3D truss girder was modelled including every single CHS member. This was Scia model #2. See figure 6.2.

In Scia model #1, the bridge girders were simplified to single beams with stiffness properties equivalent to those of the full truss. Validating the properties of these equivalent beams is described in Annex E.

A third model, Scia model #3, was made. This model was an exact copy of the equivalent prismatic beam girders modelled in Scia model #1. In Scia model #3 the rest of the bridge structure (the pontoons and anchoring system) was replaced by a set of new boundary conditions. Scia model #3 was made to check whether modelling imposed deformations on a structure in Scia gives reliable results.



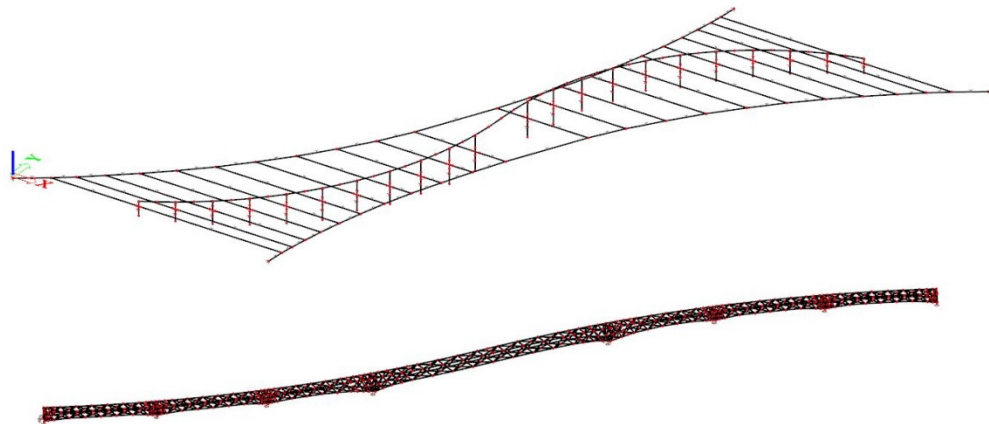


FIGURE 6.2: MODEL OF THE WHOLE SOGNEFJORD BRIDGE WITH THE GIRDERS MODELLED AS SINGLE EQUIVALENT BEAMS (SCIA MODEL #1, TOP) AND MODEL OF ONLY A PART OF THE 3D TRUSS (SCIA MODEL #2, BOTTOM)

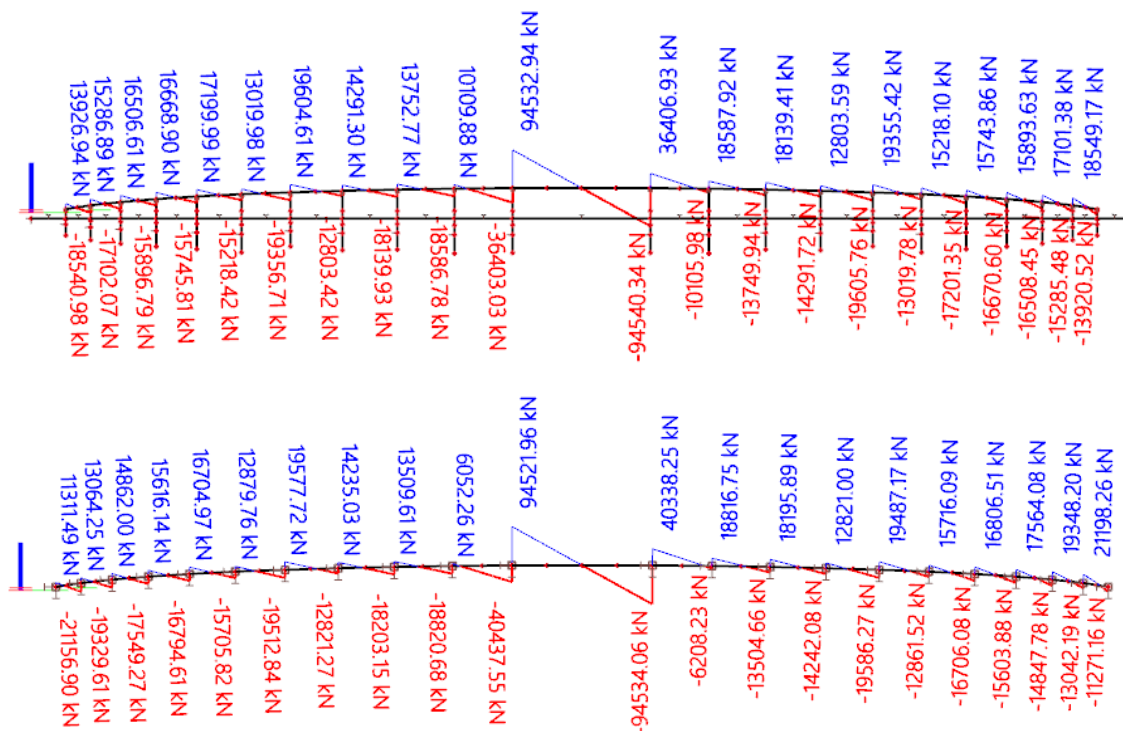


FIGURE 6.3: GLOBAL FORCES RESULTS UNDER LC4 IN SCIA MODEL #1 (TOP), AND IN SCIA MODEL #3 (BOTTOM), WHERE THE PONTOONS AND ANCHORING SYSTEM WERE REPLACED BY A SET OF IMPOSED DEFORMATIONS. THE DIFFERENCES IN RESULTS ARE SMALL.

In Scia model #3, the girder supports, which were the tops of the pontoons in Scia model #1, were replaced by clamped supports. For the boundary conditions, the deformations of the top of the pontoons in Scia model #1 under a ULS storm situation were retrieved. Then, these exact deformations were modelled as imposed deformations on the bridge girders in Scia model #3. This was done by displacing and rotating the clamped supports in Scia model #3.

If under these imposed storm deformations the girders of Scia model #3 would give the same results as the girders of Scia model #1 under storm loads, then it could be concluded that in modelling, parts of a structure can be

replaced by imposing equivalent deformations. This was found to be the case. By this it was concluded allowable to replace parts of a structure in Scia Engineer by equivalent imposed deformations. See figure 6.3 for the comparison of results.

### 6.3 Boundary conditions and imposed deformations in Scia model #2 of the full truss girder

The same modelling of equivalent imposed deformations was used in the truss girder research. In Scia model #2 of the full truss girder, the rest of the bridge structure was replaced by a set of equivalent imposed deformations. The deformations were again imposed by displacing and rotating the clamped supports.

This was done by modelling the rubber blocks that support the bridge girder as two dummy bars, hinged connected to the superstructure. The hinges prevented additional member forces from clamping effects. The two dummy bars were connected by a third dummy bar in the middle. Deformations were imposed through a clamped support in the middle. See figure 6.4.

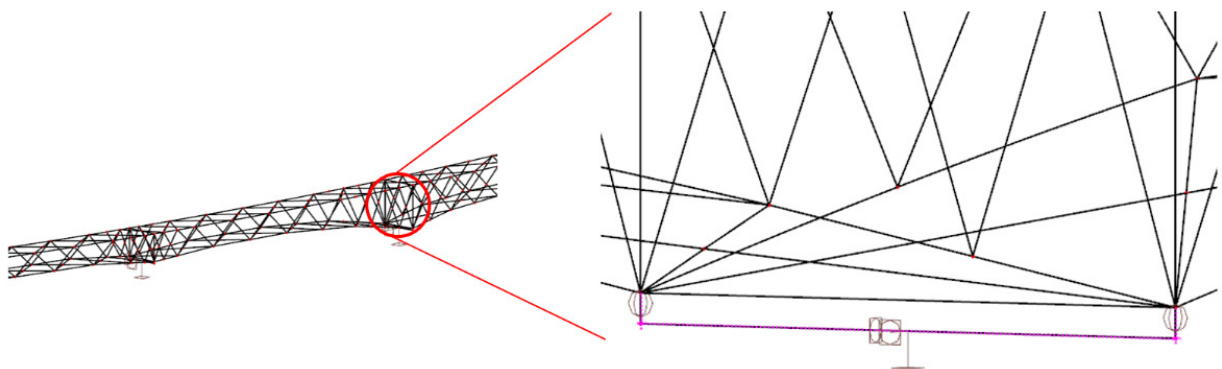


FIGURE 6.4: MODELLING THE BOUNDARY CONDITIONS IN THE FULL TRUSS GIRDER MODEL. ON THE RIGHT, THE HINGES AND THE SUPPORT CAN BE SEEN, LOCATED ON THE (PINK) DUMMY BARS.

The rubber blocks on which the superstructure rests will act like springs. When loaded they will deform and allow some displacements of the superstructure. The rubber blocks were however modelled as hinges that cannot displace. As this is a slightly conservative approach, this was deemed acceptable in this stage of design. More on the modelling of the girder supports in Scia model #2 is discussed in Annex K.

Of the deformations imposed on the girders, the most important aspect is deformation differences between adjacent pontoons. As an indication, the values of these deformation differences in LC4 (ULS storm) are given in Annex L. The maximum difference in lateral displacement was 3.2 m. The values of the imposed deformations differ per span and per load situation. This means that for every load case, a different force arises in every member of the truss.

### 6.4 Global forces and bending moments in ULS storm situation in girders

First the global forces and bending moments under LC4 (ULS storm) in every span of the bridge were calculated, using the Scia model #3. For this, the displacements of the girder in LC4 were again settled with the self-weight displacements (refer to chapter 5.5 for more on this). The results for normal forces and bending moments  $M_y$  and  $M_z$  are given in figure 6.5.

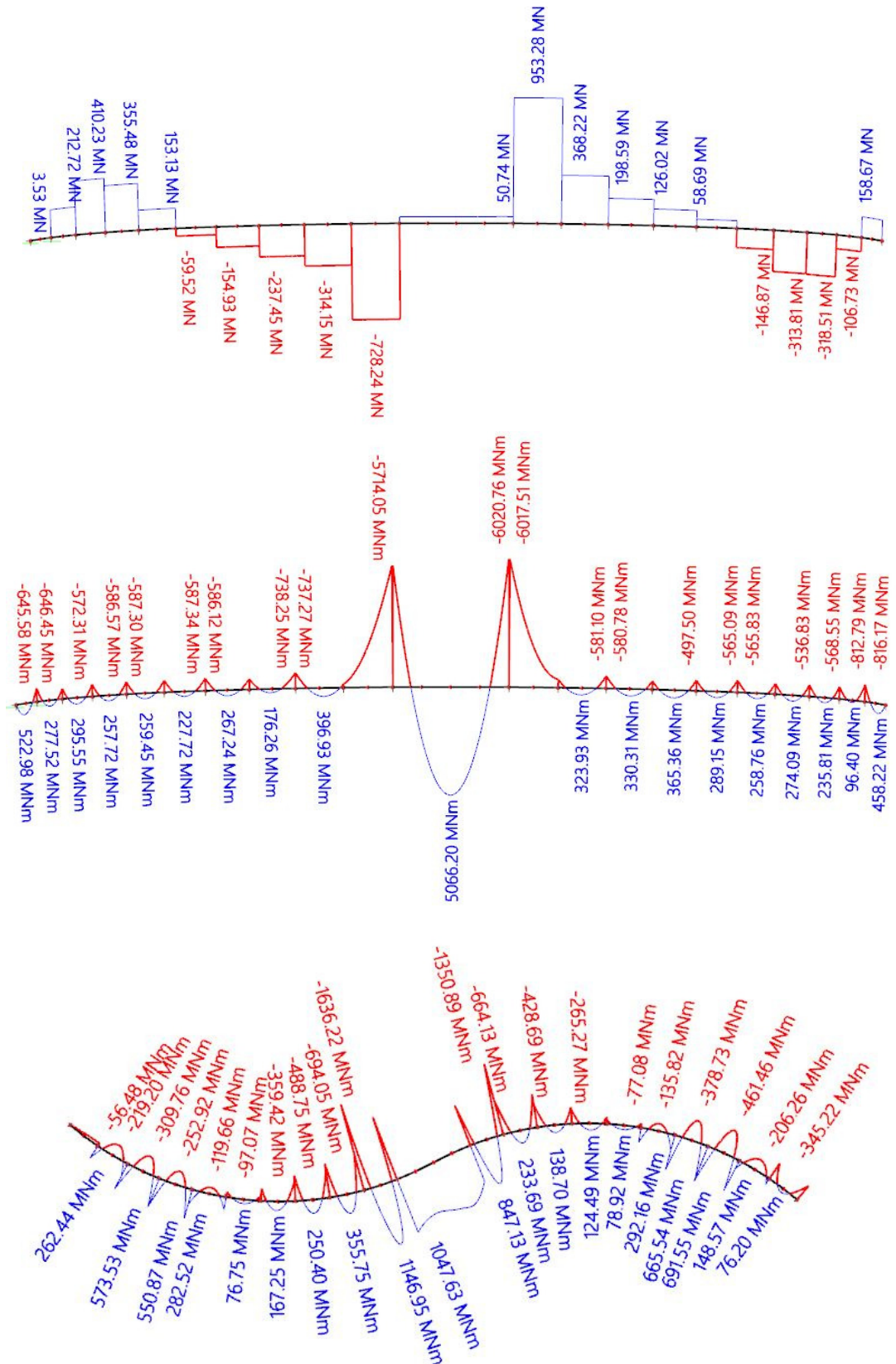


FIGURE 6.5: GLOBAL FORCES IN THE GIRDERS. FROM TOP TO BOTTOM: N FORCES [MN], MY AND MZ BENDING MOMENTS [MNm].

The highest normal forces were found in the two girders directly next to the main span, with a maximum value of 953 MN. The highest  $M_z$  bending moment was -1636 MNm, located at the span directly adjacent to the main span.  $M_y$  bending moments were on average about 4 times higher than  $M_z$  bending moments. The highest  $M_y$  bending moment was located at the main span, being -6021 MNm. The results for all loads can be found in Annex L.

The girders were also subjected to self-weight and wind loads only, to investigate the effects of bridge deformations on the global forces in the superstructure. Global forces in the bridge girders were twenty times smaller when the girders were subjected to self-weight and wind loads only. These results can be found in Annex L.

## 6.5 Forces and bending moments in ULS storm situation in truss girder members

Forces in individual members were investigated. Members in the main span and the side span imposed to the largest displacements (under a ULS storm) are presented as an indication. The results of the members at mid-span and at the support are presented. See figure 6.6.



FIGURE 6.6: LOCATIONS ON TRUSS GIRDER WHERE INDIVIDUAL MEMBERS WERE EVALUATED

See tables 6.1 and 6.2 for internal forces and bending moments in the members. Since these are the largest span and the side span with the largest imposed loads in Scia model #2, these results were deemed representative for the magnitude of forces in the girder members in other spans as well.

TABLE 6.1: FORCES IN INDIVIDUAL MEMBERS IN MAIN SPAN GIRDER

Members at support	Member # in Scia model	N [MN]	$M_y$ [MNm]	$M_z$ [MNm]	Stress [N/mm <sup>2</sup> ]
Chord top right	B6807	96.45	-19.11	23.13	189
Chord top left	B6806	-22.13	-4.02	4.59	42
Chord bottom right	B6022	-143.97	-28.98	-34.10	192
Chord bottom left	B6023	-139.10	-11.87	5.75	146
Brace right	B5855	-15.41	-0.89	-4.32	116
Brace left	B5857	-6.96	0.60	-2.23	56
Brace top	B5823	-17.26	1.81	1.14	63
Brace bottom	B6077	5.06	-5.51	0.64	184
Members at mid-span	Member # in Scia model	N [MN]	$M_y$ [MNm]	$M_z$ [MNm]	Stress [N/mm <sup>2</sup> ]
Chord top right	B6031	-88.16	39.30	13.70	160
Chord top left	B6030	-236.36	40.86	14.49	334
Chord bottom right	B6026	94.93	8.83	4.55	252
Chord bottom left	B6027	17.84	9.56	3.17	82

**TABLE 6.2: FORCES IN INDIVIDUAL MEMBERS IN SIDE GIRDER BETWEEN PONTOONS #13 AND #14**

Members at support	Member # in Scia model	N [MN]	My [MNm]	Mz [MNm]	Stress [N/mm <sup>2</sup> ]
Chord top right	B6526	56.92	-16.64	-4.68	438
Chord top left	B6527	48.82	-8.73	6.51	336
Chord bottom right	B6531	-27.02	-11.22	0.35	241
Chord bottom left	B6530	15.79	-6.34	0.04	139
Brace right	B6420	-6.24	-0.38	-1.68	286
Brace left	B6419	-4.85	-0.28	-1.42	232
Brace top	B6528	-3.37	0.36	0.10	120
Brace bottom	B6525	-5.88	-3.62	-0.07	457
Members at mid-span	Member # in Scia model	N [MN]	My [MNm]	Mz [MNm]	Stress [N/mm <sup>2</sup> ]
Chord top right	B6812	0.52	3.32	-0.84	38
Chord top left	B6811	16.81	2.83	0.37	106
Chord bottom right	B6814	30.35	1.76	-1.21	152
Chord bottom left	B6813	38.68	1.42	-0.37	193

Forces and bending moments differ significantly per member of the truss. Normal forces in the considered members range from -236 MN to 95 MN. Bending moments range from -34 MNm to 41 MNm. The stresses shown are von Mises stresses.

The bending moment in a truss varies along the span of the girder and therefore axial forces in the chords vary as well. However, the variance in normal forces in chords in the Sognefjord truss is different from that of bending moment effects only. Normal forces resulting from bending moments are normally the same on each side of the cross-section. Now the normal forces differ significantly between either side of the cross-section. This is caused by the behaviour of the pontoons.

This is illustrated in figure 6.7, where the normal forces in the four chords are displayed along the length of the girder. The differences between the left and right side of the girder are significant. Moreover, forces differ significantly per span, whereas normally they are of comparable magnitude. Maximum axial forces in the chords where -244 MN and 142 MN under a ULS storm situation.

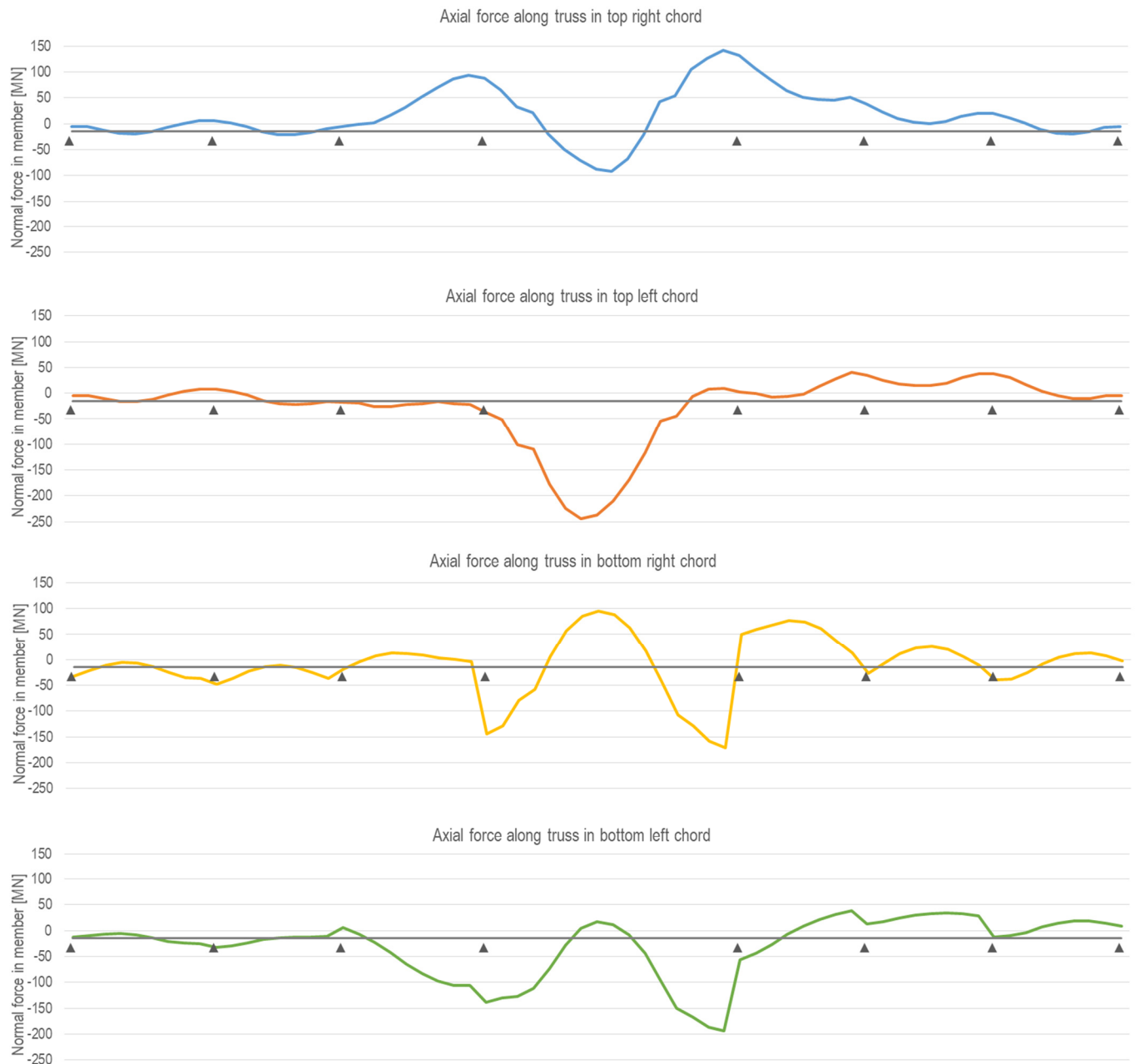


**FIGURE 6.7: NORMAL FORCES IN ALL FOUR CHORDS OF THE TRUSS, ALONG THE LENGTH OF THE SPANS**

The difference in load patterns is due to the deformations imposed on the girders by the displacing pontoons, which are different for each truss span. See figure 6.8 for an illustration. This holds for every span and therefore every member of the truss. Maximum forces are located in different members every load situation. This makes predicting maximum force levels in members of the truss girders challenging.



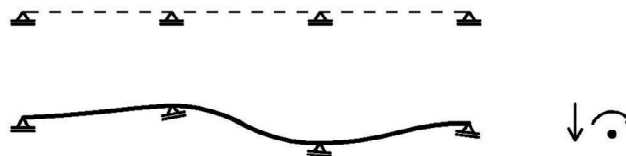


FIGURE 6.8: DIFFERENT DISPLACING PONTOONS CAUSES DIFFERENT IMPOSED DEFORMATIONS ON THE GIRDERS.

## 6.6 Stress levels

Figure 6.9 shows the stress levels in individual members in the truss under a ULS storm. The stress level lies between 100 and 250 N/mm<sup>2</sup> in most members. The maximum member stress in the truss in Scia model #2 is 590 N/mm<sup>2</sup> under LC4 (ULS storm). This results in a unity check for stability of 1.36. Stress levels strongly vary between individual members. A clear pattern in stress levels cannot be found. However, under larger imposed deformations stress levels do shift up. There is no difference between stresses in chords and stresses in braces.

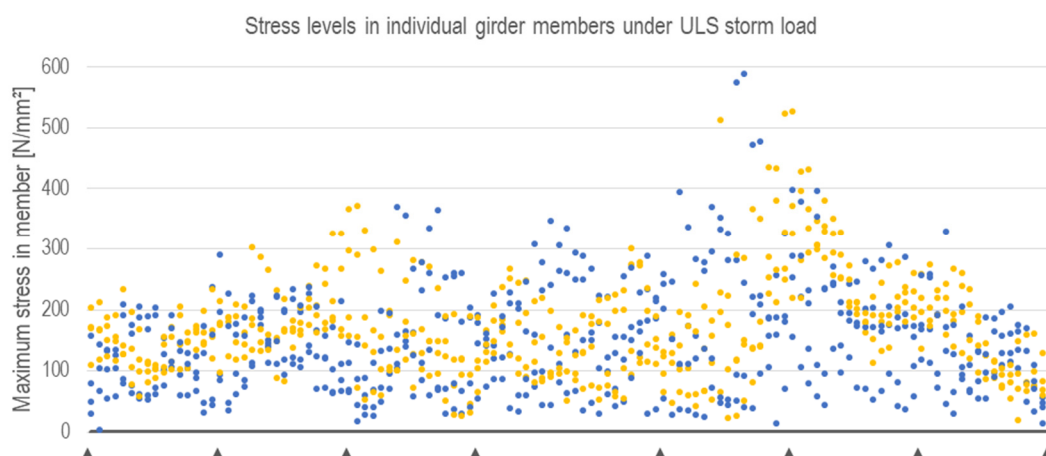


FIGURE 6.9: STRESS LEVELS IN INDIVIDUAL TRUSS MEMBERS ALONG THE SPANS. STRESSES IN CHORDS ARE INDICATED IN BLUE, STRESSES IN BRACES ARE INDICATED IN YELLOW.

## 6.7 Effect of stiffer pontoons

### 6.7.1 Global forces and bending moments on girders

Chapter 5 concluded that increasing rotational stiffness of the pontoons had a significant effect in decreasing bridge girder deformations. The effect of smaller bridge deformations on forces in the bridge girders was therefore checked.

The truss girder was subjected to ULS storm deformations of the Sognefjord bridge with twice the pontoon rotational stiffness. The values of deformation differences between adjacent pontoons under ULS storm loads with double pontoon rotational stiffness are given in Annex L. These are on average 2.5 times lower compared to displacement differences with original pontoon rotational stiffness. The maximum lateral displacement difference was 1.3 m.



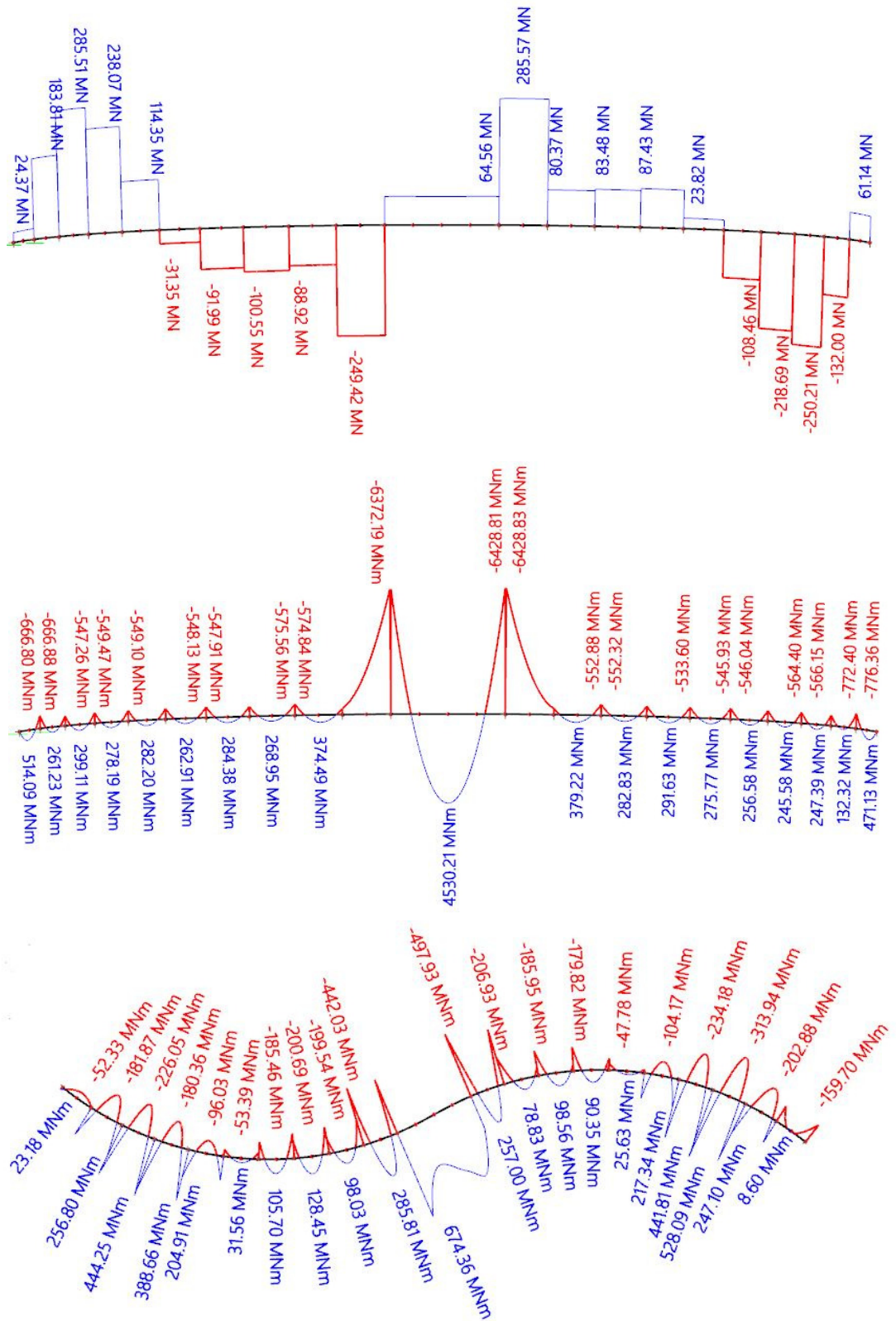
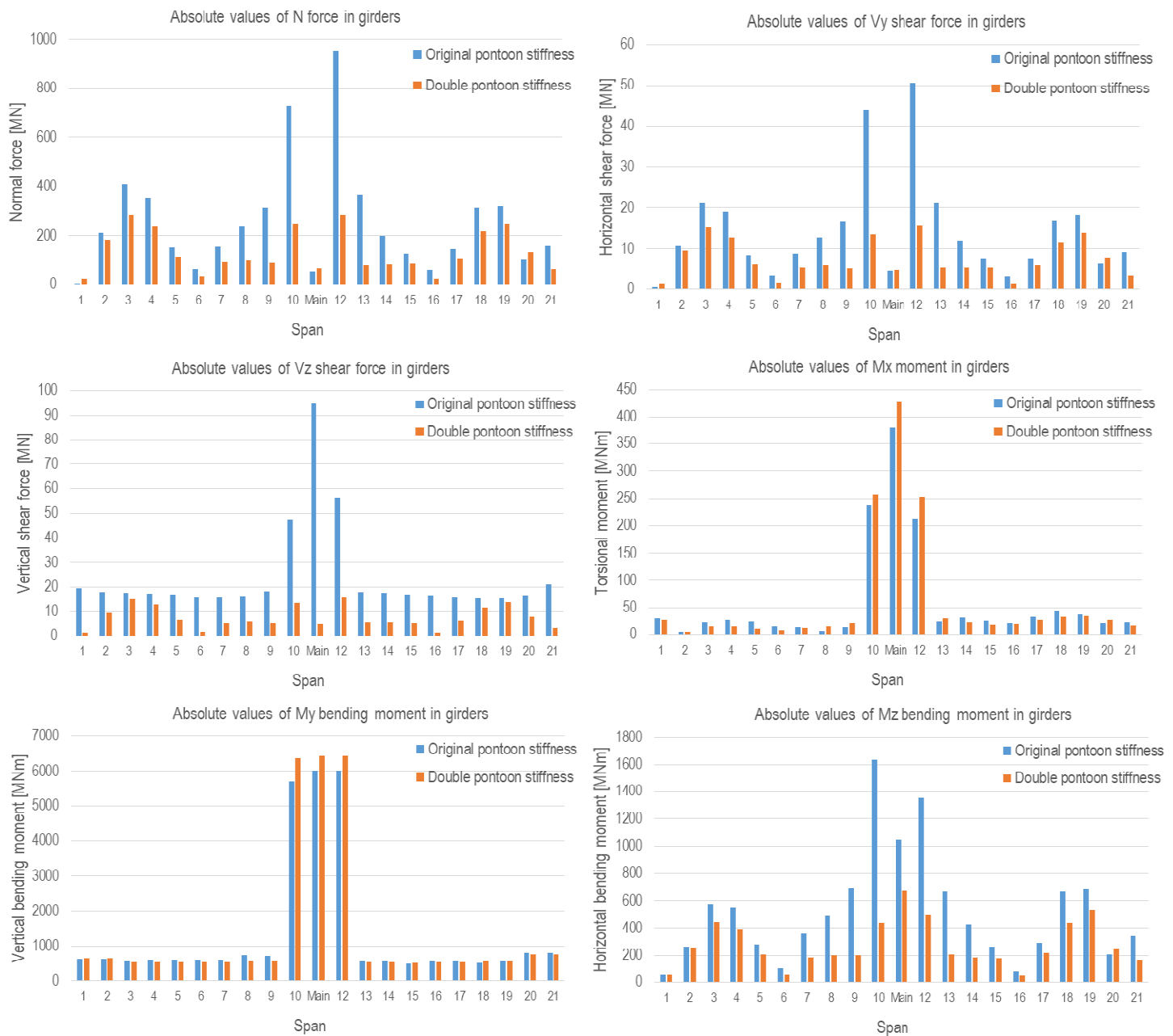


FIGURE 6.10: GLOBAL FORCES AND BENDING MOMENTS IN THE GIRDERS UNDER ULS STORM DEFORMATIONS WITH DOUBLE PONTOON ROTATIONAL STIFFNESS. FROM TOP TO BOTTOM: N FORCES, MY AND MZ BENDING MOMENTS.

Global forces in the bridge girders were again calculated using Scia model #3. Figure 6.10 displays the global normal forces and My and Mz bending moments. Most global forces in the girders under LC4 are significantly lower for a two times higher pontoon rotational stiffness. The maximum global axial force in a bridge girder is 286 MN, in the girders adjacent to the main span. This is 70% lower compared to the axial force with original pontoon stiffness. Maximum Mz bending moment is 674 MNm, which is 59% lower than the original value.

With a maximum value of -6429 MNm, the maximum My bending moment is 7% higher than the maximum horizontal bending moment under the original pontoon stiffness. For the whole bridge My bending moments values change little. It is expected this is due to the governing nature of vertical loads (the unchanged self-weight) over imposed deformations. The results for all global forces on the bridge girders for double pontoon rotational stiffness are given in Annex L.



**FIGURE 6.11: ABSOLUTE VALUES OF GLOBAL FORCES AND BENDING MOMENTS IN THE GIRDERS FOR BOTH ORIGINAL PONTON ROTATIONAL STIFFNESS AND DOUBLE PONTON ROTATIONAL STIFFNESS**

Figure 6.11 compares global forces in the girders under a ULS storm with the original pontoon rotational stiffness and with double pontoon rotational stiffness. The amount of change in global forces in the girders varies. With higher pontoon rotational stiffness, normal and shear forces decline significantly for most spans. Mz bending moments decrease significantly, although not in every span. Mx bending moments and My bending moments in the girders do not change significantly when the rotational stiffness of the pontoons is doubled.

## 6.7.2 Forces and bending moments in truss members under reduced storm deformations

Using Scia model #2, the same four locations were evaluated for the forces and bending moments in individual members, but now for member forces under a ULS storm with double pontoon rotational stiffness. The results are given in tables 6.3 and 6.4.

**TABLE 6.3: FORCES IN INDIVIDUAL MEMBERS IN MAIN SPAN GIRDER UNDER REDUCED STORM DEFORMATIONS**

Members at support	Member # in Scia model	N [MN]	My [MNm]	Mz [MNm]	Stress [N/mm <sup>2</sup> ]
Chord top right	B6807	76.56	-15.83	18.58	151
Chord top left	B6806	53.73	-13.00	-11.40	105
Chord bottom right	B6022	-160.52	-24.40	-35.39	205
Chord bottom left	B6023	-151.78	-19.16	8.62	167
Brace right	B5855	-12.40	-0.40	-3.11	89
Brace left	B5857	-8.15	-0.10	-0.66	44
Brace top	B5823	5.77	0.34	0.89	48
Brace bottom	B6077	-13.62	-4.10	-0.32	142
Members at mid-span	Member # in Scia model	N [MN]	My [MNm]	Mz [MNm]	Stress [N/mm <sup>2</sup> ]
Chord top right	B6031	-116.37	38.81	6.90	190
Chord top left	B6030	-184.86	39.70	4.80	270
Chord bottom right	B6026	73.92	4.74	2.22	196
Chord bottom left	B6027	38.42	4.15	1.21	108

**TABLE 6.4: FORCES IN INDIVIDUAL MEMBERS IN SIDE GIRDER BETWEEN PONTOONS #13 AND #14 UNDER REDUCED STORM DEFORMATIONS**

Members at support	Member # in Scia model	N [MN]	My [MNm]	Mz [MNm]	Stress [N/mm <sup>2</sup> ]
Chord top right	B6526	19.73	-9.59	-1.39	190
Chord top left	B6527	22.73	-5.62	2.69	166
Chord bottom right	B6531	-28.83	-7.33	1.57	208
Chord bottom left	B6530	-2.27	-4.66	0.02	60
Brace right	B6420	-4.65	-0.17	-0.85	174
Brace left	B6419	-4.19	-0.12	-0.65	146
Brace top	B6528	-0.75	0.14	0.01	41
Brace bottom	B6525	-4.09	-1.94	-0.02	263
Members at mid-span	Member # in Scia model	N [MN]	My [MNm]	Mz [MNm]	Stress [N/mm <sup>2</sup> ]
Chord top right	B6812	-9.07	3.16	0.11	74
Chord top left	B6811	-8.97	2.96	-0.19	72
Chord bottom right	B6814	14.37	0.29	-0.29	70
Chord bottom left	B6813	10.79	0.21	-0.57	55

The results again vary significantly between different members. Compared to tables 6.1 and 6.2 the overall magnitude of forces is similar. Maximum forces and moments have however relocated to different members. The peak forces in members have become significantly smaller. Normal forces in the considered members range from -185 MN to 77 MN, a reduction of 22% compared to the force peaks in tables 6.1 and 6.2. Bending moments range from -35 MNm to 40 MNm.

### 6.7.3 Stress levels under reduced storm deformations due to increased pontoon rotational stiffness

With higher pontoon rotational stiffness member stress peaks were greatly reduced. With double pontoon rotational stiffness, most member stresses in LC4 lay between 50 and 200 N/mm<sup>2</sup>. The highest stress peak in the truss girder was reduced to 293 N/mm<sup>2</sup>, a reduction of 50%. See figure 6.12. The unity check for stability is 0.67.

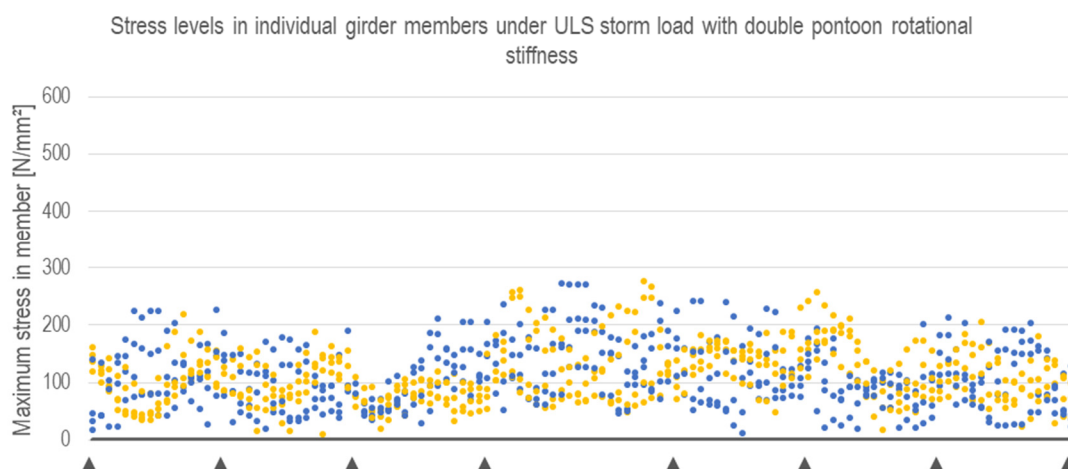


FIGURE 6.12: STRESS LEVELS IN INDIVIDUAL TRUSS MEMBERS ALONG THE SPANS UNDER REDUCED STORM DEFORMATIONS. STRESSES IN CHORDS ARE INDICATED IN BLUE, STRESSES IN BRACES ARE INDICATED IN YELLOW.

## 6.8 Discussion

As a whole, the Sognefjord bridge deforms homogeneous, but differences in deformations between adjacent pontoons cause force peaks in the girders that would normally not occur. Lateral deformation differences range from 2.2 to 3.2 m for the considered spans. The relative small scale of these deformation differences makes predicting and controlling imposed forces on girders challenging. On the scale of a 4.5 kilometre long bridge, a 3 m displacement is small.

Stress levels differ strongly between individual members. In some members, deformations in different degrees of freedom add up to the load, in others they balance each other out. Foreseeing one particular stress level in one particular member, under a certain load, is very difficult. Only one load situation was considered in this research, and with many different load situations stress levels could change significantly in other situations. It is strongly recommended to investigate other load situations in further research.

Furthermore only the 7 center spans of the Sognefjord bridge were investigated. As imposed deformations differ per span, it is recommended that in further research all spans of the superstructure are fully modelled and checked. The severest load situation (ULS storm) and spans with the largest deformations were investigated. It is therefore expected that the result in this research are representative for this stage of design.

## 6.9 Conclusion

This chapter investigated the effects of storm displacements of the Sognefjord bridge on its bridge girders. In the original bridge design, imposed loads on the girders are too high for the current design to withstand. The rotational stiffness of the pontoons can be increased. When the rotational stiffness of the pontoons is doubled, deformations imposed on the bridge girders decrease significantly. This results in lower member forces and member stresses in

the girder. Maximum member stress in the superstructure becomes  $293 \text{ N/mm}^2$ , resulting in a unity check for stability of 0.67. The truss girder design is then structurally feasible for a ULS storm situation.

A clear causal inference between storm loads and individual member forces cannot be distinguished. It is not possible to make reliable predictions for the bridge girder behaviour under other load situations. Research into girder behaviour under other load situations is therefore needed.

Managing the deformations imposed on the bridge girders is very challenging. One pontoon accidentally could displace differently from the others, because of a single big wave for example. This could immediately cause relative displacements that are too large for the girder to withstand, which would risk the structural integrity of the bridge. It is recommended to design the superstructure taking a safety margin for member stress into account.

## 7. INVESTIGATING SHIP COLLISION

A major threat when considering feasibility of the Sognefjord bridge is collision with a marine vessel. A preliminary investigation of impact of a ship with a pontoon of the Sognefjord bridge was therefore conducted.

This was done by first researching the amount of displacement of the bridge under a ship collision event. To do this, an energy balance model was made. With the results of this, the consequences of a ship collision event for the structural integrity of the bridge were discussed. The focus of the ship impact analysis lay on the bridge girder and the buoyancy of a broken pontoon.

In the energy balance analysis, the design ship impact as defined in chapter 2.5 was used. This is a bulk carrier of 40,000 T, colliding with a speed of 6.2 m/s, yielding an impact energy of 781 MNm. The calculations were made by programming an energy balance calculation in the Python script language.

### 7.1 Modelling ship impact

Ship impact is a complex dynamic phenomenon, in which normally large plastic deformations occur. Because the Sognefjord bridge is floating, the stiffness of the bridge under a ship collision event is difficult to predict. A complete impact analysis was considered too laborious for the preliminary design stage. It was therefore decided to simplify the model.

The analysis was done by writing a numeric approximation in Python code and making a large number of energy-displacement calculations at small time steps. This was done by assuming a combined pontoon-ship mass after impact, taking into account energy dissipation through plastic ship bow deformation. At each time step, the energy dissipating by the drag of the seawater and by the displacement of the bridge girder was calculated. Then the kinetic energy of the system was reduced by the dissipated energy, until it reached zero. By making the time steps sufficiently small (10 milliseconds), in this way the total displacement and rotation of the pontoon could be calculated.

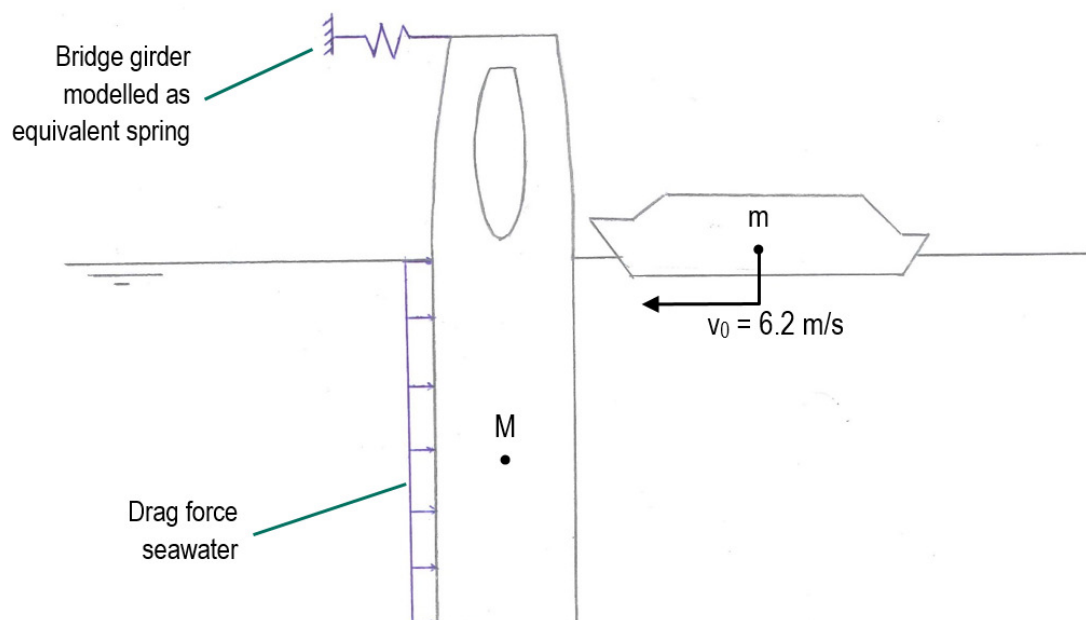


FIGURE 7.1: SHIP IMPACT MODEL SCHEMATISATION

See figure 7.1 for a sketch of the calculation approach. For a full explanation on the analysis set-up and numeric method, refer to Annex M. The Python script written for this analysis can also be found here.

In the energy model, only a single pontoon (the pontoon next to the fairway) was considered. See figure 7.1. On the top of the pontoon, the bridge girder was replaced by an equivalent spring. In a collision event, the seawater will resist movements of the pontoon. This was modelled by incorporating the drag force of the water on the pontoon.

To simplify the model, it was chosen to not take the anchoring cables into account, since determining an equivalent cable stiffness was not feasible. Since the cables will likely have a large effect on reducing pontoon displacement, this is a very conservative simplification. Likewise, the pontoon was assumed to not rotate, which means the rotational stiffness of the pontoon would not be activated. For a first preliminary investigation however, these conservative simplifications were deemed acceptable.

It was expected that the ship hull (made of steel plates) would deform drastically and that the pontoon (a thick concrete buoy) would deform less significant (DNV-RP C204, 2010). Through the deforming ship hull, impact energy will dissipate. Based on the study by (Engseth and Wasjø, 2016) the initial dissipated energy was set at 175 MJ. As a conservative simplification, the pontoon was assumed to not deform at impact.

Only the most severe collision case was regarded: head-on bow collision between a large ship and one of the pontoons at the edge of the fairway. It was assumed that if the bridge is sufficiently strong for this impact case, it will be feasible for other cases as well. Other loads, such as wind loads, wave loads and traffic loads, were not considered in this analysis. In future ship impact research, it is however recommended these loads are taken into account as well.

## 7.2 Ship collision analysis results

It was found that the maximum displacement of the pontoon in a ship collision event was 6.9 meters. The impact duration was 4.5 seconds. See figure 7.2. In a collision event, the pontoon is expected to be towed (partly) back to its original position by the rest of the bridge structure. In this preliminary study however, the focus was on forward displacement only.

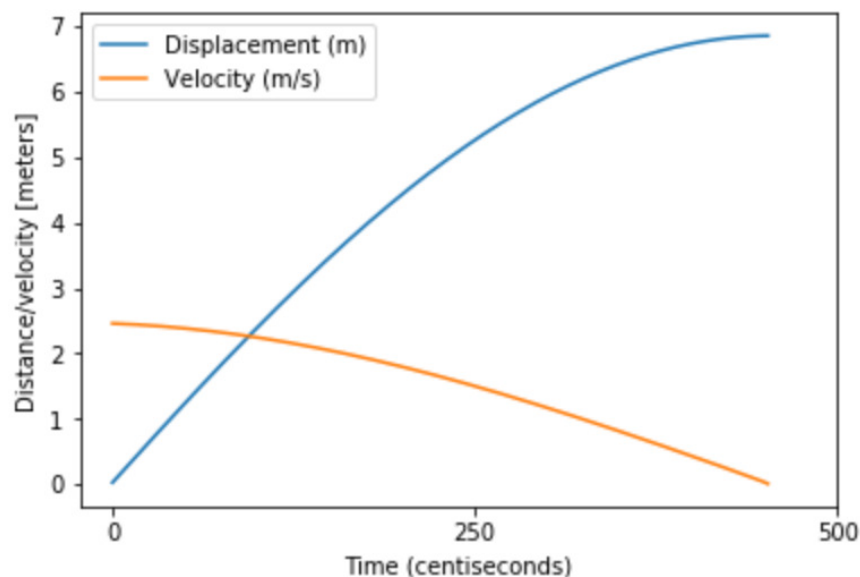


FIGURE 7.2: DISPLACEMENT AND VELOCITY RESULTS FROM THE IMPACT ANALYSIS



### 7.3 Bridge behaviour under impact

In chapter 6 it was found that lateral displacements in the range of 3 m were too large for the truss girder to take up. An almost 7 m displacement of one pontoon at ship impact is therefore problematically high. Pontoon displacements of this scale will result in the loss of structural integrity of the bridge girder.

However, in the model it was assumed only the hit pontoon would displace, while other pontoons would stay in place. In real-life however, upon ship impact, the displacing pontoon will drag the rest of the Sognefjord bridge along. See figure 7.3. This would activate a very large amount of water drag that was not yet taken into account. The anchoring cables are expected to suppress pontoon movement as well. This will significantly reduce the movement of the pontoon, possibly preventing collapse of the Sognefjord bridge. The exact amount of reduction will have to be determined in more precise research, though.

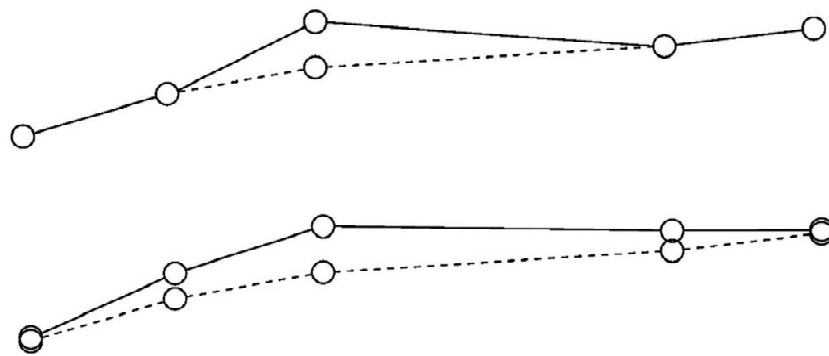


FIGURE 7.3: ONLY ONE PONTOON DISPLACING UPON IMPACT (TOP), OR OTHER PONTOONS GETTING DRAGGED ALONG (BOTTOM)

### 7.4 Dynamic response under impact

$T_{\text{impact}}/T_{\text{pontoon}}$  is about 0.5. According to Biggs (1964), this leads to a dynamic load amplification factor of 1.2. Because the impact duration lies far from the eigenperiods of the pontoon (see Annex N), resonance of the pontoon from ship impact is not expected to occur.

In a ship collision event, one lateral anchoring cable will be further tensioned by the displacing pontoon, while the other cable will be temporary unloaded. When the latter cable again deflects to its self-weight curve, it will be subjected to a large sudden impulse load from being reloaded by its self-weight.

The shortest lateral anchoring cable at the main span pontoon is 171 m. The maximum allowed strain for this cable therefore is 0.6 m ( $\epsilon_{\text{max}} = 3.5\%$ ). A larger displacement will result in forces large enough to make the cable snap. The pontoon displacement under ship impact is therefore a large concern for the lateral anchoring cables. It is therefore strongly recommended to incorporate the anchoring cables in further ship collision research.

### 7.5 Pontoon buoyancy under impact

It was suspected that in a collision event, the major amount of plastic deformation will occur in the ship hull. Even then, the concrete pontoons are likely to crack though. The pontoons are however not allowed to sink. It was therefore decided to divide the pontoons in compartments. In this way, instead of the whole pontoon sinking, only a small part of the pontoon would flood with water. In this way the buoyancy of the pontoon would be limitedly effected only.

The buoyancy of a pontoon with compartments was investigated. For this an indicative design of a pontoon compartment layout was made. This consisted of a 'ring' of compartments in the pontoon, which was 20 m in height and had its centre at 5 m below sea-level. This abides the Eurocode guideline for ship impact area. See figure 7.4.

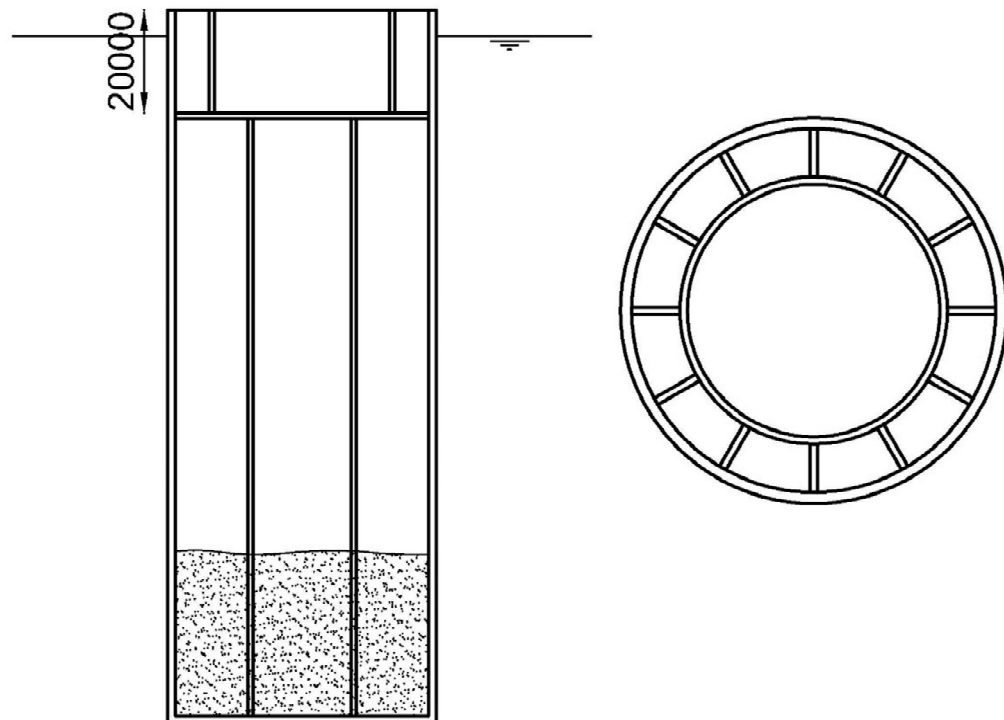


FIGURE 7.4: PRELIMINARY DESIGN FOR COMPARTMENTATION OF A PONTOON

Then, the pontoon buoyancy before impact and the buoyancy after impact (with two flooded compartments) were calculated. It was found that if two compartments would flood from a collision event, the pontoon would sink 2.4 m, or 1.8% of its total submerged length. See Annex M for the calculations made. In chapter 6, it was found that for vertical forces in the bridge girders, girder self-weight was governing. Indeed, a change in the imposed vertical deformation of this magnitude showed insignificant changes in global forces in the girders. A deflection of 2.4 m of one pontoon was therefore deemed acceptable.

By this, compartmentation of the pontoons was deemed a sufficient measure for ship collision protection of the pontoons. It was also concluded that local pontoon failure will not pose a threat to overall Sognefjord bridge feasibility.

## 7.6 Conclusions

In a ship collision event the Sognefjord bridge could lose its structural integrity, with catastrophic results. In this chapter a preliminary investigation in maximum displacement of the bridge under ship impact was therefore conducted.

The lateral displacement of a pontoon upon ship impact was found to be higher than what is acceptable for the bridge girder. If one pontoon would displace 6.9 m relative to the others, global forces on the adjacent bridge girders would become higher than what the girders can withstand. However, multiple conservative simplifications were made in the model used. It is expected that with more precise and realistic modelling, the bridge displacement upon ship impact will be lower. It is recommended in further research to elaborate modelling. It is furthermore recommended to investigate other collision events, such as sideway collision, as well.

---

When the pontoon displaces from ship impact, the lateral anchoring cables could be unloaded and reloaded. The impulse coming from the reloading could make the cable snap. This is a severe concern for the bridge feasibility that needs to be addressed.

It is expected that the pontoon and superstructure will plastically deform upon impact. When the pontoons are divided into compartments, they will deflect little after ship impact. However, any broken pontoons should still need to be fixed. The same holds for the bridge girders. A bridge repair design is outside the scope of this research, but it is recommended that in further research this is investigated.

## 8. BRIDGE DYNAMICS

In previous research, dynamic effects on the whole Sognefjord bridge had not been taken into account. However, because of its floating nature, the Sognefjord bridge is prone to dynamic response. A preliminary analysis of dynamic behaviour was therefore made.

Due to the complexity of the Sognefjord bridge structure, a full dynamic analysis would be laborious enough to devote a complete thesis research in itself to. Therefore it was decided to limit the analysis to investigating possible dynamic behaviour and ways to address this.

Furthermore an analysis of eigenfrequencies of bridge components was conducted. The results from this analysis were compared with frequencies of dynamic loads, to investigate threats of resonance effects.

### 8.1 Possible dynamic behaviour

Dynamic loads on the Sognefjord bridge are the wind, wave, traffic and current loads. Because of the extreme slenderness of the cables, the largest dynamic risk was expected in the anchoring system. Under the steady current, vortex-induced vibrations of the cables can arise. The bridge girder could show a dynamic response to the wind load and flow of traffic. If these loads would occur in the girder's natural frequency, heavy swaying of the girder could occur. The pontoons could show a dynamic response if the wave load is in the same frequency as the eigenfrequency of the pontoon. Furthermore, theoretically vortex-induced vibrations of a pontoon might occur under the steady current as well.

In the Sognefjord bridge, a part that is displacing under a dynamic load could drag its adjoining parts along. Bridge components could therefore be excited by other components as well. The Sognefjord bridge could also show a dynamic response as a whole. Summarising, the following dynamic responses are considered:

- Vortex-induced vibrations of the anchoring cables
- Resonance of the pontoons
- Resonance of the superstructure
- Resonance of sub-structures of the Sognefjord bridge
- Resonance of the Sognefjord bridge as a whole

The Sognefjord bridge could also show a dynamic response in ship collision event. This is discussed in chapter 7 and will not be further discussed in this chapter.

### 8.2 Eigenfrequency analysis modelling

In predicting a dynamic response, eigenfrequencies are very instructive. When the natural frequencies of a structure are known, they can be compared to the load frequencies to check for any risk of resonance.

However, conducting a full dynamic analysis to find all the natural frequencies of the bridge would be outside the scope of this research. Therefore, natural frequencies of individual components of the Sognefjord bridge were calculated using Scia Engineer. See figure 8.1 For every component, a separate model was made in Scia Engineer. In these models, the components considered were copied from the Scia model #1 of the whole Sognefjord bridge. As boundary conditions, the rest of the Sognefjord bridge was replaced by a set of equivalent springs. See Annex N for more on this.

The following bridge components were analysed:

- Main anchoring cable
- Longest side anchoring cable (at pontoon #1)
- Both lateral anchoring cables at mid-span (pontoon #11)
- Pontoon #11 (largest pontoon)
- Pontoon #1 (smallest pontoon)

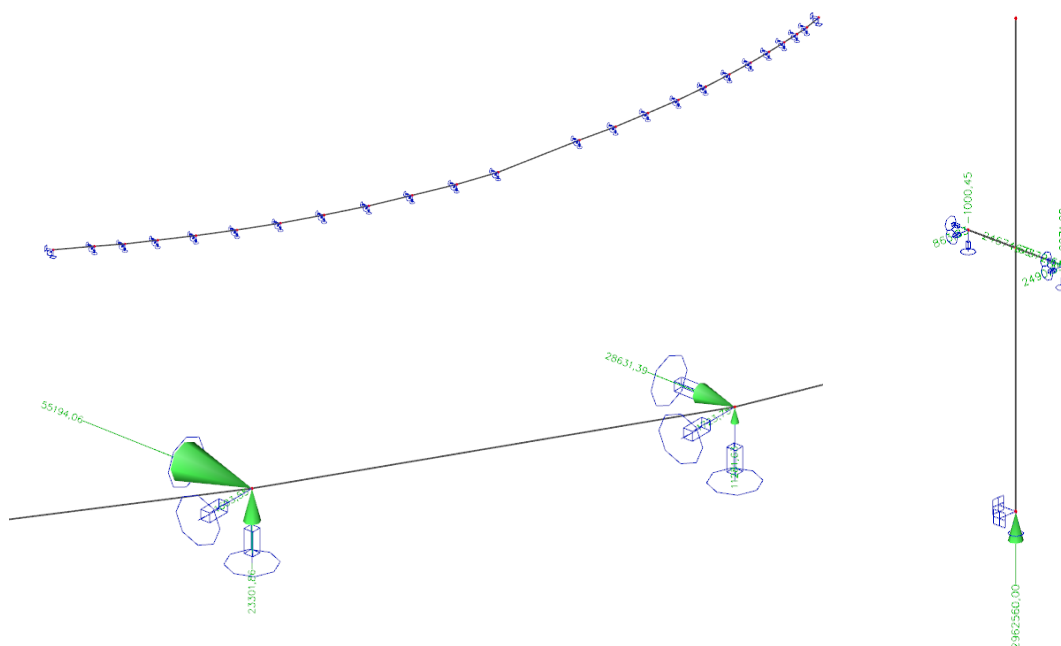


FIGURE 8.1: EIGENFREQUENCY ANALYSIS MODELLING OF CABLES (LEFT) AND PONTOONS (RIGHT)

### 8.3 Eigenfrequency analysis results

In table 8.1, the first two eigenperiods of each component are given. A list of the first 10 eigenperiods of the considered bridge components can be found in Annex N.

TABLE 8.1: FIRST TWO EIGENPERIODS OF DIFFERENT BRIDGE COMPONENTS

Part of the bridge	First eigenperiod [s]	Second eigenperiod [s]
Main anchoring cable	112.3	84.4
Longest side anchoring cable	1123.9	1123.9
Long lateral cable at pontoon #11	167.6	167.5
Short lateral cable at pontoon #11	46.0	44.6
Largest pontoon	61.3	24.6
Smallest pontoon	102.3	20.8

The anchoring system is subjected to current and wind wave loads. Besides these loads the pontoons have to resist wind loads as well. As chapter 2.3 indicates, the periods of wind waves are around 5 seconds. Of the longest anchoring cables, the first ten eigenperiods were found to be much higher than this. Therefore for these components, wave loads were not expected to pose dynamic threats.

However, the short lateral anchoring cable at pontoon #11 and the considered pontoons showed to have eigenperiods in the same range as wind wave loads. Despite these results resonance was not considered a threat. However, to eliminate all concerns more investigation is needed.

### 8.4 Vortex-induced vibrations

When an object is placed in a steady flow, turbulent flows can arise, causing vortex-induced vibrations of the object. See figure 8.2. VIV could occur in bridge girder members under wind flows and the pontoons and the anchoring cables under current flows. Especially for the very slender anchoring cables VIV is a serious concern, causing

possible fatigue failure of the cables. VIV could lead to resonance of the cables when the frequency of the turbulent flow is close to the eigenfrequency of the cable. It is strongly recommended to check this in further research.



FIGURE 8.2: TURBULENT FLOW BEHIND AN OBJECT IN A STEADY CURRENT, CAUSING VIV

### 8.5 Reducing dynamic effects

Multiple measures to reduce the effects of dynamic behaviour exist. A preliminary qualitative analysis was conducted, to obtain an image of ways to address dynamic behaviour problems. The following measures to reduce dynamic behaviour in the Sognefjord bridge were investigated:

- Adding mass to members
- Placing elastomeric bearings between bridge components (see figure 8.3)
- Instalment of tuned mass dampers in the bridge
- Placement of buoyancy elements in anchoring cables to reduce cable tension
- Instalment of viscous dampers in the bridge (see figure 8.4)
- Member geometry optimisation

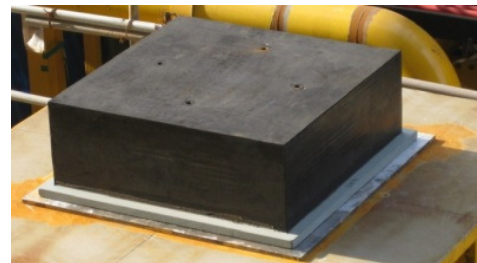
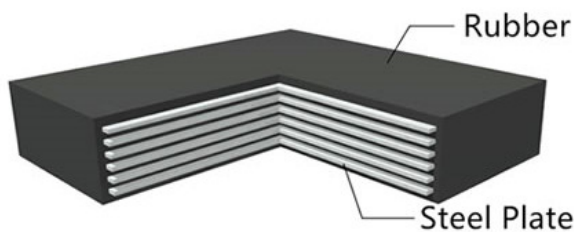


FIGURE 8.3: ELASTOMERIC BEARING

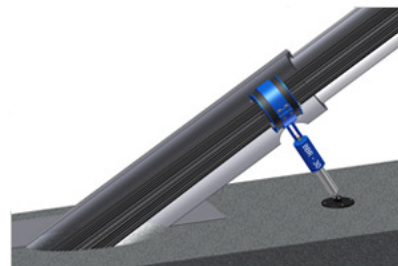
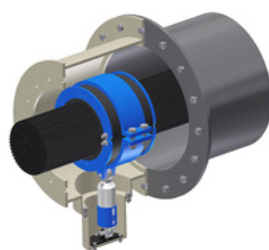


FIGURE 8.4: VISCOUS DAMPER

Each measure was investigated for its effectiveness in reducing dynamic effects, its structural feasibility, required maintenance and costs. Annex N elaborates on these evaluations.

For each measure a score of 1 (bad) to 5 (good) was given for each criterion. These scores were estimates, however, these were based on engineering experience and best practices in the field and considered to be sufficient for this stage of design. In table 8.2 the scores are displayed. In Annex N a list of comments on these scores is given for reference.

**TABLE 8.2: MULTI-CRITERIA ANALYSIS FOR MEASURES IN REDUCING DYNAMIC EFFECTS**

Measure	Reducing dynamics component	Reducing dynamics bridge	Structural feasibility	Maintenance intensity	Costs	Total score
Adding mass elements	3	3	2	5	1	14
Tuned mass damper	3	2	3	4	3	15
Reducing cable tension	2	1	2	5	5	15
Adding viscous dampers	4	4	4	5	3	20
Elastomeric bearings	2	4	5	4	4	19
Adjusting member geometry	4	2	4	5	4	19

In the analysis, using viscous dampers and elastomeric bearings in the bridge were found to be the best options to mitigate dynamic effects. For VIV in the anchoring cables, helical strakes (named under 'adjusting member geometry' was found an efficient measure. Viscous dampers could decrease resonance. Elastomeric bearings would up to a certain degree allow members to displace freely without affecting each other. By this, the effect of the interconnected floating nature of the bridge would be reduced. Helical strakes could significantly decrease the vibrations of cables under turbulent flows.

## 8.6 Conclusions

A full dynamic analysis was not the scope of this research. This chapter was limited to a first analysis of dynamic responses and mitigating measures. Resonance of individual bridge components is not expected to occur in the bridge. Vortex-induced vibrations are deemed a risk, especially for the anchoring cables. Further research is needed to get more exact results. Optimising the cable cross-section geometry could be a feasible way to mitigate VIV of the anchoring cables.

Insight in the eigenmodes of the whole Sognefjord bridge is still needed to have full insight in dynamic threats. It is recommended that a full study into this is to be performed. Vortex-induced vibrations need to be further researched as well, especially for the anchoring cables. As this chapter suggests, there are ways to mitigate the dynamics risks. The effect of these measures on reducing dynamic response of bridge components needs to be incorporated in further research.



## 9. MAIN CONCLUSIONS FROM RESEARCH

In chapter 1, the following research sub questions were presented:

- **What behaviour (displacements and rotations) can be expected from a bridge structure like this in conventional load situations?**
- **What loads can be expected in the superstructure of the Sognefjord in conventional load situations?**
- **Is there a risk of structural collapse of the Sognefjord bridge in a ship collision event?**
- **Can hazardous dynamic behaviour of the Sognefjord bridge be expected?**

The answers to these questions gave the knowledge required to answer the main research question:

**Is creating a continuous girder without internal hinges for the Sognefjord buoyancy bridge feasible?**

This chapter presents the main conclusions drawn in this thesis research and answers the research questions defined above.

### 9.1 Creating a continuous girder without internal hinges for the Sognefjord bridge

In chapter 5, increasing rotational stiffness of the pontoons was found a structurally feasible option in decreasing bridge deformations. By doubling the rotational stiffness of the pontoons, displacements and rotations of the Sognefjord bridge reduce by 44% maximum. This would make creating a continuous bridge girder without internal hinges for the Sognefjord buoyancy bridge structurally feasible for a 100-year ULS storm.

The feasibility of the continuous girder concept was investigated for one load situation only. Because a ULS storm is the severest storm situation, it is expected that the continuous superstructure concept will be feasible in other load situations as well.

Deformations imposed on the superstructure depend on the deformation differences between adjacent pontoons, which differ from global bridge deformations. Because of the 10 times smaller scale, deformation differences between adjacent pontoons do not necessarily reduce when global bridge deformations reduce. Stresses in the superstructure are therefore not necessarily lower in other load situations. The feasibility of a continuous bridge girder is therefore only completely proven when more load situations are researched.

To make the superstructure concept feasible in a ULS storm situation, the rotational stiffness of the pontoons would have to be doubled. The pontoons compose of 92% of the total mass of the bridge. Doubling this mass would significantly increase costs of construction. It has to be decided whether these costs are worth the benefits.

Concluding, creating a continuous bridge girder without internal hinges for the Sognefjord buoyancy bridge is structurally feasible. This was found for a ULS storm situation, and therefore it is expected that it will be feasible in other situations as well. More research and design work for this other load situations needs to be done however. Moreover, to make a continuous bridge girder feasible the rotational stiffness of the pontoons needs to be increased, which comes with great costs.

### 9.2 Behaviour of the Sognefjord bridge in conventional load situations

Bridge deformations under six different load situations were investigated. The maximum lateral displacement of the Sognefjord bridge is 27 meters, while the maximum longitudinal displacement is 46 meters. These values were deemed acceptable.

For the severest load situation, a ULS storm, the influence of different bridge parameters on bridge deformations was investigated. In figure 9.1, the sensitivity of lateral bridge displacements at mid-span to every parameter is displayed. Three parameters mainly influence bridge behaviour. These are in order of magnitude the wind loads, the rotational stiffness of the pontoons and the axial stiffness of the anchoring cables. A two times higher rotational stiffness of the pontoons leads to a maximum reduction in lateral bridge displacements of 44%. The stiffness of the superstructure was found to have only minor effect on bridge behaviour.

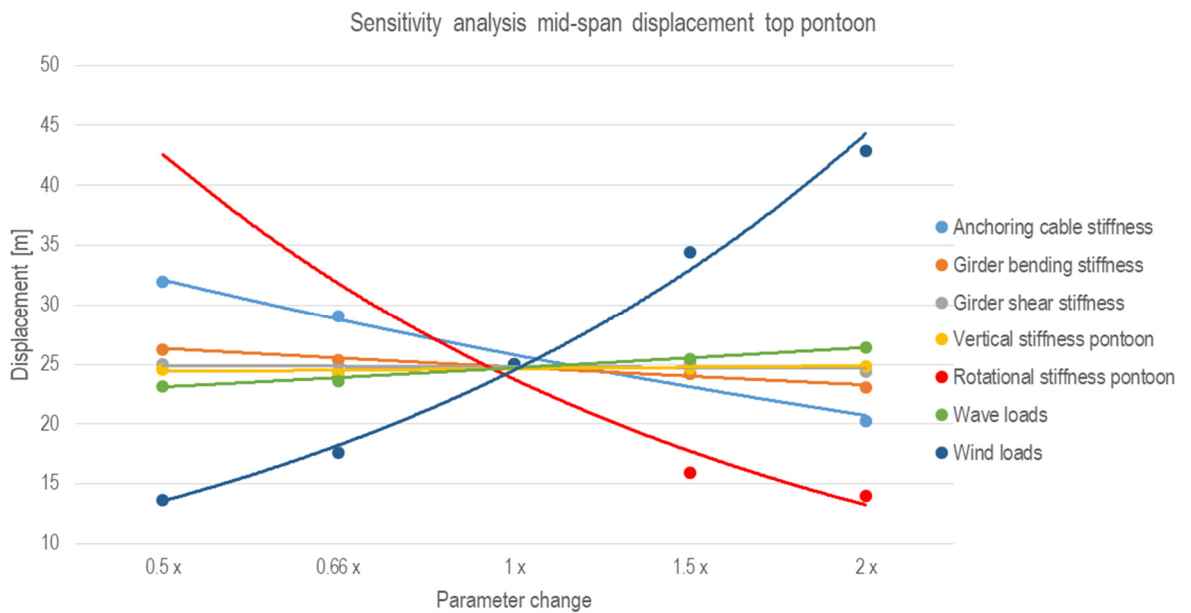


FIGURE 9.1: PARAMETER SENSITIVITY ON LATERAL DISPLACEMENTS OF THE BRIDGE AT MID-SPAN. THE STEEPER THE CURVE, THE BIGGER THE INFLUENCE OF THE PARAMETER ON DISPLACEMENTS.

No single part of the bridge structure is fixed and the loads can be diverse. A wide range of deformations under different load situations therefore exists. See figure 9.2. This increases the difficulty in predicting and managing the behaviour of the Sognefjord bridge compared to a fixed structure.

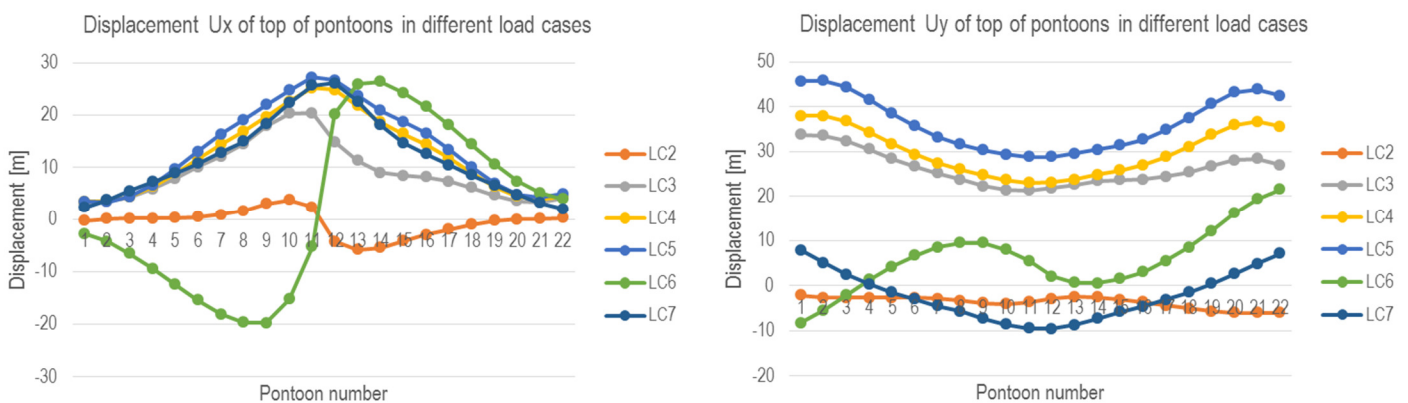


FIGURE 9.2: BRIDGE DEFORMATIONS VARY SIGNIFICANTLY UNDER DIFFERENT LOAD SITUATIONS

In a ULS storm, differences in lateral displacements between adjacent pontoons are around 3 meters. The maximum difference in lateral displacement between adjacent pontoons was 3.2 m. The difference in deformations between adjacent pontoons varies for every span.

### 9.3 Behaviour of the superstructure in conventional load situations

In the superstructure, internal loads were found to be mainly determined by the displacements of the pontoons. The differences in the displacements of adjacent pontoons impose deformations on the girders. See figure 9.3.

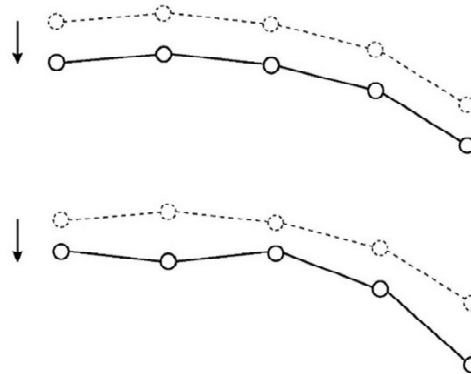


FIGURE 9.3: ALL PONTOONS DISPLACING THE SAME (TOP) OR ADJACENT PONTOONS DISPLACING DIFFERENTLY (BOTTOM). THE LATTER GIVES STRESS IN THE GIRDERS.

Under ULS storm deformations, the stress level is different in every truss member. The maximum member stress in a ULS storm was 590 N/mm<sup>2</sup>, resulting in a unity check for stability of 1.36. See figure 9.4. It is not considered efficient to exactly predict the maximum stress in one particular member, in a particular load situation. It is considered a better approach to define certain boundaries between which stress levels generally are expected to lie.

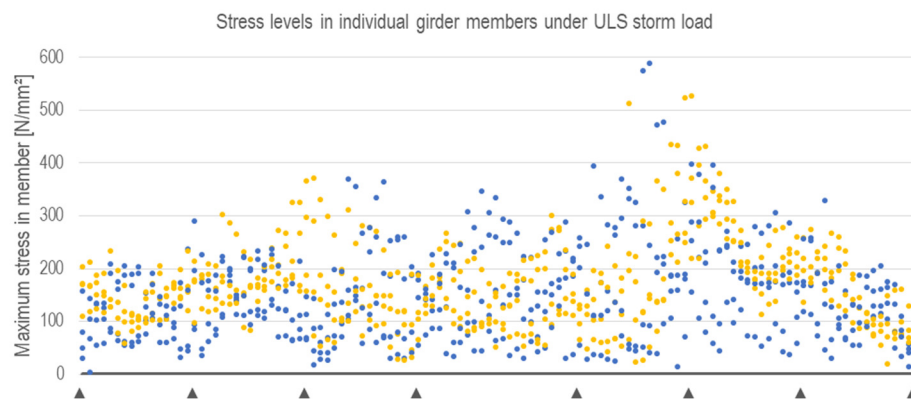
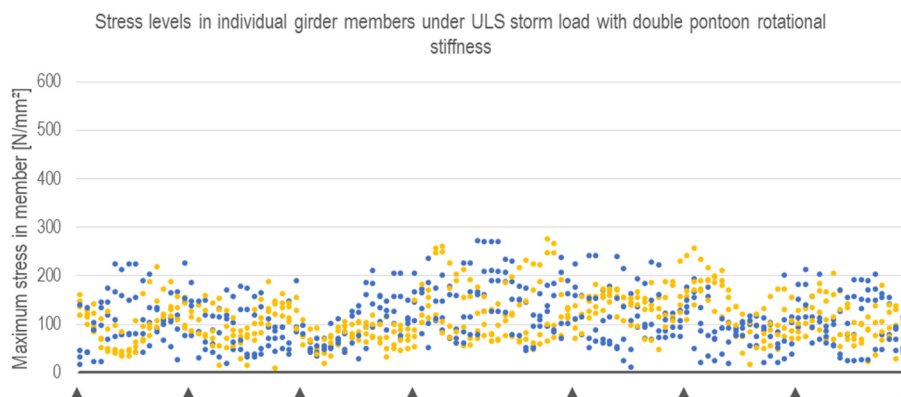


FIGURE 9.4: STRESS LEVELS IN THE TRUSS MEMBERS UNDER ULS STORM. STRESSES IN CHORDS INDICATED IN BLUE, STRESSES IN BRACES INDICATED IN YELLOW.

When the rotational stiffness of the pontoons is doubled, stress levels in the bridge girders generally drop to about half their value. The maximum member stress is then 293 N/mm<sup>2</sup>, a decrease of 50%. The unity check for stability is then 0.67. Stress values become low enough to make the continuous girder concept feasible. The maximum stress peaks relocate to other members. See figure 9.5.



**FIGURE 9.5: STRESS LEVELS IN THE TRUSS MEMBERS UNDER ULS STORM, WITH DOUBLE PONTOON ROTATIONAL STIFFNESS. STRESSES IN CHORDS INDICATED IN BLUE, STRESSES IN BRACES INDICATED IN YELLOW.**

## 9.4 Ship collision and bridge dynamics

In a conservative investigation, a ship collision event was found to give displacements that are problematically large for the bridge girder to withstand. However, it is expected that more precise modelling will lead to less conservative results. An important concern is unloading and reloading of the lateral anchoring cables by the displacing pontoon.

The Sognefjord bridge was also preliminary checked for hazardous dynamic behaviour. It was expected that resonance of individual bridge components would not threaten feasibility of the Sognefjord bridge. Vortex-induced vibration of bridge parts is a concern which needs more investigation. Measures to mitigate dynamic threats are available.

## 9.5 Limitations in this research

In chapter 3 it was found that modelling multiple load-steps in Scia Engineer gives incorrect results. The displacement results for the cable anchoring system in Scia Engineer were too high. The error in the results (about 20%) was deemed high, but manageable, and assuming higher displacements than is actually the case is a conservative approach.

A second limitation in this research was that the truss girder could not be fully modelled without problems of model stability occurring. The part of the superstructure that was modelled was considered representative for the girder behaviour. However, since imposed deformations are different for every bridge girder, all the girders should be modelled to have complete results about the superstructure behaviour.

Furthermore, the truss girder could not be implemented in Scia model #1 of the whole Sognefjord bridge. In this model the truss was therefore replaced by a prismatic beam with equivalent stiffness properties. The full truss girder was modelled separately, where the rest of the bridge structure was replaced by equivalent imposed deformations. These were found correct methods to replace parts of the bridge structure in a model. It is however expected that modelling the complete Sognefjord bridge will give more precise results.

## 9.6 Recommendations for further research

The behaviour of both the Sognefjord bridge as a whole as well as of the superstructure in particular can vary a lot under different load situations. In this research however only six load combinations were considered, of which only one was analysed in-depth. Since it is expected that in some other load combinations the bridge will behave very different, it is recommended to perform more research into bridge behaviour in other load situations.

It is recommended to optimise modelling, so the complete bridge can be modelled correctly. The current modelling was a conservative approach. It is expected that when the limitations discussed in chapter 9.5 are omitted, results will be more accurate and less conservative.

It is expected that pontoon design can be optimised, which would be very effective in decreasing bridge deformations. More investigation into pontoon design is therefore recommended.

Both ship collision and Sognefjord bridge dynamics have been looked upon preliminary only. The results give a first impression, but more research is needed to get complete results. It is recommended this is done in further research.

A number of important bridge aspects still have not been investigated. At both shore ends, the Sognefjord bridge will show large displacements. Special girder solutions will have to be designed to facilitate these displacements. Furthermore, a bridge erection design is still missing. The unprecedented size of this structure will however present large challenges for construction. Both aspects need to be investigated in further research.

The design of the Sognefjord bridge is still in a preliminary stage. Detailed design therefore has not been performed yet. The supports of the superstructure, the connections of the anchoring system to the shores and pontoons and especially fatigue details of the superstructure are large challenges to the structural feasibility of the bridge. It is recommended these are investigated in later research.

## 10. REFERENCES

- Biggs, J.M., *Introduction to Structural Dynamics: Rigorous analysis of one-degree systems*, McFraw-Hill College, 1964.
- Chey, M., Chase, J.G., Mander, J.B., Carr, A.J., *Semi-active tuned mass damper building systems: Application*, Earthquake engineering and structural dynamics, Wiley, 2009.
- DNV-RP-C204: Design against accidental loads*, Det Norske Veritas, 2010.
- DNV-RP-C205: Environmental conditions and environmental loads*, Det Norske Veritas, 2010.
- Engseth, M., Wasjø, K., *Bjørnafjorden submerged floating tube bridge ship impact*, Norwegian Public Road Administration, Oslo, 2016.
- Estes, A.C., Frangopol, D.M., *Minimum expected cost-oriented optimal maintenance planning for deteriorating structures: application to concrete bridge decks*, Reliability Engineering and System Safety, 2001.
- NEN-EN 1337-3: Structural bearings – Part 3: Elastomeric bearings*, NEN, Delft, 2005.
- NEN-EN 1990-A1: Eurocode: Basis of structural design*, NEN, Delft, 2011.
- NEN-EN 1990-A1: Eurocode: Basis of structural design, Dutch National Annex*, NEN, Delft, 2015.
- NEN-EN 1991-1-4: Eurocode 1: Actions on structures – Part 1-4: General actions – Wind actions*, NEN, Delft, 2005.
- NEN-EN 1991-1-5: Eurocode 1: Actions on structures – Part 1-5: General actions – Thermal actions*, NEN, Delft, 2011.
- NEN-EN 1991-1-7: Eurocode 1: Actions on structures – Part 1-7: General actions – Accidental actions*, NEN, Delft, 2015.
- NEN-EN 1991-1-4: Eurocode 1: Actions on structures – Part 2: Traffic loads on bridges*, NEN, Delft, 2015.
- Fang, H., Mao, Y., Liu, W., Zhu, L., Zhang, B., *Manufacturing and evaluation of Large-scale Composite Bumper System for bridge pier protection against ship collision*, Composite Structures, Elsevier, 2016.
- Fjeld, A. et al., *Feasibility study for crossing Sognefjorden – Submerged Floating Tunnel*, Statens Vegvesen, Oslo, 2012.
- Gerritsen, M., *Assessment of structural types for bridging the Sognefjord*, Delft University of Technology, Delft, 2013.
- Granor, *Elastomeric laminated bearings product portfolio*, Granor Rubber & Engineering, Victoria.
- Hansen, M.G., Randrup-Thomsen, S., Askeland, T., Ask, M., *Bridge crossings at Sognefjorden – Ship collision risk studies*, Collision and Grounding of Ships and Offshore Structures, Taylor & Francis Group, London, 2013.
- Hua, J., Chorzepa, M.G., *Evaluation of a Floating Steel Fender System for Bridge Pier Protection against Vessel Collision*, Journal of Bridge Engineering, ASCE, 2016.
- Hermans, R.T.H., *Buoyancy aided Crossing for Bridging Extreme Widths*, Delft University of Technology, Delft, 2014.
- Jakobsen, S.E. et al., *Sognefjorden Feasibility Study of Floating Bridge*, Statens Vegvesen, Oslo, 2013.

- De Jonge, T., Laukeland, L., *Collision between a spar platform and a tanker*, Collision and Grounding of Ships and Offshore Structures, Taylor & Francis Group, London, 2013.
- Larsen, A., Larose, G.L., *Dynamic wind effects on suspension and cable-stayed bridges* *Journal of Sound and Vibration*, Elsevier, 2015.
- Lee, D.A., Taylor, D.P., *Viscous damper developments and future trends*, Tall and Special Buildings, Wiley, 2002.
- Lothe, A.E., Brørs, B., *SINTEF Rapport: Mulighetsstudie for kryssing av Sognefjorden Opedal – Lavik estimat på bølger og strøm*, Statens Vegvesen, Oslo, 2010.
- Maurer Söhne GmbH, *Elastomeric bearing product portfolio*, Maurer Söhne GmbH, Munich, 2012.
- Metrikine, A., *Structural dynamics course, lecture notes*, Delft University of Technology, Delft, 2017.
- Nussbaumer, A., Borges, L., Davaine, L., "Fatigue Design of Steel and Composite Structures", European Convention for Constructional Steelwork, 2011
- Romeijn, A., *Steel Bridges lecture notes*, Delft University of Technology, Delft, 2006.
- Simone, A., *An Introduction into the Analysis of Slender Structures*, Delft University of Technology, Delft, 2011.
- Statens vegvesen - Håndbok N100 Veg- og gateutforming, Statens Vegvesen, Oslo, 2014.
- Spuler, T., Loehrer, R., O'suilleabhain, C., *Life-cycle considerations in the selection and use of bridge expansion joints*, Report 18<sup>th</sup> Congress of IABSE, International Association for Bridge and Structural Engineering, Seoul, 2012.
- Wang, L., Yang, L., Huang, D., Zhang, Z., Chen, G., *An impact dynamics analysis on a new crashworthy device against ship-bridge collision*, International Journal of Impact Engineering, Elsevier, 2008.
- Wang, W., Dalton, D., Hua, X., Wang, X., Chen, Z., Song, G., *Experimental Study on Vibration Control of a Submerged Pipeline Model by Eddy Current Tuned Mass Damper*, Applied Sciences, MDPI, 2017.
- Wei, F., Yuan, W., Chen, B., *Steel Fender Limitations and Improvements for Bridge Protection in Ship Collisions*, *Journal of Bridge Engineering*, ASCE, 2014.
- World Sea Temperatures ([www.seatemperature.org](http://www.seatemperature.org)), requested on 19 June 2017.
- Yip, T., *Long Span Buoyancy Bridge with Submerged Cable Anchoring*, Delft University of Technology, Delft, 2015.



## ANNEX A: BRIDGE CONCEPT FROM PREVIOUS RESEARCH

### A.1 Bridge design from previous study

As mentioned in chapter 2.3, prior to this research, two theses about a feasible fixed-link crossing for the Sognefjord have been submitted. Further optimizing the latest design by Yip (2015) was used as a starting point for this research. The full report of this study can be found under "*Long span buoyancy bridge with submerged cable anchoring*", 2015, by T. Yip. This study in turn started with the research conducted by Hermans (2014) as a background. Then, the design resulting from that study was investigated by Yip and adjusted where found necessary. This annex will give an overview of the properties of the design by Yip. Chapter 2.3.2 discusses conclusions and remarks on this research. The design concept by Yip (2015) is given in figure A.1.

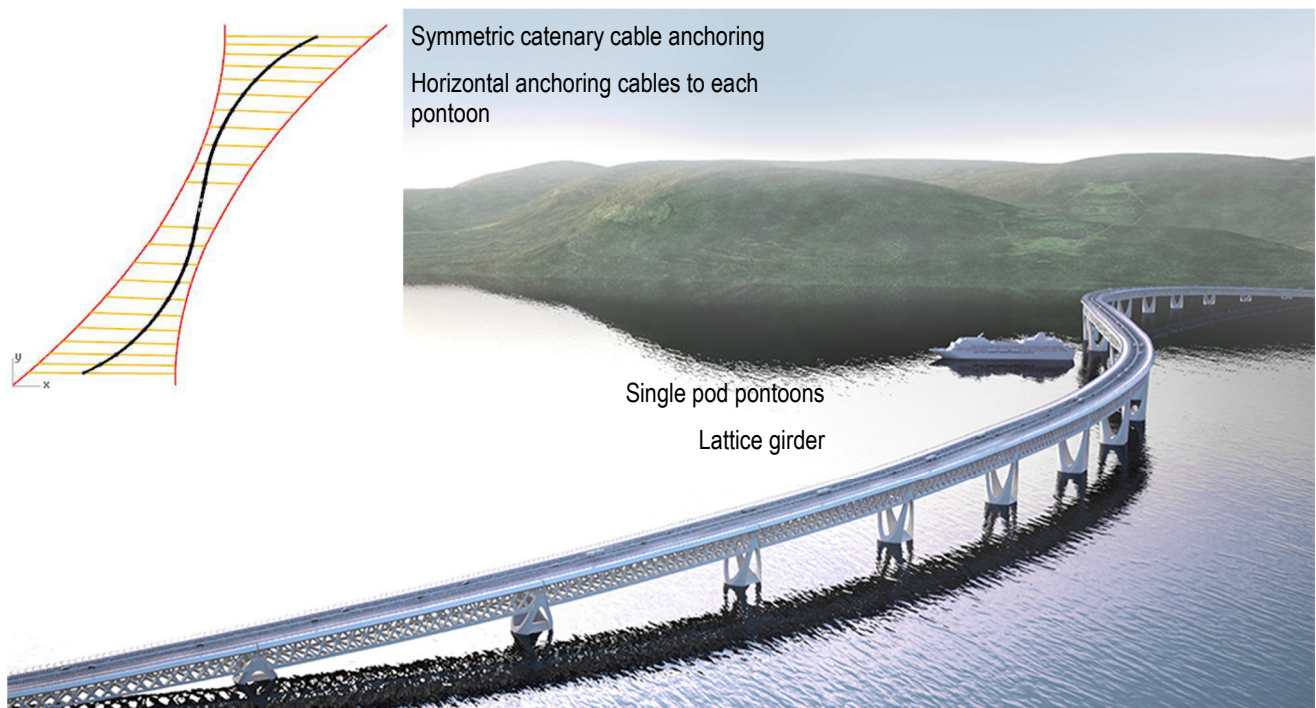


FIGURE A.1: DESIGN CONCEPT FROM REPORT BY YIP (2015)

### A.2 Bridge design by Yip (2015) characteristics

#### A.2.1 New pontoon design

The first thesis on this subject) studied different pontoon layouts (Hermans, 2014). Eventually it was decided on using simple cylindrical spar pontoons for most of the points. However, at the points where the bridge was anchored by cables (at four points), three spars were combined into one tripod, for more rotational stability (which results in lower torsional forces in the superstructure).

The bigger tripods were in both reports considered not aesthetically competing. The heavy bracing would not confirm to the minimalistic design preferred by the architects and also decreased the main span width clearance. Tripods were therefore omitted by Yip (2015), which was decided together with anchoring all pontoons instead of only four (more on that in section A.2.2). For sake of practical simplicity, a spar pontoon shape was introduced. This concept has proven itself in the offshore industry for its dynamic and stability capacities. No further research into pontoon design optimisation was conducted.



FIGURE A.2: PONTON DESIGN FROM YIP (2015)

Furthermore, a form study on the non-submerged top of the pontoons was conducted together with the architects. Starting points for their shape were evoking an image of robustness, transparency and lightness. The eventual choice for pontoons is displayed in figure A.2.

In previous design, the radii of all non-anchored pontoons was 15 m. Yip (2015) adjusted the pontoon radii to loads and displacements of the superstructure (which of course vary along the span). This led to pontoons with radii varying from 12 to 20 m. The latter were the pontoons at the main span, which had to support the biggest span (and thus carry the largest loads).

### A.2.2 Catenary cable anchoring system

Anchoring only four pontoons led to uncertainties and stability issues. Therefore Yip (2015) decided on changing the layout of the anchoring system to a horizontal suspension system (see figure A.3). Since every pontoon is anchored, separate pontoon movements don't need to be transferred through the superstructure, drastically decreasing the forces in this part of the bridge. Also, the risk of colliding tendons is reduced.

Hermans (2014) proposed prestressing the tendons by their own submerged weight, by reducing the sag. Even though Yip (2015) mentions this required tendon prestressing as a negative aspect, in her report prestressing the tendons by their own weight is also proposed.

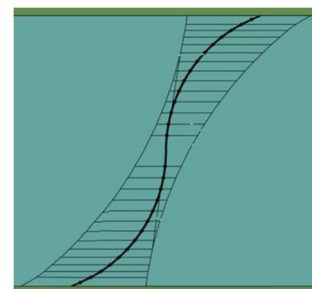


FIGURE A.3: HORIZONTAL SUSPENSION ANCHORING SYSTEM

### A.2.3 Lattice bridge girders

The continuous girder system eventually proposed by Hermans (2014) gave rise to unfavourable properties in construction and response to movements. Furthermore, by adopting a new cable anchoring system, resisting lateral movements of the pontoons through the bridge girder wasn't necessary anymore. Therefore in the research by Yip (2015) it was decided to make bridge girder parts hinged connected to the pontoons, so the effect of pontoon movements will induce less forces into the girders.

Furthermore, an important aesthetical requirement was that the girder was to be a single line, with no parts standing out. Based on this requirement, a suspension bridge, cable stayed bridge or arch bridge concept was ruled out. It was decided that the superstructure would be a lattice girder. Reasons for not investigating a box girder layout without parts standing out were not given.

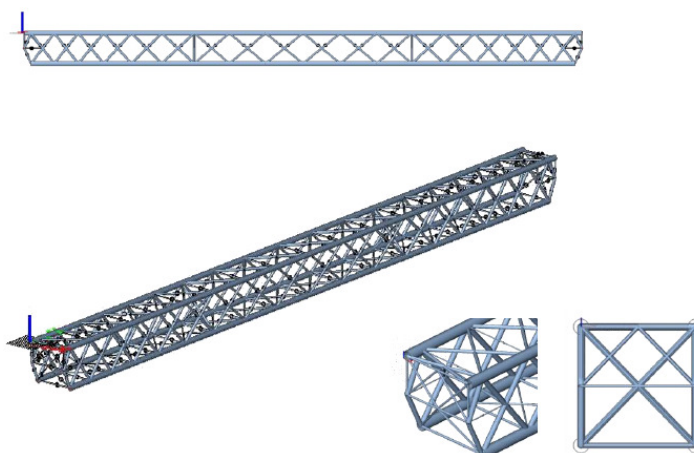


FIGURE A.4: BRIDGE GIRDER LAYOUT FROM YIP (2015)

Because of the large self-weight of concrete, using concrete flanges was ruled out. A lattice girder with steel box girder flanges is mentioned, but not further investigated. After a form finding study, a girder with diagonally crossing braces (in X-shapes) was proposed. To cope with torsional and shear forces, the layout varies along the length of the girder (see figure A.4).

It was decided that bridge girder parts would have to be straight and not curved according to the S-shape, as to not introduce any traffic-induced torsional stresses. This means the bridge S-curve would be built up out of straight pieces, even though the bridge girders are displayed in the architectural renders as being curved. To still accommodate the road curves, a minimum girder width of 23.2 m for the main girder was calculated.

#### A.2.4 Omitting arch action and prestressing of the girder

Hermans (2014) proposed introducing arch action by prestressing the girder, in order to reduce lateral movements. This would make the horizontal girder arch prone to instability and increases the size of the girder. Also, when the arch is actually two arches combined to an S-curve, the effect of arch action would probably be severely less. Therefore prestressing tendons in the girder were omitted in the design by Yip (2015).

#### A.2.5 Bridge joints

In her research, Yip (2015) proposed a first support layout at the top of the pontoons. This design had two components. First of all, a pin in the middle of the bridge girder end was proposed, in order to resist horizontal movements but allow horizontal rotations. Second, two deformable bearing blocks would be placed at the corners of a bridge girder end (see figure A.5). These should transfer vertical forces to the pontoons, but allow for some horizontal rotations and rotations in the vertical plane of the span. It was however commented that this design was a rough assumption and that more design was needed.

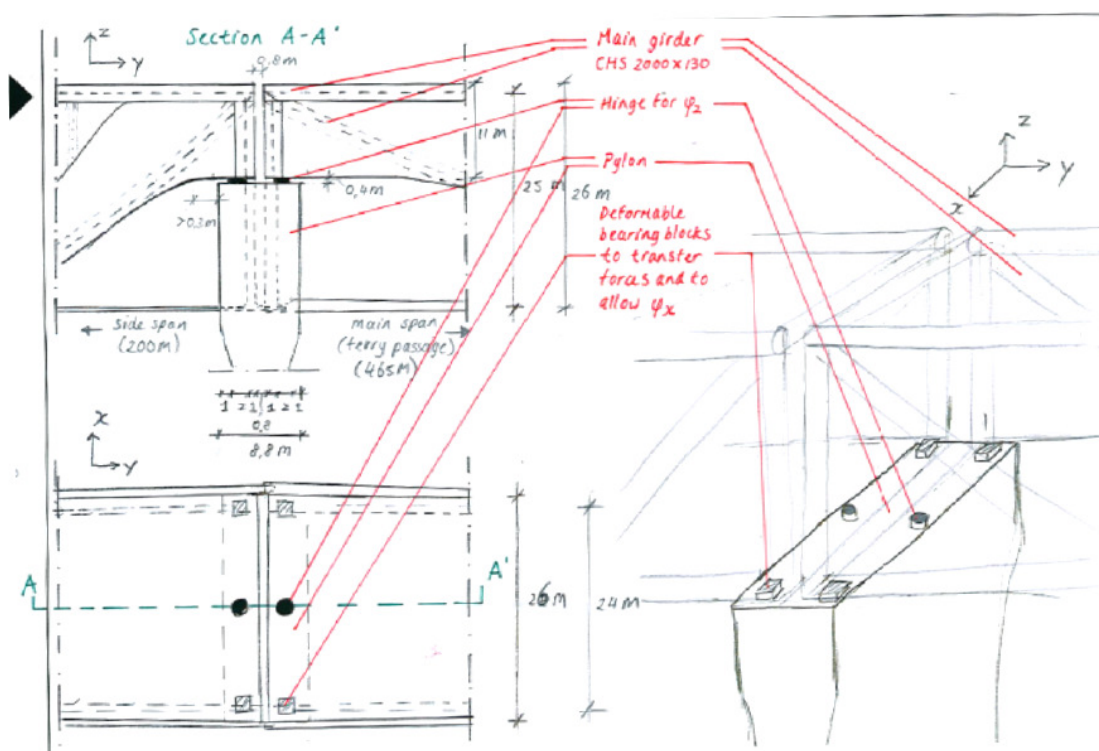


FIGURE A.5: PROPOSED CONCEPTUAL SUPPORT DESIGN AT PONTOON TOP

## A.2.6 Erection method

For erecting the bridge the following process is proposed. First, the pontoons bottoms are constructed at a fabrication site, after which they can be towed over water to nearby the construction site, where they will be further topped up to their eventual length. Ballast is added to the pontoons while the upper parts are constructed, in order to keep a practical draught. In this way, most of the construction can be done nearby site.

More or less at the same time, the anchoring cables are towed to site and the main cables are anchored to the shore. During this phase, the cables are connected to buoyancy elements to make them float at surface level. Once the cables are in place, the finished pontoons will be brought into their final position and connected to the anchoring cables.

After this, the buoyancy elements will be disconnected from the cables, making them sag and thereby pretensioning themselves. Then the superstructure is placed on top of the pontoons, making the pontoons sink a little further in the sea. When everything is placed, ballast will be added per pontoon if necessary, to obtain the final desired draught. An image of this process is given in figure A.6.

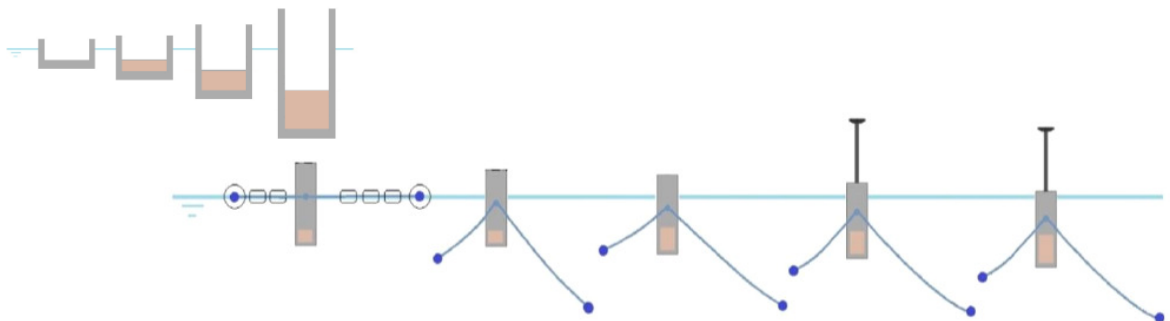


FIGURE A.6: ILLUSTRATION OF PROPOSED PONTOON ERECTION METHOD

## A.3 Modelling and calculations

### A.3.1 Loads on pontoons

Yip (2015) used the recommendations made by Hermans (2014) in modelling traffic loads. These consist of imposing a uniform traffic load of  $35 \text{ kN/m}^2/\text{m}$  and a double axle load of  $1200 \text{ kN}$  on the bridge. Horizontal (longitudinal) traffic loads from braking were however omitted, on the basis that these are negligible according to Eurocode 1-2 for a road with this radius. Upon inspection, it proved that EC1 only allows lateral centrifugal forces to be omitted. Longitudinal braking forces must always be taken into account (EC1:1-2). However, traffic braking forces are insignificant in comparison with other longitudinal forces on the girder. They can still be disregarded. It proved that in the static calculations (performed by a Maple sheet), double axle forces were not taken into the vertical loads acting on the pontoons. These do however cause significant vertical forces (higher than vertical forces coming from uniform traffic loads) and thus can't be neglected.

Hermans (2014) designed a steel box girder for the superstructure, with an according self-weight based on the cross-section area. This gave a rather precise self-weight of  $114.396 \text{ kN/m}$  for side span girders. Since Yip (2015) assumed a new girder concept, this value was not relevant anymore. In the new calculations the self-weight of the girder was therefore assumed to be  $265 \text{ kN/m}$ , making for a total uniform load of  $300 \text{ kN/m}$ .

The dimensions of the girders in the designs of Hermans (2014) and Yip (2015) are around  $16 \times 4.5 \text{ m}$  with an additional truss of on average around  $12 \times 7 \text{ m}$ , and  $24 \times 25 \text{ m}$ , respectively. In other words, the girder concept by Yip (2015) is both 1.5 times wider and 2 times higher. The self-weight by Yip (2015) is assumed to be just 2.3 times larger, without any further validation. Considering this property has a significant effect on the pontoon size, further calculation of the girder self-weight could be considered. The bridge deck weight is by Yip (2015) assumed to be  $20 \text{ kN/m}$  and not further mentioned in the calculation file, although it might be incorporated in the  $300 \text{ kN/m}$  value. However, a bridge deck weight of  $20 \text{ kN/m}$  seems unreasonably low in this case, considering this value corresponds to a concrete deck of under  $40 \text{ mm}$  thickness, without any further components.

For calculation of the environmental loads, extreme environmental values (for wind, waves, etc.) were used as calculated by Hermans (2014) and these values were used to calculate loads according to the Eurocode. Dynamic effects were not considered.

### **A.3.2 Modelling in several steps**

First, a layout for the anchoring system, including spans, cable dimensions and stiffnesses, was assumed. Erecting this cable layout would impose loads by self-weight, which in turn cause settlements (deflections and rotations) of the system. These were all modelled using SCIA. This was also done to model the erection phase of the design.

Using the pontoon loads as input, a Maple sheet was made to calculate the necessary pontoon length (as to create enough buoyancy) and the corresponding rotational pontoon stiffness. When the pontoon buoyancy or rotational stiffness didn't prove to be sufficient, the pontoon was enlarged. Larger pontoons have a larger self-weight, resulting in larger loads, resulting in larger pontoons again. Therefore a few iterations in their design were made. This eventually resulted in a list of properties for all the pontoons, which were then used as input in a SCIA model.

These pontoons and the loads being put in the SCIA model of course affected the loads on the cable anchoring system. When the resulting loads on the cables proved to be too large, the cables were enlarged, resulting in larger loads on the pontoons, resulting in larger pontoons, resulting in large loads on the cables again. Again, a few iteration steps were made, until a final design was proposed that when modelled against extreme load cases, showed displacements and rotations that are within limits. Connecting the pontoons to the anchoring system would result in movements of the whole system, because it would settle again. These movements were however considered insignificant and therefore neglected.



## ANNEX B: FULL CONCLUSIONS ON RESEARCH BY YIP (2015)

Yip (2015) investigated a new concept for the Sognefjord bridge, focussing on the anchoring system and a new bridge girder. As a starting point, this research has been read thoroughly. Elaborate conclusions on the research, together with conclusions on points to be investigated in this thesis, are given below.

- Yip (2015) started by changing the anchoring concept from anchoring just four pontoons, to applying a double horizontal suspension anchoring system. In this way, each pontoon is individually anchored and no contribution from the girder to restrain the pontoons in lateral direction is needed anymore, drastically reducing forces in the girder. Furthermore, risk of colliding tendons is heavily reduced. However, this system has its downsides as well. First of all, a very large number of cable connections, which are difficult and expensive to construct, has to be made. This is even more problematic considering these connections will be submerged. Furthermore, the two main suspension cables will have to be of a size currently unprecedented.

Because of their sheer weight (roughly 40,000 tonnes each), erection of the main cables will be very difficult, since equipment capable of handling this is lacking. However, taking this all into consideration, the catenary anchoring system was still found to be the best choice at the moment for restraining pontoon movement. This because in this system, every pontoon is anchored and alternatives (such as bottom anchoring) are considered less feasible. Therefore this will be maintained as a starting point for this research.

- The architects clearly stated their desire for a singular, clear line for the superstructure. Different concepts were mentioned, but for this reason a suspension, arch or cable stayed bridge was ruled out. Because of its large self-weight, a composite concrete – steel lattice girder was also ruled out. The choice was eventually made on designing a steel lattice girder with circular hollow sections. Reasons for not considering other options that at first sight also comply to aesthetics (for example a box girder or a lattice girder with steel box girder flanges) were however not given.

Also, justification for the girder dimensions was found to be partly lacking. The girder height is 25 m, but a reason for choosing this value is absent, although it is stated that this height will vary along the bridge span. In the proposed design the bridge girders were straight (with a curved road on top of them), to not induce any unwanted torsional forces from traffic loads. This however makes for a girder width largely exceeding the required bridge deck width. Since calculations on these torsional forces are absent as well, and considering a lack of girder height calculations, it was concluded that opportunities exist for optimization of the girder dimensions.

The report states that quite some modelling on forces in the superstructure still has to be done (p.85). Taking all these remarks into consideration, it is expected that there is room for optimisation of the superstructure design. Therefore, this study will consider alternative girder concepts and include extensive calculations and modelling. The goal is to reach an optimised design both in terms of aesthetics and dimensions of the girder.

- The research only made rough assumptions for the layout of the supports of the bridge girders at the top of the pontoons. These consist of a vertical pin to restrain horizontal movement and two large bearing blocks to transfer vertical forces. The report remarks that more research on these supports is needed and the current design was indeed found to have limitations, for example in functioning of the pin or durability of the bearing blocks. Furthermore, requirements on bridge maintenance set by the Norwegian government will require large alterations to the current support design. Therefore this study will reconsider girder design and girder joints at the support and research design alternatives. This will of course have a big influence on girder design as well. Therefore these two design aspects can be considered as going hand in hand.

- One of the consequences of the new anchoring system design was that it became unnecessary to enlarge the buoyancy of four of the pontoons. Furthermore, it was stated that the initial tripod concept for these pontoons was not aesthetically competing, as it didn't abide the requirements for continuity and lightness as set by the architects. Therefore the decision was made on making all pontoons single cylindrical spar structures. In order to reach the right upward buoyant forces, rotational stiffness and draught, the dimensions of these pontoons have been calculated extensively. However, research into impact redundancy of different pontoon concepts was not conducted. The current pontoon design has opportunities for optimisation, especially in terms of ship impact redundancy. Therefore this research will make an effort in designing for more redundancy.
- Dynamics of the Sognefjord bridge hasn't been investigated yet. Since the anchoring system is a relatively complex net of very slender cables, dynamic excitation and resonance of cables are serious risks. Because of the relatively un-fixed nature of the bridge, all members (including pontoons and bridge girder) could also be dynamically amplified. Therefore it was concluded that dynamics for this bridge needs to be addressed.



## ANNEX C: MODEL VALIDATION IN ANSYS

Due to its size and geometry, the anchoring system is very sensitive to movements and loads, making it hard to predict its behaviour. Therefore it was chosen to investigate whether, for this moment, SCIA Engineer gives precise enough results when modelling the anchoring system. This was done by creating a comparable cable system in Ansys, a FEA-suite generally considered and often proven to give results very close to reality. If two different models of the same structure will give the same results, it can be assumed that at least in this stage of design the quality of the SCIA-model is high enough to provide realistic results in deformation and forces of the anchoring system.

### C.1 Difficulties in modelling

As stated before, one would like to apply loads on the cable system in the right order, e.g. the cable self-weight first, such that the cables stiffen, and external loading only second (as would be the case in real-life). However, in SCIA Engineer it's not possible to apply loads in order; all loads are applied at the same time. This means the external loads will be applied to a system that is not stiffened by self-weight yet, which could result in different cable behaviour.

Ansys does have the possibility to apply loads in order, but cable models in Ansys tend to become unstable a lot quicker. This is due to the nature of FE-modelling: this is a process of incremental steps where in each step a small part of stress and deformation is calculated, after which in a new step, a new part of the load is applied and stresses and deformations calculated. When these steps are big, the incremental differences in displacement of nodes becomes very high. This makes it harder for software to approach the next value, since it's not close to the current value of a node. When this difference is too big, the software won't be able to find the next point to calculate and instability will occur, making the calculation to shut down. This process is accelerated once cables deform in two directions (as is the case here). SCIA Engineer works according to the same calculation procedure (the Newton-Raphson method) for non-linear calculations, but has a bigger tolerance for the incremental difference and less calculation parameters that can be adjusted (making the calculations more stable but giving the user less options and in some occasions less precise results).

These difficulties in calculation stability can be overcome by trying to give the structure an initial shape that approximates the final shape. This is done by applying the loads in small, increasing steps, so that the structure deforms in smaller steps. However, in Ansys, even then the anchoring system still is prone to instability. Modelling the complete system in Ansys might very well be a thesis topic in itself – a thorough attempt was made by an experienced engineer at Iv-Consult, which even then only succeeded in creating a system that was stable at a self-weight of only 1/20 of actual gravity. To omit these problems, but still validate the SCIA model, it was decided to model a similar, but simplified, anchoring system. The exact same structure was modelled in SCIA Engineer as well, to compare forces and displacements. This approach was chosen to both validate the modelling, as keep the amount of work limited. This under the assumption that if a simplified but similar model shows the same results, modelling the bridge in SCIA Engineer will give results that are for now useable and accurate enough. In both models, beam elements were used for more stable calculations. As stated in Annex B, for these geometries, beam elements show the same behaviour as cable elements and are therefore suited for this research.

### C.2 Stepwise elaboration in modelling

This validation research has been conducted in several steps. This started with a very simple rectangular 110x50 m cable system, already with 2 70mm diameter main cables and 4 20mm diameter sub cables. This was modelled in both programs, which gave the same results for deformations and stresses. After this, the model was elaborated into two curved main cables and more (7) side cables. Again, this gave the same deformations and internal forces. The third step was to fully elaborate the geometry into two further curved main cables and 11 sub cables, in a geometry mimicking the anchoring system of the Sognefjord bridge in a 238x195 m model. Again, both programs showed roughly the same results. See figures C.1 to C.6 for the models. This validation research has been conducted in several steps. This started with a very simple rectangular 110x50 m cable system, already with 2 70mm diameter main cables and 4 20mm diameter sub cables. This was modelled in both programs, which gave the same results for deformations and stresses. After this, the model was elaborated into two curved main cables and more (7) side cables. Again, this gave the same deformations and internal forces. The third step was to fully

elaborate the geometry into two further curved main cables and 11 sub cables, in a geometry mimicking the anchoring system of the Sognefjord bridge in a 238x195 m model. Again, both programs showed roughly the same results. See figures C.1 to C.6 for the models.

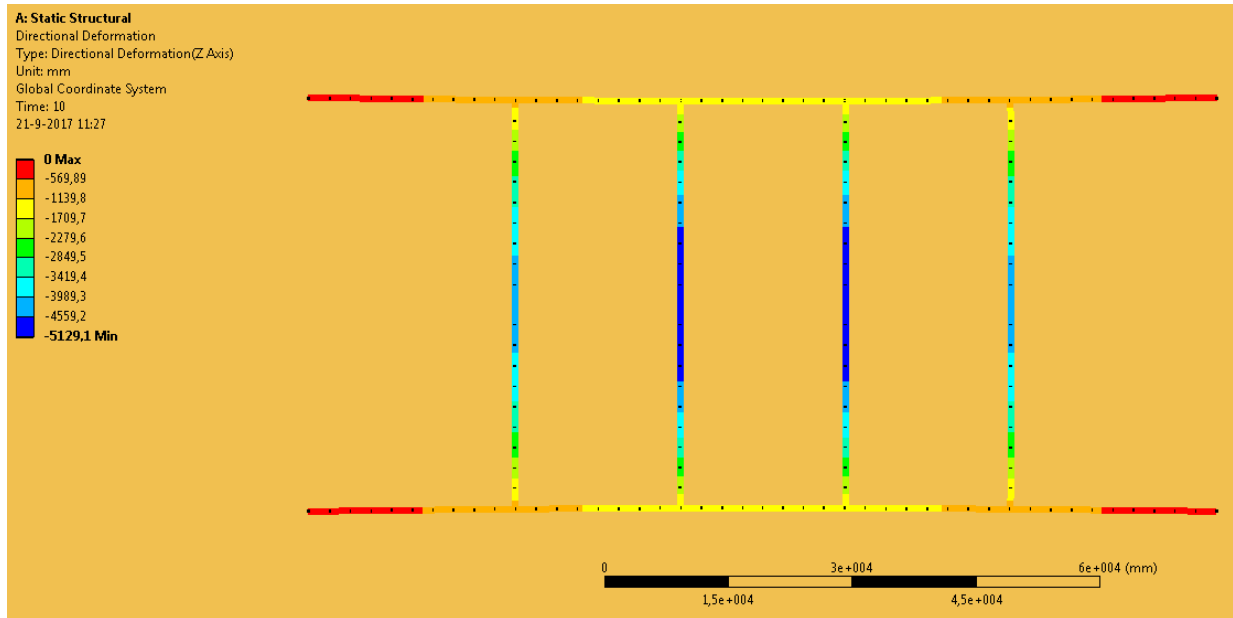


FIGURE C.1: MODEL #1 IN ANSYS, MAXIMUM VERTICAL DISPLACEMENT IS 5129 MM

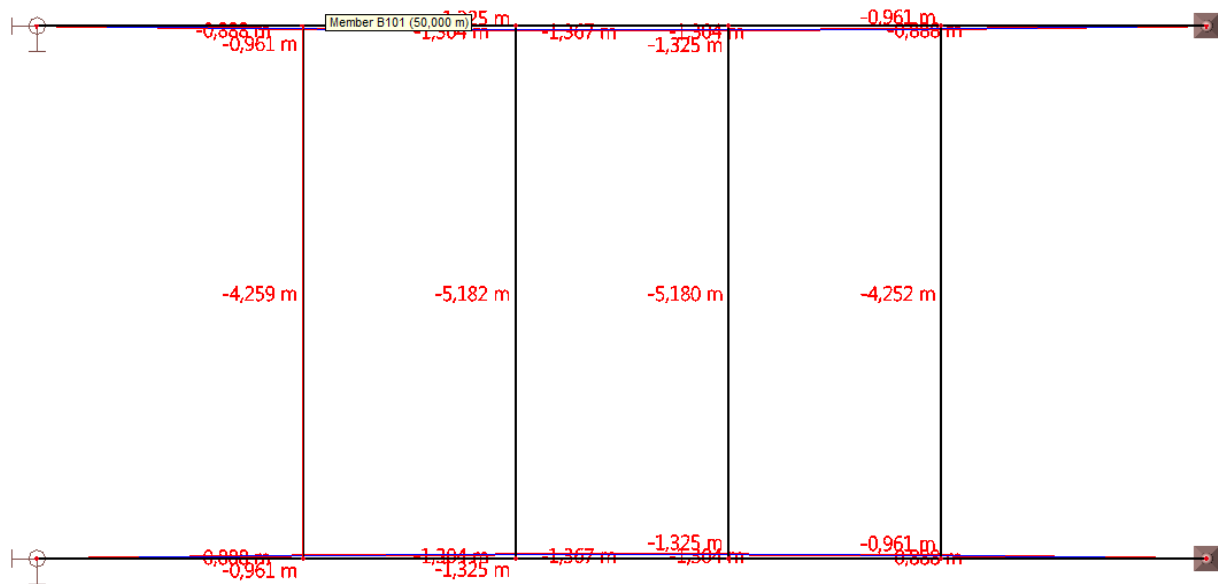


FIGURE C.2: MODEL #1 IN SCIA, MAXIMUM VERTICAL DISPLACEMENT IS 5182 MM.

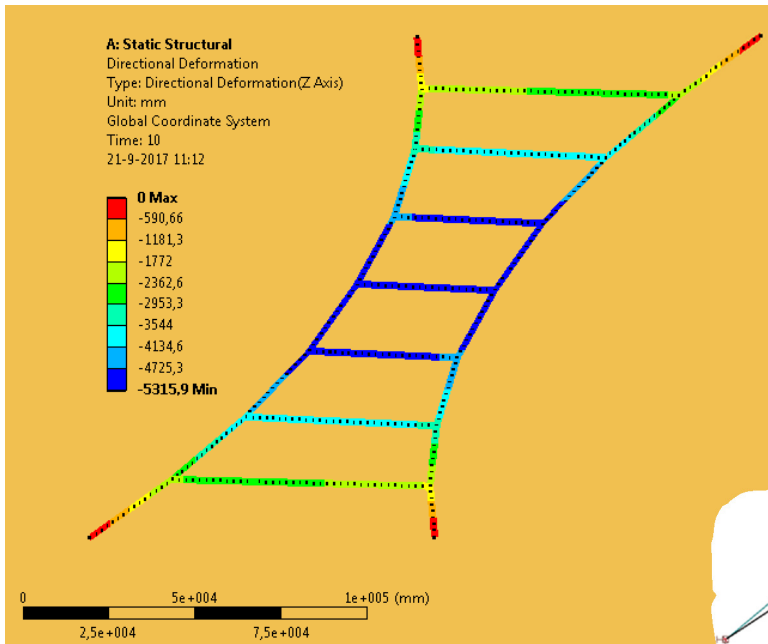


FIGURE C.3: MODEL #2 IN ANSYS, MAXIMUM VERTICAL DISPLACEMENT IS 5316 MM

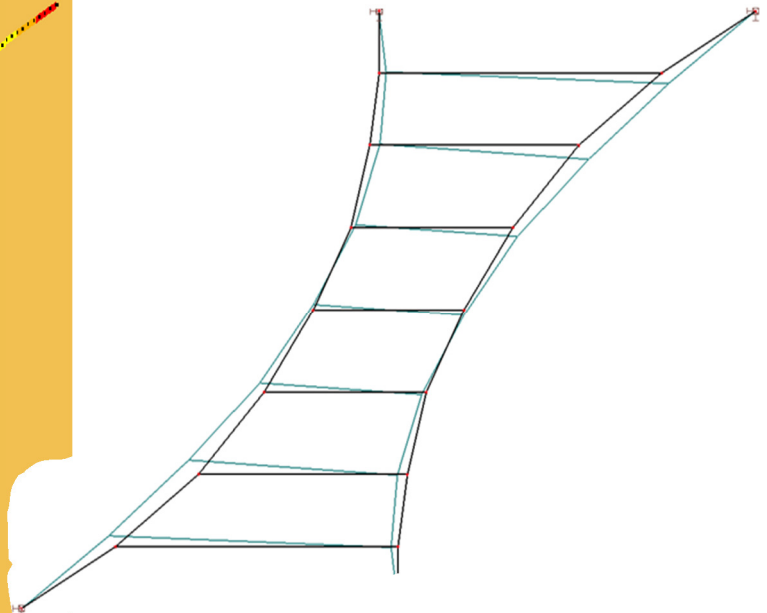


FIGURE C.4: MODEL #2 IN ANSYS, MAXIMUM VERTICAL DISPLACEMENT IS 5316 MM

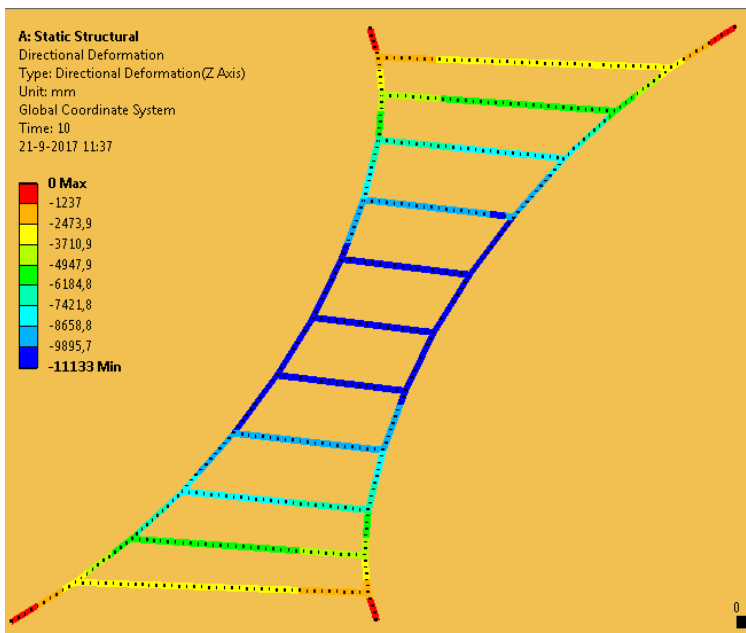


FIGURE C.5: MODEL #3 IN ANSYS, MAXIMUM VERTICAL DISPLACEMENT IS 11133 MM

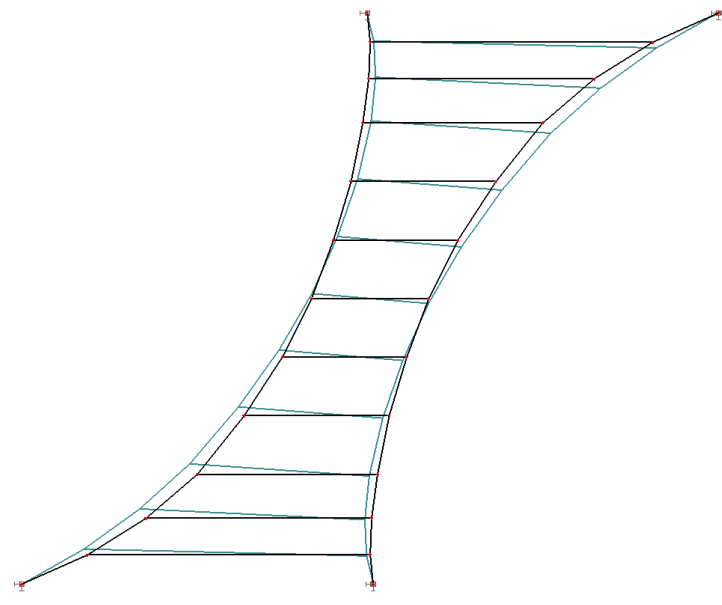


FIGURE C.6: MODEL #3 IN SCIA, MAXIMUM VERTICAL DISPLACEMENT IS 11329 MM

Eventually, pontoons were also added to this model. However, just as with modelling cables in general, modelling these comes with some stability challenges. First of all because of the more complex shape of the deformed cables, but also because large flexible (spring) supports tend to buckle in Ansys, making for large, unwanted rotations and imposed displacements. Therefore, it was decided, again to keep the modelling work within bounds, to simplify the pontoons to sliding supports that can freely displace in any lateral direction, but are restrained from movement in vertical direction. See figures C.7 and C.8 for the models.

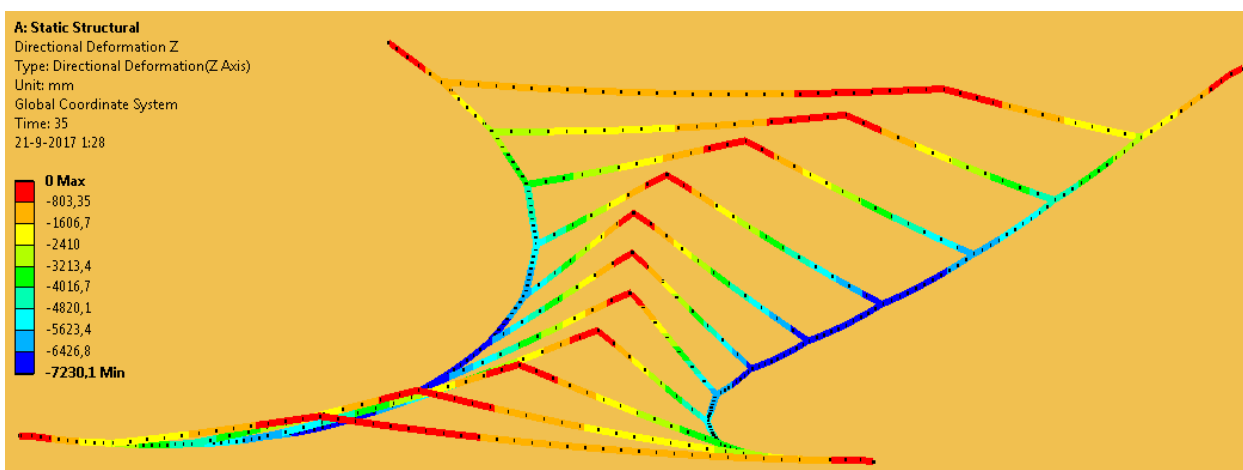


FIGURE C.7: MODEL #4 IN ANSYS, MAXIMUM VERTICAL DISPLACEMENT IS 7230 MM

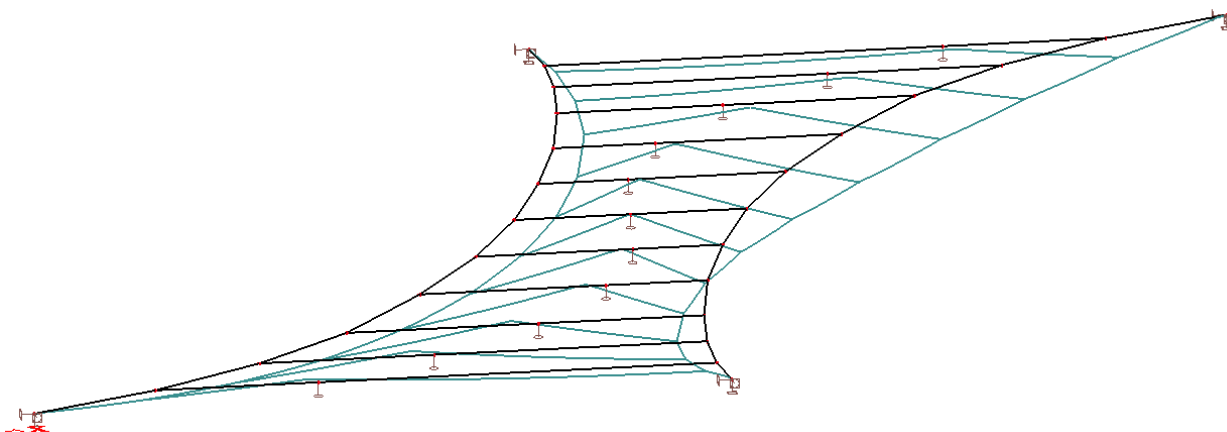


FIGURE C.8: MODEL #4 IN SCIA, MAXIMUM VERTICAL DISPLACEMENT IS 7359 MM

The last modelling step was keeping the same structure, but adding a second, external force to the structure. This was done because one property of loading in SCIA Engineer, is that this program imposes all loads (both self-weight and external loading) at once on the structure. This is considered to be a flaw in the software, because in real-life, the anchoring system will first be loaded by its self-weight, which will stiffen the cables through tensioning. After this the rest of the bridge will be constructed, which will impose external loads on the now stiffened cables. However, in SCIA these external loads will, at the same time as the self-weight, be imposed on an un-stiffened cable structure. Unstiffened cables will show different results from stiffened cables. In Ansys, it is possible to adjust the order of loads, so that external loads are imposed on a cable system stiffened by self-weight. It was expected that therefore the two modelling tools would now show different results (and because of the stiffened cables, deformations in Ansys would be smaller). See table C.1 for an overview of properties and boundary conditions of the models. The results, especially of the last model (#5), are discussed in C.3.

**TABLE C.1: MODEL PROPERTIES AND BOUNDARY CONDITIONS**

Property	Value
Main cable diameter	70 mm
Side cable diameter	20 mm
Length main cable	110 m (model #1) – 243 m (models #4 and #5)
Length sub cable	50 m (model #1) – 40 m to 96.5 m (models #4 and #5)
Boundary conditions	Main cables fixed supported, pontoons free for x, y direction and fixed for z-direction (models #4 and #5)
Applied load	Self-weight only (models #1-4), self-weight + external load on pontoons (model #5)
Analysis type	Geometrical non-linear

### C.3 Results

In the first three models, the maximum displacement logically occurs in the middle of the structure. In models #4 and #5, the middle is supported for vertical displacement and maximum vertical displacement occurs in the main cable, at around 2/3 of its length. As stated before, when only one load case (self-weight) is imposed, the difference between displacement results from models in SCIA Engineer and models in Ansys is insignificant. See table C.2 for an overview.

**TABLE C.2: COMPARISON OF VERTICAL DISPLACEMENTS IN DIFFERENT MODELLING SOFTWARE**

Model #	Description	Max. $u_z$ in Ansys [mm]	Max. $u_z$ in SCIA [mm]	Difference
1	Rectangle system with 4 sub cables	5129	5182	1.0%
2	Slightly curved system with 7 sub cables	5316	5344	0.5%
3	Proper curved system with 11 sub cables	11133	11329	1.8%
4	Proper curved system, 11 sub cables and pontoons	7230	7359	1.8%
5	Proper curved system, 11 sub cables, pontoons and external load	7619	9551	20.2%

In models #4 and #5, pontoons were added to the system. These pontoons show horizontal displacements in x and y-direction. Just as with vertical displacements, SCIA and Ansys give the same results for lateral displacements of the pontoons (when the structure is only loaded by self-weight). The results are given in table C.3. As can be expected, the displacements results are rotational symmetric (as is the system), with barely any displacement in the centre.

TABLE C.3: LATERAL DISPLACEMENTS OF PONTOONS IN MODEL #4

Pontoon # (from bottom to top)	Lateral displacements in Ansys [mm]		Lateral displacements in SCIA [mm]	
	$u_x$	$u_y$	$u_x$	$u_y$
1	-1729	1888	-1792	1937
2	-3344	2595	-3419	2638
3	-4090	2055	-4171	2085
4	-3132	943	-3202	959
5	-1724	357	-1784	368
6	51	12	0	0
7	1820	-378	1784	-368
8	3211	-954	3102	-959
9	4146	-2051	4171	-2085
10	3373	-2567	3419	-2638
11	1732	-1827	1792	-1937

When modelling multiple load cases, the limitations of SCIA Engineer become clear. Without the ability to impose different loads at different times, predictions of deformations of a cable system become less reliable. Cable systems that are loaded by their self-weight become stiffened, the self-weight loading acting as prestressing, and will deform less. This means that systems where all loads are imposed simultaneously show larger displacements, and thus give conservative results. Even though results from SCIA Engineer, with its inability to model load steps, differ significantly from Ansys, they are on the conservative side. More elaborate modelling in the future will show better cable system results (lower displacements). It is therefore concluded that for this moment (the design is still in its conceptual phase), in modelling the anchoring system, SCIA Engineer gives results that are accurate enough. Therefore for this design phase SCIA Engineer will remain to be used to model the bridge. With better modelling in the future, and thus less conservative results, the cable system may even be executed less heavy.

## ANNEX D: RESEARCHING DIFFERENT SUPERSTRUCTURE CONCEPTS

### D.1 Torsional check for preliminary investigation feasibility curved girder

To quickly check whether a curved bridge girder would be feasible in terms of member stress, a check was made on maximum torsional stresses. For this, a truss girder fully loaded by traffic on one half of the deck was assumed.

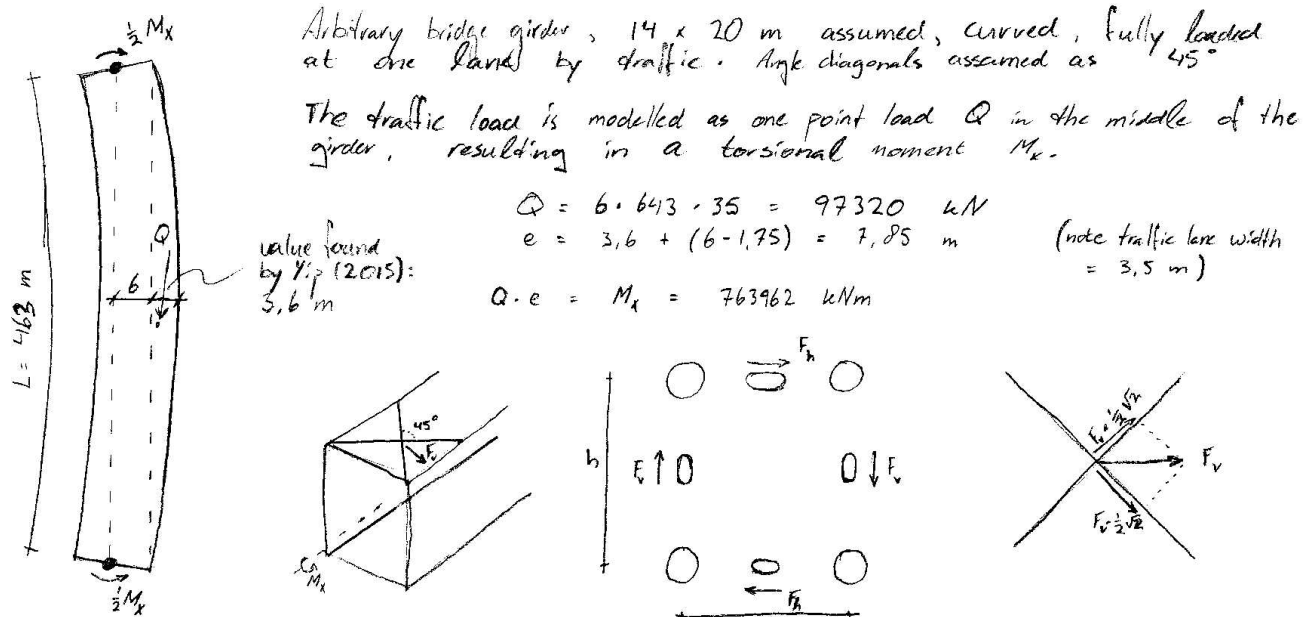
Arbitrary bridge girder, 14 x 20 m assumed, curved, fully loaded at one hand by traffic. Angle diagonals assumed as 45°

The traffic load is modelled as one point load  $Q$  in the middle of the girder, resulting in a torsional moment  $M_x$ .

value found by Yip (2015): 3,6 m

$$Q = 6 \cdot 643 \cdot 35 = 97320 \text{ kN}$$

$$e = 3,6 + (6 - 1,75) = 7,85 \text{ m} \quad (\text{note traffic lane width} = 3,5 \text{ m})$$

$$Q \cdot e = M_x = 763962 \text{ kNm}$$


$M_x = F_h \cdot h + F_v \cdot b \rightarrow F_v = \frac{\frac{1}{2} M_x}{2 \cdot b} = \frac{\frac{1}{2} \cdot 763962}{2 \cdot 14} = 13642 \text{ kN}$

We assume diagonal members  $\phi 1300 \times 30 \text{ mm}$ .

$$\sigma_{\text{diagonal}} = \frac{F_v \cdot \frac{1}{2} \sqrt{2}}{A_{\text{diag}}} = \frac{13642 \cdot 10^3 \cdot \frac{1}{2} \sqrt{2}}{\pi \cdot 1300 \cdot 30} = 78,7 \text{ N/mm}^2$$

By this value, further investigation into a curved girder is concluded as being feasible.

### D.2 Calculations to check simple preliminary bridge girder concepts

Different simple bridge girder concepts were designed and checked for their structural feasibility in terms of deflections and cross-sectional properties. These calculations are given on the following pages.



restart; unprotect (gamma); interface (imaginaryunit = j)

### First rough estimation comparison of girder designs

#### Some simple checks for a new box girder design

A new simple box girder design was introduced as a means to compare a box girder to the truss already designed. See the attached sketch. In this calculation, the following assumptions were made:

Simple design - effective width not considered - all values in N and mm, unless otherwise indicated - bridge deck self-weight of 40 kN/m assumed - traffic load LMI and axle load assumed.

$$I_{gir} := 20 : I_{stiff} := 16 : b_{gir} := 12 \cdot 10^3 : h_{gir} := 16.2 \cdot 10^3 : b_{stiff} := 150 : b_{stiff2} := 90 : h_{stiff} := 330 : b_{stiffweb} := 300 :$$

$$A_{box} := b_{gir} \cdot t_{gir} \cdot 2 + h_{gir} \cdot t_{gir} \cdot 2 : A_{stiff} := 2 \cdot \text{sqrt}(b_{stiff}^2 + b_{stiff2}^2) \cdot t_{stiff} + b_{stiff} \cdot t_{stiff} : A_{stiffweb} := (b_{stiffweb} + h_{stiff}) \cdot t_{stiff} :$$

$$A_{gir} := \text{evalf}(A_{box} + A_{stiff} \cdot (20.2 + 27.2)) :$$

$$b_{stiff} \cdot t_{stiff} \cdot h_{stiff} + \frac{2 \cdot \text{sqrt}(b_{stiff}^2 + b_{stiff2}^2) \cdot t_{stiff} \cdot h_{stiff}}{2}$$

$$e_{stiff} := \frac{A_{stiff}}{A_{gir}} :$$

$$I_{stiff,flange} := \frac{1}{12} \cdot b_{stiff}^3 \cdot t_{stiff} + b_{stiff} \cdot h_{stiff} \cdot (h_{gir} - e_{stiff})^2 + 2 \cdot \left( \frac{1}{12} \cdot t_{stiff} \cdot h_{stiff}^3 + t_{stiff} \cdot \text{sqrt}(b_{stiff}^2 + b_{stiff2}^2) \cdot \left( \frac{h_{stiff}}{2} - e_{stiff} \right) \right) :$$

$$I_{stiff,web} := \frac{1}{12} \cdot t_{stiff} \cdot h_{stiff}^3 + \frac{1}{12} \cdot b_{stiffweb} \cdot t_{stiff} :$$

$$I_{box} := \frac{1}{12} \cdot b_{gir} \cdot h_{gir}^3 - \frac{1}{12} \cdot (b_{gir} - 2 \cdot t_{gir}) \cdot (h_{gir} - 2 \cdot t_{gir})^3 :$$

$$I_{gir} := \text{evalf} \left( I_{box} + 2 \cdot 20 \cdot \left( I_{stiff,flange} + A_{stiff} \cdot \left( \frac{h_{gir}}{2} - e_{stiff} \right)^2 \right) + 2 \cdot 27 \cdot \left( I_{stiff,web} + A_{stiffweb} \cdot \left( \frac{h_{gir}}{4} \right)^2 \right) \right) :$$

$$E := 2.1 \cdot 10^5 :$$

$$A_{gir} := 2.382494304 \cdot 10^6$$

$$I_{gir} := 8.781414734 \cdot 10^{13}$$

Now calculating loads and displacements using standard mechanics:

$$q_{traffic} := 35 : Q_{traffic} := 1200 \cdot 10^3 :$$

$$q_{sw} := \text{evalf}(A_{gir} \cdot 10^{-9} \cdot 7850 \cdot 9.81 + 40) : q_{tot} := q_{traffic} + q_{sw} :$$

$$w_{mid,hinged} := \text{evalf} \left( \frac{5 \cdot q_{tot} \cdot (462 \cdot 10^3)^4}{384 \cdot E \cdot I_{gir}} + \frac{Q_{traffic} \cdot (462 \cdot 10^3)^3}{48 \cdot E \cdot I_{gir}} \right) : [mm] :$$

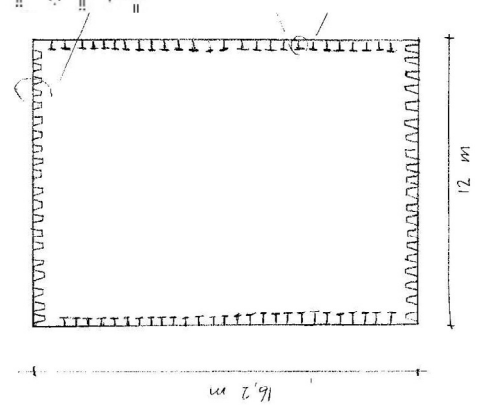
$$w_{mid,clamped} := \text{evalf} \left( \frac{q_{tot} \cdot (462 \cdot 10^3)^4}{384 \cdot E \cdot I_{gir}} + \frac{Q_{traffic} \cdot (462 \cdot 10^3)^3}{192 \cdot E \cdot I_{gir}} \right) : [mm] :$$

$$q_{sw} := 3226.387675$$

$$\left[ \frac{kN}{m} \right]$$

$$w_{mid,hinged} := 3872.878213$$

$$[mm]$$



$$(1) \quad q_{traffic} := 35 : Q_{traffic} := 1200 \cdot 10^3 : q_{sw} := \text{evalf}(A_{gir} \cdot 10^{-9} \cdot 7850 \cdot 9.81 + 40) : \left[ \frac{kN}{m} \right] : q_{tot} := q_{traffic} + q_{sw} : w_{mid,hinged} := \text{evalf} \left( \frac{5 \cdot q_{tot} \cdot (462 \cdot 10^3)^4}{384 \cdot E \cdot I_{gir}} + \frac{Q_{traffic} \cdot (462 \cdot 10^3)^3}{48 \cdot E \cdot I_{gir}} \right) : [mm] : q_{sw} := 3226.387675$$

$$\left[ \frac{kN}{m} \right]$$

$$w_{mid,hinged} := 5849.002415$$

$$[mm]$$

When assuming a pre-cambered girder, the displacement due to the load only will be:

$$w_{mid,hinged,prec} := \text{evalf} \left( \frac{5 \cdot q_{traffic} \cdot (462 \cdot 10^3)^4}{384 \cdot E \cdot I_{gir}} + \frac{Q_{traffic} \cdot (462 \cdot 10^3)^3}{48 \cdot E \cdot I_{gir}} \right) : [mm] :$$

$$w_{mid,hinged,prec} := 70.13308067$$

$$[mm]$$

However, it is clear that the weight of this girder far exceeds all maximum limitations on lifting capacity world wide. Furthermore, the increased cross-section complexity makes fabrication complicated and expensive. Therefore this girder was found not feasible. This is even without considering the over-simplification of the cross-sectional design.

#### An attempt at reaching a higher efficiency

To reach a still higher efficiency, plate thickness is reduced significantly. The same assumptions are made in calculations.

$$(2) \quad I_{gir} := 65 : t_{stiff} := 30 : t_{stiff2} := 25 : b_{gir} := 12 \cdot 10^3 : h_{gir} := 22 \cdot 10^3 : b_{stiff} := 400 : h_{stiff} := 700 : b_{stiff,web} := 300 :$$

$$A_{box} := b_{gir} \cdot t_{gir} \cdot 2 + h_{gir} \cdot t_{gir} \cdot 2 : A_{stiff} := 2 \cdot \text{sqrt}(b_{stiff}^2 + b_{stiff2}^2) \cdot t_{stiff} + b_{stiff} \cdot t_{stiff} : A_{stiff,web} := b_{stiff,web} \cdot t_{stiff} :$$

$$A_{gir} := \text{evalf}(A_{box} + 2 \cdot A_{stiff} \cdot (12.6) + (2.5 + 1) \cdot b_{gir} \cdot t_{gir} + A_{stiff2} \cdot 5.4 \cdot 2) :$$

$$\frac{b_{stiff} \cdot t_{stiff} \cdot h_{stiff} + \frac{2 \cdot \text{sqrt}(b_{stiff}^2 + b_{stiff2}^2) \cdot t_{stiff} \cdot h_{stiff}}{2}}{A_{gir}}$$

$$e_{stiff} := \frac{A_{stiff}}{A_{gir}}$$

$$I_{stiff} := \frac{1}{12} \cdot b_{stiff}^3 \cdot t_{stiff} + b_{stiff} \cdot h_{stiff} \cdot (h_{gir} - e_{stiff})^2 + 2 \cdot \left( \frac{1}{12} \cdot t_{stiff} \cdot h_{stiff}^3 + t_{stiff} \cdot \text{sqrt}(b_{stiff}^2 + b_{stiff2}^2) \cdot \left( \frac{h_{stiff}}{2} - e_{stiff} \right) \right) :$$

$$w_{web} := \frac{1}{12} \cdot b_{stiff,web} \cdot t_{stiff}^3 :$$

$$:= \frac{1}{12} \cdot b_{gir} \cdot h_{gir}^3 - \frac{1}{12} \cdot (b_{gir} - 2 \cdot t_{gir}) \cdot (h_{gir} - 2 \cdot t_{gir})^3 + \frac{1}{12} \cdot b_{gir} \cdot t_{gir}^3 \cdot 10 + 2 \cdot (b_{gir} \cdot t_{gir} \cdot 1000^2 + b_{gir} \cdot t_{gir} \cdot 2000^2) + b_{gir} \cdot t_{gir} \cdot 3000^2 + b_{gir} \cdot t_{gir} \cdot 4000^2 + b_{gir} \cdot t_{gir} \cdot 5000^2 :$$

$$:= \text{evalf}(I_{box} + 12 \cdot I_{stiff} \cdot 3.2 + 2 \cdot 12 \cdot (A_{stiff} \cdot (1 \cdot 10^3 - e_{stiff})^2 + A_{stiff} \cdot (10 \cdot 10^3 - e_{stiff})^2) + A_{stiff} \cdot (9 \cdot 10^3 - e_{stiff})^2) + 5 \cdot 4 \cdot 2 \cdot (I_{stiff,web} + A_{stiff,web} \cdot 5000^2) :$$

$$= 2.1 \cdot 10^5 :$$

$$W_{mid, clamped} := 774.8220806 \quad [mm]$$

(3)

When assuming a pre-cambered girder, the displacement due to the load only will be:

$$W_{mid, hinged, prec} := evalf\left(\frac{5 \cdot q_{traffic} \cdot (462 \cdot 10^3)^4}{384 \cdot E \cdot I_{gir}} + \frac{Q_{traffic} \cdot (462 \cdot 10^3)^3}{48 \cdot E \cdot I_{gir}}\right); [mm];$$

$$W_{mid, clamped, prec} := evalf\left(\frac{q_{traffic} \cdot (462 \cdot 10^3)^4}{384 \cdot E \cdot I_{gir}} + \frac{Q_{traffic} \cdot (462 \cdot 10^3)^3}{192 \cdot E \cdot I_{gir}}\right); [mm];$$

$$W_{mid, hinged, prec} := 46.43815490$$

$$[mm]$$

$$W_{mid, clamped, prec} := 9.534068952$$

$$[mm]$$

(4)

When a deflection limit of 1/350 of the span is taken, the requirement for deflection is met when the girder is considered pre-cambered, for a hinged connected girder. The deflections for clamped girders are about 1/5 of the deflection of a hinged connected member. This is calculation is just a first estimate though.

### Creating a more elaborative box girder design

In order to create a more efficient bridge girder, the cross-section design was changed, by adding more flanges to the top and bottom sides of the girder and adjusting stiffener geometry. See the attached image. The same assumptions are made in calculations.

$$t_{gir} := 100; t_{web} := 80; t_{st2} := 50; b_{gir} := 12 \cdot 10^3; h_{gir} := 22 \cdot 10^3; b_{web} := 400; h_{web} := 700; b_{st, web} := 300;$$

$$A_{box} := b_{gir} \cdot t_{gir} \cdot 2 + h_{gir} \cdot t_{st2} \cdot 2; A_{web} := 2 \cdot \sqrt{t_{web}^2 + b_{web}^2} \cdot t_{web} + b_{web} \cdot t_{web}; A_{st, web} := b_{st, web} \cdot t_{web};$$

$$A_{gir} := evalf(A_{box} + 2 \cdot A_{web} \cdot (12 \cdot 6) + (2 \cdot 5 + 1) \cdot b_{gir} \cdot t_{gir} + A_{st, web} \cdot 5 \cdot 4 \cdot 2);$$

$$e_{stif} := \frac{b_{web} \cdot t_{web} \cdot h_{web} + \frac{2 \cdot \sqrt{t_{web}^2 + b_{web}^2} \cdot t_{web} \cdot h_{web}}{2}}{A_{web}}$$

$$I_{web} := \frac{1}{12} \cdot b_{web}^3 \cdot t_{web} + b_{web} \cdot h_{web}^3 + t_{web} \cdot \sqrt{t_{web}^2 + b_{web}^2} \cdot \left(\frac{h_{web}}{2} - e_{stif}\right);$$

$$I_{stif, web} := \frac{1}{12} \cdot b_{stif, web}^3 \cdot t_{stif};$$

$$I_{box} := \frac{1}{12} \cdot b_{gir}^3 \cdot h_{gir} - \frac{1}{12} \cdot (b_{gir} - 2 \cdot t_{gir}) \cdot (h_{gir} - 2 \cdot t_{gir})^3 + \frac{1}{12} \cdot b_{gir} \cdot t_{gir}^3 \cdot 10 + 2 \cdot (b_{gir} \cdot t_{gir} \cdot 1000^2 + b_{gir} \cdot t_{gir}^3 \cdot 2000^2 + b_{gir} \cdot t_{gir} \cdot 3000^2 + b_{gir} \cdot t_{gir} \cdot 4000^2 + b_{gir} \cdot t_{gir} \cdot 5000^2);$$

$$I_{gir} := evalf(I_{box} + 12 \cdot I_{web} \cdot 3 \cdot 2 + 2 \cdot 12 \cdot (A_{web} \cdot (11 \cdot 10^3 - e_{stif})^2 + A_{stif} \cdot (10 \cdot 10^3 - e_{stif})^2 + A_{web} \cdot (9 \cdot 10^3 - e_{stif})^2) + 5 \cdot 4 \cdot 2 \cdot (I_{stif, web} + A_{stif, web} \cdot 5000^2));$$

$$E := 2.1 \cdot 10^7;$$

$$A_{gir} := 4.137709052 \cdot 10^7$$

$$I_{gir} := 1.577106649 \cdot 10^{15}$$

(5)


Now calculating loads and displacements using standard mechanics:

$$A_{gir} := 2.139140894 \cdot 10^7$$

$$I_{gir} := 7.569510465 \cdot 10^{14}$$

(8)

Now calculating loads and displacements using standard mechanics:

$$q_{traffic} :=$$


$$q_{sv} := e$$

$$W_{mid, hinged} := \frac{\left(\frac{kN}{m}\right) \cdot \left(\frac{462 \cdot 10^3}{48 \cdot E \cdot I_{gir}} + q_{sv}\right)}{4} + \frac{Q_{traffic} \cdot (462 \cdot 10^3)^3}{48 \cdot E \cdot I_{gir}}; [mm];$$

$$q_{sv} := 1687.320315$$

$$\left[\frac{kN}{m}\right]$$

$$W_{mid, hinged} := 6442.882029$$

$$[mm]$$

(9)

When assuming a pre-cambered girder, the displacement due to the load only will be:

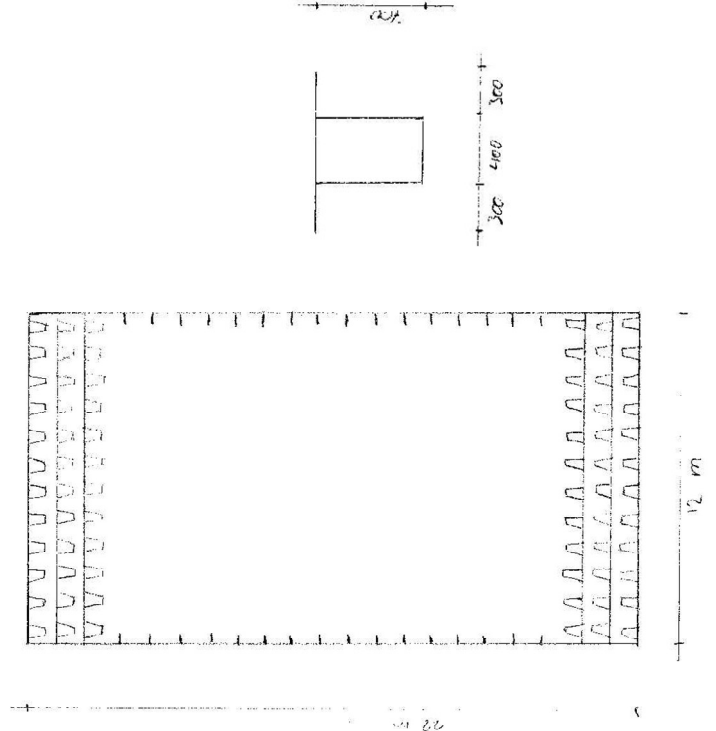
$$W_{mid, hinged, prec} := evalf\left(\frac{5 \cdot q_{traffic} \cdot (462 \cdot 10^3)^4}{384 \cdot E \cdot I_{gir}} + \frac{Q_{traffic} \cdot (462 \cdot 10^3)^3}{48 \cdot E \cdot I_{gir}}\right); [mm];$$

$$W_{mid, hinged, prec} := 146.1221943$$

$$[mm]$$

(10)

Apparently, contrary to initial assumptions, decreasing thicknesses has a detrimental effect on deflection. It is finally concluded that a box girder is not the best design for a girder.



restart; unpractc(gamma); interface(imaginaryunit=i)

### First rough estimation of a box-truss combination girder

A new simple truss girder design with box girder flanges was introduced as a means to compare a box girder to the truss already designed. See the attached sketch. In this calculation, the following assumptions were made:

Simple design - effective width not considered - all values in N and mm, unless otherwise indicated - bridge deck self-weight of 40 kN/m assumed - traffic load LM1 and axle load assumed.

#### New box/truss combination girder

$$I_{gir} := 120 \cdot I_{stif} := 80 \cdot b_{box} := 12 \cdot 10^3; h_{box} := 3 \cdot 10^3; b_{stif} := 200; b_{stif2} := 100; h_{stif} := 600;$$

$$I_{stifweb} := 1000;$$

$$I_{stifweb} := 80 \cdot b_{stifweb} := 400;$$

$$A_{box} := b_{box} \cdot t_{gir} \cdot 2 + h_{box} \cdot t_{gir} \cdot 2; A_{stif} := (b_{stif} + 2 \cdot h_{stif}) \cdot t_{stif}; A_{stifweb} := b_{stifweb} \cdot t_{stifweb}; A_{brace} := 2 \cdot \Pi$$

$$A_{gir} := evalf(2 \cdot A_{box} + A_{stif} \cdot 12 \cdot 3 \cdot 2 + A_{stifweb} \cdot 3 \cdot 4 \cdot 2 + 4 \cdot A_{brace});$$

$$e_{stif} := \frac{b_{stif} \cdot t_{stif} \cdot h_{stif} + \frac{2 \cdot I_{stif} \cdot h_{stif} \cdot h_{stif}}{2}}{A_{stif}};$$

$$I_{stif,flange} := \frac{1}{12} \cdot b_{stif} \cdot t_{stif}^3 + b_{stif} \cdot t_{stif} \cdot (h_{stif} - e_{stif})^2 + 2 \cdot \left( \frac{1}{12} \cdot t_{stif} \cdot h_{stif}^3 + I_{stif} \cdot h_{stif} \cdot \left( \frac{h_{stif}}{2} - e_{stif} \right)^2 \right);$$

$$I_{stifweb} := \frac{1}{12} \cdot t_{stifweb} \cdot b_{stifweb}^3 \cdot I_{brace} := \Pi \cdot r_{brace}^4 \cdot t_{gir};$$

$$I_{box} := \frac{1}{12} \cdot b_{box} \cdot h_{box}^3 - \frac{1}{12} \cdot (b_{box} - 2 \cdot t_{gir}) \cdot (h_{box} - 2 \cdot t_{gir})^3;$$

$$I_{gir} := evalf(2 \cdot (I_{box} + A_{box} \cdot 8000^2) + 2 \cdot 12 \cdot (I_{stif,flange} + A_{stif} \cdot (11000 - e_{stif})^2) + 2 \cdot 12 \cdot (I_{stifweb} + A_{stifweb} \cdot 9500^2) + 4 \cdot (I_{brace} + A_{brace} \cdot 4000^2));$$

$$E := 2.1 \cdot 10^5;$$

$$A_{gir} := 1.904792895 \cdot 10^7$$

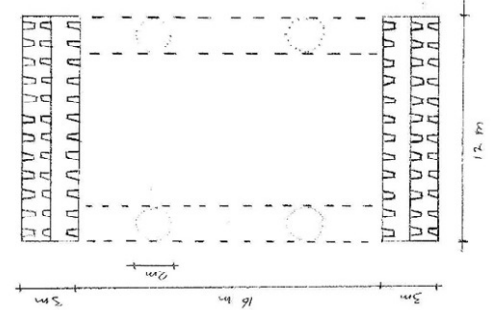
$$I_{gir} := 1.534764643 \cdot 10^{15}$$

We calculate deflections again:

$$q_{traffic} := 35 \cdot Q_{traffic} := 1200 \cdot 10^3;$$

$$q_{sw} := A_{gir} \cdot 10^{-9} \cdot 7850 \cdot 9.81 + 40 \cdot q_{tot} := evalf(q_{traffic} + q_{sw});$$

$$w_{mid,hinged} := evalf\left(\frac{5 \cdot q_{tot} \cdot (462 \cdot 10^3)^4}{384 \cdot E \cdot I_{gir}} + \frac{Q_{traffic} \cdot (462 \cdot 10^3)^3}{48 \cdot E \cdot I_{gir}}\right);$$



(1) Conclusion: the deflection at mid-span reduced around 1 m for each increase of the girder height with 2 meters. This girder is too slender for deflections without preambering.

### Reducing the height of the girder to 19 m and reducing the member thickness

$$I_{gir} := 100 \cdot I_{stif} := 60 \cdot b_{box} := 12 \cdot 10^3; h_{box} := 3 \cdot 10^3; b_{stif} := 200; b_{stif2} := 100; h_{stif} := 600;$$

$$I_{stifweb} := 1000;$$

$$I_{stifweb} := 60 \cdot b_{stifweb} := 400;$$

$$A_{box} := b_{box} \cdot t_{gir} \cdot 2 + h_{box} \cdot t_{gir} \cdot 2; A_{stif} := (b_{stif} + 2 \cdot h_{stif}) \cdot t_{stif}; A_{stifweb} := b_{stifweb} \cdot t_{stifweb}; A_{brace} := 2 \cdot \Pi$$

$$I_{brace} \cdot t_{gir};$$

$$A_{gir} := 2 \cdot A_{box} + A_{stif} \cdot 12 \cdot 3 \cdot 2 + A_{stifweb} \cdot 3 \cdot 4 \cdot 2 + 4 \cdot A_{brace};$$

$$e_{stif} := \frac{b_{stif} \cdot t_{stif} \cdot h_{stif} + \frac{2 \cdot I_{stif} \cdot h_{stif} \cdot h_{stif}}{2}}{A_{stif}};$$

$$I_{stif,flange} := \frac{1}{12} \cdot b_{stif} \cdot t_{stif}^3 + b_{stif} \cdot t_{stif} \cdot (h_{stif} - e_{stif})^2 + 2 \cdot \left( \frac{1}{12} \cdot t_{stif} \cdot h_{stif}^3 + I_{stif} \cdot h_{stif} \cdot \left( \frac{h_{stif}}{2} - e_{stif} \right)^2 \right);$$

$$I_{stifweb} := \frac{1}{12} \cdot t_{stifweb} \cdot b_{stifweb}^3 \cdot I_{brace} := \Pi \cdot r_{brace}^4 \cdot t_{gir};$$

$$I_{box} := \frac{1}{12} \cdot b_{box} \cdot h_{box}^3 - \frac{1}{12} \cdot (b_{box} - 2 \cdot t_{gir}) \cdot (h_{box} - 2 \cdot t_{gir})^3;$$

$$I_{gir} := 2 \cdot (I_{box} + A_{box} \cdot 8000^2) + 2 \cdot 12 \cdot (I_{stif,flange} + A_{stif} \cdot (9500 - e_{stif})^2) + 2 \cdot 12 \cdot (I_{stifweb} + A_{stifweb} \cdot 8000^2) + 4 \cdot (I_{brace} + A_{brace} \cdot 3250^2);$$

$$E := 2.1 \cdot 10^5;$$

We calculate deflections again:

$$q_{traffic} := 35 \cdot Q_{traffic} := 1200 \cdot 10^3;$$

$$q_{sw} := A_{gir} \cdot 10^{-9} \cdot 7850 \cdot 9.81 + 40 \cdot q_{tot} := evalf(q_{traffic} + q_{sw});$$

$$w_{mid,hinged} := evalf\left(\frac{5 \cdot q_{tot} \cdot (462 \cdot 10^3)^4}{384 \cdot E \cdot I_{gir}} + \frac{Q_{traffic} \cdot (462 \cdot 10^3)^3}{48 \cdot E \cdot I_{gir}}\right);$$

$$q_{tot} := 1047.155304$$

$$w_{mid,hinged} := 3439.253368$$

$$w_{mid,hinged,prec} := evalf\left(\frac{5 \cdot q_{traffic} \cdot (462 \cdot 10^3)^4}{384 \cdot E \cdot I_{gir}} + \frac{Q_{traffic} \cdot (462 \cdot 10^3)^3}{48 \cdot E \cdot I_{gir}}\right);$$

$$w_{mid,hinged,prec} := 128.0942080$$

Conclusion: this girder height gives a deflection at mid-span comparable to the deflection of the girder



designed by Yip (2015).

### New box/truss combination girder, design II

A new, slightly more realistic design was made, see the attached image. In this design, the flanges have two extra webs to increase the punching shear resistance of the truss members. Furthermore, the middle flange in the box was removed to make fabrication more feasible.

$$t_{gir} := 100 \cdot t_{stif} := 60 \cdot b_{box} := 12 \cdot 10^3 \cdot h_{box} := 3 \cdot 10^3 \cdot b_{stif} := 200 \cdot b_{stif2} := 100 \cdot h_{stif} := 600 ;$$

$$t_{brace} := 1000 ;$$

$$t_{stifweb} := 60 \cdot b_{stifweb} := 400 ;$$

$$A_{box} := b_{box} \cdot t_{gir} \cdot 2 + h_{box} \cdot t_{gir} \cdot 4 ; A_{stif} := (b_{stif} + 2 \cdot h_{stif}) \cdot t_{stif} ; A_{stifweb} := b_{stifweb} \cdot t_{stifweb} \cdot A_{brace} := 2 \cdot \Pi \cdot t_{brace} \cdot t_{gir} ;$$

$$A_{gir} := evalf(2 \cdot A_{box} + A_{stif} \cdot 12 \cdot 2 \cdot 2 + A_{stifweb} \cdot 6 \cdot 5 \cdot 2 + 4 \cdot A_{brace}) ;$$

$$e_{stif} := \frac{b_{stif} \cdot t_{stif} \cdot h_{stif} + \frac{2 \cdot t_{stif} \cdot h_{stif} \cdot h_{stif}}{2}}{A_{stif}} ;$$

$$I_{stif,flange} := \frac{1}{12} \cdot b_{stif} \cdot t_{stif}^3 + b_{stif} \cdot t_{stif} \cdot (h_{stif} - e_{stif})^2 + 2 \cdot \left( \frac{1}{12} \cdot t_{stif} \cdot h_{stif}^3 + t_{stif} \cdot h_{stif} \cdot \left( \frac{h_{stif}}{2} - e_{stif} \right)^2 \right) ;$$

$$I_{stifweb} := \frac{1}{12} \cdot t_{stifweb}^3 \cdot b_{stifweb} + t_{stifweb} \cdot b_{stifweb} \cdot I_{brace} := \Pi \cdot t_{brace}^3 \cdot t_{gir} ;$$

$$I_{box} := \frac{1}{12} \cdot b_{box} \cdot h_{box}^3 - \frac{1}{12} \cdot (b_{box} - 2 \cdot t_{gir}) \cdot (h_{box} - 2 \cdot t_{gir})^3 + 2 \cdot \frac{1}{12} \cdot t_{gir} \cdot h_{box} ;$$

$$I_{gir} := evalf(2 \cdot (I_{box} + A_{box} \cdot 8500^2) + 2 \cdot 12 \cdot (I_{stif,flange} + A_{stif} \cdot (10000 - e_{stif})^2) + 2 \cdot 12 \cdot (I_{stifweb} + A_{stifweb} \cdot 3500^2) + A_{stif} \cdot (7000 + e_{stif})^2) + 2 \cdot 5 \cdot 6 \cdot (I_{stifweb} + A_{stifweb} \cdot 8500^2) + 4 \cdot (I_{brace} + A_{brace} \cdot 3500^2) ;$$

$$E := 2.1 \cdot 10^5 ;$$

$$A_{gir} := 1.518527412 \cdot 10^7$$

$$I_{gir} := 9.639714633 \cdot 10^{14}$$

(13)

We calculate deflections again:

$$q_{traffic} := 35 \cdot Q_{traffic} := 1200 \cdot 10^2 ;$$

$$q_{sw} := A_{gir} \cdot 10^{-9} \cdot 7850 \cdot 9.81 + 40 \cdot q_{tot} := evalf(q_{traffic} + q_{sw}) ;$$

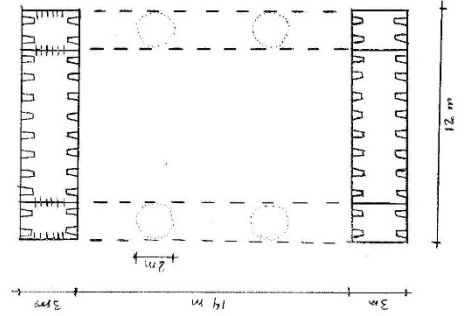
$$w_{mid,hinged} := evalf \left( \frac{5 \cdot q_{tot} \cdot (462 \cdot 10^3)^4}{384 \cdot E \cdot I_{gir}} + \frac{Q_{traffic} \cdot (462 \cdot 10^3)^3}{48 \cdot E \cdot I_{gir}} \right) ;$$

$$q_{tot} := 1244.395182$$

$$w_{mid,hinged} := 3658.722792$$

$$w_{mid,hinged,prec} := evalf \left( \frac{5 \cdot q_{traffic} \cdot (462 \cdot 10^3)^4}{384 \cdot E \cdot I_{gir}} + \frac{Q_{traffic} \cdot (462 \cdot 10^3)^3}{48 \cdot E \cdot I_{gir}} \right) ;$$

(5)



$$q_{tot} := 1541.852437$$

$$w_{mid,hinged} := 2845.492320$$

$$w_{mid,hinged,prec} := evalf \left( \frac{5 \cdot q_{traffic} \cdot (462 \cdot 10^3)^4}{384 \cdot E \cdot I_{gir}} + \frac{Q_{traffic} \cdot (462 \cdot 10^3)^3}{48 \cdot E \cdot I_{gir}} \right) ;$$

$$w_{mid,hinged,prec} := 72.06795411$$

This gives deflections lower than the truss designed by Yip (2015). A more slender girder might be possible.

### Reducing the height of the girder to 20 m

$$t_{gir} := 120 \cdot t_{stif} := 80 \cdot b_{box} := 12 \cdot 10^3 \cdot h_{box} := 3 \cdot 10^3 \cdot b_{stif} := 200 \cdot b_{stif2} := 100 \cdot h_{stif} := 600 ;$$

$$t_{brace} := 1000 ;$$

$$t_{stifweb} := 80 \cdot b_{stifweb} := 400 ;$$

$$A_{box} := b_{box} \cdot t_{gir} \cdot 2 + h_{box} \cdot t_{gir} \cdot 2 ; A_{stif} := (b_{stif} + 2 \cdot h_{stif}) \cdot t_{stif} ; A_{stifweb} := b_{stifweb} \cdot t_{stifweb} \cdot A_{brace} := 2 \cdot \Pi \cdot t_{brace} \cdot t_{gir} ;$$

$$t_{brace} \cdot t_{gir} ;$$

$$A_{gir} := 2 \cdot A_{box} + A_{stif} \cdot 12 \cdot 3 \cdot 2 + A_{stifweb} \cdot 3 \cdot 4 \cdot 2 + 4 \cdot A_{brace} ;$$

$$e_{stif} := \frac{b_{stif} \cdot t_{stif} \cdot h_{stif} + \frac{2 \cdot t_{stif} \cdot h_{stif} \cdot h_{stif}}{2}}{A_{stif}} ;$$

$$I_{stif,flange} := \frac{1}{12} \cdot b_{stif} \cdot t_{stif}^3 + b_{stif} \cdot t_{stif} \cdot (h_{stif} - e_{stif})^2 + 2 \cdot \left( \frac{1}{12} \cdot t_{stif} \cdot h_{stif}^3 + t_{stif} \cdot h_{stif} \cdot \left( \frac{h_{stif}}{2} - e_{stif} \right)^2 \right) ;$$

$$I_{stifweb} := \frac{1}{12} \cdot t_{stifweb}^3 \cdot b_{stifweb} + t_{stifweb} \cdot b_{stifweb} \cdot I_{brace} := \Pi \cdot t_{brace}^3 \cdot t_{gir} ;$$

$$I_{box} := \frac{1}{12} \cdot b_{box} \cdot h_{box}^3 - \frac{1}{12} \cdot (b_{box} - 2 \cdot t_{gir}) \cdot (h_{box} - 2 \cdot t_{gir})^3 + 2 \cdot \frac{1}{12} \cdot t_{gir} \cdot h_{box} ;$$

$$I_{gir} := 2 \cdot (I_{box} + A_{box} \cdot 8500^2) + 2 \cdot 12 \cdot (I_{stif,flange} + A_{stif} \cdot (10000 - e_{stif})^2) + 2 \cdot 12 \cdot (I_{stifweb} + A_{stifweb} \cdot 8500^2) + 4 \cdot (I_{brace} + A_{brace} \cdot 3500^2) ;$$

$$E := 2.1 \cdot 10^5 ;$$

We calculate deflections again:

$$q_{traffic} := 35 \cdot Q_{traffic} := 1200 \cdot 10^2 ;$$

$$q_{sw} := A_{gir} \cdot 10^{-9} \cdot 7850 \cdot 9.81 + 40 \cdot q_{tot} := evalf(q_{traffic} + q_{sw}) ;$$

$$w_{mid,hinged} := evalf \left( \frac{5 \cdot q_{tot} \cdot (462 \cdot 10^3)^4}{384 \cdot E \cdot I_{gir}} + \frac{Q_{traffic} \cdot (462 \cdot 10^3)^3}{48 \cdot E \cdot I_{gir}} \right) ;$$

$$q_{tot} := 1309.600272$$

$$w_{mid,hinged} := 3009.722703$$

$$w_{mid, hinged, prec} := 114.7413093 \quad (15)$$

This gives a deflection comparable to that of the truss designed by Yip (2015). This gives possibilities for designing a more slender girder.

(6)

$$w_{mid, hinged, prec} := evalf\left(\frac{5 \cdot q_{traffic} \cdot (462 \cdot 10^3)^4}{384 \cdot E \cdot I_{gir}} + \frac{Q_{traffic} \cdot (462 \cdot 10^3)^3}{48 \cdot E \cdot I_{gir}}\right);$$

$$w_{mid, hinged, prec} := 89.70328028$$

Deflections increase but not significantly.

**Reducing both the height of the girder to 20 m as the member thickness**

$$t_{gir} := 100; t_{sif} := 60; b_{box} := 12 \cdot 10^3; h_{box} := 3 \cdot 10^3; b_{sif} := 200; b_{sif2} := 100; h_{sif} := 600;$$

$$t_{brace} := 1000;$$

$$t_{sifweb} := 60; b_{sifweb} := 400;$$

$$A_{box} := b_{box} \cdot t_{gir} \cdot 2 + h_{box} \cdot t_{gir} \cdot 4; A_{sif} := (b_{sif} + 2 \cdot h_{sif}) \cdot t_{sif}; A_{sifweb} := b_{sifweb} \cdot t_{sifweb}; A_{brace} := 2 \cdot \Pi \cdot t_{brace} \cdot t_{gir};$$

$$A_{gir} := 2 \cdot A_{box} + A_{sif} \cdot 12 \cdot 2 + A_{sifweb} \cdot 3 \cdot 4 \cdot 2 + 4 \cdot A_{brace};$$

$$e_{sif} := \frac{b_{sif} \cdot t_{sif} \cdot h_{sif} + \frac{2 \cdot t_{sif} \cdot h_{sif} \cdot h_{sif}}{2}}{A_{sif}};$$

$$I_{sif, flange} := \frac{1}{12} \cdot b_{sif} \cdot t_{sif}^3 + b_{sif} \cdot t_{sif} \cdot (h_{sif} - e_{sif})^2 + 2 \cdot \left(\frac{1}{12} \cdot t_{sif} \cdot h_{sif}^3 + t_{sif} \cdot h_{sif} \cdot \left(\frac{h_{sif}}{2} - e_{sif}\right)^2\right);$$

$$I_{sifweb} := \frac{1}{12} \cdot t_{sifweb}^3 \cdot b_{sifweb} + I_{brace} := \Pi \cdot t_{brace}^3 \cdot t_{gir};$$

$$I_{box} := \frac{1}{12} \cdot b_{box} \cdot h_{box}^3 - \frac{1}{12} \cdot (b_{box} - 2 \cdot t_{gir}) \cdot (h_{box} - 2 \cdot t_{gir})^3;$$

$$I_{gir} := 2 \cdot (I_{box} + A_{box} \cdot 8500^2) + 2 \cdot 12 \cdot (I_{sif, flange} + A_{sif} \cdot (10000 - e_{sif})^2) + 2 \cdot 12 \cdot (I_{sifweb} + A_{sifweb} \cdot 8500^2) + 4 \cdot (I_{brace} + A_{brace} \cdot 3500^2);$$

$$E := 2.1 \cdot 10^5;$$

We calculate deflections again:

$$q_{traffic} := 35; Q_{traffic} := 1200 \cdot 10^3;$$

$$q_{sw} := A_{gir} \cdot 10^{-9} \cdot 7850 \cdot 9.81 + 40 \cdot q_{tot} := evalf(q_{traffic} + q_{sw});$$

$$w_{mid, hinged} := evalf\left(\frac{5 \cdot q_{tot} \cdot (462 \cdot 10^3)^4}{384 \cdot E \cdot I_{gir}} + \frac{Q_{traffic} \cdot (462 \cdot 10^3)^3}{48 \cdot E \cdot I_{gir}}\right);$$

$$q_{tot} := 1047.155304$$

$$w_{mid, hinged} := 3053.515588$$

$$w_{mid, hinged, prec} := evalf\left(\frac{5 \cdot q_{traffic} \cdot (462 \cdot 10^3)^4}{384 \cdot E \cdot I_{gir}} + \frac{Q_{traffic} \cdot (462 \cdot 10^3)^3}{48 \cdot E \cdot I_{gir}}\right);$$

**Same as original, but now with 19 m height**

$$t_{gir} := 100; t_{sif} := 60; b_{box} := 12 \cdot 10^3; h_{box} := 3 \cdot 10^3; b_{sif} := 200; b_{sif2} := 100; h_{sif} := 600;$$

$$t_{brace} := 1000;$$

$$t_{sifweb} := 60; b_{sifweb} := 400;$$

$$A_{box} := b_{box} \cdot t_{gir} \cdot 2 + h_{box} \cdot t_{gir} \cdot 4; A_{sif} := (b_{sif} + 2 \cdot h_{sif}) \cdot t_{sif}; A_{sifweb} := b_{sifweb} \cdot t_{sifweb}; A_{brace} := 2 \cdot \Pi \cdot t_{brace} \cdot t_{gir};$$

$$A_{gir} := 2 \cdot A_{box} + A_{sif} \cdot 12 \cdot 2 + A_{sifweb} \cdot 5 \cdot 6 \cdot 2 + 4 \cdot A_{brace};$$

$$e_{sif} := \frac{b_{sif} \cdot t_{sif} \cdot h_{sif} + \frac{2 \cdot t_{sif} \cdot h_{sif} \cdot h_{sif}}{2}}{A_{sif}};$$

$$I_{sif, flange} := \frac{1}{12} \cdot b_{sif} \cdot t_{sif}^3 + b_{sif} \cdot t_{sif} \cdot (h_{sif} - e_{sif})^2 + 2 \cdot \left(\frac{1}{12} \cdot t_{sif} \cdot h_{sif}^3 + t_{sif} \cdot h_{sif} \cdot \left(\frac{h_{sif}}{2} - e_{sif}\right)^2\right);$$

$$I_{sifweb} := \frac{1}{12} \cdot t_{sifweb}^3 \cdot b_{sifweb} + I_{brace} := \Pi \cdot t_{brace}^3 \cdot t_{gir};$$

$$I_{box} := \frac{1}{12} \cdot b_{box} \cdot h_{box}^3 - \frac{1}{12} \cdot (b_{box} - 2 \cdot t_{gir}) \cdot (h_{box} - 2 \cdot t_{gir})^3 + 2 \cdot \frac{1}{12} \cdot t_{gir} \cdot h_{box};$$

$$I_{gir} := 2 \cdot (I_{box} + A_{box} \cdot 8000^2) + 2 \cdot 12 \cdot (I_{sif, flange} + A_{sif} \cdot (9500 - e_{sif})^2) + 2 \cdot 12 \cdot (I_{sifweb} + A_{sifweb} \cdot 3250^2);$$

$$E := 2.1 \cdot 10^5;$$

We calculate deflections again:

$$q_{traffic} := 35; Q_{traffic} := 1200 \cdot 10^3;$$

$$q_{sw} := A_{gir} \cdot 10^{-9} \cdot 7850 \cdot 9.81 + 40 \cdot q_{tot} := evalf(q_{traffic} + q_{sw});$$

$$w_{mid, hinged} := evalf\left(\frac{5 \cdot q_{tot} \cdot (462 \cdot 10^3)^4}{384 \cdot E \cdot I_{gir}} + \frac{Q_{traffic} \cdot (462 \cdot 10^3)^3}{48 \cdot E \cdot I_{gir}}\right);$$

$$q_{tot} := 1244.395182$$

$$w_{mid, hinged} := 4124.135632$$

$$w_{mid, hinged, prec} := evalf\left(\frac{5 \cdot q_{traffic} \cdot (462 \cdot 10^3)^4}{384 \cdot E \cdot I_{gir}} + \frac{Q_{traffic} \cdot (462 \cdot 10^3)^3}{48 \cdot E \cdot I_{gir}}\right);$$

$$w_{mid, hinged, prec} := 129.3371352 \quad (17)$$

This gives as expected a worse performance.

$$W_{mid, hinged, prec} := 113.7274923$$

(8) Same as original, but now with a height of 18 m and box flanges of 2 m height

The deflection at mid-span stays around the same; the girder self-weight reduces significantly. However, it is still far higher than the self-weight of the truss girder.

**Reducing the height of the girder to 16 m and reducing the member thickness**

$$t_{gir} := 100 : t_{stif} := 60 : b_{box} := 12 \cdot 10^3 : h_{box} := 3 \cdot 10^3 : b_{stif} := 200 : b_{stif2} := 100 : h_{stif} := 600 : t_{brace} := 1000 :$$

$$I_{stifweb} := 60 : b_{stifweb} := 400 :$$

$$A_{box} := b_{box} \cdot t_{gir} \cdot 2 + h_{box} \cdot t_{gir} \cdot 2 : A_{stif} := (b_{stif} + 2 \cdot h_{stif}) \cdot t_{stif} : A_{stifweb} := b_{stifweb} \cdot t_{stifweb} : A_{brace} := 2 \cdot \Pi \cdot t_{brace} \cdot t_{gir} :$$

$$A_{gir} := 2 \cdot A_{box} + A_{stif} \cdot 12 \cdot 3 \cdot 2 + A_{stifweb} \cdot 3 \cdot 4 \cdot 2 : + 4 \cdot A_{brace} :$$

$$e_{stif} := \frac{b_{stif} \cdot t_{stif} \cdot h_{stif} + \frac{2 \cdot t_{stif} \cdot h_{stif} \cdot h_{stif}}{2}}{A_{stif}} :$$

$$I_{stif, flange} := \frac{1}{12} \cdot b_{stif} \cdot t_{stif}^3 + b_{stif} \cdot t_{stif} \cdot \left( h_{stif} - e_{stif} \right)^2 + 2 \cdot \left( \frac{1}{12} \cdot t_{stif} \cdot h_{stif}^3 + t_{stif} \cdot h_{stif} \cdot \left( \frac{h_{stif}}{2} - e_{stif} \right)^2 \right) :$$

$$I_{stifweb} := \frac{1}{12} \cdot t_{stifweb}^3 \cdot b_{stifweb} : I_{brace} := \Pi \cdot t_{brace}^3 \cdot t_{gir} :$$

$$I_{box} := \frac{1}{12} \cdot b_{box} \cdot h_{box}^3 - \frac{1}{12} \cdot (b_{box} - 2 \cdot t_{gir}) \cdot (h_{box} - 2 \cdot t_{gir})^3 :$$

$$I_{gir} := 2 \cdot (I_{box} + A_{box} \cdot 8000^2) + 2 \cdot 12 \cdot (I_{stif, flange} + A_{stif} \cdot (8000 - e_{stif})^2) + 2 \cdot 12 \cdot (I_{stifweb} + A_{stifweb} \cdot 6500^2) + 4 \cdot (I_{brace} + A_{brace} \cdot 2500^2) :$$

$$E := 2.1 \cdot 10^5 :$$

We calculate deflections again:

$$q_{traffic} := 35 : Q_{traffic} := 1200 \cdot 10^3 :$$

$$q_{sw} := A_{gir} \cdot 10^{-9} \cdot 7850 \cdot 9.81 + 40 : q_{tot} := evalf(q_{traffic} + q_{sw}) :$$

$$W_{mid, hinged} := evalf \left( \frac{5 \cdot q_{tot} \cdot (462 \cdot 10^3)^4}{384 \cdot E \cdot I_{gir}} + \frac{Q_{traffic} \cdot (462 \cdot 10^3)^3}{48 \cdot E \cdot I_{gir}} \right) :$$

$$q_{tot} := 1047.155304$$

$$W_{mid, hinged} := 5155.798767$$

$$W_{mid, hinged, prec} := evalf \left( \frac{5 \cdot q_{traffic} \cdot (462 \cdot 10^3)^4}{384 \cdot E \cdot I_{gir}} + \frac{Q_{traffic} \cdot (462 \cdot 10^3)^3}{48 \cdot E \cdot I_{gir}} \right) :$$

$$W_{mid, hinged, prec} := 192.0265502$$

(9)

(10)

$$t_{gir} := 100 : t_{stif} := 60 : b_{box} := 12 \cdot 10^3 : h_{box} := 2 \cdot 10^3 : b_{stif} := 200 : b_{stif2} := 100 : h_{stif} := 600 : t_{brace} := 1000 :$$

$$I_{stifweb} := 60 : b_{stifweb} := 400 :$$

$$A_{box} := b_{box} \cdot t_{gir} \cdot 2 + h_{box} \cdot t_{gir} \cdot 4 : A_{stif} := (b_{stif} + 2 \cdot h_{stif}) \cdot t_{stif} : A_{stifweb} := b_{stifweb} \cdot t_{stifweb} : A_{brace} := 2 \cdot \Pi \cdot t_{brace} \cdot t_{gir} :$$

$$A_{gir} := 2 \cdot A_{box} + A_{stif} \cdot 12 \cdot 2 \cdot 2 + A_{stifweb} \cdot 3 \cdot 6 \cdot 2 : + 4 \cdot A_{brace} :$$

$$e_{stif} := \frac{b_{stif} \cdot t_{stif} \cdot h_{stif} + \frac{2 \cdot t_{stif} \cdot h_{stif} \cdot h_{stif}}{2}}{A_{stif}} :$$

$$I_{stif, flange} := \frac{1}{12} \cdot b_{stif} \cdot t_{stif}^3 + b_{stif} \cdot t_{stif} \cdot \left( h_{stif} - e_{stif} \right)^2 + 2 \cdot \left( \frac{1}{12} \cdot t_{stif} \cdot h_{stif}^3 + t_{stif} \cdot h_{stif} \cdot \left( \frac{h_{stif}}{2} - e_{stif} \right)^2 \right) :$$

$$I_{stifweb} := \frac{1}{12} \cdot t_{stifweb}^3 \cdot b_{stifweb} : I_{brace} := \Pi \cdot t_{brace}^3 \cdot t_{gir} :$$

$$I_{box} := \frac{1}{12} \cdot b_{box} \cdot h_{box}^3 - \frac{1}{12} \cdot (b_{box} - 2 \cdot t_{gir}) \cdot (h_{box} - 2 \cdot t_{gir})^3 + 2 \cdot \frac{1}{12} \cdot t_{gir} \cdot h_{box} :$$

$$I_{gir} := 2 \cdot (I_{box} + A_{box} \cdot 8000^2) + 2 \cdot 12 \cdot (I_{stif, flange} + A_{stif} \cdot (9000 - e_{stif})^2) + 2 \cdot 12 \cdot (I_{stifweb} + A_{stifweb} \cdot 3500^2) + 4 \cdot (I_{brace} + A_{brace} \cdot 3500^2) :$$

$$E := 2.1 \cdot 10^5 :$$

We calculate deflections again:

$$q_{traffic} := 35 : Q_{traffic} := 1200 \cdot 10^3 :$$

$$q_{sw} := A_{gir} \cdot 10^{-9} \cdot 7850 \cdot 9.81 + 40 : q_{tot} := evalf(q_{traffic} + q_{sw}) :$$

$$W_{mid, hinged} := evalf \left( \frac{5 \cdot q_{tot} \cdot (462 \cdot 10^3)^4}{384 \cdot E \cdot I_{gir}} + \frac{Q_{traffic} \cdot (462 \cdot 10^3)^3}{48 \cdot E \cdot I_{gir}} \right) :$$

$$q_{tot} := 944.8880160$$

$$W_{mid, hinged} := 3520.918983$$

$$W_{mid, hinged, prec} := evalf \left( \frac{5 \cdot q_{traffic} \cdot (462 \cdot 10^3)^4}{384 \cdot E \cdot I_{gir}} + \frac{Q_{traffic} \cdot (462 \cdot 10^3)^3}{48 \cdot E \cdot I_{gir}} \right) :$$

$$W_{mid, hinged, prec} := 145.2667898$$

By decreasing the box height, more material is brought to the outer edges of the girder, where it is most efficient. This gives good performance. However, the girder self-weight is still almost 3 times as high as the truss girder designed by Yip (2015). It is therefore concluded that a truss girder is the most efficient for this bridge.





### E.3 Pontoon modelling

The pontoons of the Sognefjord bridge have a certain buoyancy and rotational stiffness. Because of the large size of the pontoons in comparison to the rest of the bridge structure, the pontoon properties have a big effect on the behaviour of the Sognefjord bridge. Therefore this properties should be modelled correctly. In the research by Yip (2015) the pontoon rotational stiffness was determined by calculating the restoring moment of the pontoon under a certain rotation. This restoring moment was assumed to be created by the mass of the pontoon and the ballast. See figure E.2 for the principle. This was upon evaluation considered to be a broad assumption, but still deemed fit for this preliminary stage of research. Therefore this method was maintained for this thesis and the pontoon properties as determined by Yip (2015) were maintained in Scia model #1 of the whole Sognefjord bridge.

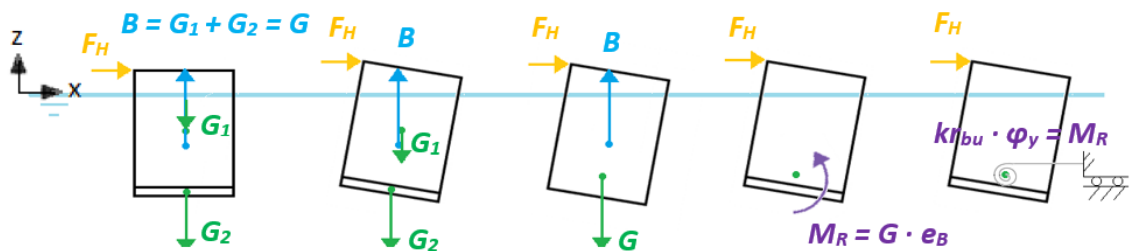


FIGURE E.2: CALCULATING ROTATIONAL STIFFNESS OF THE PONTOONS. RETRIEVED FROM YIP (2015).

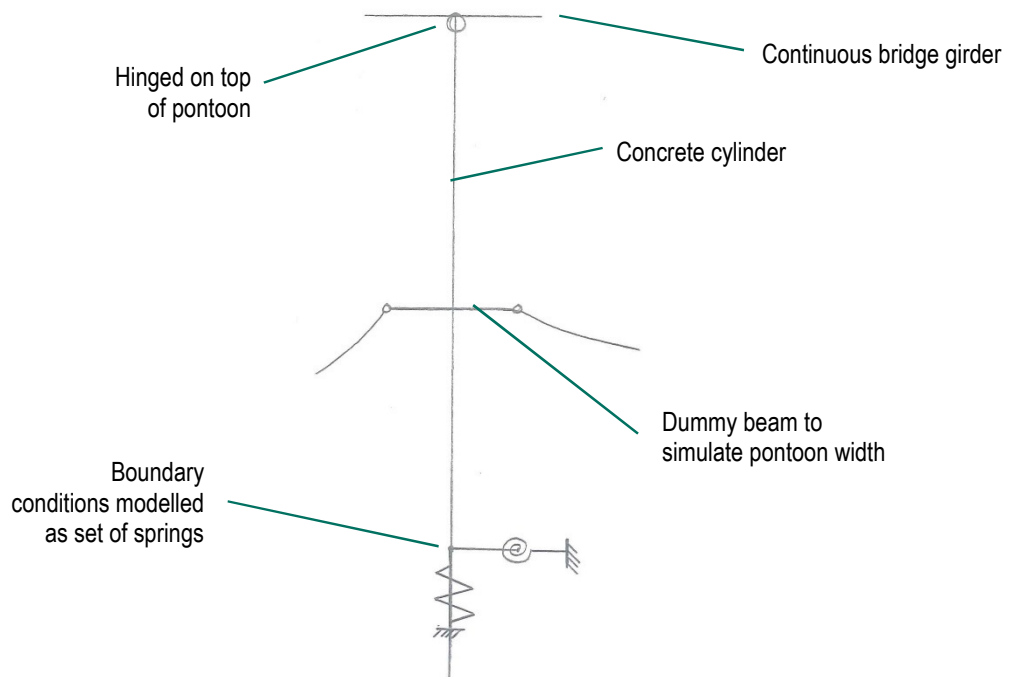
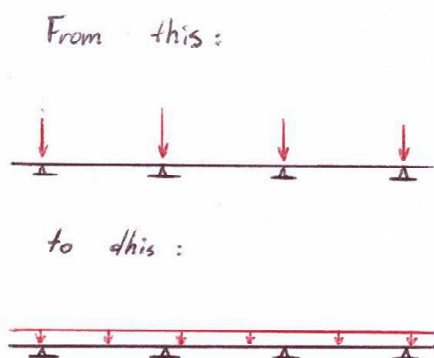


FIGURE E.3 SCHEMATIC REPRESENTATION OF HOW THE PONTOONS WERE MODELLED IN SCIA MODEL #1

The stiffness properties of the pontoons, being the buoyancy and the rotational stiffness, were modelled in Scia model #1 as a set of springs located at the centre of buoyancy of each pontoon. Since the lateral anchoring cables are fixed to the side of a pontoon, two weightless dummy beams were modelled to incorporate this. The cables are connected at 20 m below the water level. See figure E.3 for a sketch.

## E.4 Loads

In the SCIA-model by Yip (2015), self-weight of the superstructure was modelled as an external load. By modelling a cross-section with the appropriate self-weight, this was not necessary anymore. Furthermore, in the Scia model by Yip (2015) all the loads from the superstructure (including traffic loads) were modelled as concentrated loads on the pontoons. This omits the external moments resulting from these loads, which is unrealistically optimistic. By adding a self-weight, this load will become distributed (as is the case in real life) which also introduces resulting external moments. See figure E.2.



increased to 75 kN/m.

**FIGURE E.2: MORE REALISTIC WAY OF MODELLING SELF-WEIGHT LOADS IN SCIA**

Because of their complicated geometry, the pylons (the parts of the pontoon above water) weren't given their own cross-section yet. Therefore in Scia model #1 their self-weight value has been adjusted. The pylon self-weight in the model used by Yip (2015) was evaluated to be very low. For this thesis it has been adjusted to correspond to the pylon height, with a value of 28410 kN per 70 m height, a number used by Yip (2015) in Maple calculation files. When later in this research more properties of the pylon geometry are known, this value could be adjusted.

Lastly, in the model used by Yip (2015) all the self-weight loads from the superstructure as well as wind and traffic loads were modelled as acting on the centre of gravity of the pontoons. This was done on purpose to not affect rotations of the pontoons. However, since in this thesis the interests lies partly in these rotations, these should be modelled differently. The wind loads were therefore applied at the top of the pontoons. It was deemed more realistic to model these as distributed loads, as is the case in real-life. In modelling, loads were adjusted according to their location (e.g. large wind load at higher elevation, or lower current load at larger depth) and were given the right angle (instead of only modelling these orthogonally). See figures E.3 and E.5 for an overview and a view of loads in the SCIA model. As comparison, figure E.4 displays the way loads were modelled in the research by Yip (2015).

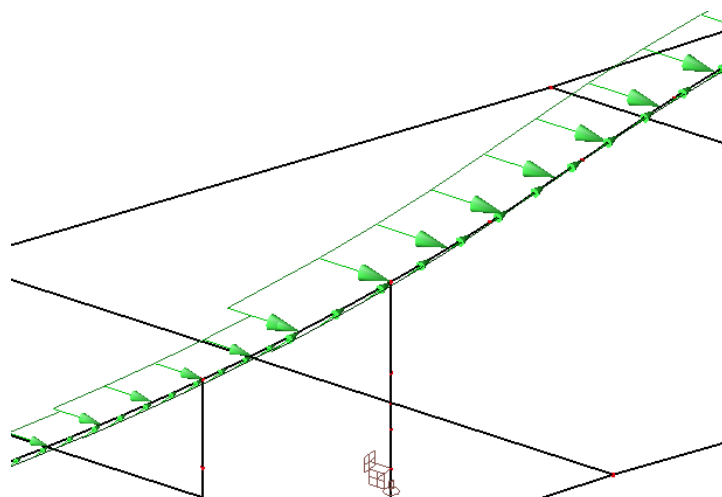


**FIGURE E.3: DISTRIBUTED WIND LOAD MODELLING, ADJUSTED FOR GIRDER HEIGHT**

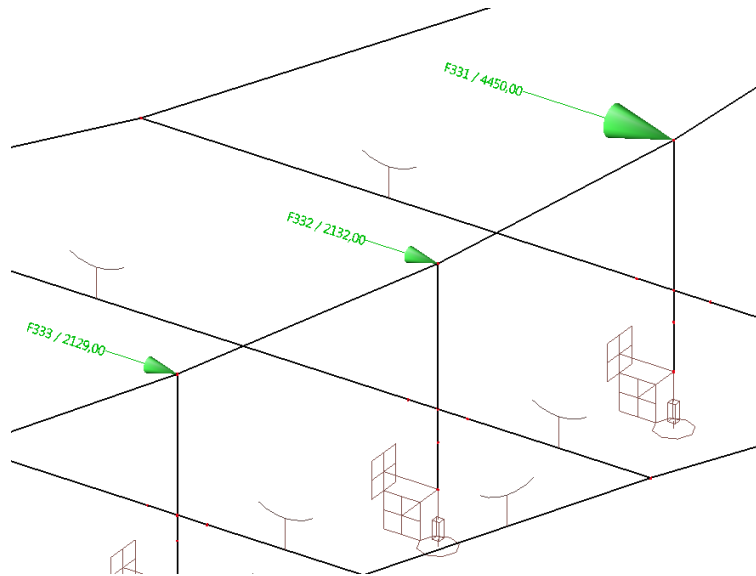


FIGURE E.4: WIND LOADS MODELLED IN RESEARCH BY YIP (2015)

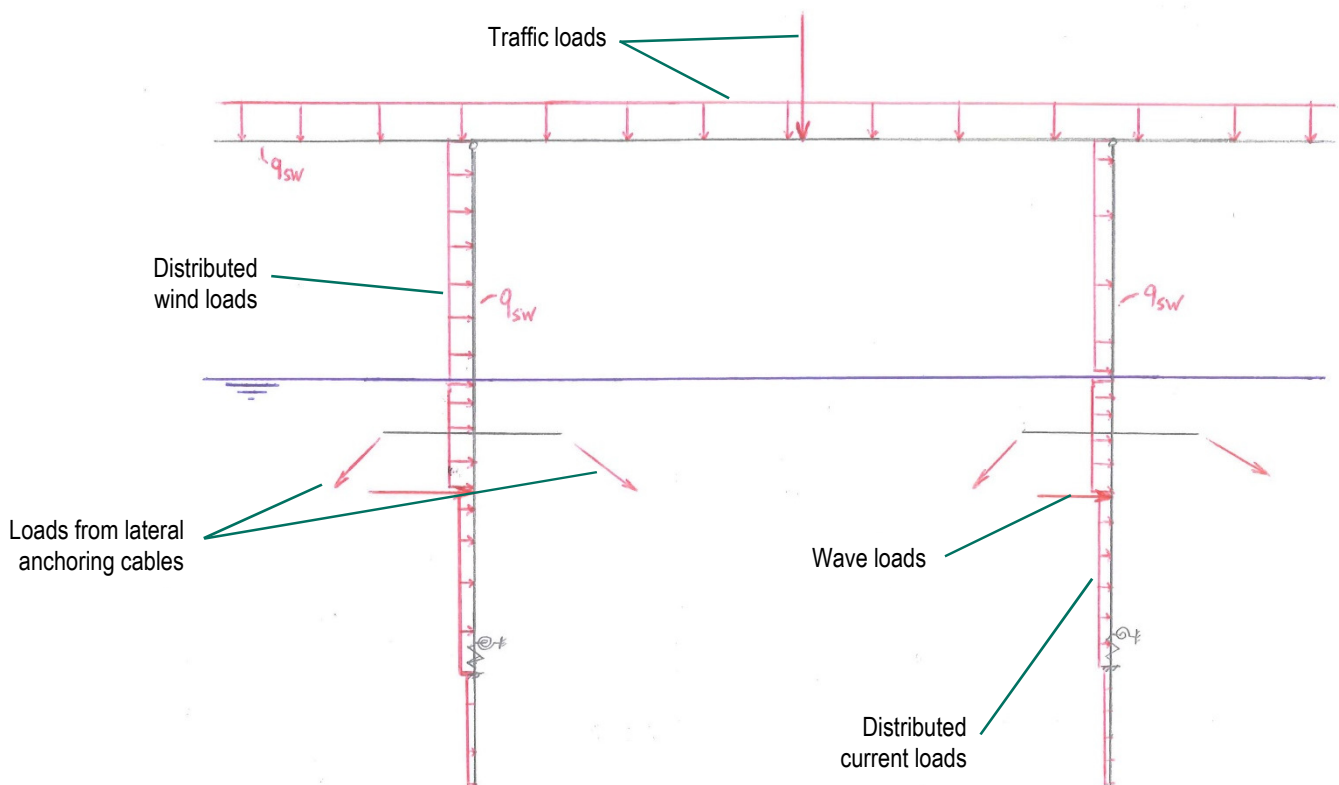


FIGURE E.5: MODELLING OF LOADS IN SCIA MODEL #1 OF THE WHOLE SOGNEFJORD BRIDGE

## ANNEX F: EXTERNAL LOADS CALCULATION FILE OUTPUT

### Calculation of environmental loads for SCIA model

In this file, all external load calculations are made. Unless specified differently, all values are in [kN], [m] and [kN/m].

#### Distributed ultimate wind loads on the bridge girders

According to NEN-EN-1991-1-4

Three wind directions taken into account: 150° (maximum wind in axial direction), 240° (maximum wind) and 270° (maximum sideways wind). Wind velocities with a 100 year return period are assumed.

The main span bridge girder is 26 m high (top to bottom), with the bottom elevating 70 m above water at the main span. The intermediate span girders are on average 13.59 m high (top to bottom). The side span girders are on average 10.88 m high (top to bottom), with the height according to the (new) SCIA model 01 of the whole bridge. All members are cylindrical and therefore a drag coefficient of 1.2 is used.

$$\begin{aligned}
 z_0 &:= 0.01 : z_{\min} := 1 : z_H := 0.05 : h_{\text{wind}} := 1 : P_w := 1.25 : c_p := 1 : C_d := 1.2 : \\
 v_{h,1,ULS} &:= 28 : v_{h,2,ULS} := 32 : \\
 z_{g,1} &:= 0 + \frac{10.88}{2} : z_{g,2} := 11.64 + \frac{10.88}{2} : z_{g,3} := 22.81 + \frac{10.88}{2} : z_{g,4} := 32.82 + \frac{10.88}{2} : z_{g,5} := 41.67 \\
 &+ \frac{10.88}{2} : z_{g,6} := 49.36 + \frac{10.88}{2} : z_{g,7} := 55.22 + \frac{10.88}{2} : z_{g,8} := 60.59 + \frac{10.88}{2} : z_{g,9} := 64.81 \\
 &+ \frac{10.88}{2} : z_{g,10} := 67.88 + \frac{13.69}{2} : z_{g,11} := 70 + \frac{26}{2} :
 \end{aligned}$$

For the main span, we assume the chords to be 3 m in diameter and the braces on average 1.6 m in diameter, with braces no crossing each other. In other words, the average area per m girder will be  $3 + 3 \cdot 1.6 = 7.6$  meters. The side area of the other spans are calculated according to the same analogy.

$$\begin{aligned}
 A_{\text{side},g,1} &:= 1.8 \cdot 2 + .8 : A_{\text{side},g,2} := 1.8 \cdot 2 + .8 : A_{\text{side},g,3} := 1.8 \cdot 2 + .8 : A_{\text{side},g,4} := 1.8 \cdot 2 + .8 : \\
 A_{\text{side},g,5} &:= 1.8 \cdot 2 + .8 : A_{\text{side},g,6} := 1.8 \cdot 2 + .8 : A_{\text{side},g,7} := 1.8 \cdot 2 + .8 : A_{\text{side},g,8} := 1.8 \cdot 2 + .8 : \\
 A_{\text{side},g,9} &:= 1.8 \cdot 2 + .8 : A_{\text{side},g,10} := 2.2 \cdot 2 + .8 : A_{\text{side},g,11} := 3 \cdot 2 + 1.6 :
 \end{aligned}$$

for i from 1 to 11 do  
for j from 1 to 2 do

$$\begin{aligned}
 v_{m,i,j,ULS} &:= .19 \cdot \left( \frac{z_0}{z_H} \right)^{.07} \cdot \ln \left( \frac{z_{g,i}}{z_0} \right) \cdot v_{h,j,ULS} : \\
 q_{pg,i,j,ULS} &:= \frac{\left[ 1 + \frac{7 \cdot k_{\text{wind}}}{c_0 \cdot \ln \left( \frac{z_{g,i}}{z_0} \right)} \right] \cdot \rho_w \cdot v_{m,i,j,ULS}^2}{2 \cdot 1000} \cdot A_{\text{side},g,i} \cdot C_d :
 \end{aligned}$$

end do  
end do

Now we can display the distributed wind load on the girders per pontoon. Each half of the girder will get the distributed load calculated for the respective pontoon.

$$\begin{aligned}
 \text{matrix}([ [ \text{Pontoon}, 1, 2, 3, 4, 5, 6, 7, 8, 9, 10, 11 ], [ q_{\text{wind girder}, ULS, 150} q_{pg,1,1, ULS} q_{pg,2,1, ULS} \\
 q_{pg,3,1, ULS} q_{pg,4,1, ULS} q_{pg,5,1, ULS} q_{pg,6,1, ULS} q_{pg,7,1, ULS} q_{pg,8,1, ULS} q_{pg,9,1, ULS} \\
 q_{pg,10,1, ULS} q_{pg,11,1, ULS} ], [ q_{\text{wind girder}, ULS, 270} q_{pg,1,2, ULS} q_{pg,2,2, ULS} q_{pg,3,2, ULS} q_{pg,4,2, ULS} \\
 q_{pg,5,2, ULS} q_{pg,6,2, ULS} q_{pg,7,2, ULS} q_{pg,8,2, ULS} q_{pg,9,2, ULS} q_{pg,10,2, ULS} q_{pg,11,2, ULS} ] ] ) : \\
 ([ [ \text{Pontoon}, 1, 2, 3, 4, 5, 6, 7, 8, 9, 10, 11 ], \\
 [ q_{\text{wind girder}, ULS, 150} 6.245494660, 8.014819824, 8.854764452, 9.379306580, 9.747090936, \\
 10.01839762, 10.20260291, 10.35758138, 10.47144678, 12.51016018, 18.62143540 ], \\
 [ q_{\text{wind girder}, ULS, 270} 8.157380785, 10.46833610, 11.56540662, 12.25052287, 12.73089428, \\
 13.08525403, 13.32584870, 13.52826956, 13.67699171, 16.33980103, 24.32187481 ] ] ) :
 \end{aligned}$$

For the wind loads in 240°-direction, we have to slightly adjust the calculation. Because SCIA can only input loads in orthogonal directions, we calculate components in x and y-directions.

$$\begin{aligned}
 v_{h,3,ULS} &:= 34 : \\
 c_{\text{angle},1} &:= \frac{1}{2} : c_{\text{angle},2} := \frac{1}{2} :
 \end{aligned}$$

for i from 1 to 11 do  
for j from 1 to 2 do

$$\begin{aligned}
 v_{m,2,i,ULS} &:= .19 \cdot \left( \frac{z_0}{z_H} \right)^{.07} \cdot \ln \left( \frac{z_{g,i}}{z_0} \right) \cdot v_{h,3,ULS} : \\
 q_{pg,2,i,j,ULS} &:= \text{evalf} \left( \frac{\left[ 1 + \frac{7 \cdot k_{\text{wind}}}{c_0 \cdot \ln \left( \frac{z_{g,i}}{z_0} \right)} \right] \cdot \rho_w \cdot v_{m,2,i,ULS}^2}{2 \cdot 1000} \cdot A_{\text{side},g,i} \cdot C_d \cdot c_{\text{angle},j} \right) :
 \end{aligned}$$

end do  
end do

$$\begin{aligned}
 \text{matrix}([ [ \text{Pontoon}, 1, 2, 3, 4, 5, 6, 7, 8, 9, 10, 11 ], [ q_{\text{wind girder}, ULS, 240} q_{pg,2,1,1, ULS} q_{pg,2,2,1, ULS} \\
 q_{pg,2,3,1, ULS} q_{pg,2,4,1, ULS} q_{pg,2,5,1, ULS} q_{pg,2,6,1, ULS} q_{pg,2,7,1, ULS} q_{pg,2,8,1, ULS} q_{pg,2,9,1, ULS} \\
 q_{pg,2,10,1, ULS} q_{pg,2,11,1, ULS} ], [ q_{\text{wind girder}, ULS, 240} q_{pg,2,1,2, ULS} q_{pg,2,2,2, ULS} q_{pg,2,3,2, ULS} \\
 q_{pg,2,4,2, ULS} q_{pg,2,5,2, ULS} q_{pg,2,6,2, ULS} q_{pg,2,7,2, ULS} q_{pg,2,8,2, ULS} q_{pg,2,9,2, ULS} q_{pg,2,10,2, ULS} \\
 q_{pg,2,11,2, ULS} ] ] ) :
 \end{aligned}$$

$$\begin{aligned}
 ([ [ \text{Pontoon}, 1, 2, 3, 4, 5, 6, 7, 8, 9, 10, 11 ], \\
 [ q_{\text{wind girder}, ULS, 240} 7.975157061, 10.23448908, 11.30705269, 11.97686445,
 \end{aligned}$$



12.44650509, 12.79294895, 13.02816911, 13.22606819, 13.37146811, 15.97479425,  
23.77856039];  
 $[q_{wind\ girder, SLS, 240, y}, 4.604459075, 5.908885025, 6.528129910, 6.914845915,$   
 $7.185993065, 7.386012520, 7.521816940, 7.636074030, 7.720020710, 9.223051760,$   
 $13.72855824]$

### Distributed serviceability wind loads on the bridge girders

According to NEN-EN-1991-1-4

The same wind directions are taken into account now, but with a wind velocity with a 5 year return period.

$v_{b,1,SLS} := 20 ; v_{b,2,SLS} := 24 ;$   
**for i from 1 to 11 do**  
**for j from 1 to 2 do**  
 $v_{m,i,j,SLS} := -19 \cdot \left( \frac{z_{g,i}}{z_{0j}} \right)^{0.7} \cdot \ln \left( \frac{z_{g,i}}{z_{0j}} \right) \cdot v_{b,i,SLS} ;$   

$$q_{pg,i,j,SLS} := \left[ \frac{1 + \frac{7 \cdot k_{wind}}{c_0 \cdot \ln \left( \frac{z_{g,i}}{z_{0j}} \right)}}{2 \cdot 1000} \cdot \rho_w \cdot v_{m,i,j,SLS}^2 \right] \cdot A_{side,g,i} \cdot C_d ;$$
  
**end do**  
**end do**

Now we can again display the distributed wind load on the girders per pontoon. Each half of the girder will get the distributed load calculated for the respective pontoon.

$matrix([ [Pontoon, 1, 2, 3, 4, 5, 6, 7, 8, 9, 10, 11], [q_{wind\ girder, SLS, 150}, q_{pg, 1, 1, SLS}, q_{pg, 2, 1, SLS}, q_{pg, 3, 1, SLS},$   
 $q_{pg, 4, 1, SLS}, q_{pg, 5, 1, SLS}, q_{pg, 6, 1, SLS}, q_{pg, 7, 1, SLS}, q_{pg, 8, 1, SLS}, q_{pg, 9, 1, SLS}, q_{pg, 10, 1, SLS}, q_{pg, 11, 1, SLS}],$   
 $[q_{wind\ girder, SLS, 270}, q_{pg, 1, 2, SLS}, q_{pg, 2, 2, SLS}, q_{pg, 3, 2, SLS}, q_{pg, 4, 2, SLS}, q_{pg, 5, 2, SLS}, q_{pg, 6, 2, SLS},$   
 $q_{pg, 7, 2, SLS}, q_{pg, 8, 2, SLS}, q_{pg, 9, 2, SLS}, q_{pg, 10, 2, SLS}, q_{pg, 11, 2, SLS}]]);$   
 $[ [Pontoon, 1, 2, 3, 4, 5, 6, 7, 8, 9, 10, 11];$   
 $[q_{wind\ girder, SLS, 150}, 3.186476869, 4.089193794, 4.517736965, 4.785360494, 4.973005578,$   
 $5.111427354, 5.205409649, 5.284480296, 5.342574880, 6.382734778, 9.500732348];$   
 $[q_{wind\ girder, SLS, 270}, 4.588526694, 5.888439058, 6.505541227, 6.890919108, 7.161128029,$   
 $7.360455384, 7.495789895, 7.609651632, 7.693307836, 9.191138081, 13.68105458]$

For the S-S wind loads in 240°-direction, again we have to slightly adjust the calculation. Because SCA can only input loads in orthogonal directions, we calculate components in x and y-directions.

$v_{b,3,SLS} := 24.5 ;$   
**for i from 1 to 11 do**  
**for j from 1 to 2 do**  
 $v_{m2,i,SLS} := -19 \cdot \left( \frac{z_{g,i}}{z_{0j}} \right)^{0.7} \cdot \ln \left( \frac{z_{g,i}}{z_{0j}} \right) \cdot v_{b,3,SLS} ;$   

$$q_{pg2,i,j,SLS} := evalf \left( \left[ \frac{1 + \frac{7 \cdot k_{wind}}{c_0 \cdot \ln \left( \frac{z_{g,i}}{z_{0j}} \right)}}{2 \cdot 1000} \cdot \rho_w \cdot v_{m2,i,SLS}^2 \right] \cdot A_{side,g,i} \cdot C_d \cdot \cos(\alpha_{angle,j}) \right);$$
  
**end do**  
**end do**  
 $matrix([ [Pontoon, 1, 2, 3, 4, 5, 6, 7, 8, 9, 10, 11], [q_{wind\ girder, SLS, 240, x}, q_{pg2, 1, 1, SLS}, q_{pg2, 2, 1, SLS},$   
 $q_{pg2, 3, 1, SLS}, q_{pg2, 4, 1, SLS}, q_{pg2, 5, 1, SLS}, q_{pg2, 6, 1, SLS}, q_{pg2, 7, 1, SLS}, q_{pg2, 8, 1, SLS}, q_{pg2, 9, 1, SLS},$   
 $q_{pg2, 10, 1, SLS}, q_{pg2, 11, 1, SLS}], [q_{wind\ girder, SLS, 240, y}, q_{pg2, 1, 2, SLS}, q_{pg2, 2, 2, SLS}, q_{pg2, 3, 2, SLS},$   
 $q_{pg2, 4, 2, SLS}, q_{pg2, 5, 2, SLS}, q_{pg2, 6, 2, SLS}, q_{pg2, 7, 2, SLS}, q_{pg2, 8, 2, SLS}, q_{pg2, 9, 2, SLS}, q_{pg2, 10, 2, SLS},$   
 $q_{pg2, 11, 2, SLS}]]);$   
 $[ [Pontoon, 1, 2, 3, 4, 5, 6, 7, 8, 9, 10, 11];$   
 $[q_{wind\ girder, SLS, 240, x}, 4.141079612, 5.314231898, 5.871157770, 6.218955789,$   
 $6.462815464, 6.642705542, 6.764843002, 6.867601577, 6.943100109, 8.294870459,$   
 $12.34695576];$   
 $[q_{wind\ girder, SLS, 240, y}, 2.390853428, 3.068173216, 3.389714518, 3.590515798,$   
 $3.731308247, 3.835167832, 3.905683927, 3.965011618, 4.008600716, 4.789045691,$   
 $7.128518230]$

### Distributed ultimate wind loads on the pylons

According to NEN-EN-1991-1-4

The same three wind directions are taken into account. For the elevation, the average height of each pontoon is taken. Wind velocities with a 100 year return period are assumed.

$z_{py,1} := 0 ; z_{py,2} := \frac{11.64}{2} ; z_{py,3} := \frac{22.81}{2} ; z_{py,4} := \frac{32.82}{2} ; z_{py,5} := \frac{41.67}{2} ; z_{py,6} := \frac{49.36}{2} ; z_{py,7} :=$   
 $\frac{55.22}{2} ; z_{py,8} := \frac{60.59}{2} ; z_{py,9} := \frac{64.81}{2} ; z_{py,10} := \frac{67.88}{2} ; z_{py,11} := \frac{70}{2} ;$

Only a broad sketch of the design has been made so far, which complicates projections of pylon area a bit. We assume that each pylon on average is half as wide as the pontoon on which it rests. The pylons have a rounded shape. This gives us the following pylon latera areas:

```
A_side,py,1 := 15 : A_side,py,2 := 18 : A_side,py,3 := 18 : A_side,py,4 := 18 : A_side,py,5 := 18 : A_side,py,6 := 18 :
A_side,py,7 := 21 : A_side,py,8 := 21 : A_side,py,9 := 21 : A_side,py,10 := 21 : A_side,py,11 := 26 :
```

for i from 1 to 11 do  
for j from 1 to 2 do

$$v_{mp,i,j,ULS} := .19 \cdot \left(\frac{z_0}{z_H}\right)^{.07} \cdot \ln\left(\frac{z_{py,i}}{z_0}\right) \cdot v_{b,j,ULS} :$$

$$q_{pp,i,j,ULS} := \frac{\left[1 + \frac{7 \cdot k_{wind}}{c_0 \cdot \ln\left(\frac{z_{py,i}}{z_0}\right)}\right] \cdot \rho_w \cdot v_{mp,i,j,ULS}^2}{2 \cdot 1000} \cdot A_{side,py,i} \cdot C_d :$$

end do  
end do

Now we can display the distributed wind load on the girders per pontoon. Each half of the girder will get the distributed load calculated for the respective pontoon.

```
matrix([[Pylon, 1, 2, 3, 4, 5, 6, 7, 8, 9, 10, 11], [q_wind_pylon,ULS,150,q_pp,1,1,ULS,q_pp,2,1,ULS,q_pp,3,1,ULS,
q_pp,4,1,ULS,q_pp,5,1,ULS,q_pp,6,1,ULS,q_pp,7,1,ULS,q_pp,8,1,ULS,q_pp,9,1,ULS,q_pp,10,1,ULS,
q_pp,11,1,ULS], [q_wind_pylon,ULS,270,q_pp,1,2,ULS,q_pp,2,2,ULS,q_pp,3,2,ULS,q_pp,4,2,ULS,q_pp,5,2,ULS,
q_pp,6,2,ULS,q_pp,7,2,ULS,q_pp,8,2,ULS,q_pp,9,2,ULS,q_pp,10,2,ULS,q_pp,11,2,ULS]]) :
```

(5)

```
[[Pylon, 1, 2, 3, 4, 5, 6, 7, 8, 9, 10, 11],
[q_wind_pylon,ULS,150,Float(∞),25.95474118,30.14178310,32.52126035,34.12650040,
35.28630043,42.07489469,42.83242800,43.38585720,43.76814608,54.50468862],
[q_wind_pylon,ULS,270,Float(∞),33.90007013,39.36885954,42.47674828,44.57338829,
46.08822914,54.95496446,55.94439580,56.66724211,57.16655812,71.18979734]]
```

For the wind loads in 240°-direction, we have to slightly adjust the calculation. Because SCIA can only input loads in orthogonal directions, we calculate component's in x and y-directions.

```
for i from 1 to 11 do  
for j from 1 to 2 do  
v_{mp,2,i,ULS} := .19 \cdot \left(\frac{z_0}{z_H}\right)^{.07} \cdot \ln\left(\frac{z_{py,i}}{z_0}\right) \cdot v_{b,3,ULS} :
```

$$q_{pp2,i,j,ULS} := \text{evalf}\left(\frac{\left[1 + \frac{7 \cdot k_{wind}}{c_0 \cdot \ln\left(\frac{z_{py,i}}{z_0}\right)}\right] \cdot \rho_w \cdot v_{m2,i,ULS}^2}{2 \cdot 1000} \cdot A_{side,py,i} \cdot C_d \cdot C_{angle,j}\right) :$$

end do  
end do

```
matrix([[Pylon, 1, 2, 3, 4, 5, 6, 7, 8, 9, 10, 11], [q_wind_pylon,ULS,240,x,q_pp2,1,1,ULS,q_pp2,2,1,ULS,
q_pp2,3,1,ULS,q_pp2,4,1,ULS,q_pp2,5,1,ULS,q_pp2,6,1,ULS,q_pp2,7,1,ULS,q_pp2,8,1,ULS,q_pp2,9,1,ULS,
q_pp2,10,1,ULS,q_pp2,11,1,ULS], [q_wind_pylon,ULS,240,y,q_pp2,1,2,ULS,q_pp2,2,2,ULS,q_pp2,3,2,ULS,
q_pp2,4,2,ULS,q_pp2,5,2,ULS,q_pp2,6,2,ULS,q_pp2,7,2,ULS,q_pp2,8,2,ULS,q_pp2,9,2,ULS,q_pp2,10,2,ULS,
q_pp2,11,2,ULS]])
```

(6)

```
[[Pylon, 1, 2, 3, 4, 5, 6, 7, 8, 9, 10, 11],
[q_wind_pylon,ULS,240,x,12.87741251,45.29985740,49.04762178,51.56799802,53.37922923,
54.73163415,64.93212369,65.84342188,66.51497456,67.26753079,85.10792414],
[q_wind_pylon,ULS,240,y,7.434777575,26.15388486,28.31765763,29.77279753,30.81851236,
31.59932370,37.48857908,38.01471734,38.40243846,38.83692700,49.13708290]]
```

### Distributed serviceability wind loads on the pylons

According to NEN-EN-1991-1-4

The same three wind directions are taken into account and wind velocities with a 5 year return period are assumed.

for i from 1 to 11 do  
for j from 1 to 2 do

$$v_{mp,i,j,SLS} := .19 \cdot \left(\frac{z_0}{z_H}\right)^{.07} \cdot \ln\left(\frac{z_{py,i}}{z_0}\right) \cdot v_{b,j,SLS} :$$

$$q_{pp,i,j,SLS} := \frac{\left[1 + \frac{7 \cdot k_{wind}}{c_0 \cdot \ln\left(\frac{z_{py,i}}{z_0}\right)}\right] \cdot \rho_w \cdot v_{mp,i,j,SLS}^2}{2 \cdot 1000} \cdot A_{side,py,i} \cdot C_d :$$

end do  
end do

Now we can display the distributed wind load on the girders per pontoon. Each half of the girder will get the distributed load calculated for the respective pontoon.



### Current loads on the pontoons

According to DNV C205, chapter 7.6.

The current differs along the water depth (for 10, 30 and 75 depth respectively) and will be project along the pontoons accordingly. The three maximum current velocities (100 year return period) are taken into account:

$$u_{c,1} := 1.27; u_{c,2} := .48; u_{c,3} := .39;$$

These are used to calculate the current velocities for the different pontoon types. Because SCIA can only input loads in orthogonal directions, we calculate components in x and y-directions.

$$d_{p,1} := 30; d_{p,2} := 36; d_{p,3} := 42; d_{p,4} := 52;$$

$$c_d := 1.5; p_{sp} := 1004.85;$$

for  $i$  from 1 to 4 do  
for  $j$  from 1 to 3 do  
for  $k$  from 1 to 2 do

$$q_{ep,i,j,k} := \text{evalf}\left(\frac{1}{2} \cdot \frac{p_{sp} \cdot d_{p,i}^2 \cdot u_{c,i}^2}{1000} \cdot c_{\text{angle},k}\right);$$

end do  
end do  
end do

Now we can display the current load on each pontoon, for each depth.

matrix([[Pontoon diameter type, 30 x, 36 x, 42 x, 52 x, 30 y, 36 y, 42 y, 52 y], [q<sub>current,10 depth,SLS</sub>,  
q<sub>ep,1,1,1</sub> q<sub>ep,2,1,1</sub> q<sub>ep,3,1,1</sub> q<sub>ep,4,1,1</sub> q<sub>ep,1,1,2</sub> q<sub>ep,2,1,2</sub> q<sub>ep,3,1,2</sub> q<sub>ep,4,1,2</sub>], [q<sub>current,30 depth,SLS</sub>,  
q<sub>ep,1,2,1</sub> q<sub>ep,2,2,1</sub> q<sub>ep,3,2,1</sub> q<sub>ep,4,2,1</sub> q<sub>ep,1,2,2</sub> q<sub>ep,2,2,2</sub> q<sub>ep,3,2,2</sub> q<sub>ep,4,2,2</sub>], [q<sub>current,75 depth,SLS</sub>,  
q<sub>ep,1,3,1</sub> q<sub>ep,2,3,1</sub> q<sub>ep,3,3,1</sub> q<sub>ep,4,3,1</sub> q<sub>ep,1,3,2</sub> q<sub>ep,2,3,2</sub> q<sub>ep,3,3,2</sub> q<sub>ep,4,3,2</sub>]])

[[[Pontoon diameter type, 30 x, 36 x, 42 x, 52 x, 30 y, 36 y, 42 y, 52 y],

[q<sub>current,10 depth,SLS</sub>, 31.58070557, 37.89684669, 44.21298780, 54.73988966,

18.23312886, 21.87975463, 25.52638040, 31.60409002],

[q<sub>current,30 depth,SLS</sub>, 4.511249651, 5.413499582, 6.315749512, 7.819499396,

2.604571200, 3.125485440, 3.646399680, 4.514590080],

[q<sub>current,75 depth,SLS</sub>, 2.978129652, 3.573755584, 4.169381514, 5.162091399,

1.719423956, 2.063308748, 2.407193539, 2.980334858]]]

### Ultimate wave loads on the pontoons

According to DNV C205, chapter 6.2

matrix([[Pylon, 1, 2, 3, 4, 5, 6, 7, 8, 9, 10, 11], [q<sub>wind,pylon,SLS,150°</sub>, q<sub>pp,1,1,SLS</sub>, q<sub>pp,2,1,SLS</sub>, q<sub>pp,3,1,SLS</sub>,  
q<sub>pp,4,1,SLS</sub>, q<sub>pp,5,1,SLS</sub>, q<sub>pp,6,1,SLS</sub>, q<sub>pp,7,1,SLS</sub>, q<sub>pp,8,1,SLS</sub>, q<sub>pp,9,1,SLS</sub>, q<sub>pp,10,1,SLS</sub>, q<sub>pp,11,1,SLS</sub>],  
[q<sub>wind,pylon,SLS,270°</sub>, q<sub>pp,1,2,SLS</sub>, q<sub>pp,2,2,SLS</sub>, q<sub>pp,3,2,SLS</sub>, q<sub>pp,4,2,SLS</sub>, q<sub>pp,5,2,SLS</sub>, q<sub>pp,6,2,SLS</sub>,  
q<sub>pp,7,2,SLS</sub>, q<sub>pp,8,2,SLS</sub>, q<sub>pp,9,2,SLS</sub>, q<sub>pp,10,2,SLS</sub>, q<sub>pp,11,2,SLS</sub>]])

[[[Pylon, 1, 2, 3, 4, 5, 6, 7, 8, 9, 10, 11],

[q<sub>wind,pylon,SLS,150°</sub>, Float(∞), 13.24221488, 15.37846075, 16.59247979, 17.41147980,

18.00321450, 21.46678301, 21.85327957, 22.13564144, 22.33068677, 27.80851460],

[q<sub>wind,pylon,SLS,270°</sub>, Float(∞), 19.06878947, 22.14498350, 23.89317089, 25.07253094,

25.92462890, 30.91216751, 31.46872261, 31.87532369, 32.15618894, 40.04426104]]]

For the wind loads in 240°-direction, we again have to slightly adjust the calculation. Because SCIA can only input loads in orthogonal directions, we calculate components in x and y-directions.

for  $i$  from 1 to 11 do  
for  $j$  from 1 to 2 do

$$v_{\text{avg},i,SLS} := .19 \cdot \left(\frac{z_0}{z_H}\right)^{.07} \cdot \ln\left(\frac{z_{py,i}}{z_0}\right) \cdot v_b,3,SLS;$$

$$q_{pp2,i,j,SLS} := \text{evalf}\left(\frac{1 + \frac{7 \cdot k_{\text{wind}}}{c_0 \cdot \ln\left(\frac{z_{py,i}}{z_0}\right)}}{2 \cdot 1000} \cdot p_w \cdot v_{\text{avg},i,SLS}^2 \cdot A_{\text{side},py,i} \cdot C_d \cdot c_{\text{angle},j}\right);$$

end do  
end do

matrix([[Pylon, 1, 2, 3, 4, 5, 6, 7, 8, 9, 10, 11], [q<sub>wind,pylon,SLS,240°</sub>, x, q<sub>pp2,1,1,SLS</sub>, q<sub>pp2,2,1,SLS</sub>,  
q<sub>pp2,3,1,SLS</sub>, q<sub>pp2,4,1,SLS</sub>, q<sub>pp2,5,1,SLS</sub>, q<sub>pp2,6,1,SLS</sub>, q<sub>pp2,7,1,SLS</sub>, q<sub>pp2,8,1,SLS</sub>, q<sub>pp2,9,1,SLS</sub>,  
q<sub>pp2,10,1,SLS</sub>, q<sub>pp2,11,1,SLS</sub>], [q<sub>wind,pylon,SLS,240°</sub>, y, q<sub>pp2,1,2,SLS</sub>, q<sub>pp2,2,2,SLS</sub>, q<sub>pp2,3,2,SLS</sub>,  
q<sub>pp2,4,2,SLS</sub>, q<sub>pp2,5,2,SLS</sub>, q<sub>pp2,6,2,SLS</sub>, q<sub>pp2,7,2,SLS</sub>, q<sub>pp2,8,2,SLS</sub>, q<sub>pp2,9,2,SLS</sub>, q<sub>pp2,10,2,SLS</sub>,  
q<sub>pp2,11,2,SLS</sub>]])

[[[Pylon, 1, 2, 3, 4, 5, 6, 7, 8, 9, 10, 11],

[q<sub>wind,pylon,SLS,240°</sub>, x, 6.686563029, 23.52183341, 25.46785033, 26.77654916, 27.71702623,

28.41925898, 33.71583672, 34.18902593, 34.53772791, 34.92849080, 44.19206873],

[q<sub>wind,pylon,SLS,240°</sub>, y, 3.860488964, 13.58033685, 14.70387024, 15.45944786, 16.00243255,

16.40786682, 19.46584740, 19.73904332, 19.94036650, 20.16597356, 25.51430277]]]



For the wind wave load on the pontoons, we assume the pontoons to be fixed cylinders and apply the Morison Equation. To do this, we first need to calculate the wave particle velocity and acceleration. We assume a mass coefficient of 1.5 (customary for cylindrical bodies in water). Again, we differentiate between four pontoon types and three wind directions: 150° (maximum wind in axial direction), 240° (maximum wind) and 270° (maximum sideways wind). For each wind direction, we assume the biggest according wave height, as a conservative simplification. Wind velocities with a 100 year return period are assumed.

$$\begin{aligned} L_{wp} &:= 36; T_{wp} := 4.8; d_{ford} := 1253; g := 9.81; z_{wp} := 0; C_a := 1.5; \\ k_{wp} &:= \frac{2 \cdot P_i}{L_{wp}}; \omega_{wp} := \frac{2 \cdot P_i}{T_{wp}}; \\ H_{wp,1,ULS} &:= 1.55; H_{wp,2,ULS} := 2.00; a_{wp,1,ULS} := \frac{H_{wp,1,ULS}}{2}; a_{wp,2,ULS} := \frac{H_{wp,2,ULS}}{2}; \end{aligned}$$

for i from 1 to 2 do  
for j from 1 to 4 do

$$\begin{aligned} u_{wp,i,ULS} &:= a_{wp,i,ULS} \cdot \omega_{wp} \cdot \frac{\cosh(k_{wp} \cdot z_{wp} + k_{wp} \cdot d_{ford})}{\sinh(k_{wp} \cdot d_{ford})} \cdot 1; \\ a_{x,wp,i,ULS} &:= a_{wp,i,ULS} \cdot g \cdot k_{wp} \cdot \frac{\cosh(k_{wp} \cdot z_{wp} + k_{wp} \cdot d_{ford})}{\cosh(k_{wp} \cdot d_{ford})} \cdot 1; \end{aligned}$$

$$F_{wp,i,j,ULS} := evalf \left( \rho_{sw} \cdot \frac{d_p^2 \cdot C_a \cdot a_{x,wp,i,ULS}}{4} + \frac{1}{2} \cdot \rho_{sw} \cdot d_p \cdot d_{p,j} \cdot u_{wp,i,ULS} \cdot \text{abs}(u_{wp,i,ULS}) \right);$$

end do  
end do

Now we can display the wind-wave forces for each pontoon type. In this first calculation we only display two of the three directions:

$$\begin{aligned} &matrix \left( \left[ \left[ \text{Pontoon diameter type, 30, 36, 42, 52} \right], \left[ F_{wp,150,ULS}, F_{wp,1,1,ULS}, F_{wp,1,2,ULS}, F_{wp,1,3,ULS} \right], \left[ F_{wp,1,4,ULS} \right], \left[ F_{wp,270,ULS}, F_{wp,2,1,ULS}, F_{wp,2,2,ULS}, F_{wp,2,3,ULS}, F_{wp,2,4,ULS} \right] \right] \right); \\ &\left[ \begin{array}{cccc} \text{Pontoon diameter type} & 30 & 36 & 42 & 52 \\ F_{wp,150,ULS} & 1432.365757 & 2058.139179 & 2797.012691 & 4279.802079 \\ F_{wp,270,ULS} & 1855.187103 & 2664.031324 & 3618.811145 & 5534.412181 \end{array} \right] \quad (10) \end{aligned}$$

For the wind waves in 240°-direction, we have to slightly adjust the calculation. Because SCIA can only input loads in orthogonal directions, we calculate components in x and y-directions.

$$H_{wp,3,ULS} := 2.34; a_{wp,3,ULS} := \frac{H_{wp,3,ULS}}{2};$$

for i from 1 to 4 do  
for j from 1 to 2 do

$$\begin{aligned} u_{wp,3,ULS} &:= a_{wp,3,ULS} \cdot \omega_{wp} \cdot \frac{\cosh(k_{wp} \cdot z_{wp} + k_{wp} \cdot d_{ford})}{\sinh(k_{wp} \cdot d_{ford})} \cdot 1; \\ a_{x,wp,3,ULS} &:= a_{wp,3,ULS} \cdot g \cdot k_{wp} \cdot \frac{\cosh(k_{wp} \cdot z_{wp} + k_{wp} \cdot d_{ford})}{\cosh(k_{wp} \cdot d_{ford})} \cdot 1; \end{aligned}$$

$$F_{wp2,i,j,ULS} := evalf \left( \rho_{sw} \cdot \frac{P_i}{4} \cdot C_a \cdot a_{x,wp,3,ULS} \cdot \frac{1}{1000} \cdot c_{angle,j} + \frac{1}{2} \cdot \rho_{sw} \cdot C_d \cdot d_{p,j} \cdot u_{wp,3,ULS} \cdot \text{abs}(u_{wp,3,ULS}) \cdot c_{angle,j} \right);$$

end do  
end do

matrix \left( \left[ \left[ \text{Pontoon diameter type, 30 x, 36 x, 42 x, 52 x, 30 y, 36 y, 42 y, 52 y} \right], \left[ F\_{wp,240,ULS}, F\_{wp2,1,1,ULS}, F\_{wp2,2,1,ULS}, F\_{wp2,3,1,ULS}, F\_{wp2,4,1,ULS}, F\_{wp2,1,2,ULS}, F\_{wp2,2,2,ULS}, F\_{wp2,3,2,ULS}, F\_{wp2,4,2,ULS} \right] \right] \right);

$$\left[ \left[ \text{Pontoon diameter type, 30 x, 36 x, 42 x, 52 x, 30 y, 36 y, 42 y, 52 y} \right], \left[ F_{wp,240,ULS}, 1885.106283, 2705.735158, 3674.233241, 5616.994950, 1088.366620, 1562.156921, 2121.319550, 3242.973546 \right] \right] \quad (11)$$

### Serviceability wave loads on the pontoons

According to DNV C205, chapter 6.2

We perform the same calculation, but now with wave heights with a return period of 5 years.

$$H_{wp,1,SLS} := 1.05; H_{wp,2,SLS} := 1.40; a_{wp,1,SLS} := \frac{H_{wp,1,SLS}}{2}; a_{wp,2,SLS} := \frac{H_{wp,2,SLS}}{2};$$

for i from 1 to 2 do  
for j from 1 to 4 do

$$u_{wp,i,SLS} := a_{wp,i,SLS} \cdot \omega_{wp} \cdot \frac{\cosh(k_{wp} \cdot z_{wp} + k_{wp} \cdot d_{ford})}{\sinh(k_{wp} \cdot d_{ford})} \cdot 1;$$

$$a_{x,wp,i,SLS} := a_{wp,i,SLS} \cdot g \cdot k_{wp} \cdot \frac{\cosh(k_{wp} \cdot z_{wp} + k_{wp} \cdot d_{ford})}{\cosh(k_{wp} \cdot d_{ford})} \cdot 1;$$

$$F_{wp,i,j,SLS} := evalf \left( \rho_{sw} \cdot \frac{P_i}{4} \cdot C_a \cdot a_{x,wp,i,SLS} \cdot \frac{1}{1000} + \frac{1}{2} \cdot \rho_{sw} \cdot C_d \cdot d_{p,j} \cdot u_{wp,i,SLS} \cdot \text{abs}(u_{wp,i,SLS}) \right);$$

end do

**end do**

Now we can display the wind-wave forces for each pontoon type. In this first calculation we only display two of the three directions:

$$\begin{aligned}
 & \text{matrix}([[\text{Pontoon diameter type}, 30, 36, 42, 52], [F_{\text{wp}, 1, 50, \text{SLS}}, F_{\text{wp}, 1, 1, \text{SLS}}, F_{\text{wp}, 1, 2, \text{SLS}}, F_{\text{wp}, 1, 3, \text{SLS}}, \\
 & F_{\text{wp}, 1, 4, \text{SLS}}], [F_{\text{wp}, 2, 70, \text{SLS}}, F_{\text{wp}, 2, 1, \text{SLS}}, F_{\text{wp}, 2, 2, \text{SLS}}, F_{\text{wp}, 2, 3, \text{SLS}}, F_{\text{wp}, 2, 4, \text{SLS}}]]); \\
 & \left[ \begin{array}{ccccc}
 \text{Pontoon diameter type} & 30 & 36 & 42 & 52 \\
 F_{\text{wp}, 1, 50, \text{SLS}} & 966.2445737 & 1389.342059 & 1889.055735 & 2892.170060 \\
 F_{\text{wp}, 2, 70, \text{SLS}} & 1292.122631 & 1857.011919 & 2524.056126 & 3862.807405
 \end{array} \right] \quad (12)
 \end{aligned}$$

For the wind waves in 240°-direction, we have to slightly adjust the calculation. Because SCIA can only input loads in orthogonal directions, we calculate components in x and y-directions.

$$\begin{aligned}
 H_{\text{wp}, 3, \text{SLS}} & := 1.50 \cdot a_{\text{wp}, 3, \text{SLS}} := \frac{H_{\text{wp}, 3, \text{SLS}}}{2}; \\
 & \text{for } i \text{ from 1 to 4 do} \\
 & \text{for } j \text{ from 1 to 2 do} \\
 u_{\text{wp}, 3, \text{SLS}} & := a_{\text{wp}, 3, \text{SLS}} \cdot \omega_{\text{wp}} \cdot \frac{\cosh(k_{\text{wp}} \cdot z_{\text{wp}} + k_{\text{wp}} \cdot d_{\text{port}})}{\sinh(k_{\text{wp}} \cdot d_{\text{port}})} \cdot 1; \\
 a_{x, \text{wp}, 3, \text{SLS}} & := a_{\text{wp}, 3, \text{SLS}} \cdot g \cdot k_{\text{wp}} \cdot \frac{\cosh(k_{\text{wp}} \cdot z_{\text{wp}} - k_{\text{wp}} \cdot d_{\text{port}})}{\cosh(k_{\text{wp}} \cdot d_{\text{port}})} \cdot 1; \\
 F_{\text{wp}, 2, i, j, \text{SLS}} & := \text{evalf}\left(\frac{\text{Pi}}{4} \cdot \frac{d_p^2}{4} \cdot C_d \cdot u_{x, \text{wp}, 3, \text{SLS}} \cdot C_{\text{angle}, j} + \frac{1}{2} \cdot \frac{P_{\text{sw}} \cdot C_d \cdot d_p \cdot u_{\text{wp}, 3, \text{SLS}} \cdot \text{abs}(u_{\text{wp}, 3, \text{SLS}}) \cdot C_{\text{angle}, j}}{1000}\right);
 \end{aligned}$$

**end do**

**end do**

$$\begin{aligned}
 & \text{matrix}([[\text{Pontoon diameter type}, 30 \text{ x}, 36 \text{ x}, 42 \text{ x}, 52 \text{ x}, 30 \text{ y}, 36 \text{ y}, 42 \text{ y}, 52 \text{ y}], [F_{\text{wp}, 2, 40, \text{SLS}}, \\
 & F_{\text{wp}, 2, 1, 1, \text{SLS}}, F_{\text{wp}, 2, 1, \text{SLS}}, F_{\text{wp}, 2, 3, 1, \text{SLS}}, F_{\text{wp}, 2, 4, 1, \text{SLS}}, F_{\text{wp}, 2, 1, 2, \text{SLS}}, F_{\text{wp}, 2, 2, 2, \text{SLS}}, F_{\text{wp}, 2, 3, 2, \text{SLS}}, \\
 & F_{\text{wp}, 2, 4, 2, \text{SLS}}]]); \\
 & [[\text{Pontoon diameter type}, 30 \text{ x}, 36 \text{ x}, 42 \text{ x}, 52 \text{ x}, 30 \text{ y}, 36 \text{ y}, 42 \text{ y}, 52 \text{ y}], \\
 & [F_{\text{wp}, 2, 40, \text{SLS}}, 1199.946881, 1724.300114, 2343.441302, 3585.983176, 692.7896541, \\
 & 995.5251352, 1352.986466, 2070.368352]] \quad (13)
 \end{aligned}$$

## ANNEX G: NEW SUPERSTRUCTURE DESIGN

### G.1 Search for truss layout

Compared to the design by Yip (2015), the superstructure concept was changed. Instead of hinges at both ends, each span is now fixed to the adjoining span. The biggest consequence from this is that the mid-span bending moment will be lower, and thus the mid-span deflection will also be much lower. At the first phase of design it became clear that instead of displacements, stresses in the members would be governing for the first design of the girder.

A few different truss types were investigated: Warren trusses (both normal and with double intersections), Pratt trusses (with the braces in tension to prevent buckling) and combinations between these. See figure G.1 for preliminary designs. For this stage of design, each truss was modelled with fixed boundary conditions. Later on, boundary conditions were made more realistic by connecting the bridge girders to each other.

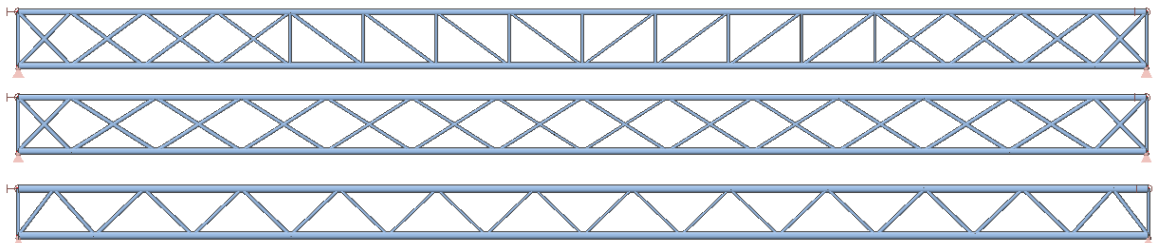


FIGURE G.1: THREE GIRDER LAYOUTS INVESTIGATED

For each type, a truss was designed with braces optimised for stresses. Then, these designs were given different girder heights and chord sizes. Each version was compared for maximum stresses and girder self-weight. The goal of this investigation was defining which truss concept had the best potential for creating a girder that was both as slender as possible, as well as light-weight.

It was found that the Warren truss gives the best relation between stress results and self-weight. Therefore it was decided to continue with the Warren truss layout. As a starting point, a Warren truss with a heart-to-heart height of 20 meters and 2500x65 mm chords was taken.

### G.2 Elaborating the Warren truss

The first next step was to adjust the member according to the bending moment diagram of a continuous beam (see figure G.2) to increase member efficiency. In continuous multi-span beams, the biggest bending moments and therefore stresses occur at the supports.

It was therefore decided to increase brace density and chord size near the supports, to lower stresses. The bending moment peaks decrease quickly, which means away from the span, member size could be decreased. For the same reason, the height of the girder could be decreased at mid-span. By doing this the girder would be both more slender and less heavy. This resulted in the following girder layout (see figure G.3) for the main span. In designing individual members were optimised for their stress level.

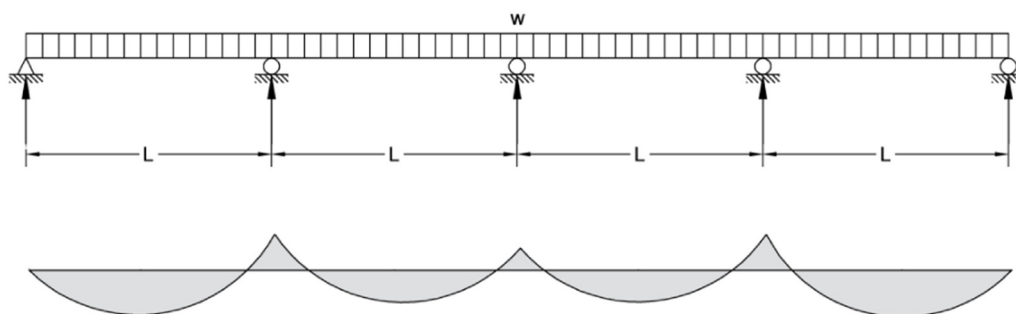


FIGURE G.2: BENDING MOMENT DIAGRAM FOR A CONTINUOUS BEAM

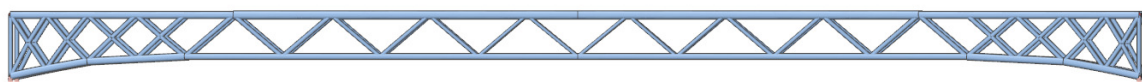


FIGURE G.3: FIRST MAIN TRUSS GIRDER LAYOUT, SIDE VIEW

### G.3 Girder properties

All members in every girder are circular hollow sections made of steel quality S460. The main span girder general properties are specified in table G.2. The size of each member is displayed in figure G.4.

TABLE G.2: MAIN GIRDER PROPERTIES

Property	Value
Girder self-weight	333 kN/m
Height	Heart-to-heart distance 17 m (mid-span) to 25 m (supports), absolute distance 20 m (mid-span) to 28 m (supports)
Girder curvature	3.1 m lateral difference









-  Main\_supporttube - Tube (3000; 120)
-  Main2 - Tube (3500; 80)
-  Main - Tube (3000; 80)
-  Main1 - Tube (2500; 55)
-  Sub - Tube (1800; 40)
-  Sub3 - Tube (1310; 27)
-  Sub2 - Tube (1450; 30)
-  Sub1 - Tube (1600; 35)

FIGURE G.4: MAIN GIRDER MEMBER SIZES

### G.4 Designing sub spans

After this, based on the main span layout, the sub span girders were designed. For the first sub spans right next to the main span a special different design was made. This because these are the transition, both in size as in force and stiffness, of the main span girder to the side span girders. Figure G.5 shows their layout.

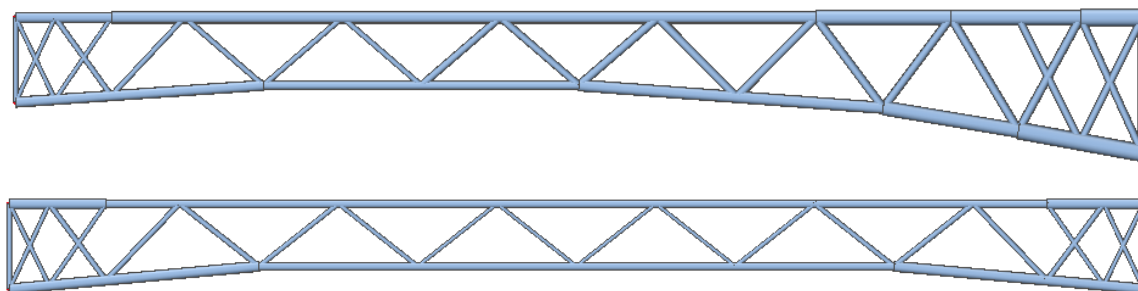


FIGURE G.5: INTERMEDIATE (ABOVE) AND SIDE SPAN (BELOW) GIRDER LAYOUT

The side girders are tapered towards the middle as well. This leads to a more slender design, in accordance with the architectural guidelines. Furthermore, to accompany a smooth transition in stiffness from the main to the side span girders, the intermediate span girder has member sizes decreasing towards the side span. In a statically undetermined system like this, stiffness has a large influence on the stress distribution in girders. Therefore the stiffness gradations were made as smooth as possible.

Table G.3 shows the general properties of the side span girders. The members of the side span girders differ in size from those of the main span girder. The intermediate span girders contain members of both; larger 'main span'-elements at the main span side, smaller 'side span'-elements towards the side span. The side span member sizes are displayed in figure G.6.

TABLE G.3: SIDE GIRDER PROPERTIES

Property	Value
Girder self-weight	Intermediate girder average <b>155 kN/m</b> Side span girder <b>87 kN/m</b>
Height	Heart-to-heart distance <b>12 m</b> (mid-span) to <b>16 m</b> (supports), absolute distance <b>13.4 m</b> (mid-span) to <b>17.8 m</b> (supports)
Girder curvature	Side span: <b>2.6 m</b> lateral difference








-  IMain - Tube (2000; 42)
-  SMain - Tube (1800; 40)
-  SSub - Tube (1000; 22)
-  SSub1 - Tube (900; 20)
-  SSub3 - Tube (900; 18)
-  SSub2 - Tube (900; 18)
-  SMain1 - Tube (1400; 32)

FIGURE G.6: SIDE GIRDER MEMBER SIZES

## G.5 Stability

During design, checks were made for stability. First, Eigenmodes of the whole structure were calculated through SCIA to check whether local or global buckling would be decisive. See figure G.7 for the first buckling shape of the bridge girder, where it is clearly visible only one member buckles out. This holds for all first five buckling shapes.

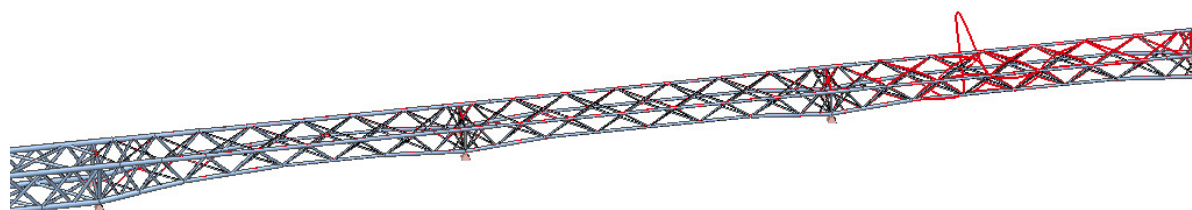


FIGURE G.7: BUCKLING MODE OF THE SUPERSTRUCTURE. LOCAL BUCKLING IS DECISIVE.

This showed that there was no global buckling shape to be taken into account. Therefore local maximum buckling stresses for all members were calculated according to Eurocode 3-1-6. The D/t ratio was kept at a minimum of 25 for each member, so all members would fall in cross-section class 1. The minimum buckling stress was found to be 435 N/mm<sup>2</sup>. The results of the calculation are given in table G.4.

TABLE G.4: BUCKLING STRESS CALCULATION RESULTS

Member type	r	t	Max. buckling length	d/t	$\lambda$	$\chi$	$\sigma_{x,Rd}$
Sub	900	40	15,808	45.00	0.37	0.98	448.6
Sub1	800	35	15,806	45.71	0.42	0.97	445.0
Sub2	725	30	15,799	48.33	0.46	0.96	441.4
Sub3	655	27	16,180	48.52	0.52	0.95	435.6
Main	1500	80	24,000	37.50	0.34	0.98	451.0
Main1	1250	55	24,000	45.45	0.40	0.97	445.9
Mainsupp	1500	120	9,450	50.00	0.13	1.00	460.0
Main2	1750	80	24,000	43.75	0.29	0.99	454.3
IMain	1000	42	16,917	47.62	0.36	0.98	449.6
SMain	900	40	16,360	45.00	0.38	0.97	447.6
Smain1	700	32	16,917	43.75	0.51	0.95	436.7
SSub	500	22	11,807	45.45	0.50	0.95	437.8
SSub1	450	20	11,105	45.00	0.52	0.95	435.6
SSub2	450	18	11,108	50.00	0.52	0.95	435.6
SSub3	450	18	11,108	50.00	0.52	0.95	435.6



## ANNEX H: BRIDGE BEHAVIOUR UNDER DIFFERENT LOAD SITUATIONS

This annex is meant to give general insight in the bridge model in SCIA Engineer that was used to make calculations, and in the general movements of Sognefjord bridge under different load cases.

### H.1 Load combinations

The following loads were taken into account in making calculations:

- Self-weight of all members, including bridge deck and cable net
- Traffic loads
- Uniform wind loads from three different angles, both for ULS as for SLS
- Current loads
- Maximum temperature difference
- Wind wave loads from three different angles, both for ULS as for SLS
- Unsymmetrical wind loads from severest angle, both for ULS as for SLS

These were combined in load combinations, of which seven different load situations were defined (see table H.1). According to Eurocode 0:NA2, the following load factors were used (see table H.2).

TABLE H.1: LOAD COMBINATIONS DEFINED FOR SCIA MODEL #1

Load combination	Description	Loads included
1	Self-weight only	Self-weight
2	Quiet warm day	SW, traffic, current
3	SLS storm with traffic	SW, traffic, current, uniform SLS 240° wind and SLS 240° wind waves
4	Maximum ULS storm / hurricane	SW, uniform 240° ULS wind, current, ULS 240° wind waves
5	Outward wind / inward current	SW, uniform 240° ULS wind, inward current (opposite direction compared to wind), 240° ULS wind waves
6	Unsymmetrical loading	SW, inward current, non-uniform ULS wind (half bridge length inwards, other half outwards wind), non-uniform wind waves
7	Maximum lateral displacement	SW, uniform 270° ULS wind, 270° wind waves

TABLE H.2: LOAD FACTORS USED IN CALCULATION MODEL

Load type	SLS	ULS
Permanent loads	1	1.25
Traffic loads	1.25	1.35
Other variable loads	1.35	1.5

## H.2 Bridge behaviour

Figures of displaced parts of Sognefjord bridge are given below, all with deformations drawn on the same scale. Figures H.2 to H.7 show the bridge girder and pontoons under each load situation. It can be seen that the shape of the girder and pontoons is roughly the same in most cases. However, the magnitude of deformation can differ quite a lot. LC2, a quiet day without wind, shows a clearly lower amount of sideways displacement of the girder than for example LC4, a severe storm. The rotations of the pontoons differ significantly as well. Also, it can be seen that the girder displaces more in the longitudinal direction under an ULS storm than under an SLS storm. This is due to the 240°-angle of the stronger winds, and the influence of traffic loads.

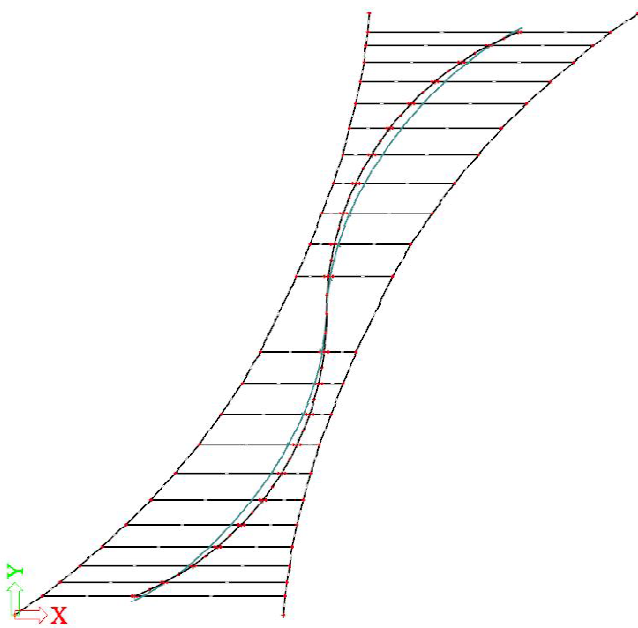


FIGURE H.2: DISPLACED GIRDER AND PONTOONS IN LC2

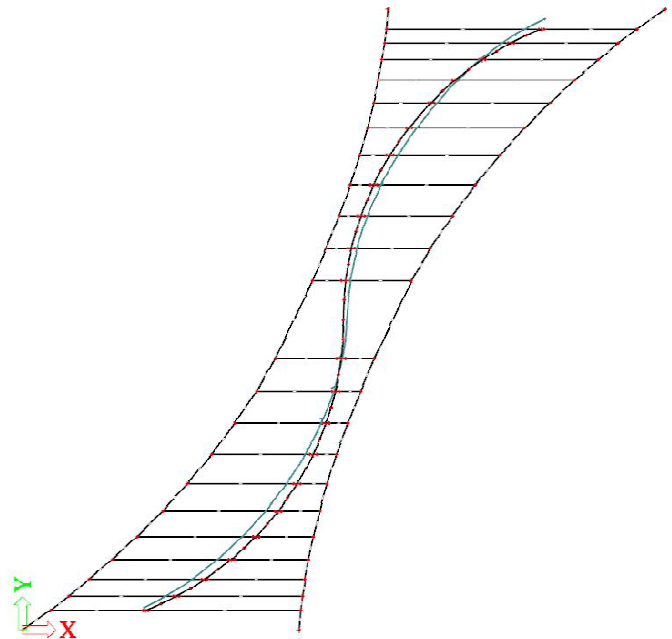


FIGURE H.3: DISPLACED GIRDER AND PONTOONS IN LC3

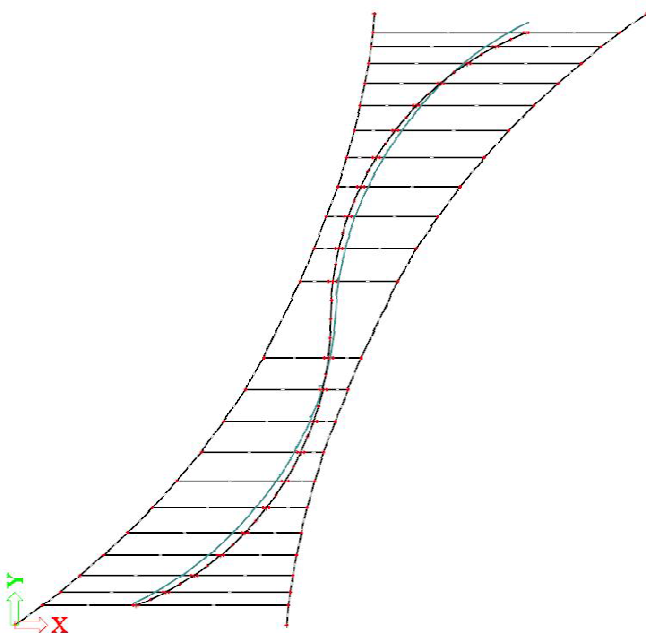


FIGURE H.4: DISPLACED GIRDER AND PONTOONS IN LC4

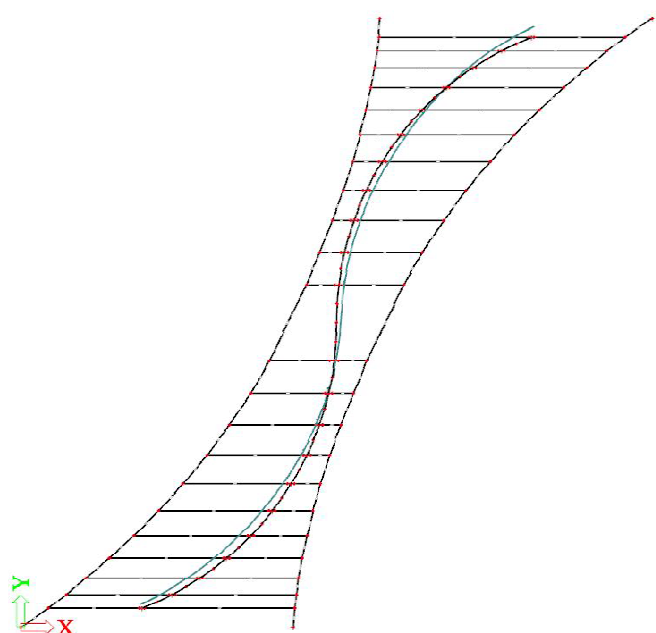


FIGURE H.5: DISPLACED GIRDER AND PONTOONS IN LC5

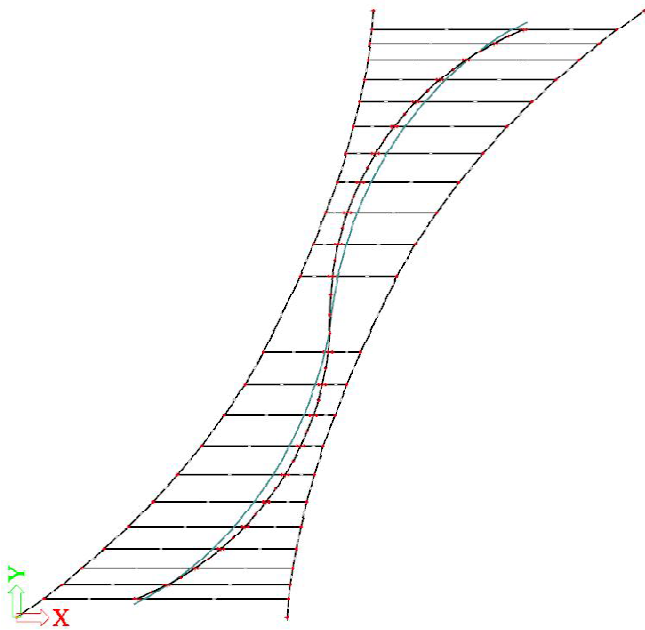


FIGURE H.6: DISPLACED GIRDER AND PONTOONS IN LC6

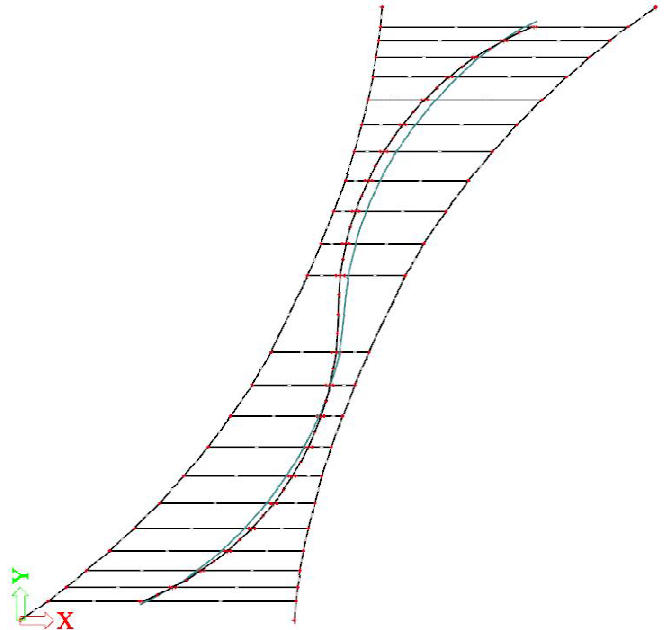


FIGURE H.7: DISPLACED GIRDER AND PONTOONS IN LC7

For the same load cases, side views of the girder and pontoons are given in figure H.8. As can be seen, the pontoons rotate less in load combinations 6 and 7. This is for LC6 due to the opposite load directions that neutralise each other. The wind loads of LC7 have no component in longitudinal bridge direction, which significantly reduces rotations in that direction.

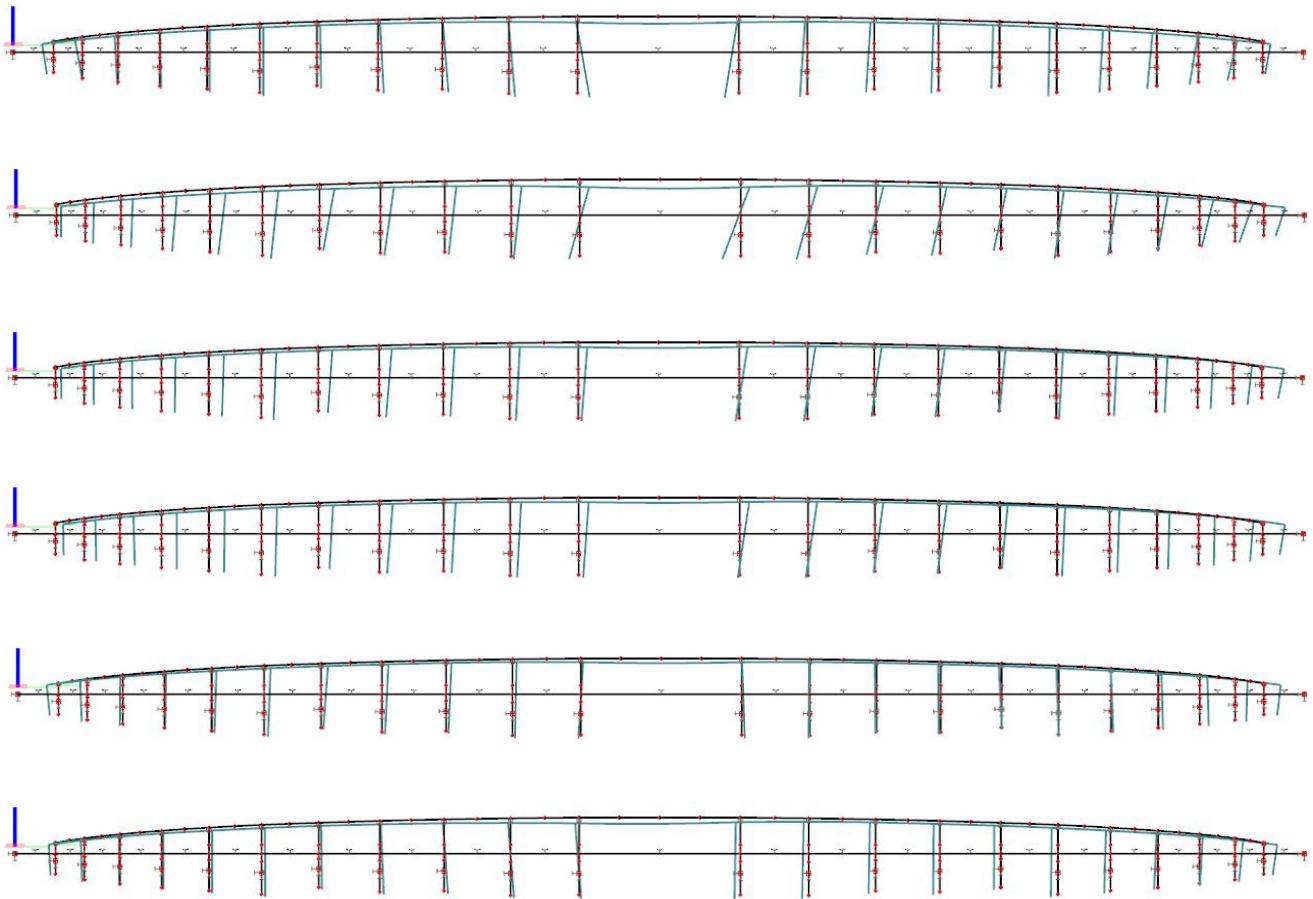


FIGURE H.8: DISPLACED GIRDER AND PONTOONS IN SIDE VIEW, FROM TOP TO BOTTOM: LC1 TO LC7, RESPECTIVELY

The anchoring system generally deforms generally in about the same shape for each load combination. As an indication, figure H.9 shows the deformed shape of the anchoring system under LC3. The figures clearly show that the side with the longest lateral anchoring cables deflects the most. Deflection on both sides of one pontoon is not equal. Figure H.10 shows a birds view of the full deformed shape of the bridge, under LC3.

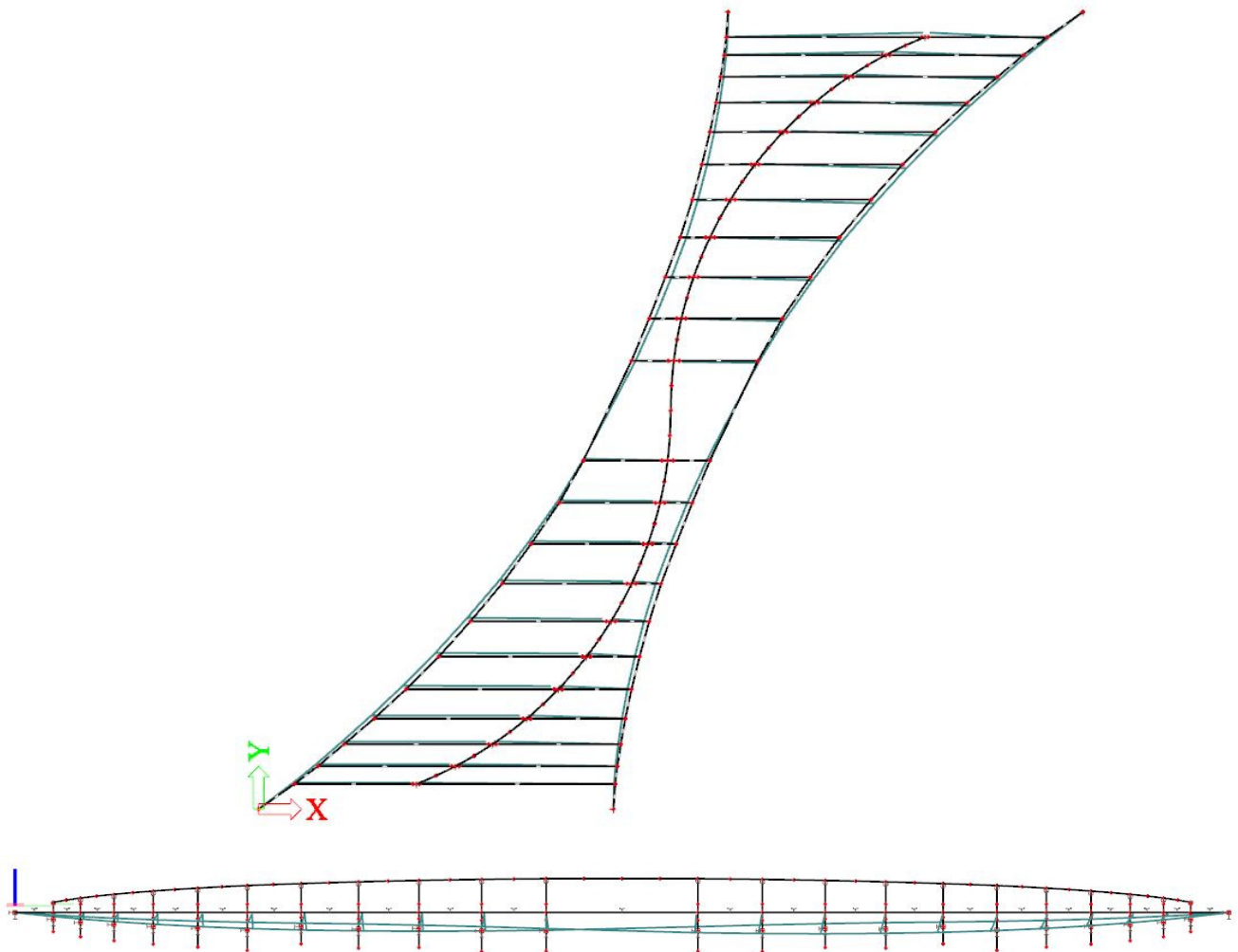


FIGURE H.9 DISPLACED ANCHORING SYSTEM IN LC3

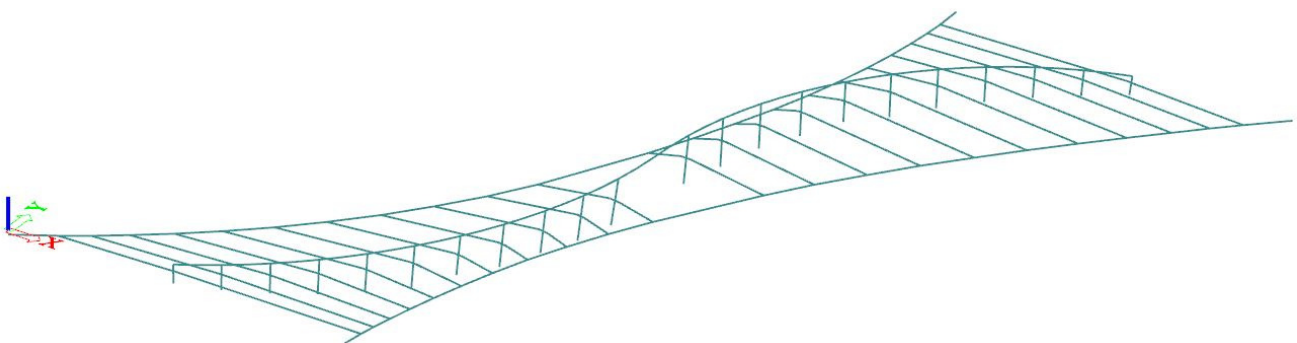


FIGURE H.10 DISPLACED SHAPE OF THE FULL SOGNEFJORD BRIDGE UNDER LC3

As an indication, table H.2 displays all deformations of the top of the pontoons for the whole bridge, under load combination LC4. Note that here, the displacements in LC4 were taken and the displacements from LC1, the self-weight only situation, were subtracted from these. This was done because the self-weight situation is the situation without any external loads, which was therefore taken as a base situation, from which all the other deformations depart.

**TABLE H.2: ALL DEFORMATIONS OF THE TOP OF PONTOONS UNDER LC4: ULS STORM**

Pontoon	Ux [m]	Uy [m]	Uz [m]	Fix [mrad]	Fiy [mrad]	Fiz [mrad]
1	3.482	37.999	0.388	-8.4366	-2.7477	1.662
2	3.517	37.987	0.15	-7.1206	-2.988	-3.7001
3	4.367	36.749	-0.006	-5.4869	-3.4279	-12.3319
4	6.337	34.359	-0.126	-4.7167	-3.348	-18.1544
5	8.935	31.731	-0.335	-4.3536	-2.7626	-18.7388
6	11.689	29.396	-0.664	-3.7226	-1.8059	-18.2424
7	14.477	27.404	-1.078	-2.9961	-0.2097	-15.7231
8	16.893	26.003	-1.577	-1.4221	2.2356	-14.9671
9	19.671	24.73	-2.067	-1.0137	6.6781	-15.8073
10	22.617	23.712	-2.799	0.8641	11.9756	-16.877
11	25.213	23.076	-3.128	1.7435	12.7961	-5.9081
12	24.86	23.102	-2.051	5.5997	11.5722	7.4422
13	21.837	23.789	-1.401	5.9705	11.4136	19.2405
14	18.657	24.835	-1.109	4.7603	11.1415	14.5615
15	16.437	25.82	-1.028	5.3906	8.9563	11.5139
16	14.424	26.976	-0.714	6.4415	6.6148	13.8969
17	11.799	28.816	-0.35	5.9144	5.6366	17.532
18	9.003	31.126	-0.196	5.1025	4.8806	18.6586
19	6.344	33.734	-0.108	4.98	3.9621	17.4896
20	4.458	35.954	-0.105	4.1829	3.8596	9.8973
21	3.941	36.646	-0.458	1.9005	4.5062	-1.5512
22	4.411	35.604	-1.222	-0.1529	4.6365	-8.9448



Finally, as means to compare all load situations, displacements of the 4 pontoons at mid-span of the bridge are given below for each load combination. Table H.3 clearly indicates the difference in displacements between a quiet day and for example a ULS storm. In LC6 some tops of the pontoons actually displace upwards rather than downwards. This is because the angle of rotation decreases compared to the self-weight situation, which raises the top of the pontoons. Again, the displacements in every load situation were subtracted by the displacements from self-weight only.

**TABLE H.3: MID-SPAN DEFORMATIONS FOR ALL LOAD CASES**

Load combination	Pontoon #	Ux [m]	Uy [m]	Uz [m]	Fix [mrad]	Fiy [mrad]	Fiz [mrad]
LC2	10	3.718	-4.048	-2.386	-2.6767	2.2720	2.5466
	11	2.330	-3.692	-3.031	-2.7526	2.9955	13.2273
	12	-4.277	-2.902	-2.764	4.3000	2.4422	13.6445
	13	-5.853	-2.505	-2.078	3.9474	2.7401	3.7037
LC3	10	20.383	21.384	-6.011	-11.2325	-6.8355	-6.1004
	11	20.389	21.347	-7.812	-10.1101	-7.2110	8.1212
	12	14.933	21.858	-7.731	8.5446	-12.5269	14.5495
	13	11.306	22.645	-5.420	9.4915	-11.9054	18.4526
LC4	10	22.617	23.712	-2.799	0.8641	11.9756	-16.8770
	11	25.213	23.076	-3.128	1.7435	12.7961	-5.9081
	12	24.860	23.102	-2.051	5.5997	11.5722	7.4422
	13	21.837	23.789	-1.401	5.9705	11.4136	19.2405
LC5	10	24.779	29.421	-2.795	1.0559	12.1938	-16.2049
	11	27.248	28.816	-3.102	1.9093	13.3736	-5.4274
	12	26.677	28.866	-2.139	5.2426	12.6815	7.8589
	13	23.731	29.535	-1.614	5.7236	13.0232	18.4816
LC6	10	-15.206	7.968	0.180	-0.6959	2.8792	-42.2487
	11	-5.306	5.465	-0.073	-0.5198	2.8428	-58.7388
	12	20.205	2.022	-0.099	0.9925	0.5157	-48.1184
	13	25.962	0.667	0.096	1.2156	0.0934	-16.2621
LC7	10	22.348	-8.656	-2.580	4.5442	23.6368	-20.7092
	11	25.659	-9.470	-2.736	5.6111	24.3058	-8.6476
	12	26.123	-9.535	-0.513	8.6893	22.8525	7.0709
	13	22.652	-8.746	0.244	8.5024	21.3718	23.0770

## ANNEX I: BRIDGE PARAMETER RESEARCH RESULTS

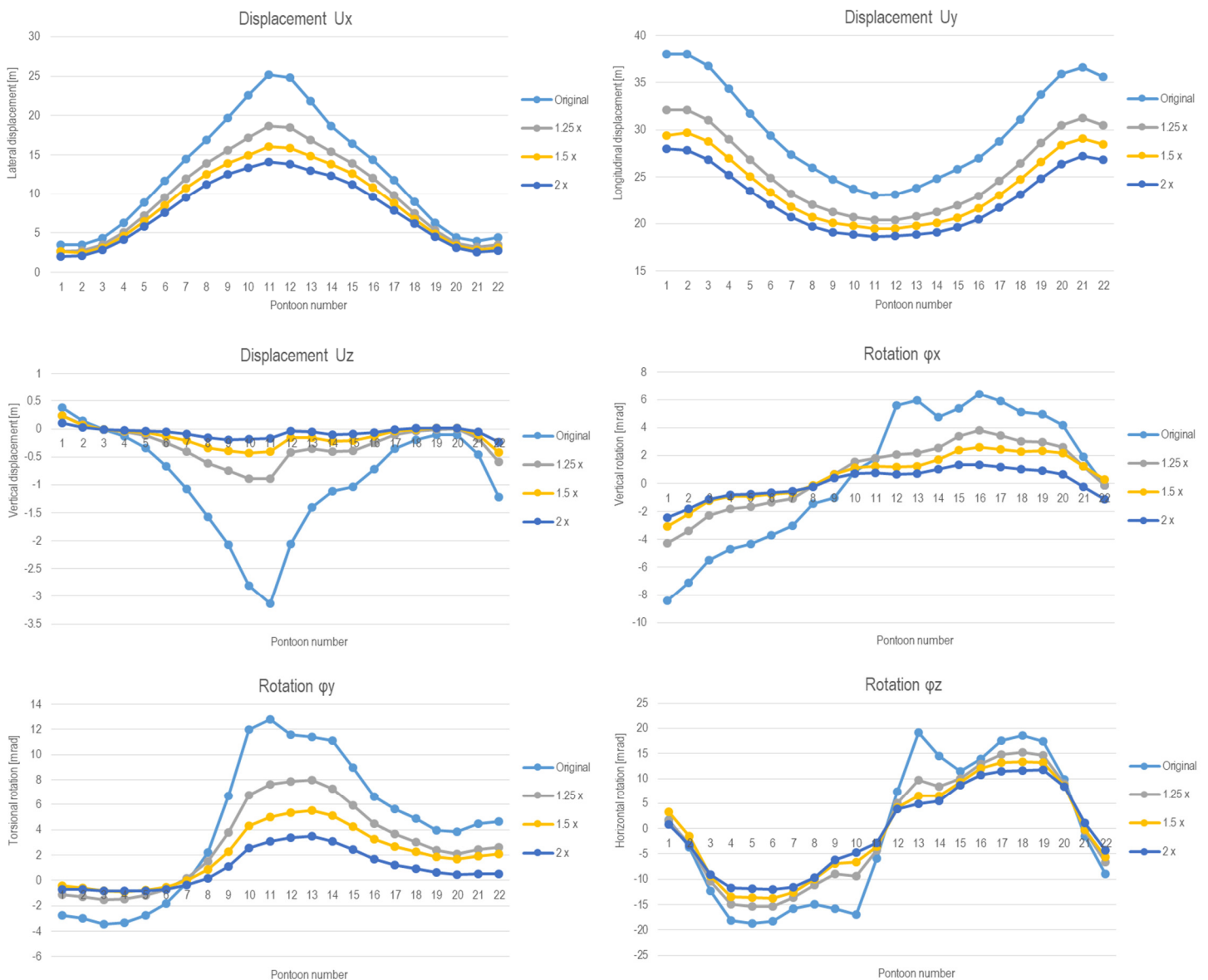
Only displacements and rotations of the top of the pontoons, e.g. the supports of the bridge girders, were considered. Displacements and rotations in all degrees of freedom were considered.

In each calculation, the results from a ULS storm situation were looked upon. From these the displacements in the self-weight situation (the base situation) were subtracted. The resulting values are displayed below.

Each parameter was raised 1.5 and 2 times and lowered 1.5 and 2 times, except for the parameters where this was not possible due to singularity in calculations. In these cases the parameter was raised only.

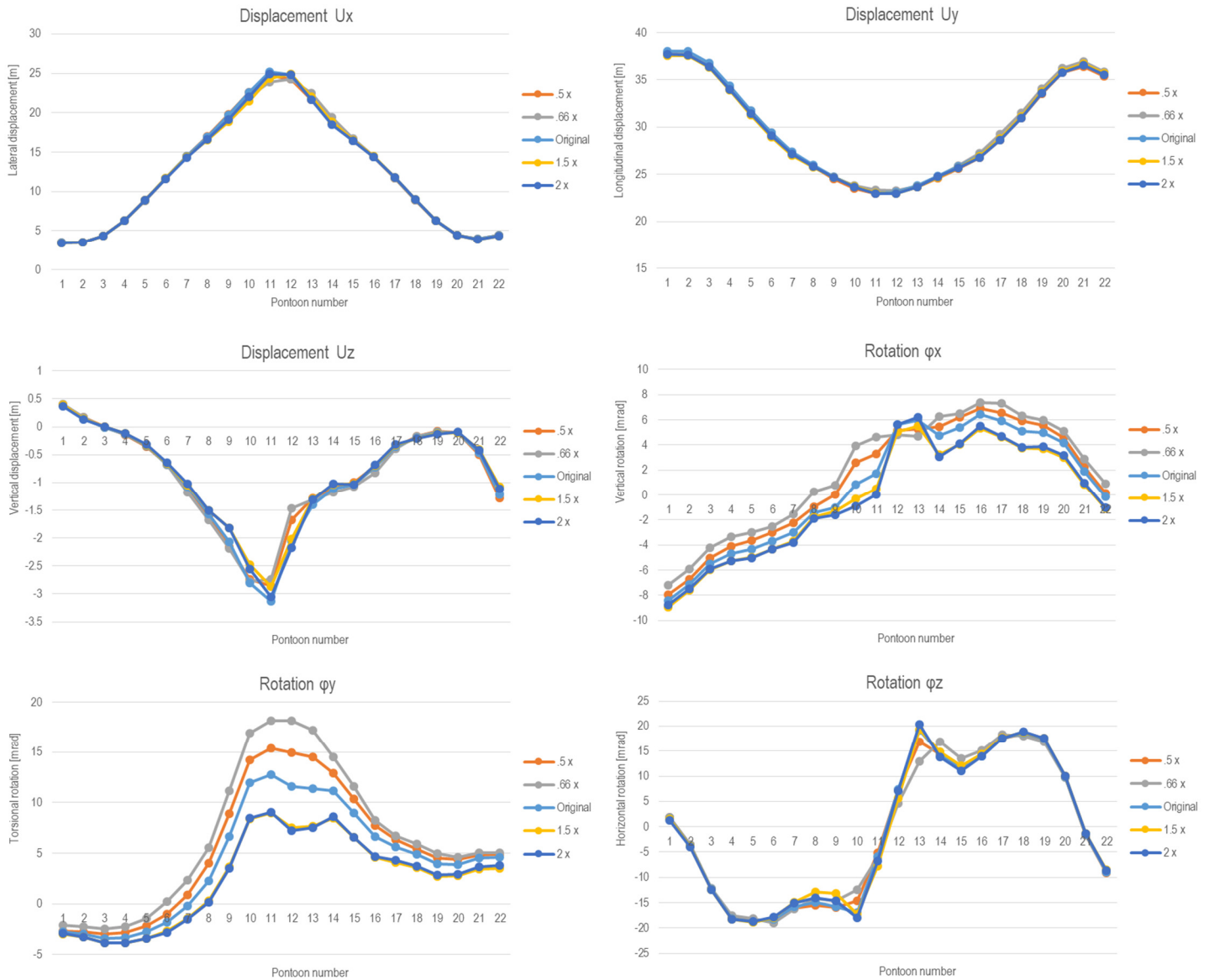
### I.1 Pontoon rotational stiffness

Only  $K_R$  of the pontoons was changed.



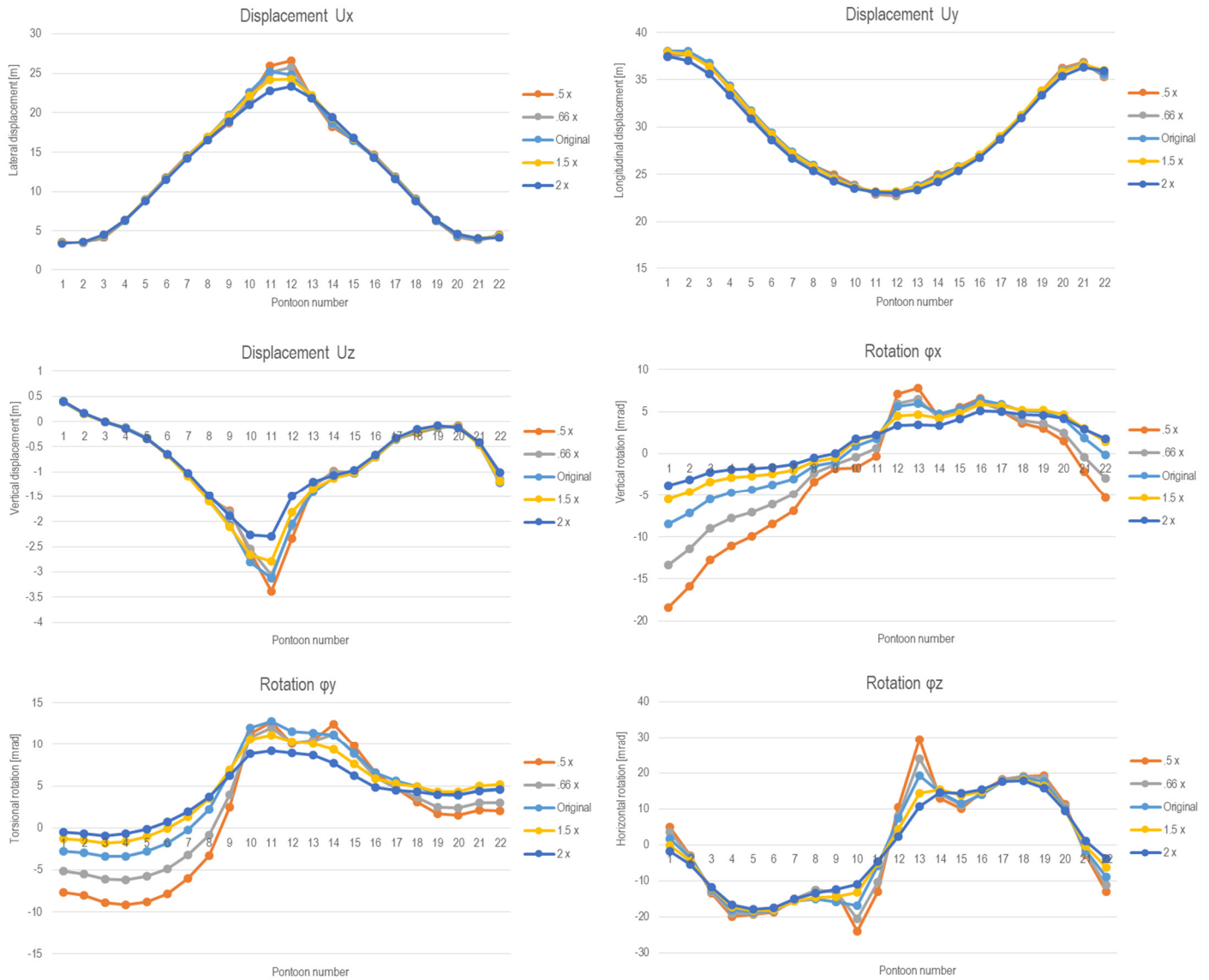
## I.2 Pontoon vertical stiffness

Only the vertical stiffness (e.g. the buoyancy) of the pontoons was changed.



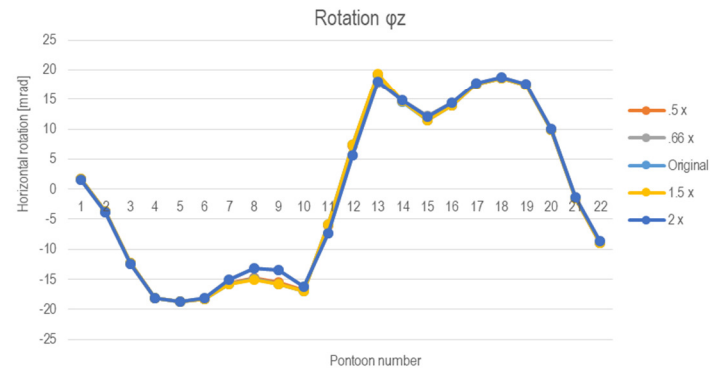
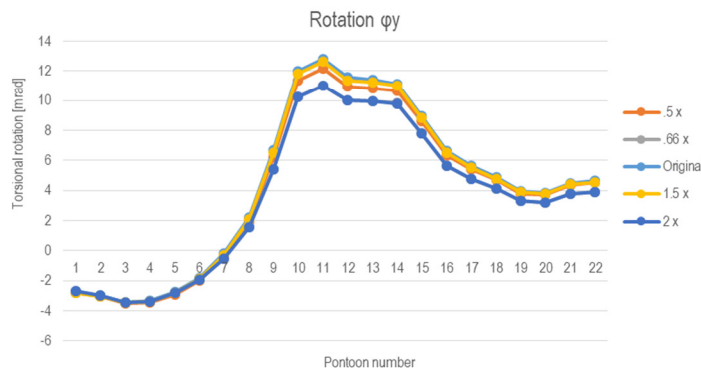
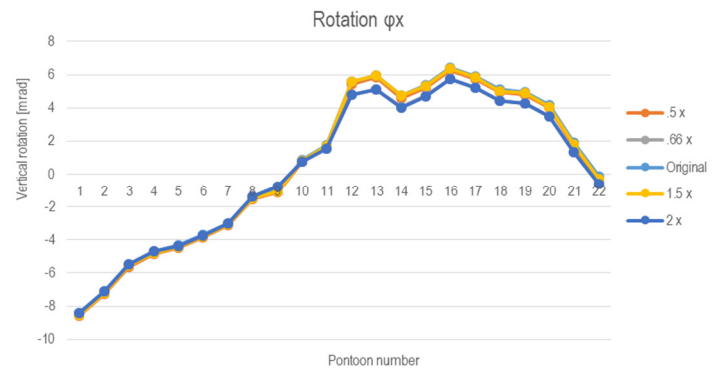
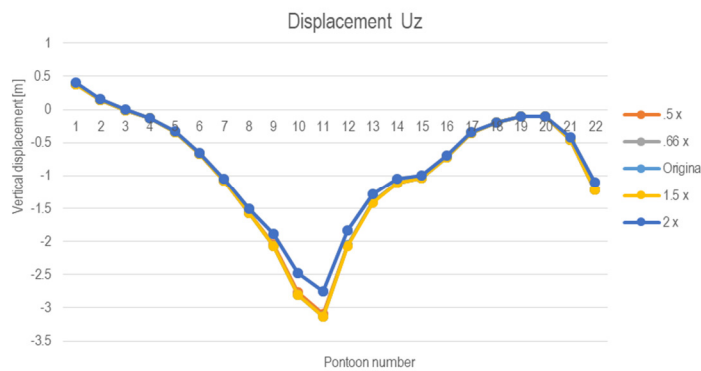
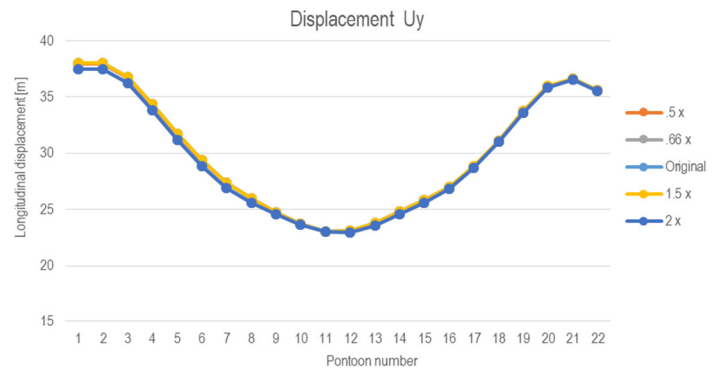
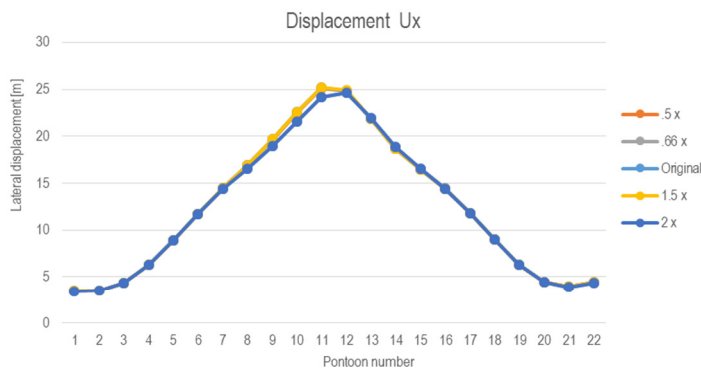
### I.3 Bending stiffness bridge girder

Only  $I_y$  and  $I_z$  of the girder cross-section were changed.



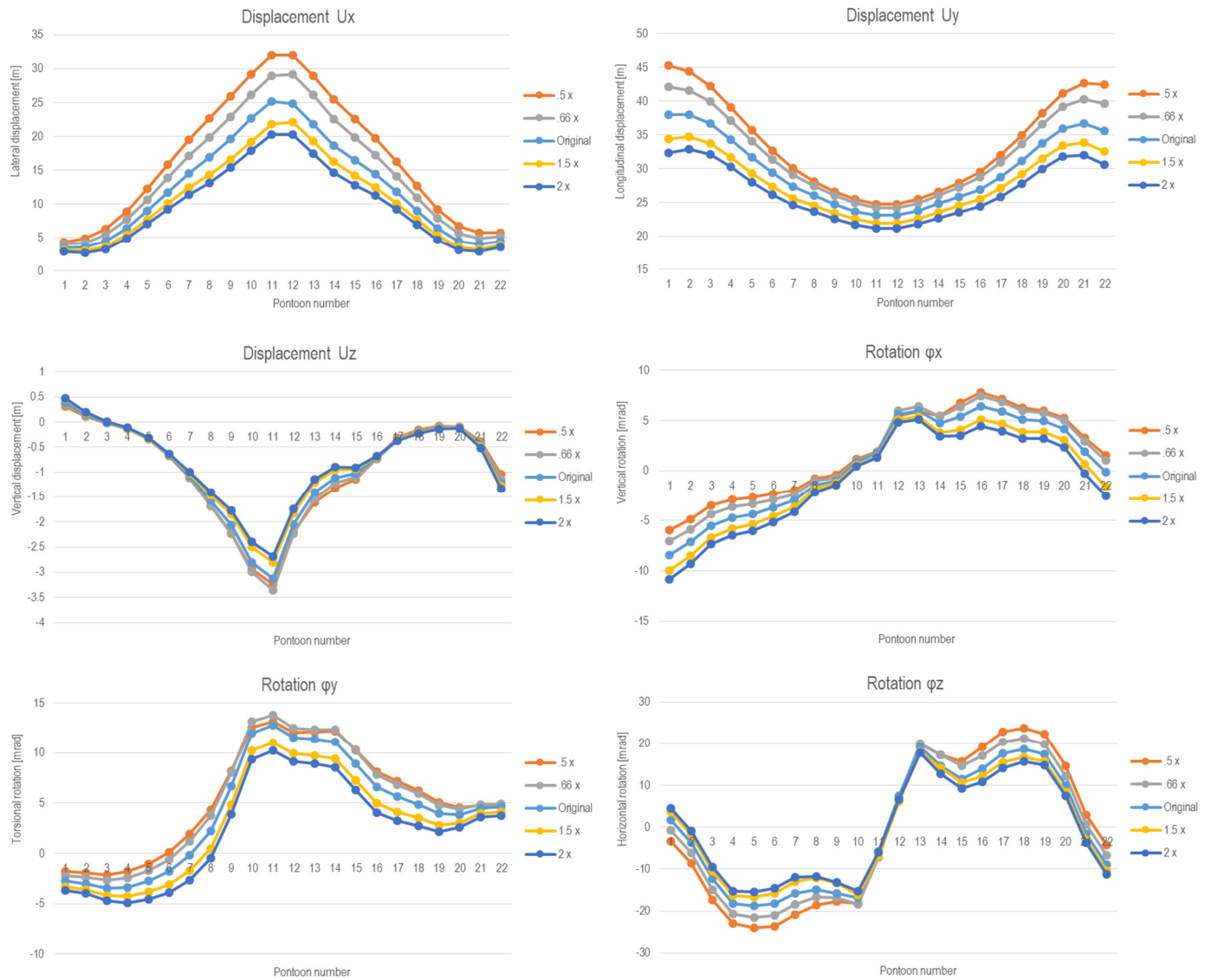
## 1.4 Shear stiffness bridge girder

Only  $A_x$ ,  $A_y$  and  $A_z$  of the bridge girder cross-section were changed. The girder steel density was adjusted accordingly, in such a way that the girder self-weight remained the same at all times. Some results are not clearly visible because they lie under other results (they are present though).



## 1.5 Anchoring system stiffness

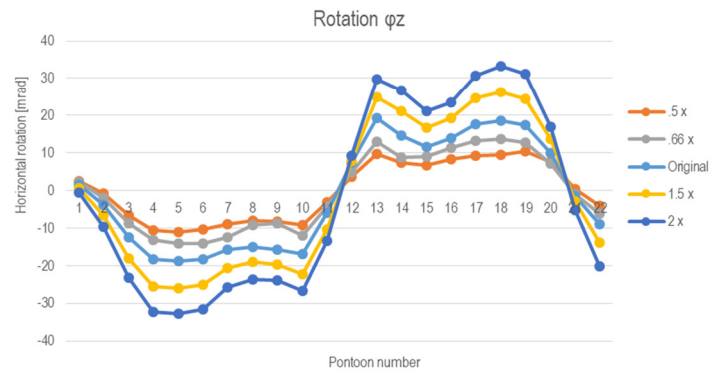
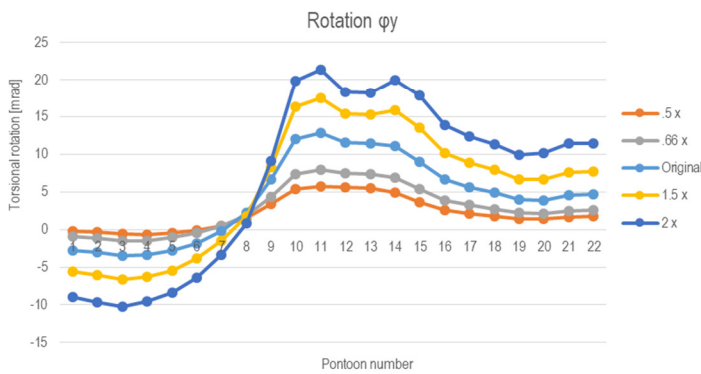
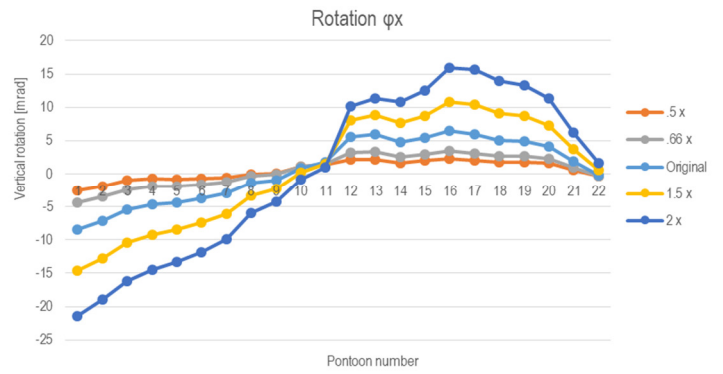
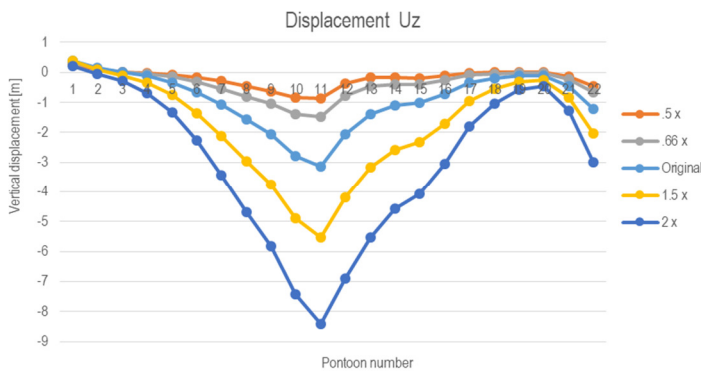
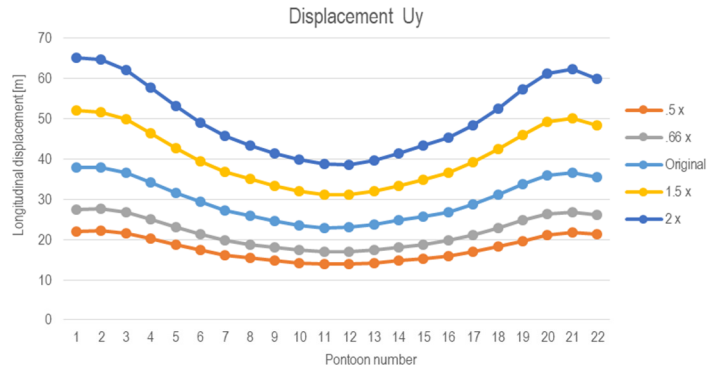
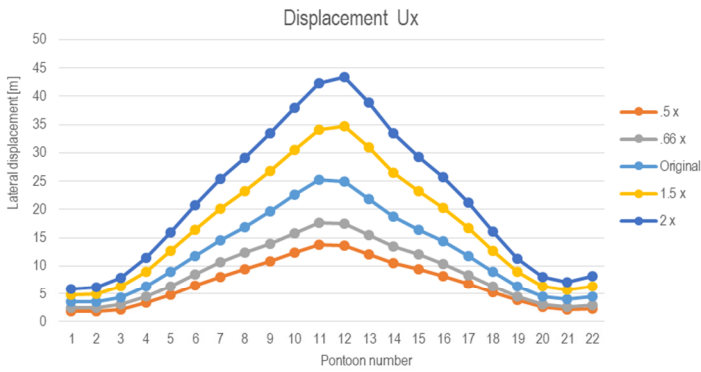
Only the (longitudinal) stiffness of the anchoring cables was changed. Only results for higher stiffness could be obtained.





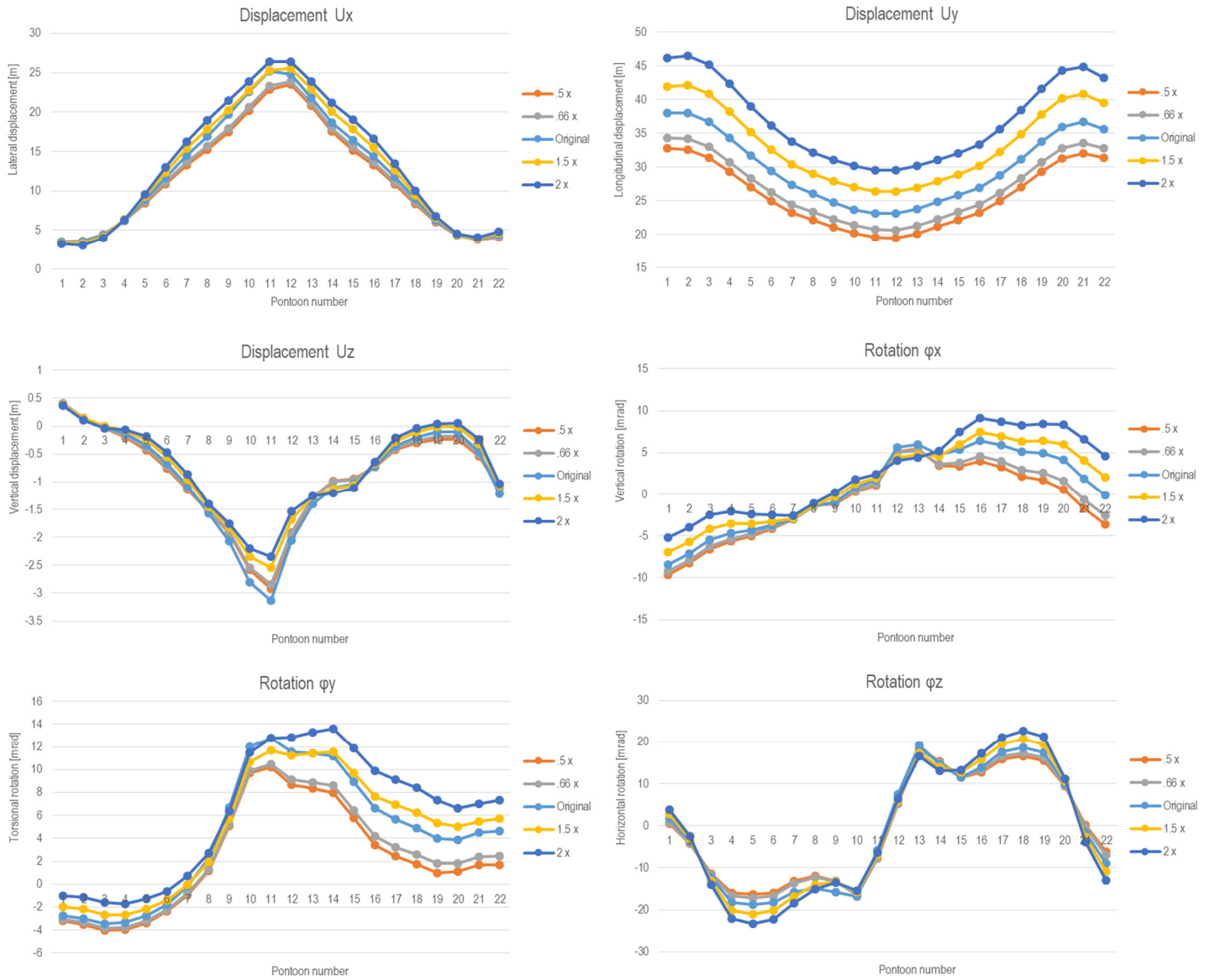
## I.6 Wind loads

Only the magnitude of environmental wind loads was changed.



## I.7 Wind wave loads

Only the magnitude of environmental wind wave loads was changed.

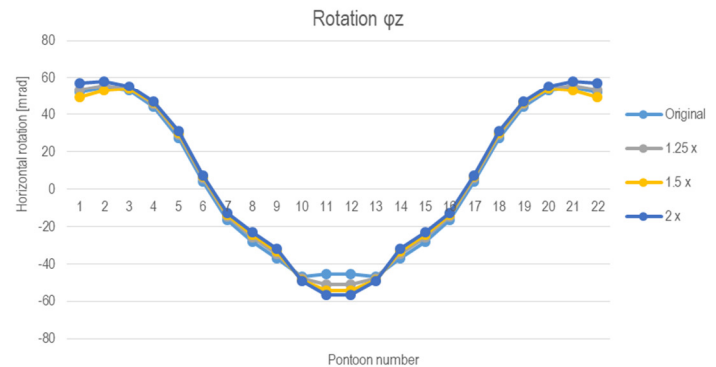
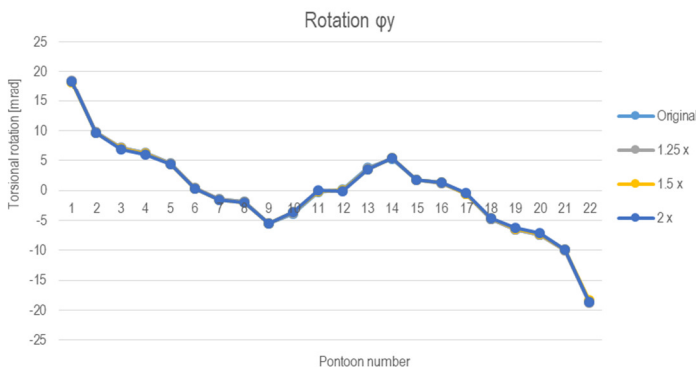
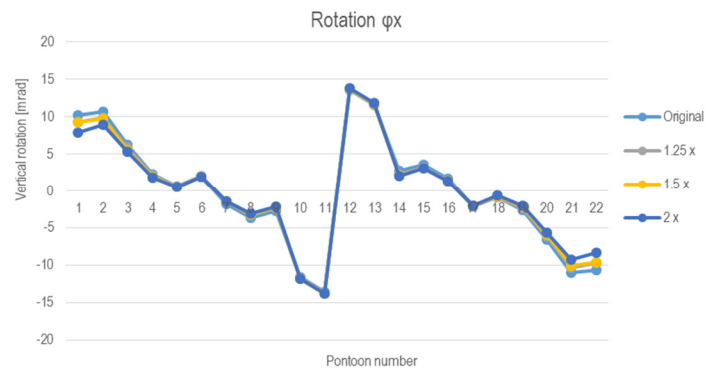
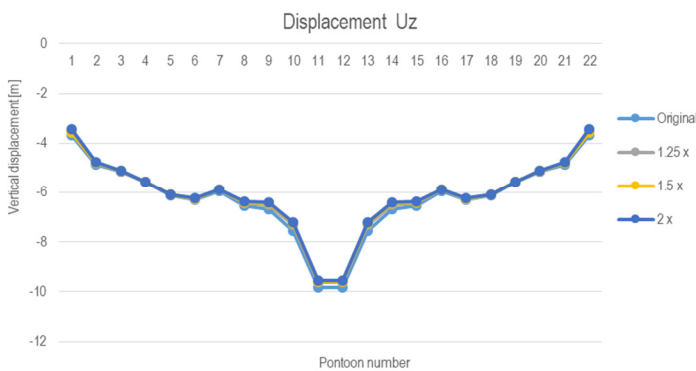
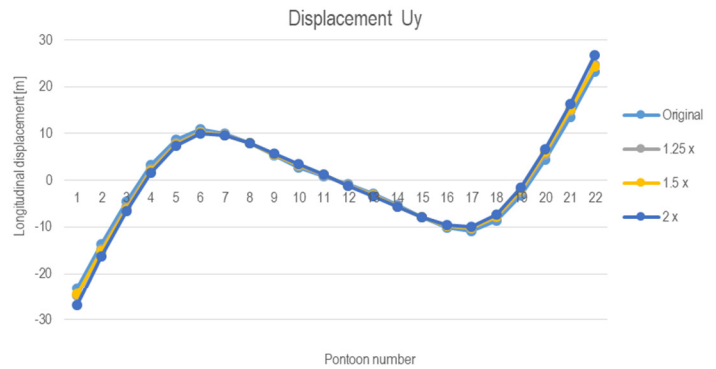
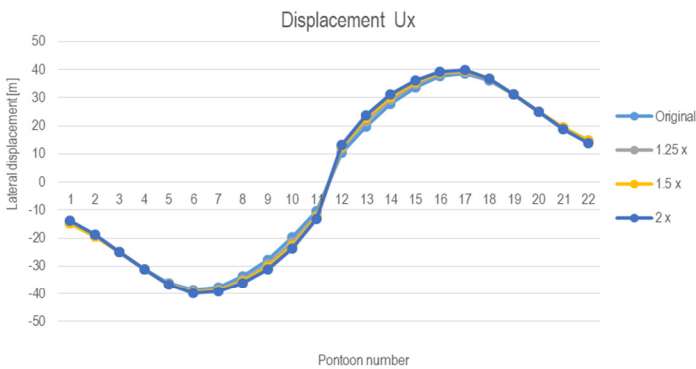


## 1.8 Effect of anchoring system on pontoon rotations

To investigate the effect of the anchoring system on pontoon rotations, pontoon rotations in self-weight situations only were investigated as well. The loads of the anchoring cables on each pontoon are not symmetrical, and therefore each pontoon is already rotated a bit in the self-weight situation because of the unsymmetrical loads. Therefore deformations in self-weight situations under different pontoon rotational stiffnesses were investigated. If these would differ, it would mean the cable system would influence the pontoon rotations, because in the self-weight situation this is theoretically the only load that rotates the pontoons.

Different stiffness would thus give different results. It can however be seen that the difference in movements for different pontoon rotational stiffness is insignificant.

This means the pontoon stiffness only gets activated when external loads (such as wind) are applied, and that therefore the anchoring cables have little effect in pontoon rotations. If the anchoring cables would have had effect on pontoon rotations, difference between curves should be seen here, because the cable system would pull the pontoons in a rotated state. Note also that, as expected because of the symmetrical load, the deformations are symmetrical in the self-weight situation.



## ANNEX J: TRIPOD PONTOON DESIGN INVESTIGATION

To investigate possibilities for improvement of the rotational stiffness of the pontoons, a design check for the spar concept was made. For this a simple preliminary design was made, of a pontoon consisting of three joined spars instead of just one. The three spars combined were given the same total diameter as the biggest pontoon in the design by Yip (2015), and the same total buoyancy. This led to spar hulls of 24.1 m in diameter and 206 m in length. See figure J.1. This requires about twice the amount of concrete compared to the single hull concept.

This led to a pontoon with 2.2 times the rotational stiffness of the single spar concept. A calculation sketch is given below (see figure J.2). Calculations are given on the next page.

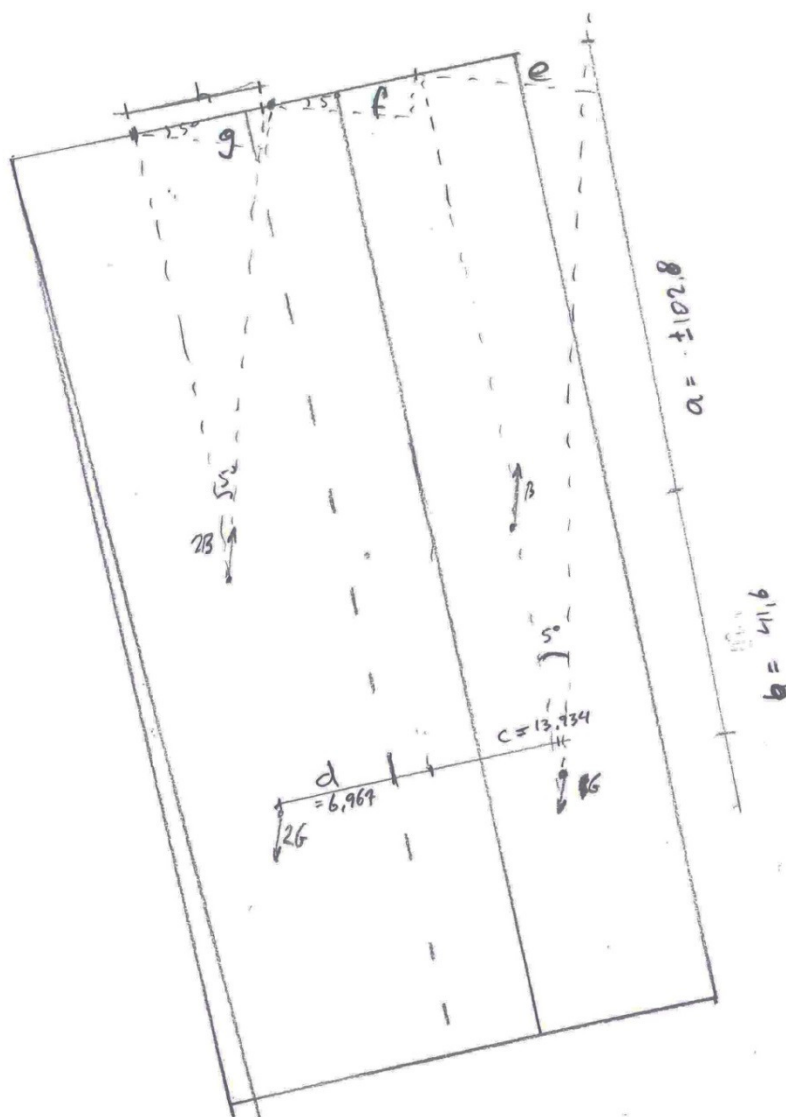
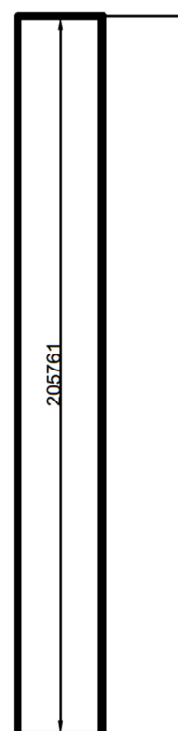
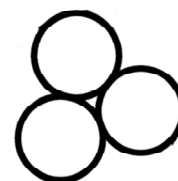
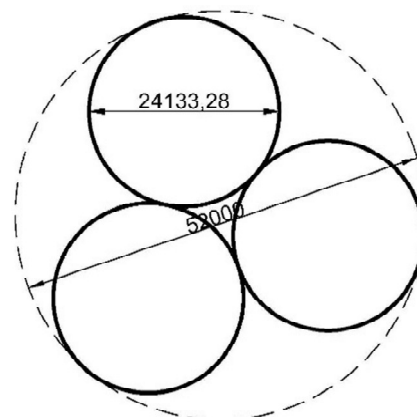


FIGURE J.1: TRIPOD SPAR DESIGN CONCEPT.

FIGURE J.2: SKETCH USED TO CALCULATE OVERTURNING MOMENT OF PONTOON UNDER IMPOSED ROTATION.

### First design check for tripod spar pontoon concept

Same total diameter and buoyancy as largest pontoon in design by Yip (2015).

All units in m, ton, kN

All distances measured from the top of the pontoon. Walls of new pontoon tubes assumed 1.5 m thick, as was old thickness.

$$L_{curr} := 133.5 \cdot L_{ball, curr} := 35.5 ;$$

$$V_{curr} := \text{Pi} \cdot 26^2 \cdot L_{curr} \cdot B_{curr} := V_{curr} \cdot 1.015 \cdot 9.81 ;$$

$$R_{new} := 12.066642 ;$$

$$B_{indiv} := \frac{B_{curr}}{3} ; V_{indiv} := \frac{B_{indiv}}{1.015 \cdot 9.81} ; L_{indiv} := \frac{V_{indiv} - \text{Pi} \cdot (R_{new} - 1)^2 \cdot 1}{\text{Pi} \cdot R_{new}^2} ;$$

$$L_{indiv} := 205.7605592$$

$$L_{ball, new} := \frac{L_{ball, curr}}{L_{curr}} \cdot L_{indiv} ;$$

$$G_{concr, indiv1} := 2 \cdot \text{Pi} \cdot R_{new} \cdot 1 \cdot L_{indiv} \cdot 2.4 \cdot G_{concr, indiv2} := \text{Pi} \cdot (R_{new} - 1)^2 \cdot 1 \cdot 2.4 \cdot G_{ball, new} := L_{ball, new} \cdot \text{Pi} \cdot (R_{new} - 1)^2 \cdot 2.1 ;$$

$$z_{B, new} := \frac{L_{indiv}}{2} ;$$

#calculation taking hollow cylinder first, then adding concrete bottom, then adding ballast

$$z_{G, new1} := \frac{G_{concr, indiv1} \cdot \frac{L_{indiv}}{2} + G_{concr, indiv2} \cdot (L_{indiv} - 0.5)}{G_{concr, indiv1} + G_{concr, indiv2}} ; z_{G, new} := \frac{(G_{concr, indiv1} + G_{concr, indiv2}) \cdot z_{G, new1} + G_{ball, new} \cdot \left( L_{indiv} - \frac{L_{ball, new}}{2} \right)}{G_{concr, indiv1} + G_{concr, indiv2} + G_{ball, new}} ;$$

$$z_{G, new} := 144.4595642$$

$$\text{rotarm} := z_{G, new} - z_{B, new} ; \alpha := \frac{5}{360} \cdot \text{Pi} ;$$

# Calculation taking the center at the top as rotation point, see sketch

$$a := \frac{L_{indiv}}{2} ; b := \text{rotarm} ; c := 13.934 ; d := 6.967 ;$$

$$e := (a + b) \cdot \sin(\alpha) ; f := c \cdot \sin(\alpha) ; g := d \cdot \sin(\alpha) ; h := a \cdot \sin(\alpha) ;$$

$$G_{indiv, tot} := G_{concr, indiv1} + G_{concr, indiv2} + G_{ball, new} ; F_{z, indiv} := G_{indiv, tot} \cdot 9.81 ; F_{B, indiv} := B_{indiv} ;$$

$$M_{overturning} := \text{evalf}(F_{z, indiv} \cdot (f + e) + 2 \cdot F_{B, indiv} \cdot (g - h) - F_{B, indiv} \cdot (f + h) - 2 \cdot F_{z, indiv} \cdot (g - e)) ;$$

$$k_{r, new} := \frac{M_{overturning}}{\alpha}$$

$$M_{overturning} := 2.644243140 \cdot 10^6$$

$$k_{r, new} := 6.060158877 \cdot 10^7 \quad (3)$$

$$k_{r, old} := 27697.762 \cdot 10^3 ;$$

$$\frac{k_{r, new}}{k_{r, old}}$$

$$2.187959763 \quad (4)$$

### Conclusion

Compared to a single spar, this simple design has 2.2 higher rotational stiffness. We calculate the required amount of concrete of the tripod compared to the spar concept:

$$\frac{V_{concr, old} := 52 \cdot \text{Pi} \cdot 1.5 \cdot L_{curr} + \text{Pi} \cdot 26^2 \cdot 1}{V_{concr, new} := 3 \cdot (R_{new} \cdot 2 \cdot \text{Pi} \cdot 1.5 \cdot L_{indiv} + R_{new}^2 \cdot \text{Pi} \cdot 1.5)} ; \frac{V_{concr, new}}{V_{concr, old}} := 2.074196805 \quad (5)$$

For the tripod pontoon concept about twice the amount of concrete is needed.



## ANNEX K: GIRDER MODELLING VALIDATION

As explained in chapter 3, to keep the calculation of Scia model #1 of the whole Sognefjord bridge stable, in this model the truss girder was replaced by an equivalent single beam. Results from this model were then transferred to Scia model #2 of the fully elaborated truss girder. Deformations of the whole bridge were inputted to calculate their results on forces and bending moments in members of the girder.

This annex shows how modelling the truss girder, its beam equivalent and the imposed deformations was validated. This started with finding a beam equivalent for the truss girder. This equivalent had to show the same displacements under different forces as the full truss girder. This process has been described in Annex E. Three equivalent beams were found for the side, intermediate and main span girders.

### K.1 Numerical cross-sections vs. geometric cross-sections

Instead of modelling the cross-sections as geometric input, in the full bridge model, these equivalent girders were modelled as numerical cross-sections. This was done so that in further research, making adjustments would require little effort. Figure K.1 shows the properties of the numerical cross-sections.

Property		Property		Property	
A [m <sup>2</sup> ]	7.86000000e+00	A [m <sup>2</sup> ]	7.56760000e+00	A [m <sup>2</sup> ]	3.01120000e+00
Ay [m <sup>2</sup> ]	3.11615100e+00	Ay [m <sup>2</sup> ]	9.06695500e-01	Ay [m <sup>2</sup> ]	8.57348200e-01
Az [m <sup>2</sup> ]	4.66828100e+00	Az [m <sup>2</sup> ]	6.06733000e+00	Az [m <sup>2</sup> ]	2.09206300e+00
AL [m <sup>2</sup> /m]	5.30000000e+01	AL [m <sup>2</sup> /m]	6.30000000e+01	AL [m <sup>2</sup> /m]	2.72000000e+01
AD [m <sup>2</sup> /m]	1.04800000e+02	AD [m <sup>2</sup> /m]	1.25000000e+02	AD [m <sup>2</sup> /m]	5.34800000e+01
cYUCS [mm]	5250	cYUCS [mm]	1750	cYUCS [mm]	1800
cZUCS [mm]	8000	cZUCS [mm]	14000	cZUCS [mm]	5000
α [deg]	0.00	α [deg]	0.00	α [deg]	0.00
Iy [m <sup>4</sup> ]	2.94591000e+02	Iy [m <sup>4</sup> ]	6.03631700e+02	Iy [m <sup>4</sup> ]	3.81305100e+01
Iz [m <sup>4</sup> ]	1.55086200e+02	Iz [m <sup>4</sup> ]	1.99517200e+01	Iz [m <sup>4</sup> ]	7.47356300e+00
Iy [mm]	6122	Iy [mm]	8931	Iy [mm]	3558
Iz [mm]	4442	Iz [mm]	1624	Iz [mm]	1575
Wely [m <sup>3</sup> ]	3.68238700e+01	Wely [m <sup>3</sup> ]	4.31165500e+01	Wely [m <sup>3</sup> ]	7.62610100e+00
Welz [m <sup>3</sup> ]	2.95402300e+01	Welz [m <sup>3</sup> ]	1.14009800e+01	Welz [m <sup>3</sup> ]	4.15197900e+00
Wply [m <sup>3</sup> ]	4.34505000e+01	Wply [m <sup>3</sup> ]	5.88513100e+01	Wply [m <sup>3</sup> ]	9.50732800e+00
Wplz [m <sup>3</sup> ]	3.26430000e+01	Wplz [m <sup>3</sup> ]	1.20475900e+01	Wplz [m <sup>3</sup> ]	4.52446400e+00
Mply+ [Nm]	2.00e+10	Mply+ [Nm]	2.71e+10	Mply+ [Nm]	4.37e+09
Mply- [Nm]	2.00e+10	Mply- [Nm]	2.71e+10	Mply- [Nm]	4.37e+09
Mplz+ [Nm]	1.50e+10	Mplz+ [Nm]	5.54e+09	Mplz+ [Nm]	2.08e+09
Mplz- [Nm]	1.50e+10	Mplz- [Nm]	5.54e+09	Mplz- [Nm]	2.08e+09
dy [mm]	0	dy [mm]	0	dy [mm]	0
dz [mm]	0	dz [mm]	0	dz [mm]	0
It [m <sup>4</sup> ]	2.95763700e+02	It [m <sup>4</sup> ]	6.30118800e+01	It [m <sup>4</sup> ]	1.92216700e+01
Iw [m <sup>6</sup> ]	1.98831800e+02	Iw [m <sup>6</sup> ]	9.05812900e+02	Iw [m <sup>6</sup> ]	2.00651500e+01
β y [mm]	0	β y [mm]	0	β y [mm]	0
β z [mm]	0	β z [mm]	0	β z [mm]	0

FIGURE K.1: NUMERICAL INPUT OF THE CROSS-SECTIONS OF MAIN (LEFT), INTERMEDIATE (MIDDLE) AND SIDE (RIGHT) EQUIVALENT BRIDGE GIRDER.

To check whether this different way of modelling the beam cross-section had any influence on the calculated forces and displacements in the bridge, two Scia models #1 were compared. One had geometrically inputted girders, one had numerically inputted girders. Their displacement and force results showed the differences between the two models were neglectable.

This means modelling a numerical cross-section gives the same results as modelling an equivalent geometrical cross-section, and thus using a numerical cross-section for further modelling is allowed. Figure K.2 shows a comparison of the results of the two different models.



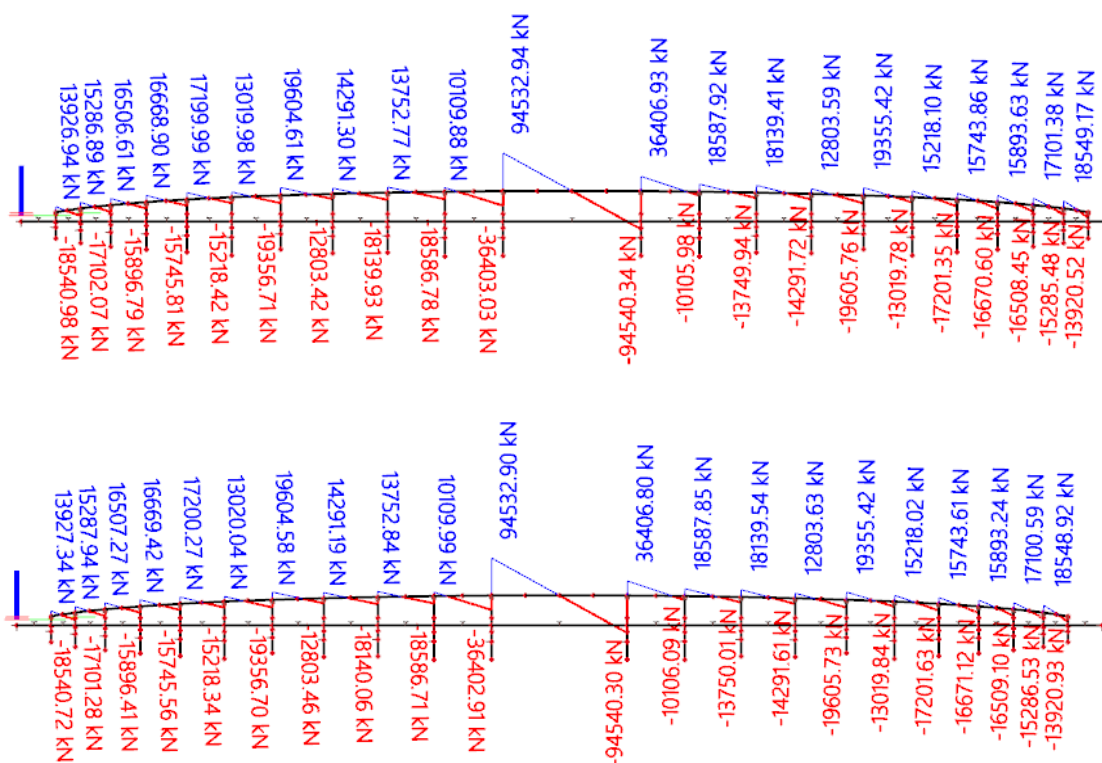


FIGURE K.2: SHEARFORCES IN Z-DIRECTION ON THE BEAM GIRDER IN THE SCIA MODEL OF THE WHOLE BRIDGE. UPPER PLOT SHOWS RESULTS OF THE FULL BRIDGE WITH A GEOMETRICALLY INPUTTED BEAM CROSS-SECTION (WITH THE PROPERTIES OF FIGURE K.1), LOWER PLOT SHOWS RESULTS OF THE EXACT SAME MODEL BUT WITH A NUMERICALLY INPUTTED BEAM CROSS-SECTION WITH THE SAME PROPERTIES. THE DIFFERENCES ARE NEGLECTABLE. THIS HOLDS FOR ALL RESULTS.

## K.2 Modelling imposed deformations

In the next step, of Scia model #1, only the equivalent bridge girder was maintained. The rest of the bridge was deleted from the model. For the remaining girder, supports were modelled in the nodes where in Scia model #1 the girder was supported by the pontoons.

From calculations with Scia model #1, the deformed shape of the whole bridge under ULS storm loads was known. Loads coming from the deleted part of the bridge were modelled then modelled in Scia model #3 by copying deformations in all six degrees of freedom from Scia model #1. This was done by giving the new supports in Scia model #3 the exact deformations of the tops of the pontoons of Scia model #1 under ULS storm loads. See figure

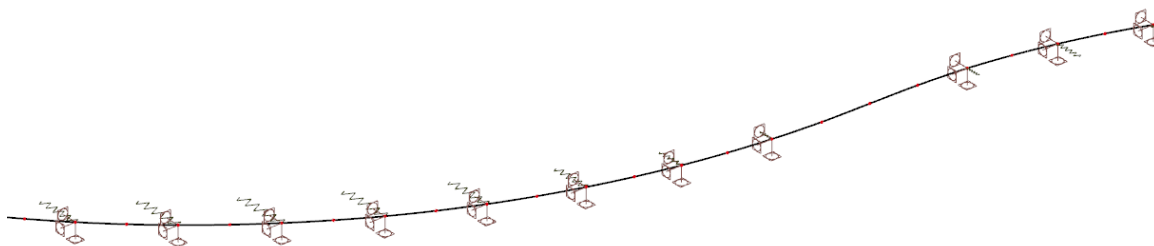


FIGURE K.3: EXACT COPY OF THE GIRDER OF SCIA MODEL #1 WITH NUMERICAL CROSS-SECTION WITH PROPERTIES OF FIGURE K.1. AT LOCATIONS OF THE TOP OF THE PONTOONS, IMPOSED DEFORMATIONS ARE GIVEN AS BOUNDARY CONDITIONS. IN THIS WAY, THE GIRDER IS GIVEN THE EXACT SAME SHAPE AS THE GIRDER IN THE WHOLE BRIDGE MODEL AND THEREFORE THE SAME FORCES AS WELL.

K.3. The idea was that, when the girders in Scia model #3 are formed in the exact same (imposed) shape as they were in Scia model #1, forces in the girders should be the same as well.

As can be seen in figure K.4, the isolated girders with imposed deformations of Scia model #3 show about the same force results as the girders in Scia model #1 of the whole bridge. Small (<5%) differences in results were deemed acceptable. By this, it was concluded that imposing deformations on the bridge girder as a means to replace the rest of the structure, is allowed.

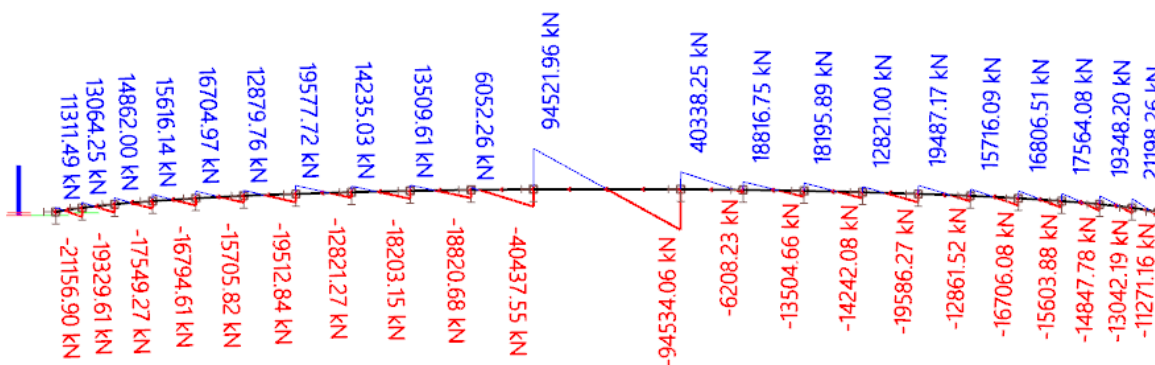


FIGURE K.4: SHEAR FORCE RESULTS IN Z-DIRECTION OF THE SAME GIRDER MODEL AS DISPLAYED IN FIGURE K.3. DIFFERENCE IN RESULTS WITH THE MODEL OF THE WHOLE BRIDGE (SEE FIGURE K.2) ARE VERY SMALL.

### K.3 Modelling deformations on the full truss girder

It was considered too elaborate to model the complete Sognefjord truss girder in Scia model #1 of the full Sognefjord bridge, because this would make calculating this model become unstable. Therefore a separate model of the truss girder only was made: Scia model #2. In this model, loads coming from the remaining part of the bridge were modelled by a set of imposed deformations in all six degrees of freedom. Looking at the previous results, this was deemed an acceptable way of replacing the rest of the bridge structure in Scia model #2.

The way the deformations are modelled however, has large influence on the results in Scia model #2. In this design phase, the truss girder was assumed to be supported by two large rubber blocks on each pontoon. This was based on support designs for continuous concrete traffic bridges. Such blocks can deform a little, thereby allow small deformations and rotations. See figure K.5 for a cross-sectional sketch of the support assumption.

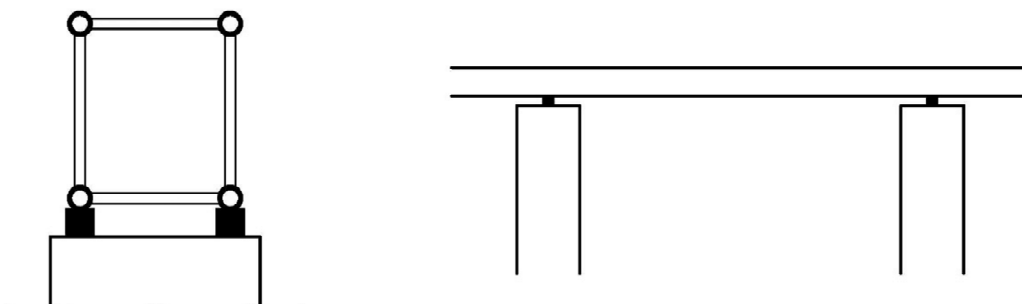
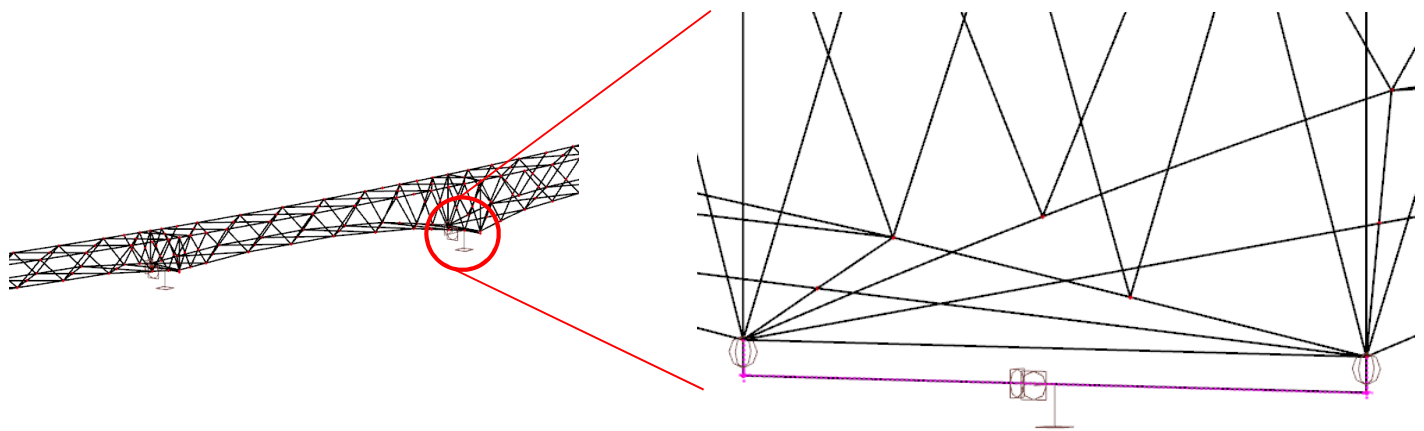


FIGURE K.5: IT WAS ASSUMED THAT THE GIRDER LIES ON TWO LARGE RUBBER BLOCKS, ON TOP OF THE PONTOONS.

Bridge deformations are imposed through these supports and therefore the boundary conditions of the truss girder have to be modelled in the right way. This would mean that in Scia model #2, the girder supports would have to be modelled as a set of springs in all six degrees of freedom, so that small displacements and rotations are allowed. However, the required stiffness that should be modelled for these springs is difficult to determine. This is because rubber block supports the size of what would be used in the Sognefjord bridge, are unprecedented.

It was therefore chosen to make a simplification. Instead of allowing small deformations of the superstructure by modelling springs, only rotations about the x-axis and y-axis were allowed. This meant small displacements of the superstructure were impeded. The rubber blocks were modelled as two dummy bars that support the truss. The (weightless and very stiff) dummy bars were hinged connected to allow rotations about the x-axis and y-axis. The two dummy bars were connected by a third dummy bar, on which, through a clamped support, the deformations in all six degrees of freedom are imposed. Since the superstructure is now impeded from displacing relative to the pontoons, it was expected this might increase global forces in the superstructure a bit. It was therefore a conservative approach, and therefore deemed acceptable for this stage of design.



**FIGURE K.6: MODELLING THE BOUNDARY CONDITIONS IN THE FULL TRUSS GIRDER MODEL. ON THE RIGHT, THE HINGES AND THE SUPPORT CAN BE SEEN, LOCATED ON THE (PINK) DUMMY BARS.**

This was deemed the best way to simulate the two rubber blocks of the girder support assumption. Just as with the rubber blocks, the two vertical dummy bars allow small  $\phi_x$  and  $\phi_y$ -rotations. By imposing deformations through a clamped support on the dummy bar, deformations were imposed on the truss indirectly. This prevented the rise of any clamping effects, which would have otherwise strongly influenced member forces. See figure K.6.

The Scia model #2 of the full 3D truss girder was then used to check forces and moments in the truss members resulting from movements of the pontoons. By this the truss girder design and feasibility could be investigated.

## ANNEX L: GIRDER DISPLACEMENT ANALYSIS RESULTS

As mentioned in chapter 5, of the deformations imposed on the girders, the most important aspect is relative deformations between adjacent pontoons. These impose loads on the bridge girders. Therefore the values of the relative deformations in LC4 (ULS storm) are given in table L.1, as an indication.

This was done because analysing truss girder behaviour was done only under the ULS storm load situation (LC4). These relative deformations are given for the middle 8 pontoons of the Sognefjord bridge, as only these were incorporated in Scia model #2 of the truss. The deformations follow the coordinate system as described in chapter 1.

TABLE L.1: DEFORMATION DIFFERENCES BETWEEN ADJACENT PONTOONS UNDER ULS STORM LOADS

Deformation differences between adjacent pontoons												
Degree of freedom	U <sub>x</sub> [m]		U <sub>y</sub> [m]		U <sub>z</sub> [m]		φ <sub>x</sub> [mrad]		φ <sub>y</sub> [mrad]		φ <sub>z</sub> [mrad]	
Pontoon rotational stiffness	1 x	2 x	1 x	2 x	1 x	2 x	1 x	2 x	1 x	2 x	1 x	2 x
Difference between #9 and #8	2.78	1.27	-1.27	-0.58	-0.49	-0.03	0.41	0.63	4.44	0.93	-0.84	3.51
Difference between #10 and #9	2.95	0.82	-1.02	-0.28	-0.73	0.00	1.88	0.33	5.30	1.41	-1.07	1.34
Difference between #11 and #10	2.60	0.74	-0.64	-0.18	-0.33	0.02	0.88	0.05	0.82	0.53	10.97	1.95
Difference between #12 and #11 (main span)	-0.35	-0.23	0.03	0.03	1.08	0.13	3.86	-0.11	-1.22	0.29	13.35	6.65
Difference between #13 and #12	-3.02	-0.81	0.69	0.19	0.65	-0.02	0.37	0.05	-0.16	0.13	11.80	1.05
Difference between #14 and #13	-3.18	-0.74	1.05	0.25	0.29	-0.05	-1.21	0.29	-0.27	-0.42	-4.68	0.66
Difference between #15 and #14	-2.22	-1.06	0.98	0.48	0.08	0.01	0.63	0.34	-2.19	-0.61	-3.05	3.18

As can be seen, the values of the imposed deformations differ for each span. This means every member in the truss will be subjected to a different load for every load case.

### L.1 Global forces and bending moments in bridge girder

First, the global forces in the bridge girders under ULS storm loads were calculated. This was done using Scia model #3, by imposing the ULS storm loads on the boundary conditions (the clamped supports) in this model. As was done in the bridge research of chapter 5, here too the self-weight displacements were taken as the base situation that was subtracted from the ULS deformations. Below, the total global forces and bending moments resulting from the ULS storm loads (LC4) are displayed. See figures L.1, L.2 and L.3.

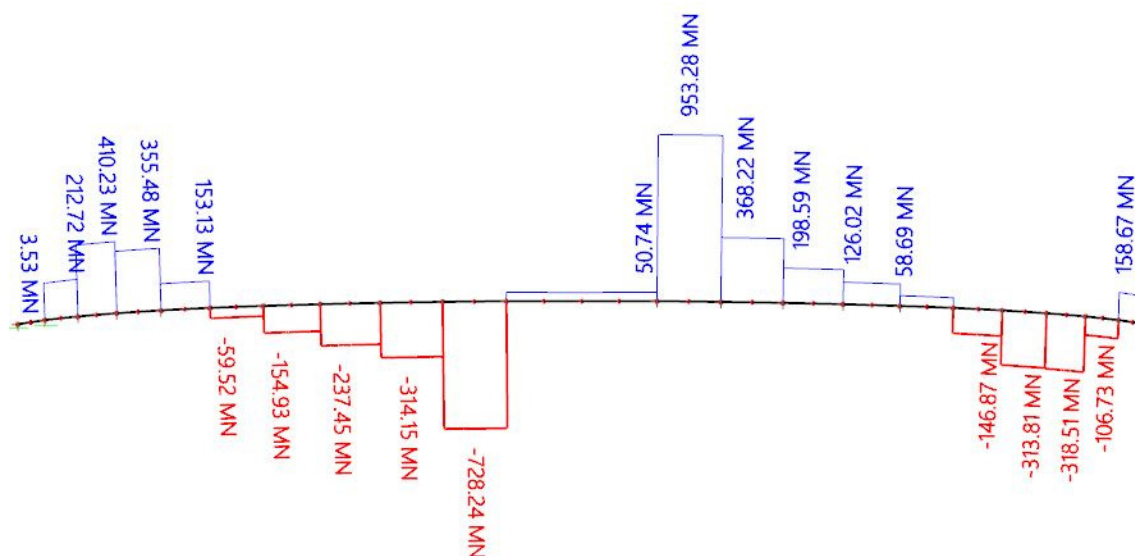


FIGURE L.1: GLOBAL FORCES IN THE GIRDERS UNDER ULS STORM LOADS. NORMAL FORCES DISPLAYED

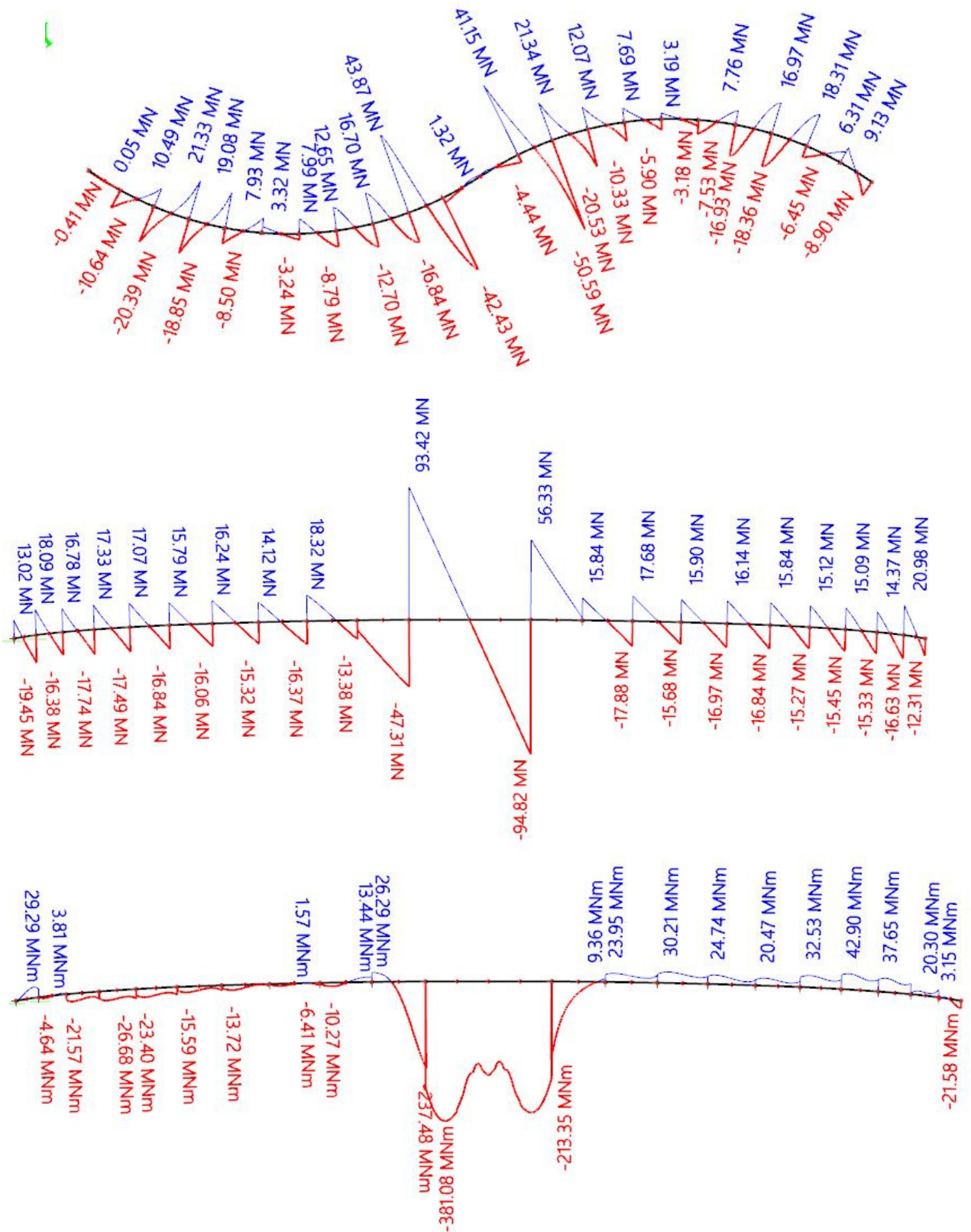


FIGURE L.2: GLOBAL FORCES IN THE GIRDERS UNDER ULS STORM LOADS. FROM TOP TO BOTTOM: VY SHEAR FORCES, VZ SHEAR FORCES, AND MX BENDING MOMENTS.



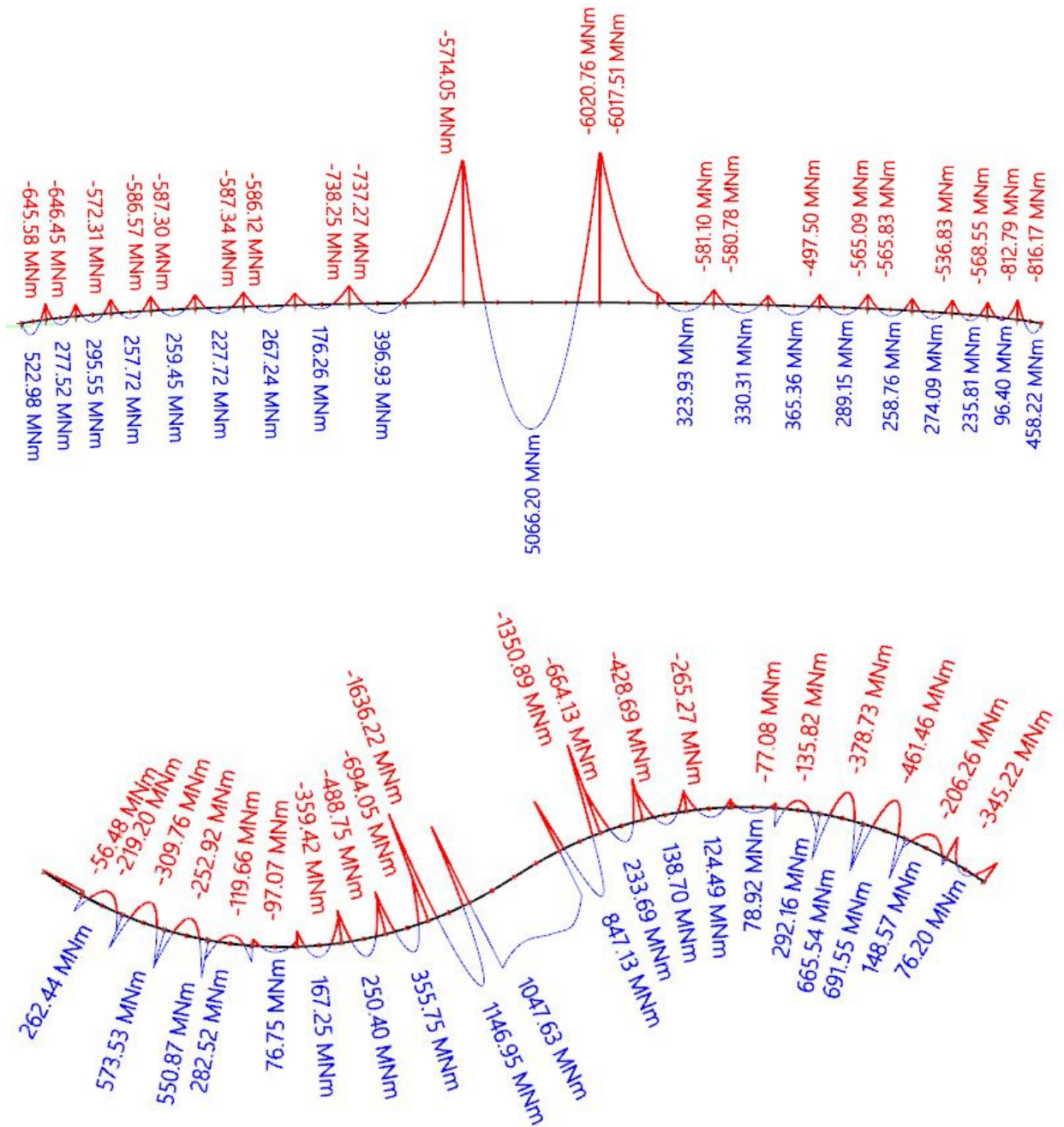


FIGURE L.3: GLOBAL FORCES IN THE GIRDERS UNDER ULS STORM LOADS. MY BENDING MOMENTS (TOP) AND MZ BENDING MOMENTS (BOTTOM).

## L.2 Global forces and bending moments in girder for double pontoon rotational stiffness

In chapter 5, it was concluded that increasing rotational stiffness of the pontoons would significantly decrease imposed deformations on the bridge girders. It was expected that this would decrease forces in the girders. Therefore, the pontoon rotational stiffness in Scia model #1 was doubled for all pontoons. Then the global forces in the bridge girders under LC4 in this new situation were calculated, again in Scia model #3. In figures L.4 and L.5, global forces on the bridge girders under LC4, but with a twice as high pontoon rotational stiffness, are displayed.



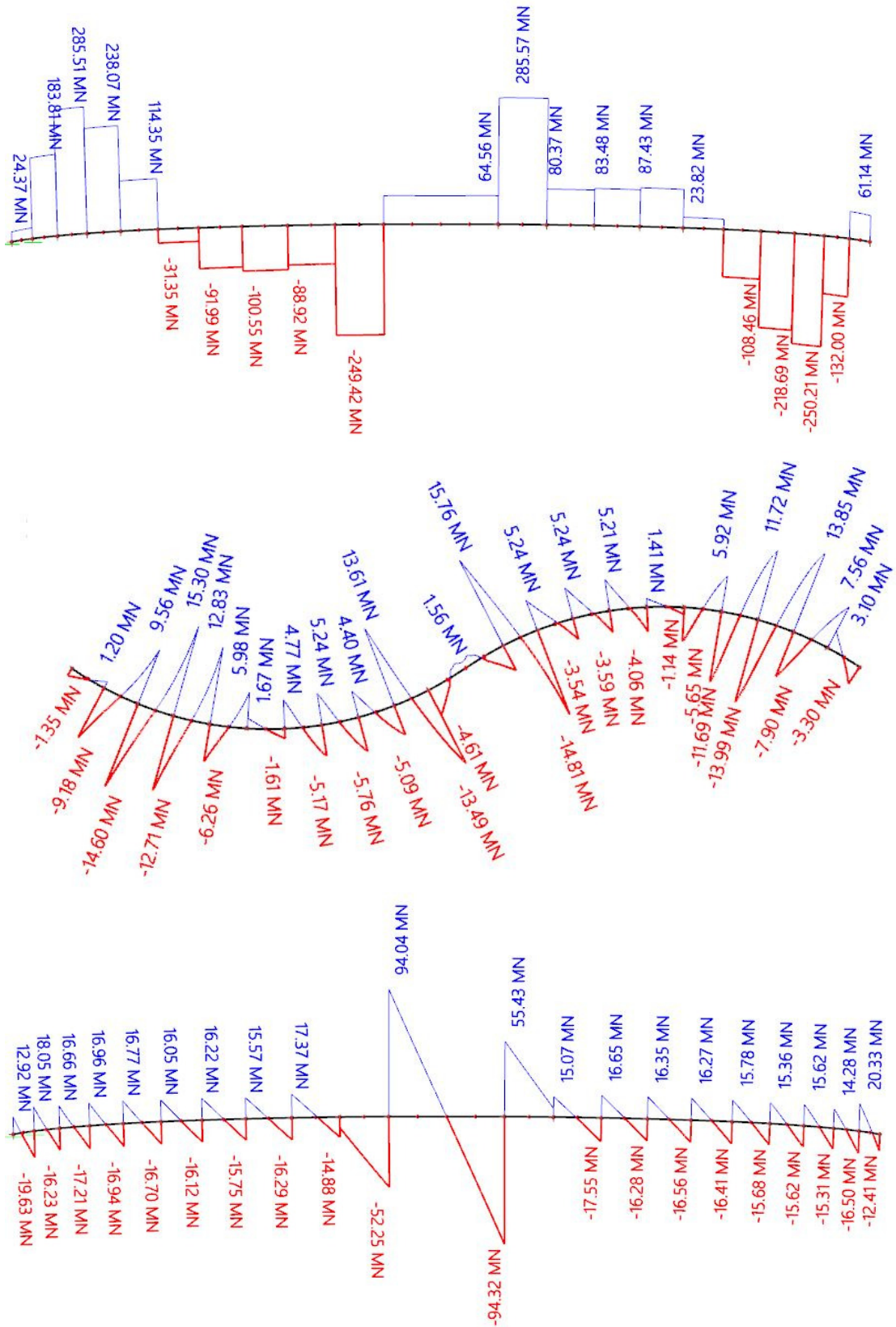


FIGURE L.4: GLOBAL FORCES IN THE GIRDERS UNDER ULS STORM LOADS WITH DOUBLE PONTOON ROTATIONAL STIFFNESS. FROM TOP TO BOTTOM: NORMAL FORCES, VY AND VZ SHEAR FORCES.

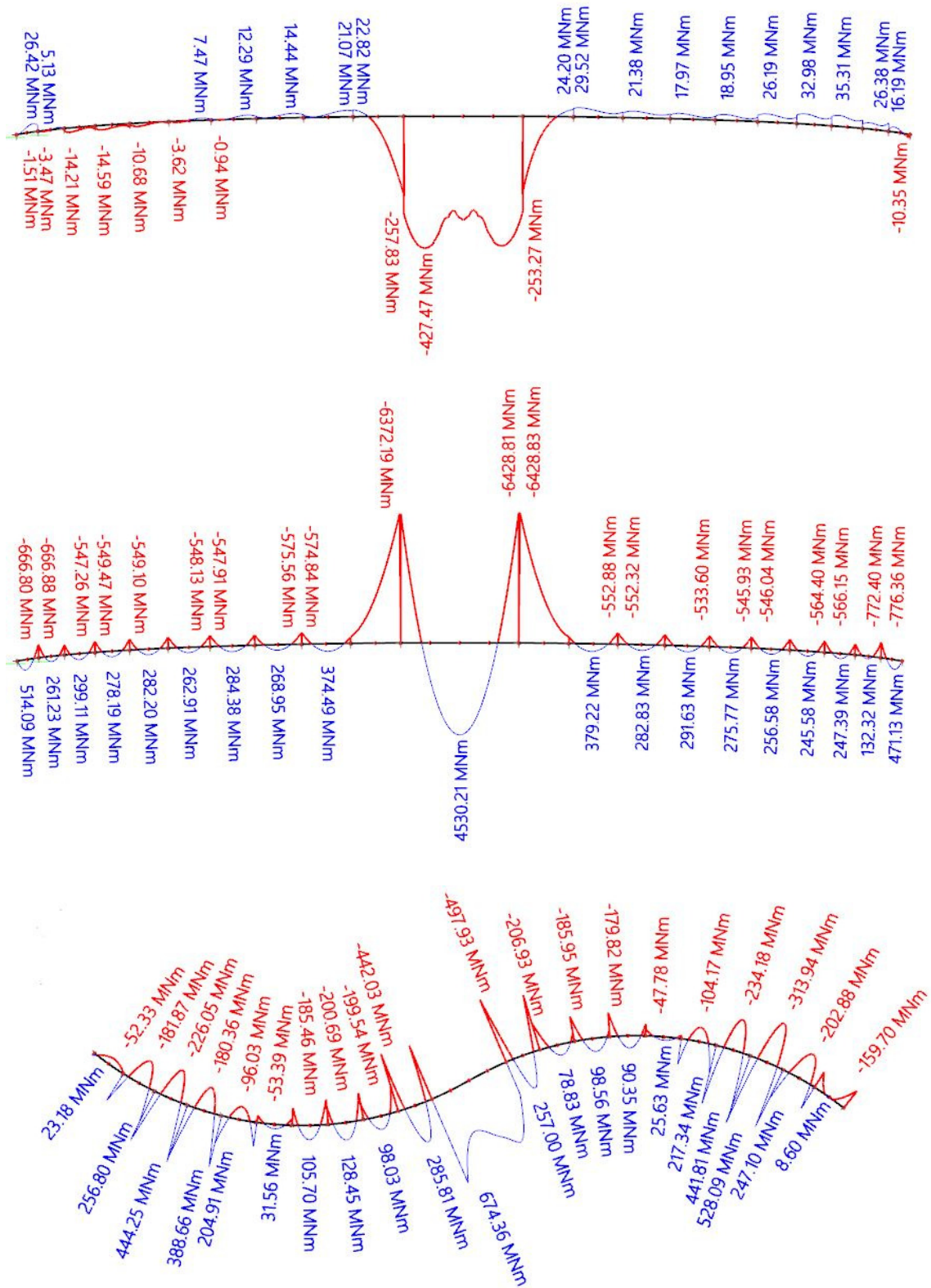


FIGURE L.5: GLOBAL FORCES IN THE GIRDERS UNDER ULS STORM LOADS WITH DOUBLE PONTON ROTATIONAL STIFFNESS. FROM TOP TO BOTTOM: MX, MY AND MZ BENDING MOMENTS.

### L.3 Global forces and bending moments in girders without imposed deformations

Global forces in the bridge girders under self-weight and lateral wind loads only were investigated as well. This means bridge deformations resulting from ULS storm deformations were not imposed. This was done to have an indication of the ratios of imposed deformations for the global forces and bending moments in the girders, as compared to the loads on the girders. These calculations were performed using Scia model #3. As expected, this sometimes results in quite different load graphs. See figures L.6 and L.7 for the results.

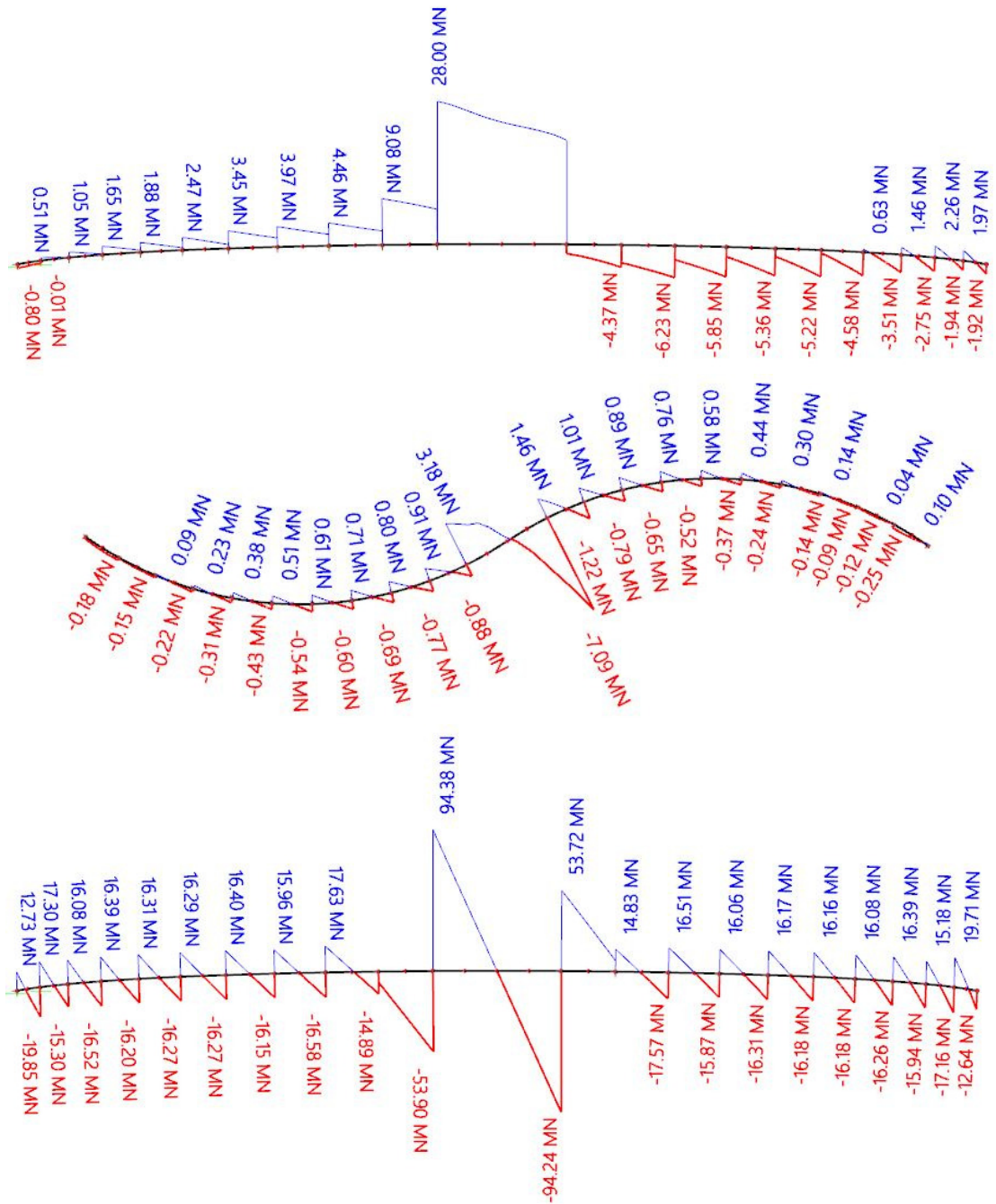


FIGURE L.6: GLOBAL FORCES IN THE GIRDERS UNDER SELF-WEIGHT AND WIND LOADS ONLY (NO IMPOSED DEFORMATIONS). FROM TOP TO BOTTOM: NORMAL FORCES, VY AND VZ SHEAR FORCES



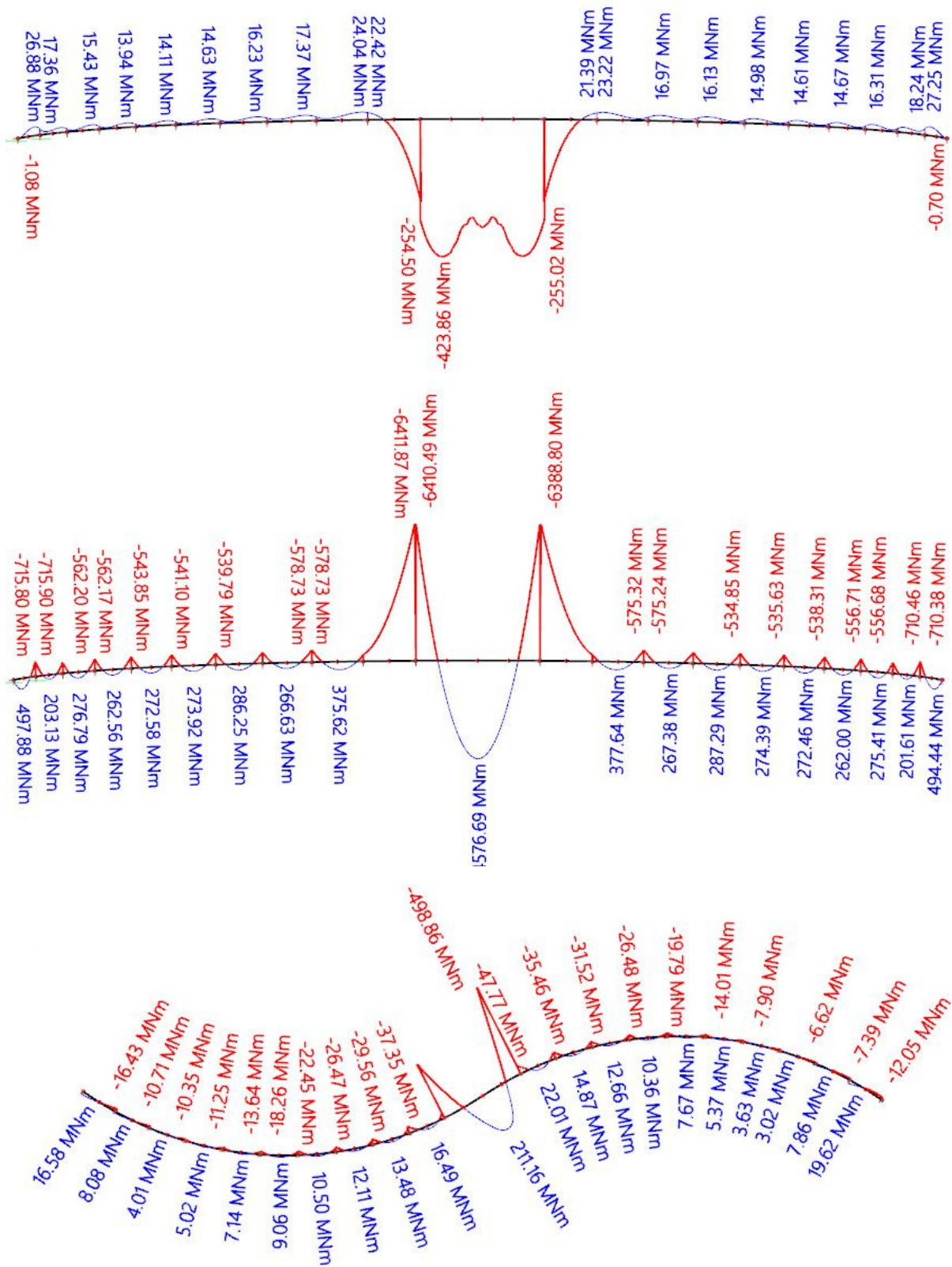


FIGURE L.7: GLOBAL FORCES IN THE GIRDERS UNDER SELF-WEIGHT AND WIND LOADS ONLY (NO IMPOSED DEFORMATIONS). FROM TOP TO BOTTOM: MX, MY AND MZ BENDING MOMENTS.

## ANNEX M: SHIP IMPACT ANALYSIS SET-UP AND SCRIPT

### M.1 Ship impact analysis model

The ship impact analysis consists of a large number of energy-displacement calculations in small time steps. Hence it was chosen to write a Python script to make these calculations. This was done in the following way.

The pontoon and ship are modelled as two masses, the former without any initial kinetic energy, the latter with a large initial kinetic energy. Upon impact, it was assumed that part of the kinetic energy of the ship would dissipate by plastic deformation of the ship bow. The remaining kinetic energy would be transferred to the pontoon and ship together, which would then act as one new combined mass. The initial dissipating energy through plastic deformation of the ship hull was determined at 175 MJ for a 40.000 t ship, based on the study by (Engseth and Wasjø, 2016).

The energy of this mass dissipated through two ways: by releasing it into the bridge girder and by releasing it to the drag force of the surrounding water. See figure M.1 for a sketch. The stiffness of the bridge girder was determined by imposing lateral displacements on the girder in Scia model #2. From the resulting lateral support reactions the bridge girder stiffness was determined. Because of the curved shape of the girder, this stiffness was non-linear. The stiffness for displacements in the range of 0-10 meters (the expected maximum range of pontoon displacements under ship impact) was determined. From the resulting girder stiffnesses, as a conservative approach, the lowest value was used as input value. This was found to be 45.7 MN/m.

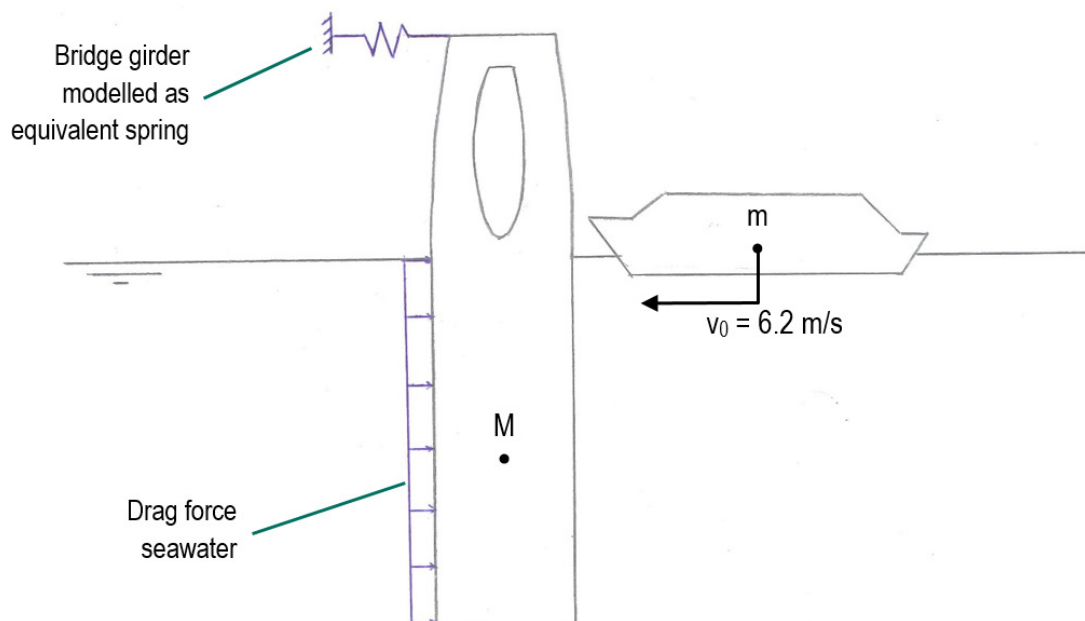


FIGURE M.1: SHIP COLLISION ANALYSIS MODEL SCHEMATISATION

Over the impact duration, the kinetic energy of the combined system would dissipate in the seawater and girder, thereby slowing the combined ship-pontoon mass down until it came to a halt. By calculating the speed and corresponding covered distance at every time step and then taking the sum of the covered distances, the total displacement of the pontoon was then calculated.

The water drag force depends on the pontoon speed, and the girder spring force on the pontoon displacement. Since these change over the impact duration, a numeric method was adopted. Small time steps were considered,

and at every time step, the kinetic energy that was transferred to the bridge girder and seawater was calculated. From the resulting kinetic energy, the resulting speed was calculated, after which the next time step could be calculated.

By making the time steps sufficiently small (10 milliseconds) and adding the covered distance at each time step, the total displacement of the pontoon was determined with close approximation. This was found to be 6.9 m. The impact duration was 4.53 s. See figure M.2. The Python script used for this analysis and the pontoon compartmentation calculation are shown on the next pages.

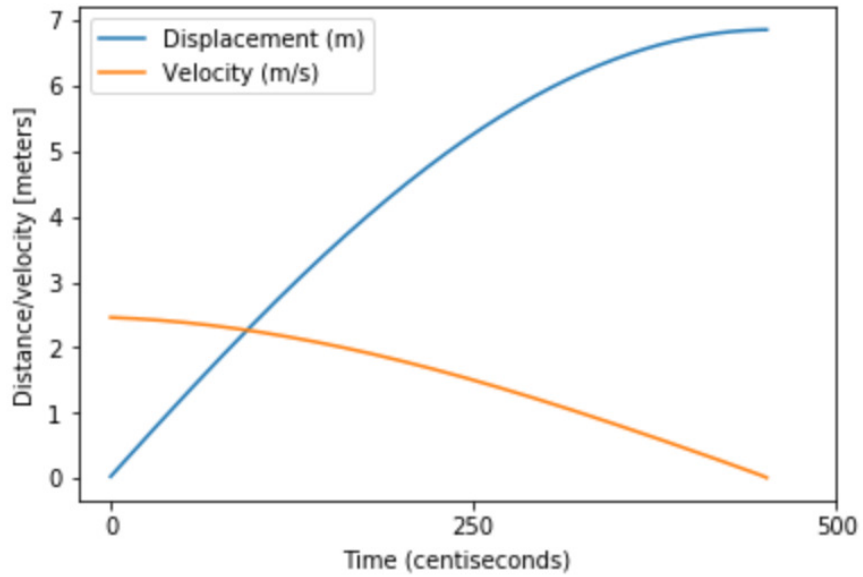


FIGURE M.2: DISPLACEMENT AND VELOCITY RESULTS FROM THE IMPACT ANALYSIS



## M.2 Python script for ship impact analysis model

In [11]:

```
import numpy as np
import matplotlib.pyplot as plt
%matplotlib inline
from math import sqrt
```

In [13]:

```
# All units in [N], [m], [J], [rad] and [Nm]

Cd = 1.5
D = 52
L = 136
rho = 1015
a1 = 82
a2 = 136/2

dt = .01
m = 40e6
M = 1.605e8
Kgirder = 45663411
Krot = 9.4375e10
u = 0
t = 0
rot = 0
v0ship = 5.0
Eplast = 175e6

#Eship = .5 * m * (v0ship**2)
Eship = 781e6
Epont0 = Eship - Eplast
v = sqrt(Epont0 / (.5 * (m + M)))
Etot = Epont0

displ = []
veloc = []
rotation = []
Etot1 = []
Edrag1 = []
Ebridge1 = []

for t in range(0,6000,1):
    if Etot > 11000: # This corresponds to a speed below 0.01 m/s
        du = v * dt
        Fdrag = .5 * rho * Cd * v**2 * D * L
        Edrag = .5 * Fdrag * du
        Fgirder = Kgirder * u
        Egirder = .5 * Fgirder * du
        Etot = Etot - Edrag - Egirder

    #Mrot = Fbridge * a1 - Fdrag * a2
    #rot = Mrot / Krot

    v = sqrt(Etot / (.5 * (m + M)))
    u = u + du
    t = t / 100 + dt
    print(t, u, v, rot)
```

```
        displ.append(u)
        veloc.append(v)
        rotation.append(rot)
        #Etot1.append(Etot)
        #Edrag1.append(Edrag)
        #Ebridge1.append(Ebridge)
    else:
        break

plt.plot(displ)
plt.plot(veloc)
#plt.plot(rotation)

plt.xticks([0,250,500])
plt.xlabel("Time (centiseconds)")
plt.ylabel("Distance/velocity [meters]")
plt.legend(['Displacement (m)', 'Velocity (m/s)'])

#plt.subplot(Etot)
#plt.subplot(Edrag)
#plt.subplot(Ebridge)
```

### M.3 Buoyancy calculation of a pontoon with compartments after ship impact

#### Calculation of buoyancy of largest pontoon after ship collision

This calculation assumes two pontoon compartments are broken and flooded with water. Unless specified differently, all values are in [kN], [m] and [kNm].

#### Pontoon weight

After a ship collision event, the pontoon weight is the original pontoon weight plus the extra weight of the water in the two compartments. First, the original weight is inputted from the file from Yip (2015).

$$G_{pont} := 2.6148 \cdot 10^6;$$

$$G_{pont} := 2.614800000 \cdot 10^6 \quad (1)$$

The pontoon volume is:

$$V_{pont} := \text{evalf}(\text{Pi} \cdot 20^2 \cdot 135);$$

$$V_{pont} := 286701.7456 \quad (2)$$

Which would give the following weight of displaced water, which should be the same as the total weight of the submerged pontoon:

$$G_{displ\ water} := V_{pont} \cdot 1.015 \cdot 9.81;$$

$$G_{displ\ water} := 2.854732286 \cdot 10^6 \quad (3)$$

This buoyancy of the pontoon per meter depth is its area times displaced water:

$$b_{pont} := \text{evalf}(\text{Pi} \cdot 20^2 \cdot 1.015 \cdot 9.81); \left[ \frac{kN}{m} \right]$$

$$b_{pont} := 21146.16509 \left[ \frac{kN}{m} \right] \quad (4)$$

Now, we assume that two compartments have flooded and are filled with water. This reduces the volume of the pontoon and it adds weight in the form of the inlet water. In an indicative design, 12 compartments were added in a ring in the pontoon. Each compartment had an area of 65.82 m<sup>2</sup> and a height of 20 m.

We calculate the inlet water weight, the original and the new pontoon draught:

$$V_{compartments} := 65.82 \cdot 20;$$

$$V_{pont, new} := V_{pont} - 2 \cdot V_{compartments};$$

$$b_{pont, new} := \left( \frac{V_{pont, new}}{135} \right) \cdot 1.015 \cdot 9.81;$$

$$b_{pont, new} := 20951.97853 \quad (5)$$

$$G_{water} := 65.82 \cdot 20 \cdot 1.015 \cdot 9.81;$$

$$G_{pont, new} := G_{pont} + 2 \cdot G_{water};$$

$$dr_{pont, old} := \frac{G_{pont}}{b_{pont}}; dr_{pont, new} := \frac{G_{pont, new}}{b_{pont, new}};$$

$$G_{pont, new} := 2.641015185 \cdot 10^6$$

$$dr_{pont, old} := 123.6536265$$

$$dr_{pont, new} := 126.0508730 \quad (6)$$

As can be seen, as a result of two flooded compartments after a ship collision, the pontoon will lower 2.4 m. This means the pontoon will lower 1.8% compared to its original length.

## ANNEX N: EIGENPERIODS, DYNAMIC BEHAVIOUR AND MEASURES

The scope of this thesis is not to conduct a full dynamic analysis research. However, a qualitative research and analysis will be conducted here, to obtain a clear image of ways to address any problems.

### N.1 Eigenperiod analysis modelling

Only the component that was analysed, was modelled. As boundary conditions, the rest of the Sognefjord bridge was replaced by a set of equivalent springs. For the spring properties, first the displacements and rotations in the self-weight situation of the bridge in Scia model #1 were taken. Then, the axial loads at the boundaries of the considered bridge component were retrieved. From the load values and from the displacement values, an equivalent spring stiffness was calculated. These springs were then modelled as boundary conditions for the bridge component to be analysed.

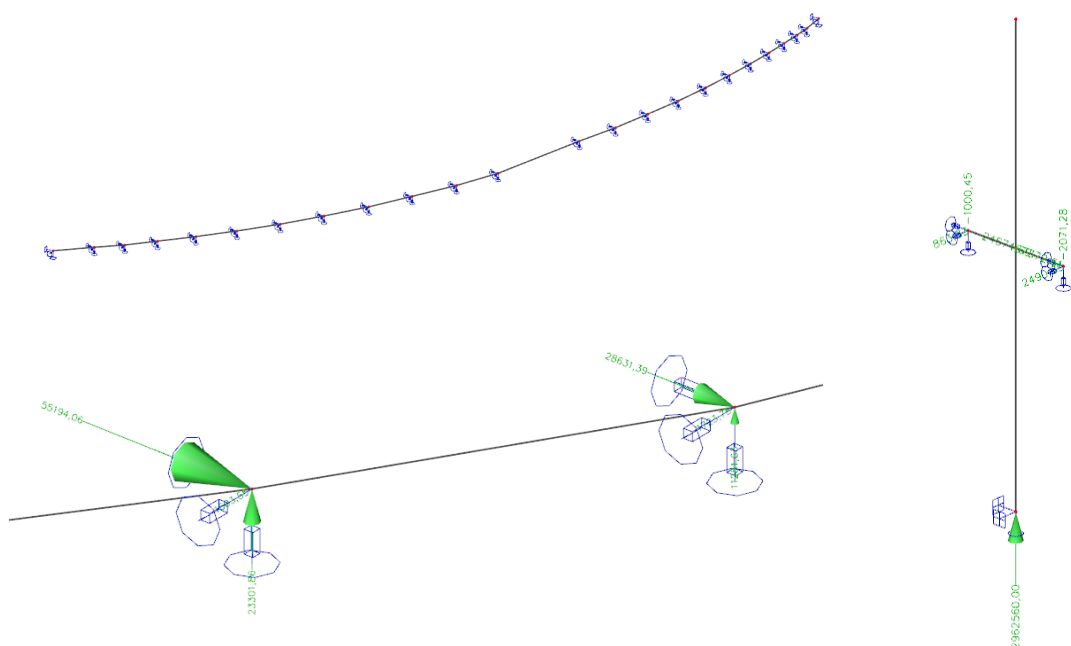


FIGURE N.1: EIGENFREQUENCY ANALYSIS MODELLING OF CABLES (LEFT) AND PONTOONS (RIGHT)

Then, the same loads from the self-weight situation were inputted at the boundary condition springs. This was to make sure the component would displace into its self-weight position. See figure 8.2 for an impression of the way the dynamic analyses were modelled.

Next to the mentioned input, at the pontoons the correct ballast weight was added, as this has a large influence on the dynamic behaviour. For the main anchoring cable, the exact same shape of the cable was maintained. This was done by copying the cable directly from Scia model #1. Each side anchoring cable was simplified using a particular unique set of springs and external forces.

When the models were set, an eigenfrequency analysis was carried out using SCIA Engineer. By modelling bridge components like this, dynamic behaviour analyses could be performed relatively quick, but with reliable results.

### N.2 Eigenperiod analysis results

For a number of bridge components that were considered to be important for dynamic behaviour, eigenfrequencies were calculated. The first ten eigenperiods of each component are given here. See table N.1.

TABLE N.1: FIRST TEN EIGENPERIODS OF MEMBERS CONSIDERED IN EIGENFREQUENCY ANALYSIS

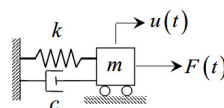
Part of the bridge	Eigenperiods									
	1	2	3	4	5	6	7	8	9	10
Main anchoring cable	112.3	84.4	73.0	70.9	61.8	59.4	55.1	52.0	49.3	43.8
Longest side anchoring cable	1123.9	1123.9	281.1	281.0	125.0	125.0	70.5	70.4	45.3	45.3
Long lateral cable at pontoon #11	167.6	167.5	42.0	41.9	18.7	18.6	10.6	10.5	6.8	6.7
Short lateral cable at pontoon #11	46.0	44.6	12.8	11.2	6.8	5.0	4.1	2.8	2.6	1.8
Largest pontoon	61.3	24.6	10.9	9.8	8.6	0.16	0.16	0.07	0.07	0.05
Smallest pontoon	102.3	20.8	15.0	10.0	8.2	0.05	0.05	0.03	0.03	0.03

### N.3 Measures to reduce behaviour

- Individual parts of the bridge can be regarded as single-degree of freedom (SDOF). With any SDOF, a way to reduce movement of the system is simply to increase its mass, since the natural damping of the system becomes higher. See figure N.1.

$$\ddot{u} + 2\zeta \omega_0 \dot{u} + \omega_0^2 u = F(t)/m$$

$$u(0) = u_0, \quad \dot{u}(0) = v_0$$



$$\omega_0 = \sqrt{k/m} \text{ is the natural frequency}$$

$$\zeta = c/c_{\text{critical}} \text{ is the damping ratio}$$

$$c_{\text{critical}} = 2\sqrt{k m} \text{ is the critical damping}$$

$$u(t) = \exp(-\zeta \omega_0 t) \left( u_0 \cos(\omega_1 t) + \frac{1}{\omega_1} (v_0 + u_0 \zeta \omega_0) \sin(\omega_1 t) \right) + \frac{1}{m \omega_1} \int_0^t F_u(\tilde{t}) \exp(-\zeta \omega_0 (t - \tilde{t})) \sin(\omega_1 (t - \tilde{t})) d\tilde{t}$$

FIGURE N.1: NATURAL DAMPING AND DYNAMIC DISPLACEMENT EQUATIONS. RETRIEVED FROM METRIKINE (2017).

Therefore it could be chosen to add mass to the bridge, for example by hanging ballast anchors to the cable system or the bridge girder. However, in the Sognefjord bridge the stress capacity of the cables in the anchoring system was already to a large extent activated (Yip, 2015). Increasing the weight of the girder would increase the already high stresses in girder members as well. Increasing the mass of the cables was therefore considered not feasible. Increasing the mass of the pontoons is more feasible, but this would come with costs of increasing pontoon size as well.

- In earthquake engineering, tuned mass dampers are used to reduce the structural acceleration due to earthquakes or wind force. These work by channelling vibration energy from the main structure to an auxiliary one (the mass), after which it will be absorbed by displacement. Disadvantages of such systems are the sensitivity related to the narrow frequency band control (this will have to fit the load frequency) and the size of the absorber mass (Chey et al., 2009). Also, mass dampers would not be practical for use in the anchoring system.

- Dynamic behaviour of anchoring cables is not only influenced by the cable properties and the dynamic loading, but by tension forces in the cables as well. Higher-tensioned cables show more dynamic displacements from the higher wave speed through the cable (see figure N.2). This results in more and bigger wave movements in the cable. Furthermore, the tensile force directly influences the eigenfrequencies of the cables.

Governing equations for free vibrations of a fixed-fixed string:

$$\frac{\partial^2 w}{\partial t^2} - c^2 \frac{\partial^2 w}{\partial x^2} = 0, \quad c = \sqrt{\frac{T}{\rho A}} \text{ - the speed of waves in the string}$$

$$w(t, x) = \sum_{n=1}^{\infty} \left\{ \Psi_n(0) \cos(\omega_n t) + \frac{1}{\omega_n} \dot{\Psi}_n(0) \sin(\omega_n t) + \frac{1}{\omega_n} \int_0^t Q_n(\tau) \sin(\omega_n(t - \tau)) d\tau \right\} \sin(\beta_n x)$$

where

$$\Psi_n(0) = \frac{2}{L} \int_0^L \varphi(x) \sin(\beta_n x) dx, \quad \dot{\Psi}_n(0) = \frac{2}{L} \int_0^L \dot{\psi}(x) \sin(\beta_n x) dx$$

$$Q_n(t) = \frac{2}{\rho A L} \int_0^L q_1(x, t) \sin(\beta_n x) dx$$

$$\beta_n = n\pi/L, \quad \omega_n = c\beta_n = n\pi c/L$$

FIGURE N.2: HIGHER CABLE EXCITATION THROUGH A HIGHER CABLE FORCE. RETRIEVED FROM METRIKINE (2017).

A way to reduce dynamic amplification is to decrease tension stress by adding buoyancy elements to the cables. Lowering tensile forces in the cables would however of course also mean that the forces that keep the pontoons in place are lowered, which is very unbeneficial for the overall behaviour of the Sognefjord bridge.

- Flutter effects in a system occur under a steady-state flow, such as current. Galloping of a structure under a wind load is a similar dynamic phenomenon. Although more things can be thought of to reduce flutter and galloping, the most important factor is structural damping (Larsen & Larose, 2015). The logical choice for this is to install viscous dampers (figure N.3). These work on resistance induced from the rapid passage of a fluid through a narrow opening. Current dampers can have damping forces easily exceeding 70 kN. A big advantage of viscous dampers is these have a very long service life and require almost no maintenance (Lee & Taylor, 2001). It is proven possible to use cable damping systems in a submerged environment (Wang et al., 2017).

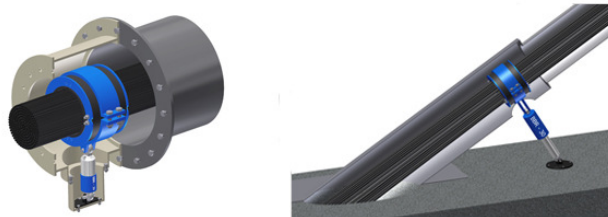


FIGURE N.3: VISCOUS DAMPERS



- It is key to investigate the absorption of displacements between different bridge components. For this a component that could absorb small displacements between two members would be needed. This can be done by placing elastomeric bearings as connections between members. These still transfer loads from one component to the other, but allow for small displacements and rotations. Existing models in the current field are up to 1280x940 mm, allow vertical forces up to 18225 kN, displacements up to 158 mm and rotations up to 21 mrad (Maurer Söhne 2012).

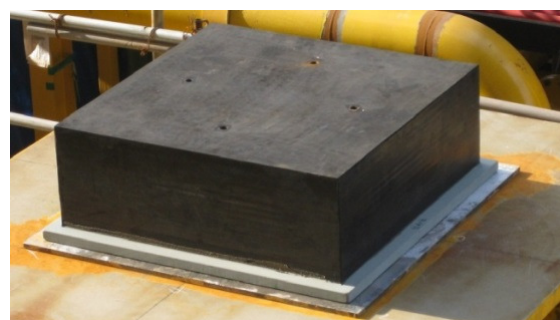
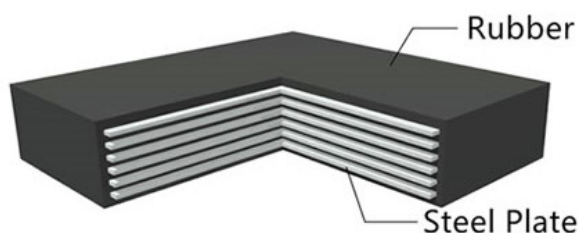


FIGURE N.5: ELASTOMERIC BEARING BLOCK

It should be investigated whether their capacity, especially for shear (typically the shear modulus of the rubber component is around 0.9 N/mm<sup>2</sup>, EN 1337-3), is sufficient. Elastomeric bearings with claims of service life of over 100 years are known in the field (Granor, 2017). This would fit the Sognefjord bridge requirements.

- The flow of both wind and water against and around the bridge is heavily influenced by member cross-section geometry. Normally, the best option would be using cylindrical cross-sections, as these are structurally practical but also have relatively favourable aerodynamic properties. About all of the member cross-sections in the Sognefjord bridge are already cylindrical. Further aerodynamic optimisation of girder members was considered structurally not efficient. VIV in the anchoring cables could be reduced by adding helical strakes to the cables. These are often used in offshore spar structures and do not require extra maintenance.

#### N.4 Qualitative analysis of dynamic behaviour measures

For each approach discussed a score of 1 (bad) to 5 (good) was given for each criterion. It has to be taken into account that these were estimates. However, these were based on engineering experience and best practices in the field and considered to be sufficient for this stage of design. In table N.2 the scores are displayed.

TABLE N.2: RESULTS FROM MULTI-CRITERION ANALYSIS

Measure	Reducing dynamics component	Reducing dynamics bridge	Structural feasibility	Maintenance intensity	Costs	Total score
Adding mass elements	3	3	2	5	1	14
Tuned mass damper	3	2	3	4	3	15
Reducing cable tension	2	1	2	5	5	15
Adding viscous dampers	4	4	4	5	3	20
Elastomeric bearings	2	4	5	4	4	19
Adjusting member geometry	4	2	4	5	4	19

---

It was chosen to let each criterion have the same weight. Some comments on the scores are given below:

- The costs of increasing mass would be very high, because next to the mass material, the structure would have to be strengthened significantly. The effectiveness of adding mass depends on the scale of application.
- The effectiveness of adding an auxiliary tuned mass damper would be limited because their effect heavily depends on the load frequency, which is semi-random. Their placement would probably be practical though, as this could be done within a pontoon or a girder. They would however add heavy mass to the bridge structure.
- Adding buoyancy elements in the cables would likely increase overall bridge displacements, especially under extreme load cases.
- Viscous dampers would be effective, but large numbers might be needed and optimisation might be challenging.
- It was assumed the service life of elastomeric bearings would be the same as the bridge service life.
- Making unusual cross-sections would bring great costs. Helical strakes for the anchoring cables are however deemed structurally very feasible.